UNIVERSITÀ DEGLI STUDI DI MILANO

PhD School in Molecular and Cellular Biology
XXXVII Cycle

Bioscience Department

UNIVERSITÀ DEGLI STUDI DI MILANO

DIPARTIMENTO DI BIOSCIENZE

Modifying phyllotaxis in *Brassica* seed crop species for yield improvement

BIOS/14

Carlotta Claudia Ferrario

Scientific Supervisor: Martin M. Kater
Tutor: Veronica Gregis - Francesca Caselli

PhD School Coordinator: Prof. Roberto Mantovani

A.A.
2023-2024

Table of contents

Abstract 4

Riassunto 5

Aim of the thesis 6

Introduction 8

1. The inflorescence architecture and its relevance 8

2. Phyllotaxis determination 11

2.1 Historical theories 11

2.2 What is known about phyllotaxis determination so far 11

3. The driving hypothesis of this thesis 15

4. The REM gene family 15

5. *Brassica napus* 19

5.1 *Brassica napus* economic relevance 19

5.2 *Brassica napus* biology and genome 21

6. A workflow for polyploid crop breeding 23

Results and discussion 25

1. Multiple mutants in *AtREM34*, *AtREM35* and *AtREM36* can produce more siliques on the main inflorescence 25

2. Study of the cluster conservation in *Brassica napus* 27

2.1 Cluster identification 27

2.2 BnaREM34, *BnaREM35/36*, *BnaREM36* and *BnaREM37* expression pattern is conserved 30

2.3 *BnaREMs* are possibly involved in phyllotaxis determination 33

2.4 Evaluation of REM protein complexes in *Brassica napus* 38

2.5 BnaREMs possibly interact with the auxin pathway 40

2.6 BnaREM and AtREM interspecific interactions 40

2.7 Summary of the results: cluster characterization 41

3. *Brassica napus* genome editing 43

3.1 gRNAs design and test 43

3.2 Strategy and Constructs 45

3.3 *Agrobaterium*-mediated transformation 47

3.4 Summary of the results 56

Conclusion and future perspectives 58

Material and Methods 61

1. Plant material and growth conditions 61

2. Phyllotactic pattern measurement and yield analysis 61

3. Bioinformatic analysis 61
3.1 Homology and phylogenetic analysis 61
3.2 Protein identity and similarity analysis 62
4. Gene expression analysis in *Brassica napus* 62
4.1 qPCR 62
4.2 *In situ* hybridization 62
5. Complementation test 63
6. Protein interaction test 63
6.1 Yeast-2-Hybrid (Y2H) 63
6.2 Bimolecular fluorescence complementation (BiFC) 63
7. Editing design and transformation 64
7.1 gRNA design 64
7.2 gRNA test by protoplast destructive assay 64
7.3 CRISPR construct cloning 65
7.4 *Brassica* transformation 65
8. Microscopical analysis of *Brassica napus* flower 68
9. GUS staining 68
10. GFP screening 69
Supplementary 70
Bibliography 75
Appendix 91

Abstract

In a world that is continuously growing and developing, it is crucial to enhance agricultural yields to ensure an adequate food supply for the population while minimizing environmental impact. Plant yield is influenced by a range of factors, among which inflorescence architecture and its geometrical organization, known as phyllotaxis. Despite centuries of studies, the mechanism behind phyllotactic patterning is still partially unknown, especially in non-model plant species. Furthermore, the direct impact of phyllotaxis on overall yield is not well understood.

In this thesis, we started to tackle these knowledge gaps. First, we reported support to the hypothesis of a direct link between phyllotaxis and yield by describing several *Arabidopsis REM* mutants with a permutated phyllotaxis and an increased number of siliques on the main stem.

Consequently to this result, we aimed to investigate the conservation of such a mechanism in the economically important crop *Brassica napus*.

We identified the candidate homologous genes in rapeseed and confirmed their expression in reproductive tissues. Moreover, we demonstrated that they can influence phyllotaxis in Arabidopsis, suggesting a retained role between these two species. Protein interaction tests further suggested that some interaction between REMs themselves and the auxin pathway can be conserved.

To finally prove the mechanism in rapeseed, we aimed to generate the homolog *REM* mutants in the species by CRISPR-Cas9 gene editing. After an *in silico* and experimental selection of the gRNAs, we focused on the *Agrobacterium* mediated transformation of rapeseed.

According to our results, both the transformation protocol as well as the editing need to be optimized if we want to apply up to date molecular techniques in *Brassica napus*.

Indeed, we detected inefficiency and high technical requirements in the transformation protocol and a low functionality of the editing machinery in transformants, the latter being reported in literature too.

Optimizing such techniques can exponentially speed up basic and applied research in rapeseed and open new possibilities in crop design. Indeed, multiple mutants are very often required to get phenotypes in high redundant genomes such as the one of *Brassica* napus and producing them by random mutagenesis is highly time consuming.

Overall, this application-driven study unveils novel genes associated with phyllotaxis and yield in the Brassicaceae family, contributing to our understanding of plant architecture and offering insights into sustainable strategies for improving crop productivity.

Riassunto

In un mondo in continua crescita è cruciale aumentare le rese agricole per garantire un adeguato accesso al cibo a tutta la popolazione mondiale, minimizzando l'impatto ambientale.

La resa di una pianta è influenzata da molti fattori, tra cui l'architettura dell'infiorescenza e la sua organizzazione geometrica, detta fillotassi.

Nonostante i secoli di studi, il meccanismo alla base della disposizione fillotattica è ancora parzialmente sconosciuto, soprattutto nelle specie che non vengono usate come modello nella ricerca. Inoltre, l'impatto della fillotassi sulla resa non è ancora chiaro.

In questa tesi, ho affrontato queste domande.

Per prima cosa ho raccolto dati a favore dell'ipotesi di un legame diretto tra fillotassi e resa, descrivendo svariati genotipi di Arabidopsis mutati in dei geni *REM*, con una fillotassi perturbata e un maggior numero di silique sull'infiorescenza primaria.

A seguito di questo risultato, ho investigato la conservazione di questo meccanismo in una coltura di rilevanza economica, *Brassica napus* (colza).

Ho identificato i candidati geni omologhi nella colza e confermato la loro espressione nei tessuti riproduttivi. In aggiunta, ho dimostrato che possono influenzare la fillotassi in Arabidopsis, risultato che suggerisce che i geni conservino il loro ruolo nelle due specie. Test di interazione proteici hanno suggerito che anche l'interazione tra i REM, e tra REM e il pathway dell'auxina possa essere in parte conservata.

Per dimostrare definitivamente il ruolo dei *REM* nella fillotassi e resa della colza, ho cercato di generare gli omologhi mutanti *REM* nella specie tramite editing mediato dalla tecnologia CRISPR-Cas9. Dopo una selezione *in silico* e sperimentale dei gRNAs, mi sono concentrati sulla trasformazione mediata da Agrobatterio.

Dai miei risultati, risultano necessarie sia un'ottimizzazione dei protocolli di trasformazione che di editing se vogliamo applicare le moderne tecnologie molecolari in *Brassica napus*.

Infatti, nella mia esperienza i protocolli di trasformazione sono risultati inefficienti e bisognosi di consolidate capacità tecniche, e la macchina di editing nei trasformanti è risultata inefficiente (in accordo con i dati in letteratura).

L' ottimizzazione di queste tecniche potrebbe esponenzialmente velocizzare sia la ricerca di base che quella applicata nella colza e aprire nuove possibilità nel disegno razionale delle colture. Infatti, mutanti multipli sono spesso richiesti per ottenere fenotipi in genomi ridondanti come quello della colza, e ottenerli tramite mutagenesi casuale richiede molto tempo.

In conclusione, questo studio applicato rivela nuovi geni associati alla fillotassi e alla resa nella famiglia delle Brassicaceae, contribuendo alla comprensione dei meccanismi alla base dell'architettura dell'infiorescenza e offrendo informazioni utili per disegnare strategie sostenibili per aumentare la produttività delle colture.

Aim of the thesis

The inflorescence architecture is a key feature of a plant. Composed by the length of the inflorescence, its branching potential and the disposal of the organs around the stem, it determines the yield of the plant.

The architecture is primarily determined by the activity of the inflorescence meristem (IM), and specific patterns of meristem maintenance and differentiation give rise to the different architectures present in nature.

Arabidopsis thaliana develops a raceme inflorescence, where the IM continuously divides to maintain itself while at the edges new floral meristems differentiate. These floral meristems will give rise to flower and fruits, which are spaced one from the other by a 137.5° angle, the so called "Golden Angle". This pattern, known as Fibonacci spiral because of its mathematical features, is the most abundant in the plant kingdom, and has been of great interest for biologists, physicist, chemists and mathematician for centuries. However, its biological role and determination are far to be understood.

Recently, in our laboratory have been uncovered how three genes of the *REM IX* family are involved in the determination of a robust phyllotactical pattern in Arabidopsis. Single and multiple mutants in *REM34*, *REM35* and *REM36*, have indeed aberrant patterns, where the divergence angle is less frequently the usual 137.5°, but is often of 90 or 180°.

The first aim of this thesis was to unveil a potential impact of this mutated pattern on the yield of the plant. To do so, we counted the siliques produced on the main inflorescence in *REM* single and double mutants, discovering that the double mutants present a 20% increase of the siliques produced.

Considering this a trait of great interest for agriculture, we evaluated the possibility to replicate it in a species of economical relevance and phylogenetically close to Arabidopsis, in a translational biology approach.

Brassica napus is part of the Brassicaceae family as *A. thaliana*, it's the third main oil crop in the world and the first in Europe. It's a young allotetraploid, born 7500 years ago from the natural hybridization of *B. rapa* and *B. oleracea* and has recently become a species of great interest for both food production and industrial processes. For these reasons we evaluated it a good candidate where to apply our research.

By a bioinformatic analysis we identified 6 candidate homologs of *REM34* and 2 genes which are homologs of *REM35* and/or *REM36*. We further included in our research the 2 detected homologs of *REM37*. Indeed, it is not expressed in Arabidopsis, but it is part of the same phylogenetic cluster and thought to be highly redundant with our three genes of interest.

Gene expression analysis by qPCR and *in situ* hybridization confirmed the expression of all our candidates in the *Brassica napus* inflorescence and floral tissues, coherently with their Arabidopsis orthologs.

Accounting for the allotetraploidy of the species and its recent origin, as well as the predicted homology of the coded REMs, we focused on the functional characterization of 4 of them, of the subgenome of *B. rapa*. By an interspecific complementation test we demonstrated that they impact the phyllotaxis in Arabidopsis, suggesting a similar role in rapeseed. Furthermore, with Y2H assays we unveiled some REM-REM and REM-ARF intra and

inter-specific interactions, suggesting a possible conservation of the molecular mechanism behind phyllotaxis determination.

Building upon these results, we designed a CRISPR-Cas9 editing strategy to get single and double *REM* mutants in rapeseed. Following an *in silico* and *in vivo* selection of the gRNAs and their cloning, we aimed to transform rapeseed by *Agrobacterium tumefaciens*.

We tested several published protocol and sub-conditions, detecting high technical requirements and low efficiency of the majority of them. We finally got 8 transformants, but none of them were edited. Transformation and editing optimization are thus suggested to more easily get mutants in rapeseed.

Taken together, during this thesis we unveiled novel genes impacting phyllotaxis and yield in the Brassicaceae family, and we got valuable information to enhance crop production by a rational genetic approach.

Introduction

1. The inflorescence architecture and its relevance

The world population is growing and is expected to reach 10 billion people by 2060 (Ritchie et al., 2024). This, together with the expected increase in meat and dairy consumption (Henchion et al., 2021), points out the need to increase our crop production (Schwarz et al., 2020a).

Dedicating more land to agriculture is not a sustainable solution, as the maintenance of wild environments is crucial to avoid biodiversity erosion and further greenhouse gases emissions related to land use change. Increasing the crop yield on the other hand, we could produce more food in the same area.

The number of fruits and seeds that a plant can bear depends on the inflorescence's architecture, meaning its length, branching potential and phyllotaxis, which is the arrangement of the organs around the stem.

The determination of the inflorescence architecture starts from the inflorescence meristem.

The meristems are niches of undifferentiated cells that have the potential to create new organs and tissues. The two principal meristems in plants are the root meristem (RAM), which develops the below-ground tissues, and the shoot apical meristem (SAM), which gives rise to the aerial part.

During the vegetative growth, the SAM produces leaves and short internodes. At a certain point, signalling pathways perceive both external and internal clues, which determine the induction to the floral transition. Specifically, the photoperiod pathway perceives the day length, the vernalization pathway the temperature, and autonomous and gibberellin pathways convey endogenous signals (Conti, 2017).

When the floral transition occurs, the stem of the plant elongates, and the SAM changes its identity into an IM (inflorescence meristem), which starts to develop new kind of meristems, the flower meristems (FM), which at the end will bring to flowers and fruits.

Different types of inflorescence architecture are present in nature (Fig. 1).

For example, the model plant *Arabidopsis thaliana* presents a raceme inflorescence, where the IM continuously maintain itself by cell division and differentiates FMs at its edges. Tomato cymose inflorescence is characterized by an IM which produces a FM on one side and a new IM on the other, reiterating the process. In some grasses, a single IM will give rise to a single spikelet meristem, which then will bear multiple FMs(Caselli et al., 2020; Prusinkiewicz et al., 2007).

More than the basic types of inflorescences, the architecture depends on the spatial organization of the organs around the stem, which is called phyllotaxis (from Greek phyllon, leaf and taxis, arrangement). Again, biodiversity presents different patterns in nature, having all in common a striking regularity.

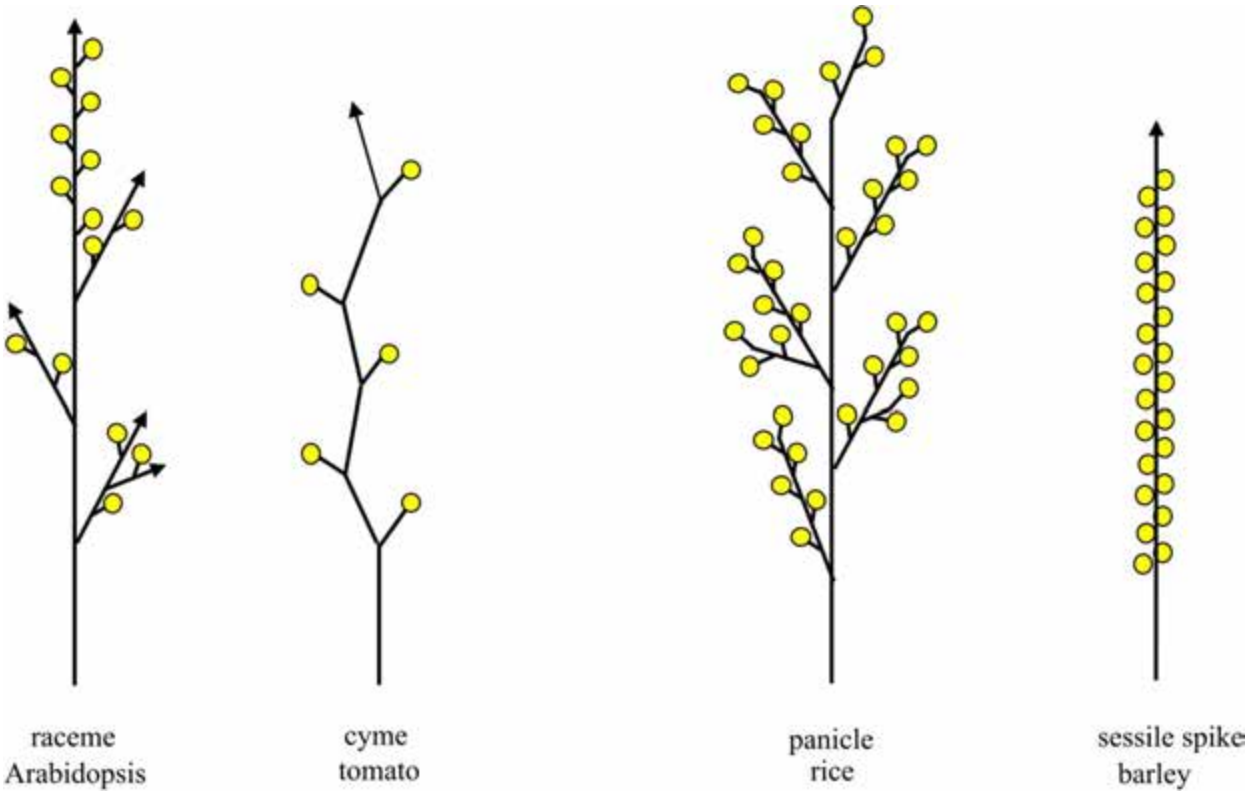

Fig. 1. Examples of inflorescences and model plants where they can be found. In inflorescences such as the raceme and the cyme, an indeterminate meristem (arrow) continuously develops while producing determinate floral meristems (yellow circles) which will become flowers. In grasses, an inflorescence meristem develops a single flower-bearing structure, which can be branched or not. In panicles, an IM develops branch meristems that then produce spikelet meristems, that bear flower meristems. In barley, a single spikelet meristem is produced from the inflorescence meristem.

The phyllotactic pattern is dictated by the number of primordia arising simultaneously from the stem (called jugacy) and the divergence angle between primordia of successive emergence events.

For example, if only 1 primordium emerges from the stem in a specific moment, a divergence angle of 47° would determine a monostichous pattern, an angle of 99.5° a Lucas spiral, angle of 137.5° a Fibonacci spiral. If all these patterns generate spirals, a divergence angle of 180° generates a distichous pattern (or alternated), where organs are disposed in lines at opposite sides of the stem.

If more primordia emerge simultaneously from the meristem, they will always be placed at the maximum distance from the other. Therefore, 2 primordia will be opposite one from the other, 3 would be spaced by angles of 120° and so on.

In case of 2 primordia emerging simultaneously, an opposite superposed pattern is designed if the successive events are spaced by 0/180° angle from the previous, while if it is 68.8° the pattern is bijugate and if it is 90° is decussate. If the primordia are 4, an angle of 45° between successive events would produce a whorled phyllotaxis (Fig. 2). For other examples of the phyllotactical patterns see Richard S. Smith, Cris Kuhlemeier, 2006.

The phyllotactic pattern is so precise that is used in taxonomic analysis, with phylogenetically close species showing a similar pattern (Reinhardt, 2005). However, it is not a rigid feature of a species, as it often changes during plant development (Bartlett & Thompson, 2014; Reinhardt, 2005; Traas, 2013). For example, in Arabidopsis, the embryonic cotyledons are placed in a decussate pattern, while subsequent leaves and flowers are arranged in a Fibonacci spiral (Reinhardt, 2005). Finally, floral organs are displaced in concentric whorls.

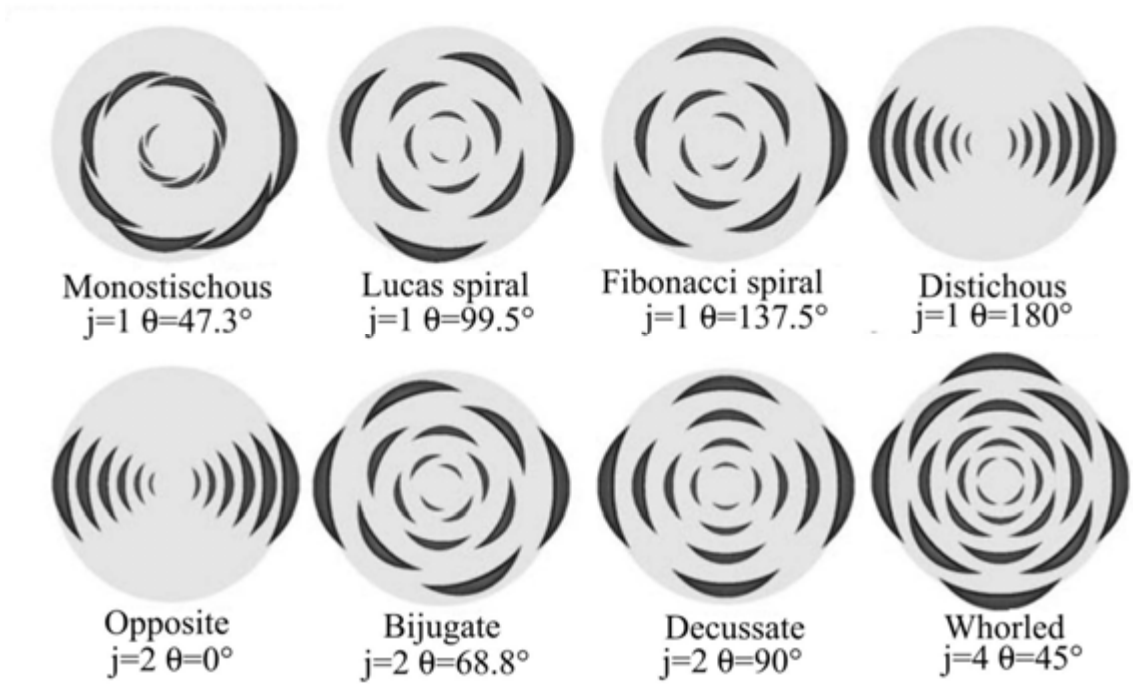

Fig. 2. Examples of the main phyllotactic patterns. j= jugacy. Adapted from Smith et al, 2006.

The most common phyllotactic pattern is the one described from the Fibonacci spiral. It characterizes different model dicots, such as tobacco, tomato and Arabidopsis (Reinhardt, 2005).

As written above, in this pattern one organ appears at a time and subsequent ones diverge by a 137.5° angle, the so-called "golden angle". This corresponds to the division of a circle (360°) by the limit of the ratio between consecutive numbers of the Fibonacci series (where each number is the sum of the two preceding it in the series), subtracted from a whole circle (360- (360/ (X_n+1/X_n in the Fibonacci series)(Godin et al., 2020).

Moreover, when looking at the shoot from the top, other spirals, differing in the orientation of the spiral bending (clock or counter-clockwise) and which differ from the one formed by the organ's succession (called generative spiral, Godin et al., 2020), can be observed. They are called parastichies and are designed by organs which are close to one another. The numbers of such spirals are consecutive numbers of the Fibonacci series (Steeves & Sussex, 1989).

The number of the parastichies depends on the relative size of the organs and the meristem. If the organs are small compared to the meristem, larger numbers of parastichies can be detected (like in sunflower, where the phyllotaxis can be described by a 34:55 pattern),

while if the organs are large compared to the meristem, lower numbers of parastichies are observed (like in tomato, 2:3)(Reinhardt, 2005). Since in many plants, the meristem size increases during growth, the pattern can shift to higher orders.

These curious mathematical observations have attracted the attention of mathematicians, physicians and biologists for centuries, who developed models and theories trying to explain such a regularity (see Yin, 2021; Adler et al., 1997, Barabé & Lacroix, 2020; Okabe, 2016).

2. Phyllotaxis determination

2.1 Historical theories

The first theory developed around phyllotaxis determination dates back to 1868, when Hofmeister proposed that a new primordium appears at the periphery of the meristem furthest from the existing ones (Hofmeister W, 1868).

This theory was tested in the pioneer experiments of scientists such as Snow and Snow and Wardlaw between 1930 and 1950. Performing surgical and chemical tests on *Lupinus* and ferns respectively, they stepped further the theory in parallel ways. According to Snow and Snow, the new primordium forms in the “first available space”, meaning that it is placed where it has a minimum available space and at a minimum distance from the tip (Snow Mary and Snow Robert, 1932b, 1932a, 1935, 1947, 1962). Wardlaw, on the other side, suggested that the older primordia have some kind of inhibitory effect on the younger ones (Wardlaw, 1949).

Further experiments and theories were subsequently developed, which produced three main models. According to the biochemical model, which is based on the evidences described above, the older primordia produce some kind of inhibitory signal that prevents the new ones from developing in their vicinity. On the other side, the biomechanical model focused on tension and compression in tissues and the geometrical model on the sizes of the meristem and the primordia.

Importantly, all these hypotheses are not exclusive and can well fit one with the other, in a wide vision that accounts for the complexity of the biological systems (as detailed later).

2.2 What is known about phyllotaxis determination so far

2.2.1 Auxin

Decades of experiments now suggest that the mechanism by which the older primordia inhibit the growth of new ones in their neighbourhood is not the excretion of an inhibitor, but the depletion of an activator. Such an activator is recognised in the phytohormone auxin.

Auxins are a family of phytohormones of which the most abundant natural form is Indole Acetic Acid (IAA). They are known to play crucial roles in almost every developmental process in plants, from gametophyte development to apical dominance, from root growth to organ initiation.

Because of its chemical features (acid dissociation constant), IAA is negatively charged inside the cell and neutral in the apoplast. This implies that IAA can enter the cell by diffusion mechanism, while it needs transporters to be excreted. Even if IAA can diffuse inside the cell, importers that facilitate this movement exist. They are known as AUX importers and are found homogeneously on the cell membrane. In contrast, the IAA

exporters, the PIN-FORMED proteins (PIN), are usually placed directionally at specific sides of the cells thus mediating the directional flow of auxin. As such, the PIN proteins are thought to be one of the main actors generating and maintaining auxin minima and maxima, which are needed for organ growth and placement.

The Arabidopsis genome codes for 8 PINs, 5 of which (PIN1 to 4 and PIN7) show a specific subcellular localization driving auxin flux (Křeček et al., 2009).

The *AtPINs* have a different expression pattern, with PIN1 being the major actor in the SAM, where it drives the creation of auxin maxima where primordia are initiated (Galvan-Ampudia et al., 2020; Křeček et al., 2009).

The stunning relevance of auxin fluxes in primordia initiation is depicted by the phenotype of *pin1* mutants, as well as wild-type Arabidopsis treated with NPA (N-1-naphthylphtalamic acid, an auxin transport inhibitor (Gälweiler et al., 1998; Okada et al., 1991)) which present naked inflorescences and fail to develop flowers. Moreover, this phenotype can be reverted by manually applying auxin on the meristem, further clarifying that auxin maxima are required at the point of new organ initiation (Reinhardt et al., 2000; Vernoux et al., 2000).

Additional support to the PIN relevance on phyllotaxis can be found in the defective organogenesis in *pid* (*PINOID*) mutants, affected in a protein kinase involved in spatial patterning of PIN (Friml Jiri, Yang Xiong, Michniewicz Marta, Weijers Dolf, 2004). Moreover, Arabidopsis mutated in *PIN* just in the target site of the PID phosphorylation presents a defective phyllotaxis (Ki et al., 2016).

Further evidence of the impact of auxin flux in phyllotaxis is given by the phenotype of the multiple auxin exporter mutant *aux1 lax1 lax2 lax3* which has irregular divergence angles and forms leaf clusters (Bainbridge et al., 2008), caused by an increased auxin diffusion in the apoplast and less regular auxin maxima.

Not only auxin transport is required for the correct phyllotaxis, but also its biosynthesis and perception.

ARF and AUX/IAA are the major factors involved in auxin perception and response.

The most accredited theory sees AUX/IAA factors repressing the ARFs in the activation of auxin-responsive genes. When auxin levels increase, the molecule works as a molecular glue between the AUX/IAA and the TIR1/AFB F-box proteins, the latter being part of an SCF E3 ubiquitin ligase complex. Therefore, upon auxin binding, the AUX/IAA are sent to proteasomal degradation and the ARF can activate the transcription of downstream genes (Fig. 3).

However, only 5 out of the 28 ARFs in *Arabidopsis thaliana* seem to have roles of transcriptional activator, while the majority are more likely to function as repressors (Guilfoyle & Hagen, 2007). Further studies are thus needed to understand the mechanisms of auxin response and to elaborate more complete functional models.

Regarding auxin biosynthesis, more than one pathway is known, with the most studied being the tryptophan-dependent pathway (Gomes & Scortecci, 2021). The two main steps of this pathway are driven by YUCCA flavin monooxygenase (YUC) and TAA aminotransferases (Y. Zhao, 2012).

Mutations in the auxin biosynthesis genes *YUC* enhance the *pin1* phenotype (Cheng et al., 2007) and *mp* mutants where the *auxin response factor 5* (*MONOTERPENOS*/*ARF5*) is not functional, phenocopy *pin1* and cannot be reverted by exogenous auxin application (Reinhardt et al., 2003; Z. Zhao et al., 2010).

Moreover, Arabidopsis mutants in *PLETHORA* genes (*plt3plt5plt7*) display an aberrant phyllotaxis, more frequently developing distichous pattern. This is supposed to be mediated by a reduced expression of the auxin biosynthetic genes *YUCCA1* and *YUCCA4* and of *PIN1* (Pinon et al., 2013; Prasad et al., 2011).

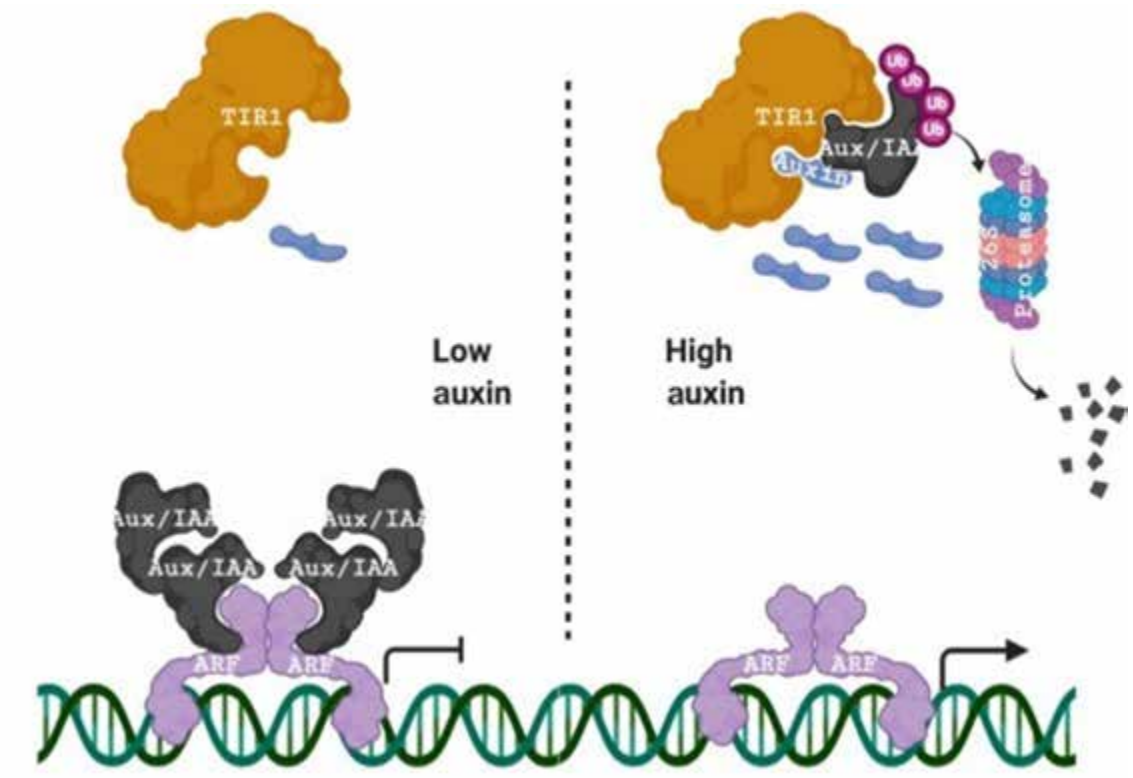

Fig. 3. Auxin response model. Adapted from Shubhajit Das et al, 2021

2.2.2 More than auxin: cell wall, cytoskeleton and meristem size

The response downstream of the auxin signalling can provide a biological explanation supporting and integrating the different hypotheses concerning phyllotaxis determination. Indeed, organ growth relies on cell division and expansion, which are related to mechanical tension (link to biomechanical model) and are regulated in space and size (geometrical model).

Organ growth involves cytoskeletal factors and cell wall modifications.

Pectin de-methyl esterification in the cell wall is indeed relevant in organ initiation (Peaucelle et al., 2008), as it makes the cell wall softer and enables the cell to expand (Braybrook & Peaucelle, 2013; Peaucelle et al., 2008, 2011). A further mechanism of softening has been related to auxin-driven apoplast acidification, providing a direct link between hormonal control and its responses (Jacobs & Ray, 1976).

Pectin de-methyl esterification is mediated by PME (pectin methyl-esterares) and while PME inhibition produces *pin*-like inflorescences, their direct ectopic application perturbs phyllotaxis (Peaucelle et al., 2008).

Moreover, pectin methyl-esterification impacts the normal PIN polarity in the SAM (Braybrook & Peaucelle, 2013), witnessing the involvement of complex feedback mechanisms in phyllotaxis determination. Many other kinds of feedback and response integration mechanisms have been described in phyllotaxis determination, elucidating pathways that can buffer cellular responses, and provide robustness to the system.

Also xyloglucans are important in defining phyllotaxis, even if the mechanism is not completely understood. Indeed, it has been hypothesised that this can be linked to organ outgrowth, to meristem shape (that appears flatter in mutants in xyloglucans pathway) or to the polar localisation of PIN (F. Zhao et al., 2019)

Regarding cytoskeletal factors, auxin impacts microtubule orientation, dictating cell anisotropy, and, in a feedback loop mechanism, mechanical stress impacts auxin distribution by PIN localisation. Indeed, microtubules are shown to orient in the same direction of the mechanic tension, and PIN preferentially localise tangentially to microtubules. Therefore, mechanical forces can impact growth by influencing microtubule positioning and auxin fluxes. (Sassi et al., 2014)

As an example of cytoskeleton involvement in phyllotaxis, mutants in *KATANIN1*, a microtubule severing protein, have defective responses to mechanical stresses and impaired phyllotaxis (Bichet et al., 2001; Burk & Ye, 2002).

Meristem size has widely been linked to phyllotactic patterns too.

Already in the 90's Doaudy and Couder demonstrated the possibility of modelling most of the phyllotactic patterns just by varying the ratio between the radius of the inhibitory field and the radius of the generative meristem (Douady & Couder, 1992, 1996a, 1996b, 1996c; R.V. Jean, 1998) providing mathematical evidence of the relevance of organ size in phyllotaxis determination, as stated by the geometrical model.

If different ratios between primordia and meristem size can generate different patterns, an altered meristem size perturbs the phyllotaxis.

This has been mainly studied in mutants in cytokinin (CK) signalling and in meristem-related genes, as they are the two main gene groups known to impact the meristem size. Notably, this adds further complexity to the mechanism, introducing a second phyto-hormone in the phyllotaxis determination.

For example, maize *abphyl1* (*ABERRANT PHYLLOTAXIS 1*) and *abphyl2* mutants, as well as rice *dec* (*DECUSSATE*), display larger meristems and a shift from alternate to decussate phyllotaxis. In *abphyl1* and *dec* a relation with the CK pathway is suggested. Moreover, *abphyl1* is also affected in *PIN* expression (Giulini et al., 2004; Itoh et al., 2012; B. H. Lee et al., 2009; F. Yang et al., 2015).

In Arabidopsis, septuple mutant in *ARR* genes, negative regulators of CK signalling, as well as RNAi lines downregulating genes of the same family, and the double mutants *ckx3 ckx5*

(mutated on cytokinin degrading enzymes) also show larger meristem and defects in phyllotaxis (Bartrina et al., 2011; Leibfried et al., 2005; Ryu et al., 2009).

CK involvement in phyllotaxis has not been just related to meristem size. Arabidopsis mutants in *ARABIDOPSIS HISTIDINE PHOSPHOTRANSFER PROTEIN6* (*AHP6*), a pseudo phosphotransferase inhibiting cytokinin signalling, have an increased frequency of permutations, which are caused by flower co-initiations (Besnard et al., 2014). Moreover, similar phenotypes have been found in mutants in genes working downstream of the CK signalling (Ranftl et al., 2016).

This also points out that phyllotaxis is not just a matter of space, but that the time of primordia outgrowth is involved. The involvement of the temporal aspect is depicted in studies such as M. K. Chen et al., 2013; Ikeda et al., 2005; Ikeda-Kawakatsu et al., 2012. All of them suggest indeed a relation between mutant phyllotaxis and plastochron (the plastochron is the time that encompasses between the emergence of two successive primordia).

Regarding meristem size genes, *clv1*, *clv2* and *clv3* display similar defects in SAM morphology and phyllotaxis, and similar phenotypes are observed in the mutants in the homologs in maize or rice. Moreover, *WUS* itself and regulators of *WUS* independent from *CLV* impact phyllotaxis (the impact of meristematic genes on phyllotaxis is deeply reviewed in Yin, 2021).

Last, while here we focused just on the meristematic determination of phyllotaxis, it has to be underlined that the final pattern is not only determined by the organ outgrowth from the meristem but also from the subsequent development of the internodes and the stem, including both their elongation and torsion (recently reviewed in Yin, 2021).

3. The driving hypothesis of this thesis

Even if more and more studies are emerging, the riddle of phyllotaxis and its biological role is far from being completely understood. However, we hypothesise that its manipulation can provide benefits to agriculture.

As proof of this, it was published that Arabidopsis *arf3,* as well as *ckx3 ckx5* mutants present a mutated phyllotaxis, an increased shoot or inflorescence apical meristem (IM or SAM) area and an increase in flowers and siliques production (Bartrina et al., 2011; K. Zhang et al., 2022).

Since in our laboratory we recently studied mutants with mutated phyllotaxis and increased IM area (Caselli et al., under revision), we wondered if we could have an impact on flower and silique production.

Thus, the first aim of my thesis was to show the impact on the yield of mutations in *REM34*, *REM35* and *REM36* in *Arabidopsis thaliana*.

4. The REM gene family

The *REM* (REproductive Meristem) genes are a family of transcription factor part of the B3 DNA binding domain superfamily together with the *ABI3/VP1, HIS* (High-level expression of Sugar Inducible gene), *RAV* (Related to Abi3/Vp1) and *ARF* (Auxin Response Factor) families (Romanel et al., 2009; Swaminathan et al., 2008). In the *Arabidopsis* genome, 87 B3 proteins

have been identified, around half of which are *REM* genes, thus being the most numerous other than divergent of these families (Romanel et al., 2009, 45 *REM*, 3 *ABI3*, 3 *HIS*, 13 *RAV*, 23 *ARF*). Even if slights differences are present in works predicting *REM* genes in Arabidopsis (Romanel et al., 2009; Swaminathan et al., 2008; Y. Wang et al., 2012), a core of 44 genes are superimposable between all of them and can be considered high-confidence *REM* (Manrique et al., 2023).

The *REM* family can be phylogenetically divided into classes (Romanel et al., 2009). In Arabidopsis, seven classes can be recognised (*REM I, V, VI, VII, VIII, IX,* and *X*), some of which are not conserved in more or less distant species such as poplar and rice and are therefore clade-specific. Specifically, they are classes *REM VII, REM IX* and *REM X*. As they account respectively for 8, 15 and 2 loci (on a total of 44 *REM* reported in the paper of reference, Romanel et al., 2009), it can be stated that a wide divergence and subsequent amplification of the *REM* family had happened in Arabidopsis-related species, which explain the high numerosity of the genes in the species.

The B3 is a DNA binding domain first observed in the *ZmVIVIPARIOUS1* gene (McCarty et al., 1991). It is composed of 100 – 120 amino acids, structured in seven ß stands folded into an open ß barrel, and two alfa-helices placed at its edges (Romanel et al., 2009; Waltner et al., 2005).

Even if the 3D structure is maintained, it is known that B3 domains of the different families show distinct DNA consensus binding motifs (Romanel et al., 2009). Since the difference between the B3 domains resides in the loops connecting some ß strands, it is supposed that these are the parts of the proteins dictating the DNA sequence specificity, while the B3 classical folding mediate a general interaction with the double strand (Romanel et al., 2009).

As the B3 domains of the *REM* family are poorly conserved when compared to the other families, they sometimes are more than one in the same protein, and they sometimes miss some conserved amino acids in the loops proposed to give the sequence specificity to the binding (Romanel et al., 2009; Waltner et al., 2005), it has been hypothesized that they might have evolved new functions more than DNA binding and that they can maybe bind the DNA in a less specific manner (Romanel et al., 2009).

However, experimental evidences suggest that the modality of binding the DNA might not be the same for all the REMs. Indeed, VRN1 (REM39) is reported to bind DNA in a non-specific way (Levy, Mesnage, Mylne, Gendall, 2002), while for REM34 an empirically defined consensus motif has been reported (Franco-Zorrilla et al., 2014).

Between the B3 superfamily, the *REM* genes are the least functionally characterised, but recently more and more studies have revealed their involvement in several developmental processes. According to their name and expression pattern, the characterized genes have mainly been linked to flowering processes as well as reproduction.

VRN1 (*REM39*), the first characterized *REM* in Arabidopsis, is involved in vernalization response and its overexpression has pleiotropic effects including siliques and flower morphology changes, early flowering, siliques phyllotaxis modification and reduced floral abscission (Levy, Mesnage, Mylne, Gendall, 2002).

REM16, REM17 (TARGET OF SVP AND FLC, TFS1), REM13, REM34 and REM46 control flowering time, inducing or repressing it (Manrique et al., 2023; Richter et al., 2019; Yu et al., 2020) and REM4 can both impact flowering time and maintain vernalization response (Heo et al., 2012).

On the strictly reproductive side, VALKYRIE (VAL, REM11) and VERDANDI (VDD, REM20) are involved in synergid degeneration and subsequent pollen bursts (Mendes et al., 2016). VDD has also a role in synergids and antipodal cell identity (Matias-Hernandez et al., 2010). REM33 (MATERNAL EFFECT EMBRYO ARREST 45, MEE45) controls seeds size by regulating cell proliferation (Y. J. Li et al., 2021), REM22 controls ovule primordia formation (Gómez-Mena et al., 2005) and in rice OsREM20 impact grain number per panicle (Wu et al., 2021).

Additionally, some years ago, Mantegazza et al., 2014 pointed out a cluster of *REM* genes thought to be particularly interesting to be studied for their possible impact on Arabidopsis flower and inflorescence development because of their expression pattern and the presence of floral integrator binding motifs in their regulatory elements. The cluster is composed of *REM34*, *REM35* and *REM36*, 3 genes located in linkage on chromosome 4 on a 10 kb DNA stretch.

Indeed, *REM34* expression is nicely correlated with the one of the floral meristem identity genes *LEAFY*, and less *AP1*, and ChIP data suggest that it is a direct target of the latter (Mantegazza et al., 2014). Moreover, promoters of both *REM34*, *REM35* and *REM36* contain consensus binding sites of AP3 and PI (Mantegazza et al., 2014) and they are upregulated in single mutants of the latter genes (Wuest et al., 2012). *REM35* also contain an SVP binding region (Mantegazza et al., 2014). However, the expression of none of them was found to change in *svp* and *ap1* mutants (Gregis et al., 2013; Kaufmann et al., 2010).

The three genes are expressed in the inflorescence and floral meristems (Mantegazza et al., 2014, fig. 4), as well as in reproductive organs and petals at different stages (Caselli et al., 2019, fig. 4).

REM34 and REM35 are known to play various roles in plant development, as they are involved in gametophyte development (Caselli et al., 2019), and regulate IM dimension and phyllotaxis, possibly interacting with some ARF proteins and modulating the expression of *PUCHI* and *LBD18* (Caselli et al, under revision). Also REM36 was shown to impact phyllotaxis (Caselli's PhD thesis 2019), but its role is less understood.

AtREM34, *AtREM35* and *AtREM36* are part of the Arabidopsis-specific *REM IX* class together with other 12 loci (Romanel et al., 2009; fig. 5).

The numerosity of this class is explained by its evolutionary history, which is studded by duplication events (Romanel et al., 2009). Indeed, the similarity between the genes of the *REM IX* class suggests that they derive from duplication events between chromosomes 2 and 4 and between the cluster on chromosome 4 itself (Franco-Zorrilla et al., 2002; Romanel et al., 2009). Furthermore, most of the genes in *REM IX* class possess more than a single B3 domain that is again thought to derive from tandem duplication events (Romanel et al., 2009).

The maintenance of such a high number of homologous genes can be explained or, as happens with MADS boxes, by sub and neo- functionalization (Duarte et al., 2006), or by the

gene buffering that redundancy can produce. The latter could be especially useful in producing robust flower development (Wellmer et al., 2006).

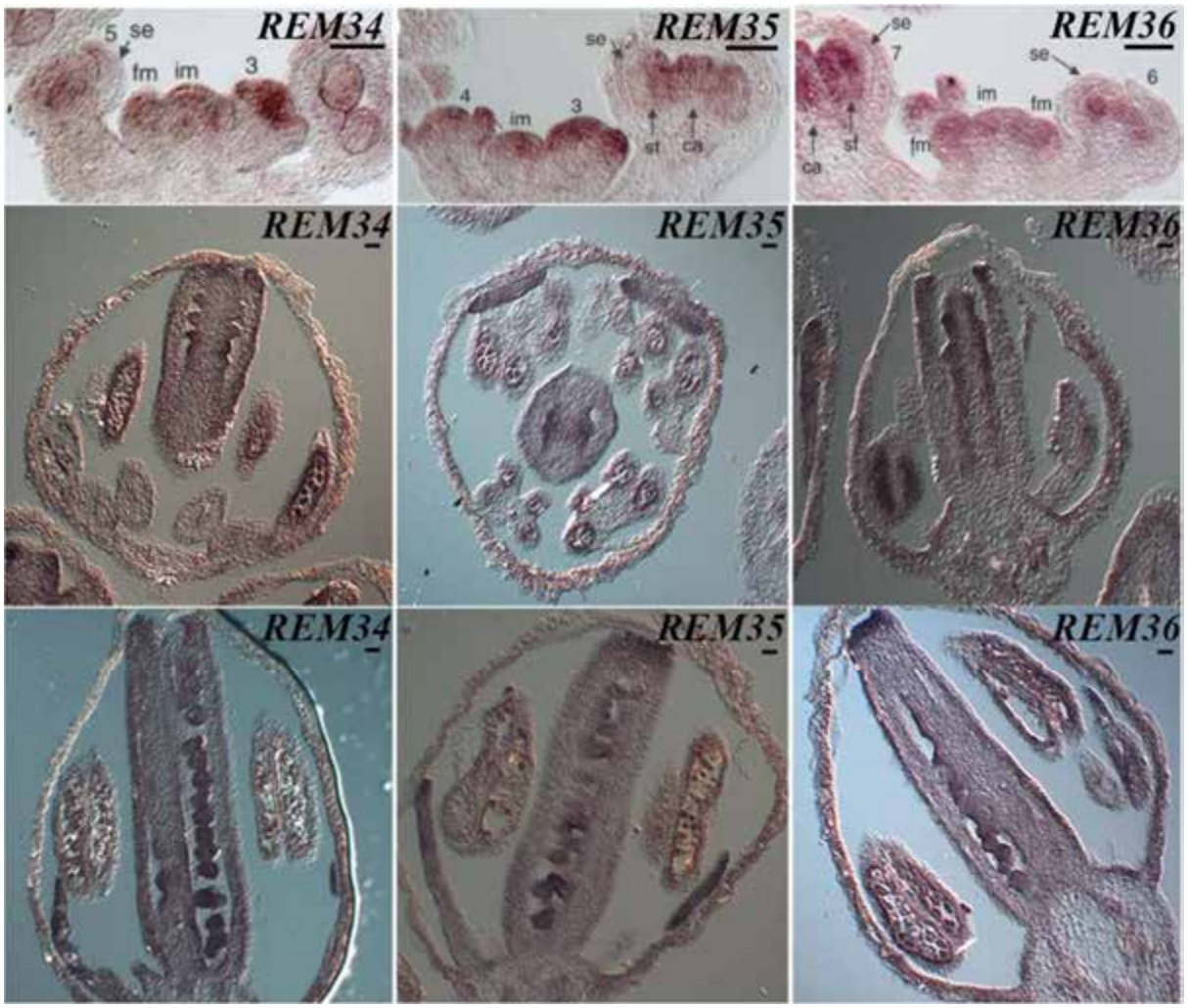

Fig. 4. *REM34*, *REM35* and *REM36* expression. Adapted from Mantegazza et al, 2014 and Caselli et al, 2019

Whatever the biological relevance is, experimentally this redundancy complicates genetic studies, as it hinders the discovery of the gene's function and requires the development of multiple mutants to get phenotypes (Caselli et al., 2019; Mantegazza et al., 2014; Caselli et al., under revision).

In such a situation, a deep comprehension of the evolution of the family and the conservation of the genes is of primary importance to determine target genes for functional genetics studies.

Importantly, in the whole *REM IX* family the genes of a cluster seem more related within the cluster than between clusters and specifically the low sequence similarity between the *REM* clusters on chromosomes 2 and 4 suggests the duplication event involving them was not recent. In support of this, *BoREM1* was found to be more related to *AtREM34* than any other *AtREM*, indicating that the chromosomal duplication producing the clusters on chromosomes 2 and 4 was previous to the divergence between *Arabidopsis* and *Brassica* genus (Franco-Zorrilla et al., 2002).

Moreover, the *REM* genes on chromosome 4 except two (*REM39* and *REM40*), do contain a specific domain, therefore composing a gene subgroup (Franco-Zorrilla et al., 2002). Specifically, it is composed of hydrophobic heptads at the C-ter, and it is supposed to be a leucine zipper involved in protein-protein interactions (Franco-Zorrilla et al., 2002; O'Shea et al., 1989; Caselli et al, under revision)

Focusing on the genes of interest for this thesis, *REM34* most similar genes are *REM35*, *REM36* and *REM37* (fig. 5), all showing 3 B3 domains and an acidic domain proposed to act as a transcriptional activator (Franco-Zorrilla et al., 2002; Mitchell & Tjian, 1989). REM35 and REM36 are more similar to each other than the other two genes(Franco-Zorrilla et al., 2002) and *REM37* was revealed to be almost not expressed in most of the tissues (Klepikova et al., 2016; Mantegazza et al., 2014).

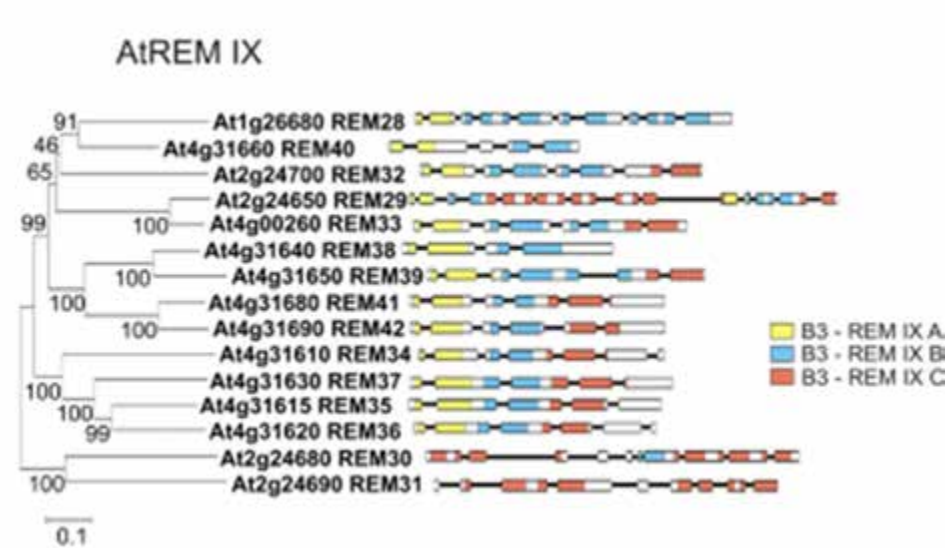

Fig. 5. *AtREM IX* phylogenetic tree. Adapted from Romanel et al, 2009. Three subgroups of B3 motifs displayed. Scale bar= 0.1 estimated amino acid substitution per residue

5. *Brassica napus*

5.1 *Brassica napus* economic relevance

After having established the yield impact of *rem34, rem35* and *rem36* mutations in *Arabidopsis*, the second aim of my thesis was to study the possibility of getting similar higher yield mutants in an economically relevant crop by a translational biology approach.

Brassica napus (or rapeseed) is the second oil crop for global production (soybean 364 million metric tons, rapeseed 71 million metric tons; Vegetable oils: global consumption 2013/14 to 2021/2022, by oil type; M. Shahbandeh, Jul 27, 2022, statista.com) and canola oil is the third most produced vegetable oil in the world (palm oil, ca 36%, soybean oil ca 30%, Global oilseed production 2021/22, by type; M. Shahbandeh, Feb 11, 2022; statista.com) and the first in Europe (Consumption of vegetable oils worldwide from 2013/14 to 2022/2023, by oil type, M. Shahbandeh, Sep 20, 2023; statista.com; oilseed and protein crops production, European commission, 2022 data).

Indeed, approximately 13–16% of the world vegetable oil comes from rapeseed (Consumption of vegetable oils worldwide from 2013/14 to 2022/2023, by oil type, M. Shahbandeh, Sep 20, 2023; statista.com; Yuan et al., 2022).

For oil content, it is even preferred over soybeans, as it can produce around 40% of oil in seed mass (also stated in K. Zhang et al., 2019) compared to just 18% in soybeans of some areas (https://www.worldatlas.com/articles/the-world-s-top-rapeseed-producing-countries.html).

Moreover, its seeds contain also good amounts of proteins. Indeed, the leftover of oil extraction, the meal, is used as a protein source for livestock, poultry and fish farming as well as fertilizer. Moreover, Canadian companies are now exploring opportunities to use canola meal as a plant-based protein source for human diets (canolacouncil.org).

About its uses, food processing holds the largest share, accounting for 72.6% of the global revenue in 2018 (Rapeseed Oil Market Size, Share & Trends Analysis Report By Application (Food Processing, Bio-fuel, Personal Care), By Region (North America, Europe, APAC, CSA, MEA), And Segment Forecasts, 2019 - 2025). As an edible oil, canola oil it is getting a lot of popularity in the USA and Canada for its healthy properties, as it is high in monounsaturated fats, Omega-3 and 6, and vitamins E and K (https://canolagrowers.com).

Furthermore, rapeseed oil has many industrial uses. It is used as an ingredient for personal care products and for biofuel, as well as inks, plastics, adhesives, bioplastics and sealants production (canolacouncil.org). 16% of the global production of biodiesel starts from rapeseed oil (third only to palm oil, 35%, and soybean oil, 26%; UFOP Chart of the week (50 2019), press release, 2019-12), pointing out its relevance also in the green transition.

The main rapeseed producers are Canada (19.5 million metric tons, 26% of the global production), the European Union (16.3 million metric tons, 22%), China (14 million metric tons, 19%), and India (8.5 million metric tons, 11.6%) (Rapeseed production volume worldwide 2020/2021, by country; M. Shahbandeh, Feb 2022, statista.com).

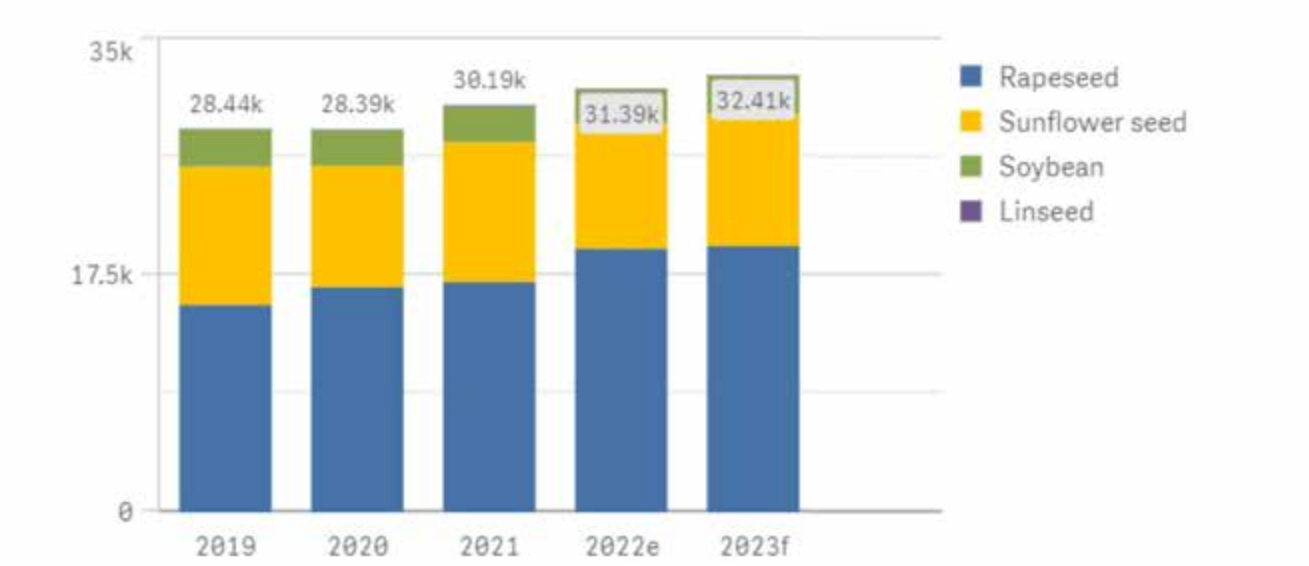

Fig. 6. Kilotons of oilseed production by type in European Union, European Commission, 2024.

Importantly, rapeseed is the first oilseed crop in the European Union, accounting for 58.6% of the oil crop gross production and a 4% increase in production in the last 5 years (oilseed and protein crops production, European Commission, 2022 data; fig 6).

Many different cultivars are cultivated nowadays according to the environmental constraints of the production site, but all the ones used for food and feed processing are types of double-low rapeseed. Indeed, already in the 50's, the rapeseed nutritional aspect, as well as the palatability for feedstock feeding, were questioned (https://www.canolacouncil.org/). High levels of erucic acid were problematic for the heart health of consumers and glucosinolates generated a pungent odour and taste that reduced the feed efficiency. Wide breeding programs were pursued to reduce the content of these two molecules in seeds, and varieties with improved characteristics have been developed, now falling around the name of double-low rapeseed.

5.2 *Brassica napus* biology and genome

Brassica napus, as *Arabidopsis thaliana*, is a species of the Brassicaceae family, and more than 86% of the protein-coding sequences are conserved between them (Cavell et al., 1998) allowing comparative studies (Parkin et al., 2005).

It is an annual or biennial species with waxy leaves and a tall raceme inflorescence that can grow up to 1.5 m. It has yellow flowers with four sepals and petals, a superior ovary and six stamens (4 long and 2 short). The siliques contain more than 15 seeds each, which are spread at dehiscence. At maturity, seeds are spherical, reddish, brown or black, and between 1.8 and 2.7 mm in diameter. It is mainly self-fertile, but outcrosses can happen when driven by wind, pollinators or contact between plants (Gulden et al., 2008). It is thought to have originated in Europe as a winter crop and then have spread all over the world, evolving new summer and semi-winter ecotypes according to the requirements of the new environments (Lu et al., 2019).

Of the *Brassica* species, six, among which *B. napus*, are described in their genetic relationships by the U's triangle model (Nagaharu, U.1935). Three diploid progenitors, *Brassica rapa* (A genome; n=10), *nigra* (B, n=8) and *oleracea* (C, n=9), can hybridize and

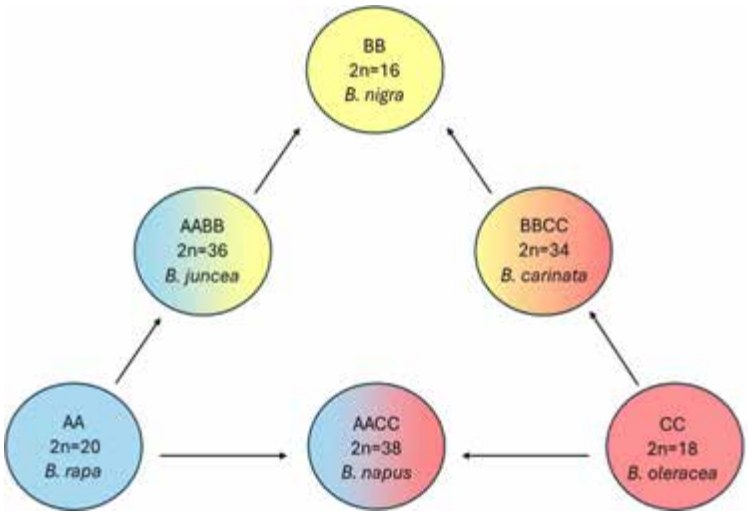

Fig. 7. U triangle model (Nagaharu, U.1935)

generate allotetraploids, *Brassica juncea* (AB, n=18), *carinata* (BC, n=17) and *napus* (AC, n=19) (Fig. 7).

Specifically, *B. napus* resulted from the interspecific hybridization between *B. oleracea* and *B. rapa*, 7500 years ago (Chalhoub et al., 2014).

Its genome is composed of 38 chromosomes (2n, 1.2 Gb, Chalhoub et al., 2014; Chen et al., 2021), 20 of which are part of the A subgenome, (*B. rapa* derived), and 18 of which of the C subgenome (*B. oleracea* derived).

Given the recent hybridization, its genome is highly redundant, even if some structural and functional interplay between the two subgenomes, as well as incipits of gene losses and expression divergence, can be observed (Chalhoub et al., 2014).

Relevant for translational gene studies, an even higher level of redundancy compared to *Arabidopsis thaliana* is expected also because of the past evolution of the *Brassica* genre. Indeed, a whole genome triplication event is known to have occurred after the *Arabidopsis* – *Brassica* clade split, around 14-24 million years ago (Bowers et al., 2003; Lysak et al., 2005; X. Wang et al., 2011).

Therefore, for each gene in Arabidopsis, 6 orthologs are theoretically expected in *Brassica napus*. This number is in some cases confirmed by comparative studies (Park et al., 2005; Town et al., 2006), but is then lowered to an empirical average of 4 because of random gene losses and a constitutive genome shrinkage for *Brassica rapa* (around 30%, Mun et al., 2009).

Functional genomics studies in *Brassica napus* started in 1991 with the publication of the first linkage map (Landry et al., 2011), but it was after the release of the first reference genome in 2014 (Darmor-bzh, (Chalhoub et al., 2014) that they exploded.

Database	Website	Description
EnsemblPlants	https://plants.ensembl.org/Brassica_napus/Info/Index	Genomic information
Genoscope	https://www.genoscope.cns.fr/brassicanapus/	Genomic information
BRAD	http://brassicadb.cn/#/	Genomic information
BrassicaEDB	https://brassica.biodb.org/	Expression profile
BnTIR	https://yanglab.hzau.edu.cn/BnTIR	Expression profile
BnaGVD	http://rapeseed.biocloud.net/home	Genomic variation
BnVIR	https://yanglab.hzau.edu.cn/BnVIR	Genomic variation
BnaGWAS	https://bnapus-zju.com/gwas/	Genome-wide association study information
BnPIR	http://cbi.hzau.edu.cn/bnapus/	Pan-genome
BnIR	https://yanglab.hzau.edu.cn/	Multi-omics

Fig. 8. *Brassica* related databases (from Tan et al, 2024)

In the following years, more and more varieties were sequenced (reviewed by Tan et al., 2024), and, based on the high-quality sequencing of 8 of them, in 2020, the first pangenome was assembled (Song et al., 2020). With the exponential growth of omics data, various databases grouping information about *Brassica napus* or the Brassicaceae family were developed (fig. 8), which display genomic, comparative genomic and transcriptomic data in a user-friendly manner. With these kinds of integrated databases, worldwide knowledge is accessible to researchers who can easily query for information and step their research upon it.

6. A workflow for polyploid crop breeding

Brassica napus breeding started only 400-500 years ago, making it a relatively recent domesticated crop (Gómez-Campo & Prakash, 1999). As a result, a lot can still be done to optimise its features for the current agriculture (Tan et al., 2024). In addition to the unexploited natural variation, current tools such as random mutagenesis and precise editing can be applied to enlarge the pool of variability and provide more resources for breeding superior varieties.

If breeding based on random mutagenesis is time-consuming and requires a lot of effort, we have now entered the era of breeding 4.0, where large-scale omics data, artificial intelligence, biotechnology and synthetic biology can drive the rational design of new crop genotypes (J. Fang, 2024; Tan et al., 2024; Wallace et al., 2018)

To perform this kind of rational breeding, we need to deepen our genetic knowledge of *Brassica napus*.

Till now, most of the studies on this species have been based on quantitative trait loci (QTL) mapping, and only less than 150 genes have been cloned and characterized (Tan et al., 2024). Importantly, they all revealed to be homologs of genes already characterized in model plants, such as Arabidopsis and rice, and most of the time to have conserved their function.

For example, genes found to impact yield in *B. napus* are involved in meristem development, hormonal signalling and nutrient efficiency, well know examples being homologs of *TFL1*, *AP1, IAA, CKX* and *MAX1* for auxin, cytokinin and strigolactones signalling, but also *WRKY47* for nitrogen utilisation and *SUT1* for sucrose transport (Cui et al., 2023; F. Li et al., 2011; H. Li et al., 2019; Schwarz et al., 2020b; Shah et al., 2018; Sriboon et al., 2020; Yan et al., 2023; Zheng et al., 2020).

This wide functional conservation suggests that translational biology can be a valuable tool to infer the genetic system of more complex organisms from the knowledge we have in model plants.

An important tool for translational studies is interspecific complementation: ectopic and specific expression of *Brassica* genes in Arabidopsis has already helped to infer the gene function in several studies (Lyu et al., 2022; M. Yang et al., 2011; Yuan et al., 2022; Q. Zhang et al., 2017). Moreover, this kind of experiment can help to reveal the sub- and neo-functionalization of genes (Babula-Skowrońska et al., 2015; Schiessl et al., 2019), a common mechanism in species where multiple copies of the same ancestral gene are present (e.g. reviewed for flowering time genes in Schiessl, 2020). This can narrow down candidate genes in case of creation of crop ideotypes by rational design approaches.

Translational biology can be increasingly important when dealing with redundant genes.

Indeed, in polyploid, more complex and wide genomes such as *Brassica napus* one, the level of redundancy can be inflated if compared to Arabidopsis.

This can make gene discovery by forward genetics very difficult, as getting a phenotype often requires the presence of multiple mutations in homologous genes (or dominant mutant alleles) just by chance.

From our point of view, this possible blindness to highly redundant gene families is a big limitation of the QTL analysis, which has been widely used till now in *Brassica napus,* and other tools are required to more deeply unwire the genetic basis of this species.

Summarizing, we think that applying translational biology is a winning strategy in the era of the *de-novo* design of varieties. Given the wide genetic knowledge that we have in model plants and the powerful evolutionary studies we can perform, we can easily predict homologous genes which can be relevant for breeding superior genotypes. In case of duplication events and hybridization of species, functional complementation can provide important hints about sub- and neo- functionalization, especially if working in phylogenetically close species, and can narrow down the targets of interest. Last, precise editing by CRISPR can rapidly generate mutants by which the gene function can, in the end, be proved in the plant of interest, or can even be used in the final genotypes' development by designing new alleles or modulating gene expression or epigenetic marks.

In this pathway, it is clear that the optimization and application of transformation techniques plays a crucial role and an effort to provide more efficient and genotype-independent protocols can be of high value for the whole scientific and agricultural field.

In this thesis, I apply this workflow in order to unwire the role of some members of the *REM* gene family in *Brassica napus* and to put the basis to develop new genotypes of increased yield in this species.

The results can be of high value in research, as provide insights on the mechanism of phyllotaxis determination in a poorly studied plant; and in agriculture, as can provide targets for increasing yield in a species of relevance for the bioeconomy and the food industry.

Results and discussion

1. Multiple mutants in *AtREM34*, *AtREM35* and *AtREM36* can produce more siliques on the main inflorescence

rem34, *rem35* and *rem36* phyllotactic phenotype, as well as the one of the double mutants, have already been described in Caselli et al, under revision and in Caselli's PhD thesis, 2019, and will be here re-capitulated just for clearness and completeness. Both single and double mutants show an aberrant phyllotactic pattern, with angles that frequently diverge from the golden angle and often cluster around 90° and 180° (data for *rem34 rem35* from Caselli, fig 9).

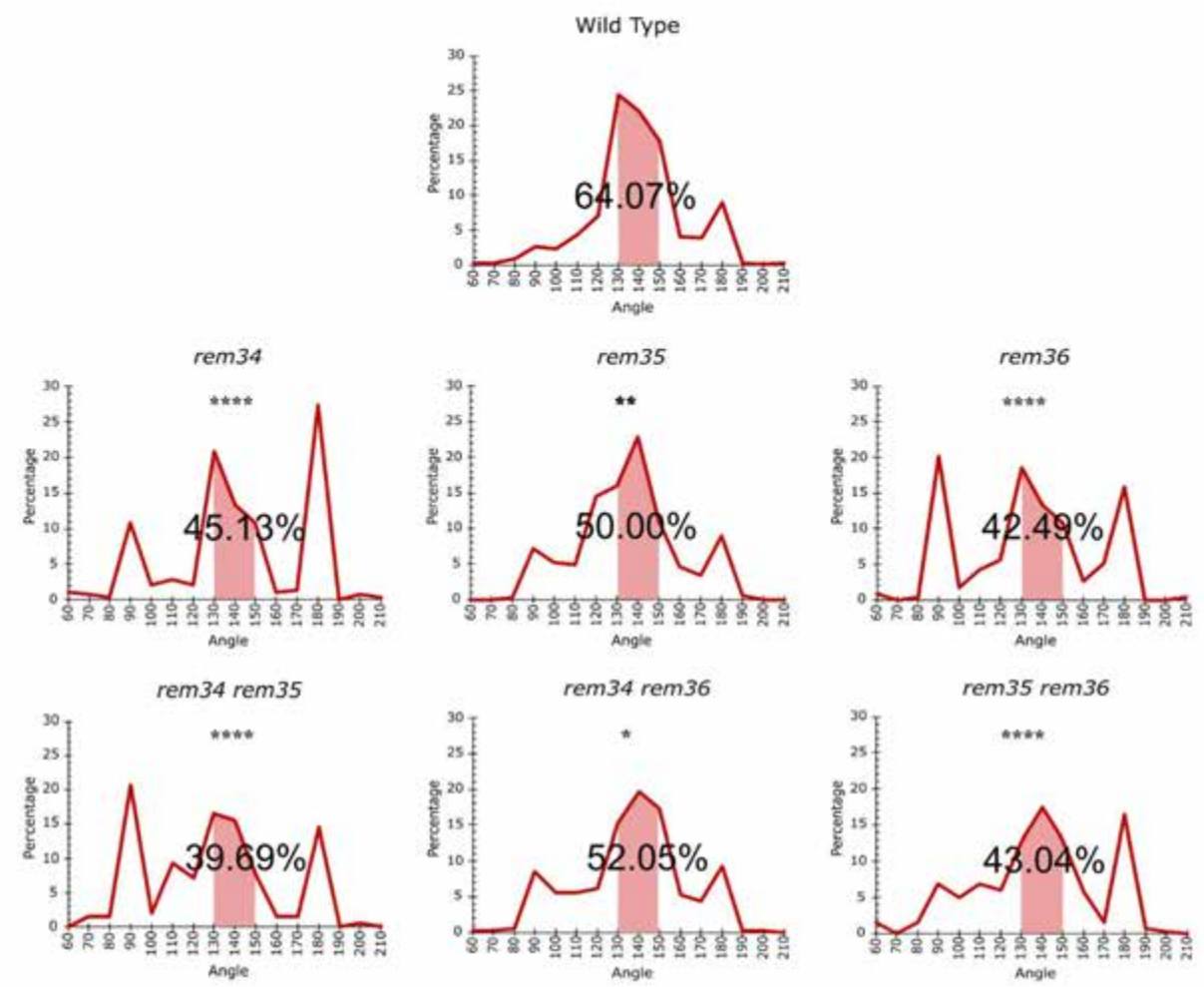

Fig. 9. The graphs show the distribution of angles between two successive siliques. The range 130°-150° is highlighted and the percentage of angles falling in that range is depicted. >9 plants per genotype were used. Statistical significance was analysed by Kruskal-Wallis and Dunn's post hoc tests ($p<0.05$; <0.01; <0.0001)

Specifically, during this thesis, we focused on differences in the percentage of angles falling between 130° and 150°, uncovering that it can be a good parameter for providing statistical evidence to our data. We think that evaluating the range around the golden angle is the best choice, given the precision of the instrument we use for phyllotaxis analysis and the natural variability of the pattern.

We then evaluated the impact of such structural changes on the plant's yield by counting the siliques produced on the main inflorescence. Interestingly, the double mutants show an increase in the number of siliques (Fig. 10).

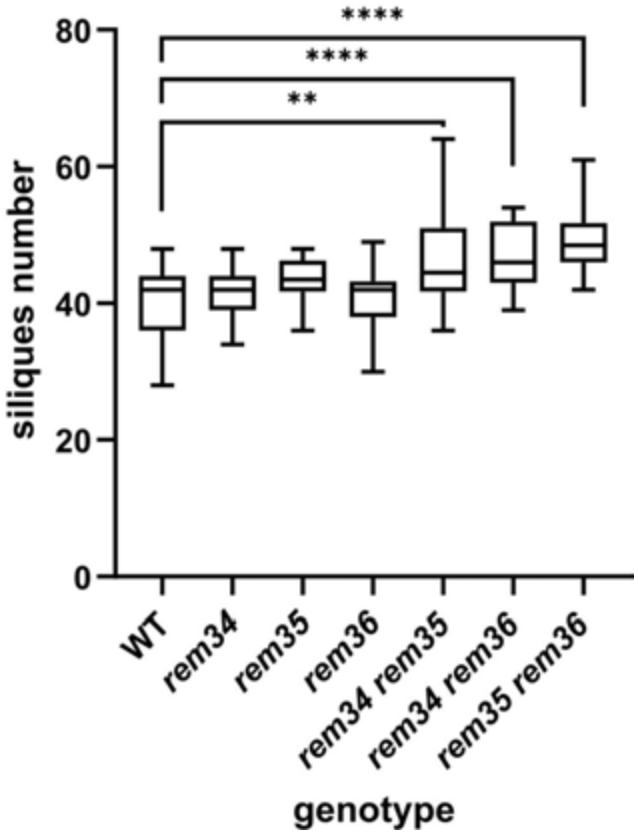

Fig. 10. Siliques on primary stem. >20 plants per genotype were analysed. Statistical significance was calculated by Kruskal-Wallis and Dunn's post hoc test according to the normality and homoscedasticity of the data ($p<0.05$, compared to WT).

Specifically, compared to an average number of 40.65 in the Wild Type, the single mutants produce a similar amount of siliques (41.46 in *rem34*; 43.54 in *rem35* and 40.86 in *rem36*), while the double mutants produce approximately 20% more. Indeed, we observe an average of siliques on the main stem of 46.23 in *rem34 rem35*, 46.59 in *rem34 rem36*, and 49.25 in *rem35 rem36*. Importantly, as the mutants maintain a consistent number of seeds per silique (fig. 11), they potentially could increase seed production.

The observation of the phyllotactic phenotype for single mutants and the yield phenotype only in the doubles suggests that the genes under study have a partially redundant function in inflorescence development.

We then studied the conservation of the gene cluster in *Brassica napus*, one of the main oil crops. In this species, genetic knowledge and results can be transferred from Arabidopsis, given their phylogenetic proximity.

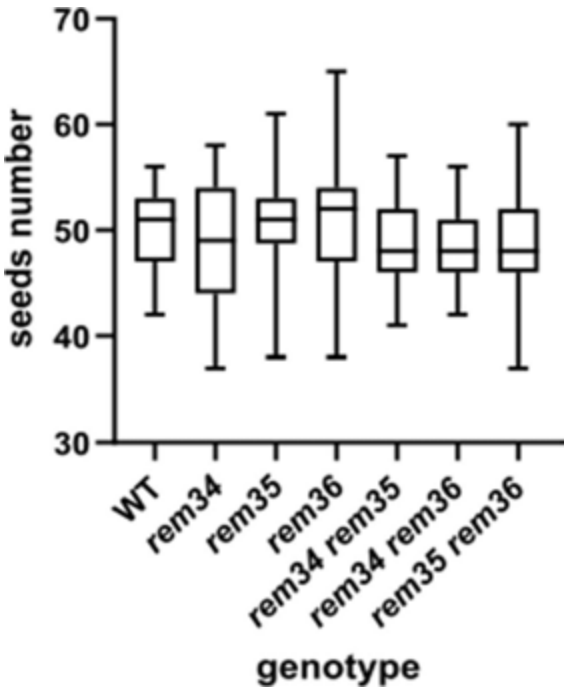

Fig. 11. Number of seeds per silique. 10 plants per genotype, 5 siliques each plant. No significant differences from WT (Kruskal Wallis – Dunn's post hoc test).

2. Study of the cluster conservation in *Brassica napus*

2.1 Cluster identification

To get the homologous and study the phylogenetic conservation of our genes of interest, we performed a phylogenetic analysis on the *REM IX* subclass of *Brassica napus* (Fig. 12).

The proteome of *B. napus* (from Ensemble plants) was queried by all the Arabidopsis proteins belonging to the *REM IX* family (*REM28-REM42*, Romanel et al., 2014) using JackHmmer and a minimum sequence identity of 40% was applied. The homologous sequences retrieved were aligned by ClustalO and a phylogeny was inferred by RAxML-NG, WAG+G substitution model.

The reliability of the tree was evaluated by comparing the phylogeny of the Arabidopsis *REM IX* genes in the tree to the previously published trees of Romanel et al., 2009 and Swaminathan et al., 2008. Moreover, the coherency with the display of the protein domains identified by MEME suite was accounted.

As detailed in the introduction, *B. napus* is an allotetraploid and both the parental diploids underwent genome triplication after the *Brassica-Arabidopsis* clades split (14-24 million years ago; Bowers et al., 2003; Lysak et al., 2005, X. Wang et al., 2011), therefore six genes are theoretically expected for every gene in Arabidopsis. However, it is known that an empirical average of 4 is observed as a consequence of fractionation and pseudogenization (Park et al., 2005; Town et al., 2006).

This is not what we observe for the *REM IX* class, supporting the evidence that this class underwent recent duplication events in Arabidopsis, as reported by Romanel et al, 2009.

Fig. 12. Phylogenesis of the *Brassica napus REM* IX class and their *Arabidopsis* counterparts. Distance as amino acid substitution per site. Different protein motifs as determined by MEME suite are displayed by different number and colours.

Focusing on the homologs of our genes of interest, we observe 6 *REM34* homologs and 2 genes which are homologs of *REM35* and *REM36* (Fig.13). These latter therefore probably duplicated after the clade split. Indeed, the estimated age of duplication of *AtREM35* and *AtREM36* is 14 Million years ago (Romanel et al., 2009), that is similar to the age of the Brassica-Arabidopsis clade split (Bowers et al., 2003; Lysak et al., 2005; X. Wang et al., 2011). The original gene might have been more similar to *AtREM36*, as one gene in *B. napus* is much more related to *REM36* than to *REM35*, while the other sets in the middle (see protein similarity in Table 2). However, more *Brassica* species should be analysed to determine precisely this genomic evolution.

As *REM37* clusters in the same phylogenetic group of our genes of interest (Romanel et al., 2009,fig 13, fig. 5) and can be redundant with them, we decided to include it in our study too. Indeed, it was not previously characterized in Arabidopsis as it is not expressed there (Mantegazza et al., 2014), but we can't assume the same for the *B. napus* homologs. In the idea of producing edited lines of increased yield and knowing that the phenotype can be hindered by redundancy (as shown in fig 10), tackling all the good-confidence redundant

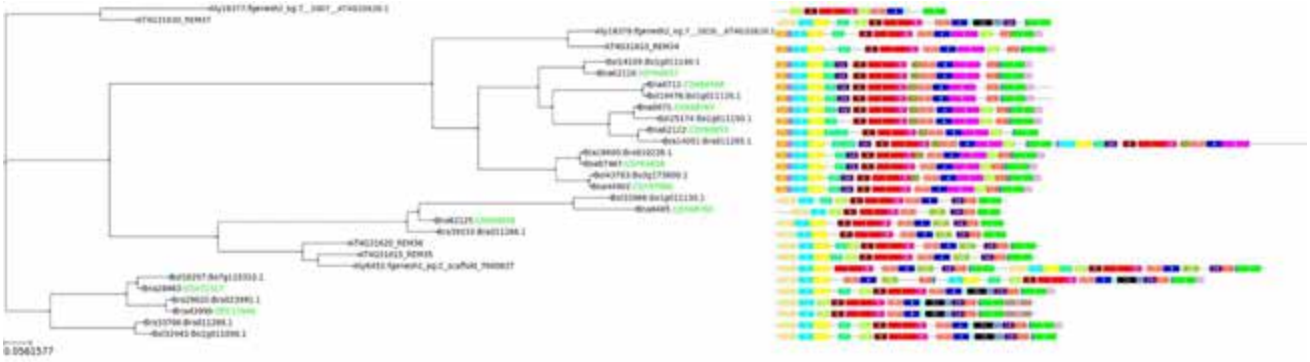

Fig. 13. *REM34, REM35, REM36* and *REM37 Brassica napus* homologs. *Brassica oleracea* and *Brassica rapa* proteins, as well as *Arabidopsis lyrata* ones, are included to provide more sound phylogenetic evidence. Distance as amino acid substitution per site. Different protein motifs as determined by MEME suite are displayed by different numbers and colours.

genes is of paramount interest. 2 *Brassica napus* homologs are reported for *AtREM37* (fig. 13).

To simplify the nomenclature, we here named our genes as *BnaREM*, a number according to the *REM* homolog in *Arabidopsis*, A or C according to the *Brassica rapa* or *Brassica oleracea* subgenome, and a successive number (Table 1).

protein code	gene code	gene name in this article
CDY60855	*BnaA01g34820D*	*BnaREM34A1*
CDY60857	*BnaA01g34830D*	*BnaREM34A2*
CDX68767	*BnaC01g06860D*	*BnaREM34C1*
CDX68769	*BnaC01g06840D*	*BnaREM34C2*
CDY65658	*BnaA08g30700D*	*BnaREM34A3*
CDY57886	*BnaC03g77300D*	*BnaREM34C3*
CDY13446	*BnaA03g51640D*	*BnaREM37A1*
CDX72317	*BnaC07g43390D*	*BnaREM37C1*
CDY60859	*BnaA01g34850D*	*BnaREM35/36A2*
CDX68768	*BnaC01g06850D*	*BnaREM36C1*

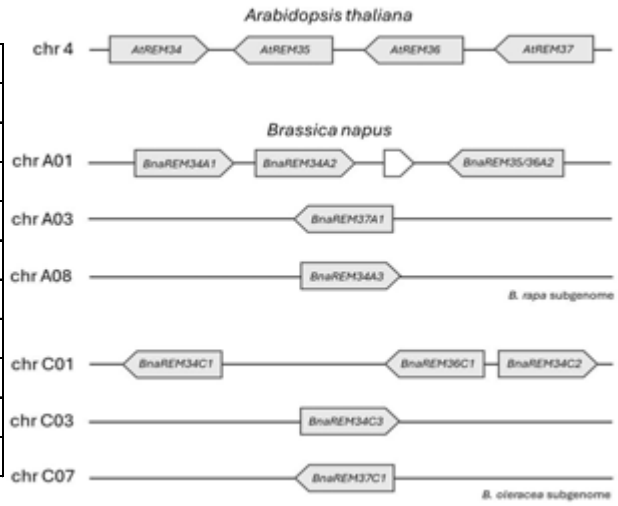

Table 1. Proteins and genes codes translation. Fig. 14. Chromosomic location of the genes studied.

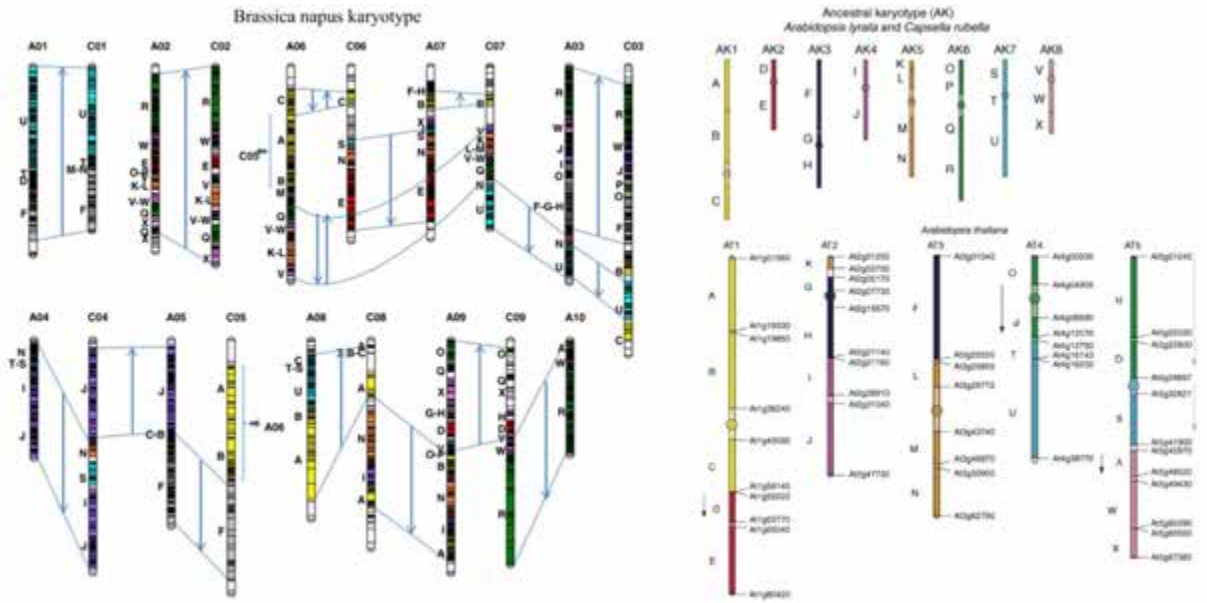

Fig. 15. Schematic representation of the karyotype of *Brassica napus* (from Delourme et al, 2013), *Arabidopsis thaliana* and *Arabidopsis lyrate* (ancestral karyotype) (from Schranz et al. 2006). Chromosomal blocks, as defined by Schranz et al. based on their collinearity with *Arabidopsis thaliana*, are indicated with the capital letters A to X on the left of each linkage group. Arrows in these homoeologous regions represent the orientation of the gene order (within the blocks) with respect to the corresponding regions in *A. thaliana*. The double arrows indicate an inversion of markers between two homoeologous regions.

Further analysis revealed the chromosome positioning of the *Brassica napus* homologs. The linkage context observed in *Arabidopsis thaliana* is at least partially maintained in both the diploid subgenomes, with the *BnaREM37*s genes that, on the other hand, are moved to a different chromosome (in Arabidopsis all the clade is linked, see fig 14) as an additional copy of *BnaREM34* (fig 14).

Specifically, our candidate genes are located on chromosome A01 (*BnaREM34A1, BnaREM34A2, BnaREM35/36A2*), C01 (*BnaREM34C1, BnaREM36C1, BnaREM34C2*), A08 (*BnaREM34A3*), C03 (*BnaREM34C3*), A03 (*BnaREM37A1*) and C07 (*BnaREM37C1*) (fig 14). These positions are coherent with the studies of collinearity between *B. napus* and *A. thaliana* presented in Delourme et al., 2013 (fig. 15)

The coded homolog proteins have high sequence similarity with the *Arabidopsis* counterpart and are very similar from one to the other (table 2). Especially the proteins coded by the twin genes of the two diploid subgenomes show poor divergence, as would be expected in a recent hybridization between related species (Chalhoub et al., 2014). The BnaREM34s display between 70 and 91% of protein similarity, the BnaREM37 display 80%, while BnaREM35/36A2 and BnaREM36C1 have diverged more, having a 68% of protein similarity (table 2).

	BnaREM34A1	BnaREM34A2	BnaREM34A3	BnaREM34C1	BnaREM34C2	BnaREM34C3
AtREM34	63	62	68	63	65	66

	BnaREM35/36A2	BnaREM36C1
AtREM35	61	50
AtREM36	64	54

	BnaREM37A1	BnaREM37C1
AtREM37	61	72

	BnaREM34A1	BnaREM34A2	BnaREM34A3	BnaREM34C1	BnaREM34C2
BnaREM34A2	77				
BnaREM34A3	69	70			
BnaREM34C1	90	79	71		
BnaREM34C2	78	78	73	80	
BnaREM34C3	70	72	91	71	74

	BnaREM35/36A2
BnaREM36C1	68

	BnaREM37A1
BnaREM37C1	80

Table 2. Similarity percentages between the *Arabidopsis* and *Brassica* and within *Brassica* proteins. A color code is given to the *BnaREM34* table to simplify the reading (conditional colour from green to red).

2.2 BnaREM34, BnaREM35/36, BnaREM36 and *BnaREM37* expression pattern is conserved

Retrieved our candidate genes, their expression profile was deeply studied by qPCR and *in situ* hybridization.

We sampled vegetative tissues, including roots, cotyledons, leaves, hypocotyl and SAM-enriched apex, as well as reproductive ones, such as IM-enriched apex (also containing small developing flowers), developed flowers and young siliques. Despite the high sequence identity between the gene sequences, specific primers were successfully designed for each candidate gene to be studied by qPCR.

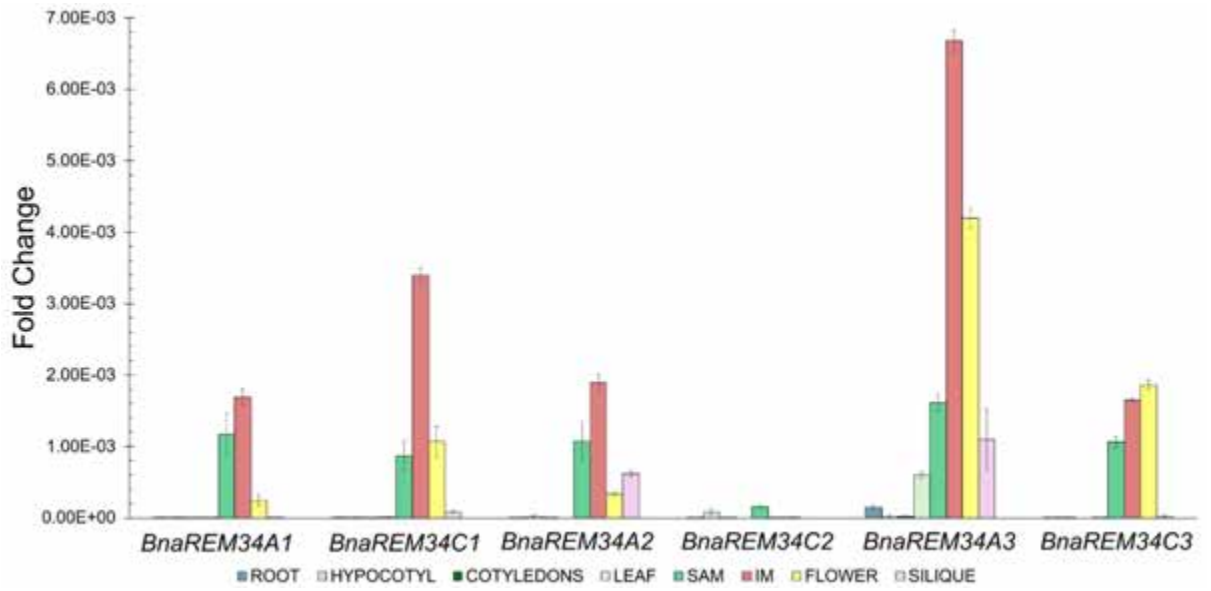

Fig. 16. *REM34* homologs expression. Average +/- Std error is displayed. The graph shows one representative biological replica out of 3. The fold change is calculated compared to the housekeeping gene *BnaACTIN-7* by the $2^{-\Delta Ct}$ method.

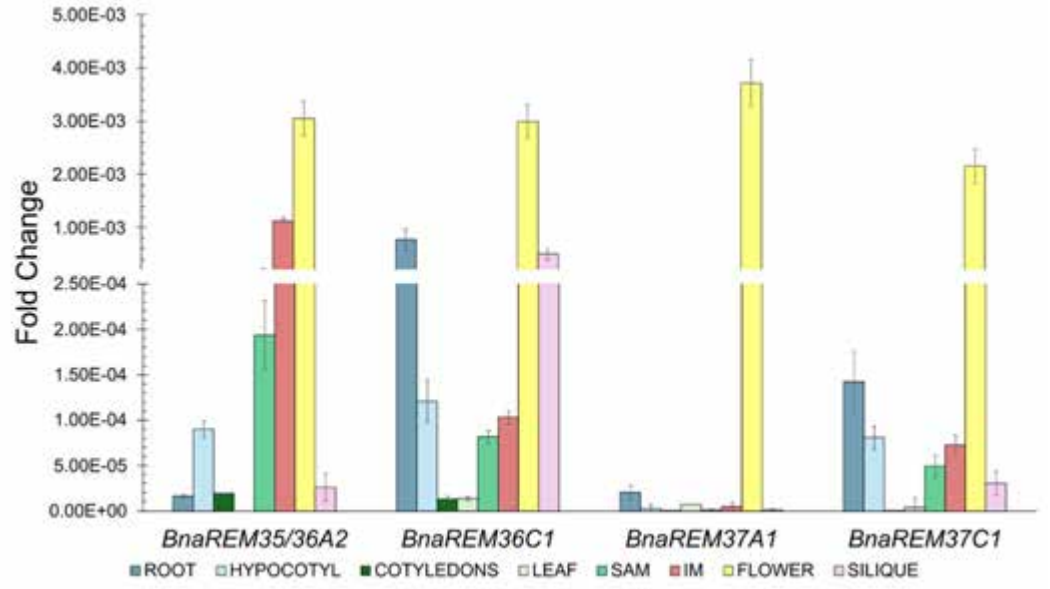

Fig. 17. *BnaREM35-36* and *BnaREM37* homologs expression. Average +/- Std error is displayed. The graph shows one representative biological replica out of 3. The fold change is calculated compared to the housekeeping gene *BnaACTIN-7* by the $2^{-\Delta Ct}$ method.

The gene expression is mainly restricted in the reproductive tissues, as would be expected for *REM*s(Mantegazza et al., 2014).

The *REM34* homologs share an almost identical expression pattern, excluding *BnaREM34C2* whose mRNA was almost not detected in any of the tested tissues (Fig. 16).

In particular, they exhibit high expression in the inflorescence meristem apex and in developed flowers, with a robust presence also in the shoot apical meristem enriched sample, consistent with the findings of Franco-Zorrilla et al., 2002; Manrique et al., 2023. Among the six *AtREM34* homologues, *REM34A3* has a broader expression profile compared to the others, as it is also present in siliques and leaves (Fig. 16).

The *REM35-36* and *REM37* homologs display the highest expression in floral tissues (fig. 17). *REM35/36* shows similarity to the *REM34* group, as it is also expressed in the IM- and slightly in the SAM-enriched samples, while *REM36C1* is modestly expressed in roots and siliques (Fig. 17). Some mild expression is visible in other tissues also for *BnaREM37s* (Fig. 17). Given the similar results we got for the two *BnaREM37* genes, we speculate that the expression of the homolog was lost in *Arabidopsis* genus, and not re-acquired in the *Brassica* ones, after the clade split.

Subsequently, to study the precise localization of the gene expression during the first phases of floral development, we performed an *in situ* hybridization analysis on the *Brassica napus* inflorescences (fig 18).

For this purpose, given the length of the probe and the high CDS sequence identity, each probe targets the twin genes of the two diploid progenitors (sense probe results are presented in appendix fig. A1).

The expression pattern of all the genes under investigation is highly consistent with the one of their Arabidopsis homologs (Fig 4; Caselli et al., 2019; Franco-Zorrilla et al., 2002;

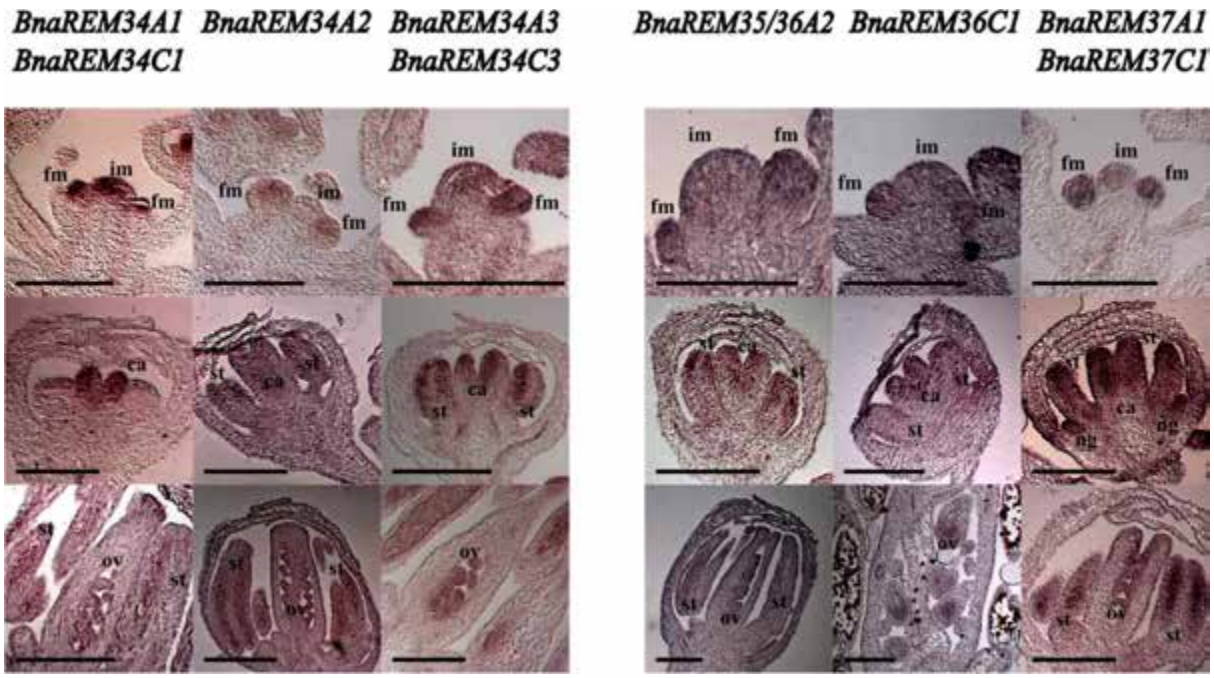

Fig. 18. *In situ* hybridization. The *REM34*, *REM35*, *REM36* and *REM37* homologs are expressed in the floral meristems (FM) and at a slighter extent, in the inflorescence dome (IM). Following flower development, the expression is restricted in the inner floral whorls (carpel=ca; stamen=st) and nectary glands (ng) and is excluded from sepals. Scale bar 200 µm.

Mantegazza et al., 2014), suggesting a possible conservation of their biological role. *BnaREM37s* pattern is superimposable with the one of the other genes under study.

For all the genes, the probe signal strongly localizes in the floral meristems and in the inflorescence meristem dome. Across the floral development, the expression is excluded from the first floral whorl and restricted to petals, anthers, pistil and nectary glands of different developmental stages. Later, the signal is clearly visible also in developing ovules (Fig. 18).

Given the results of the *in situ hybridization* we can state that all the *BnaREM* under investigation show expression in IM and FM and might therefore have a role in the phyllotaxis determination.

2.3 *BnaREMs* are possibly involved in phyllotaxis determination

To analyse the interspecific functional conservation of the genes we set up a complementation test in the homolog *Arabidopsis* single mutants.

Since the twin genes of the two subgenomes of *Brassica napus* are predicted to code for proteins with very high percentages of similarity (table 2) we focused on a single subgenome (subgenome A, *Brassica rapa* derived). We therefore cloned under the 35S constitutive promoter *BnaREM34A1*, *BnaREM34A3*, *BnaREM35/36A2* and *BnaREM37A1*. We excluded *BnaREM34A2* as the protein that codes is similar to BnaREM34A1 (table 2).

The Arabidopsis homolog mutants were transformed by floral dip and the phenotypical complementation was analysed evaluating the percentage of angles falling around the golden angle (130-150° range).

Specifically, *BnaREM34A1* and *BnaREM34A3* constructs were transformed in *rem34* mutants and *BnaREM35/36A2* was transformed in both *rem35* and *rem36* mutants. As we couldn't evaluate the functional conservation of *BnaREM37* by the same method (missing *AtREM37* expression and, therefore, a functional mutant), we decided to try to transform *BnaREM37A1* construct in the *Arabidopsis* mutant of the closest homolog. In this case, *rem35*

	BnaREM37A1	BnaREM37C1
AtREM34 id	155/491(32%)	191/549(35%)
AtREM34 simil	225/491(45%)	281/549(51%)
AtREM35 id	218/489(45%)	245/526(47%)
AtREM35 simil	286/489(58%)	327/526(62%)
AtREM36 id	210/496(42%)	243/528(46%)
AtREM36 simil	279/496(56%)	323/528(61%)
AtREM37 id	267/520(51%)	311/526(59%)
AtREM37 simil	320/520(61%)	378/526(71%)

Table 3. Identity and similarity of BnaREM37 with the AtREM included in this study (number of identical/similar aa are depicted, and the percentage). Excluding AtREM37, AtAtREM35 gets the best results.

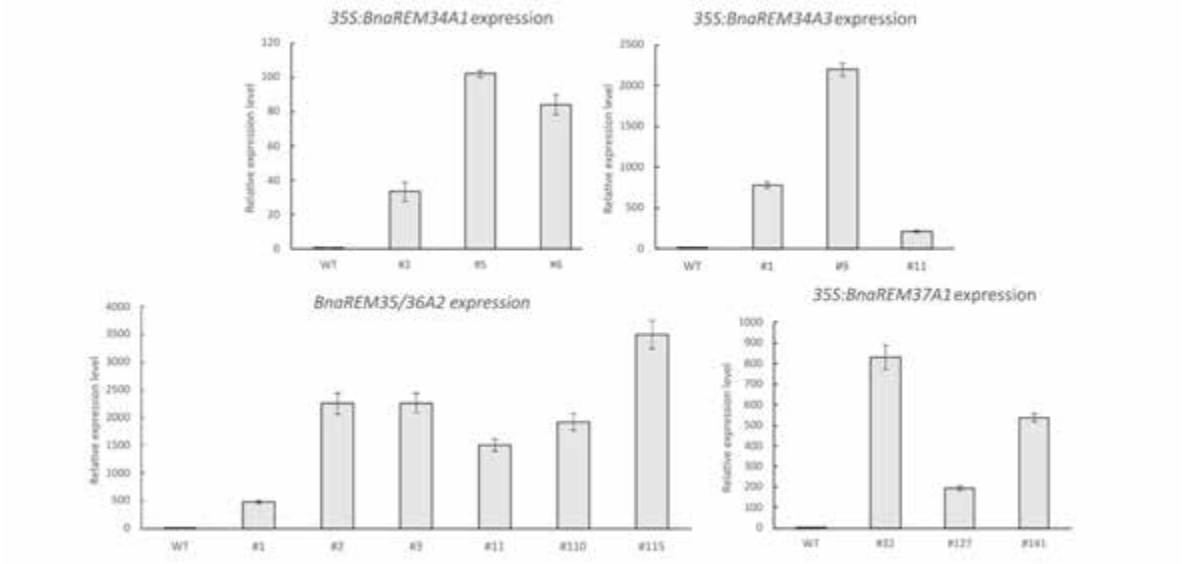

Fig. 19. Relative expression levels of *Brassica* genes in *Arabidopsis* complementation lines, generation T1. The expression in the WT is manually set at 1. For conciseness, only the number of the line is depicted. The *35S:BnaREM34A1* and *35S:BnaREM34A3* constructs are in a *rem34* background, *35S:BnaREM37A1* construct is in a *rem35* background and 35S:BnaREM35/36A2 construct is in *rem35* background for lines #1, 2, 3 and in *rem36* background for #11, 110, 115 respectively. The lines selected for the phenotype complementation have different levels of expression of the transgene. Mean +/- standard error is displayed. 3 technical replicas per line were used.

was selected according to the protein similarity (table 3). We hypothesized that if *BnaREM37A1* has a role in the phyllotaxis establishment, we could have observed some kind

of perturbation in the pattern of the background mutant by constitutively expressing the gene. Moreover, if some important protein motif is conserved, maybe at least a partial complementation could have been observed.

For each *Brassica's* gene constitutive expression, 3 independent lines showing different degrees of expression of the transgene (fig.19) were evaluated. We included *rem34 35S:REM34* and *rem35 35S:REM35* lines as a control for the effect of the constitutive expression of homologous REMs genes.

All the lines expressing *BnaREM34A1* (line 2; 68.54% - line 5; 67.74% - line 6; 68.11% of angles in the 130°-150° range), as well as the lines expressing *BnaREM34A3* (line 1; 62.58% - line 9; 66.24% - line 11; 61.07%), complement the *Arabidopsis rem34* mutant (45.13%), bringing the percentage of angles around the golden angle back to a WT situation (67.47%) and suggesting a functional conservation of the proteins coded (Fig 20).

The expression of *BnaREM35/36A2* can complement *rem36* mutant but not *rem35*. Indeed, observing a WT golden angle percentage of 61.35% and a *rem36* one of 42.49%, *rem36 35S:BnaREM35/36A2* #11, 110 and 115 presented respectively percentages of 56.28%; 60.35% and 56.44%, which are statistically equal to the WT percentage (Fig. 21). On the other hand, compared to a WT percentage of 67.86% and a *rem35* one of 50%, *rem35 35S:BnaREM35/36A2* #1, 2 and 3 presented percentages of 48.17%, 51.61% and 36.76%, equal to the *rem35* mutant (Fig. 21). This suggest the conservation of AtREM36 and BnaREM35/36A2 protein function and support the hypothesis that *REM36* was the original gene in *Arabidopsis* and that *REM35* is the result of a recent duplication and divergence.

Finally, the phenotype of the *rem35 35S:BnaREM37A1* lines suggests a role of this gene in the phyllotaxis determination and the possible presence of some protein motifs similar to the ones of AtREM35. Indeed, compared to a WT ratio of golden angles of again 67.86% and *rem35* of 50%, line #32 and #141 partially complemented the mutant displaying 65.10% and 61.72% of golden angles, behaving like the *35S:AtREM35* expression line, and #127 didn't complement, displaying 44.07% of golden angles, similarly to the *rem35* mutant (Fig. 21).

According to the results, it can be speculated that some relevant protein motifs are partially shared between BnaREM37A1 and AtREM35. The phenotype of line #127 could be due or to the T-DNA location in the genome or to the lower level expression of the construct (fig 19), and more lines should be analysed to state it.

Overall, we can conclude that an interspecific conservation of the protein function exists and that possibly *Brassica*'s genes are involved in phyllotaxis determination.

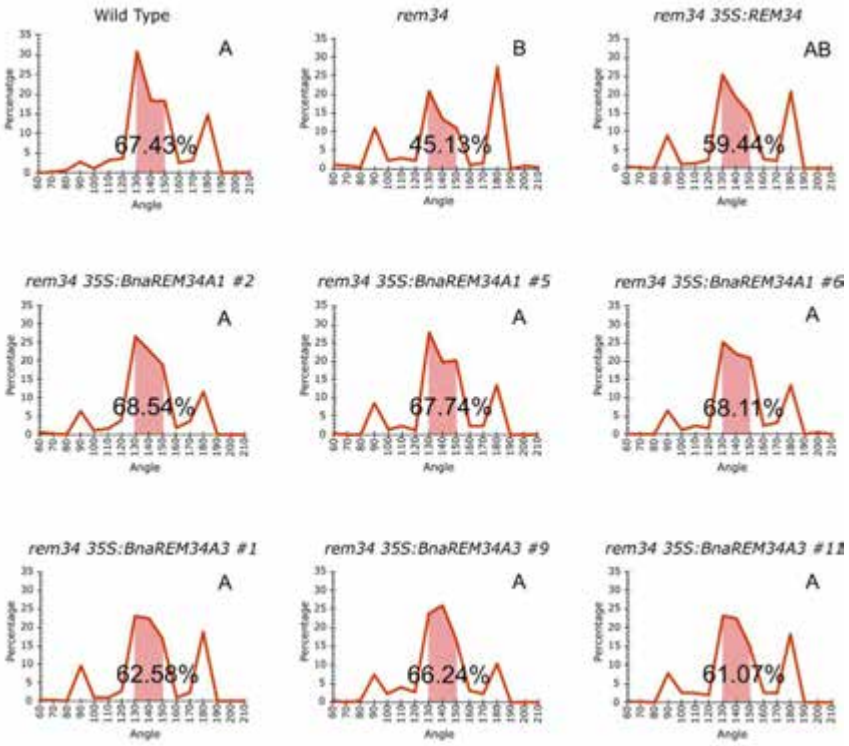

Fig. 20. Complementation test, REM34 group. The graphs show the distribution of angles between two successive siliques. The range 130°-150°, used to evaluate the phenotype complementation, is highlighted and the percentage is reported. WT, mutants and constitutive expression lines are depicted. *rem34 35S:AtREM34* is included as an additional control. For each *Brassica*'s gene constitutive expression, 3 independent lines were evaluated. 9-15 plants per genotype were used. For *35S:AtREM34* a low expression of the protein was observed; this might be the cause of the partial complementation observed. Statistical significance was analysed by Kruskal-Wallis and Dunn's test ($p<0.05$, tests according to the normality and homoscedasticity of the data). Different letters are given to significantly different genotypes.

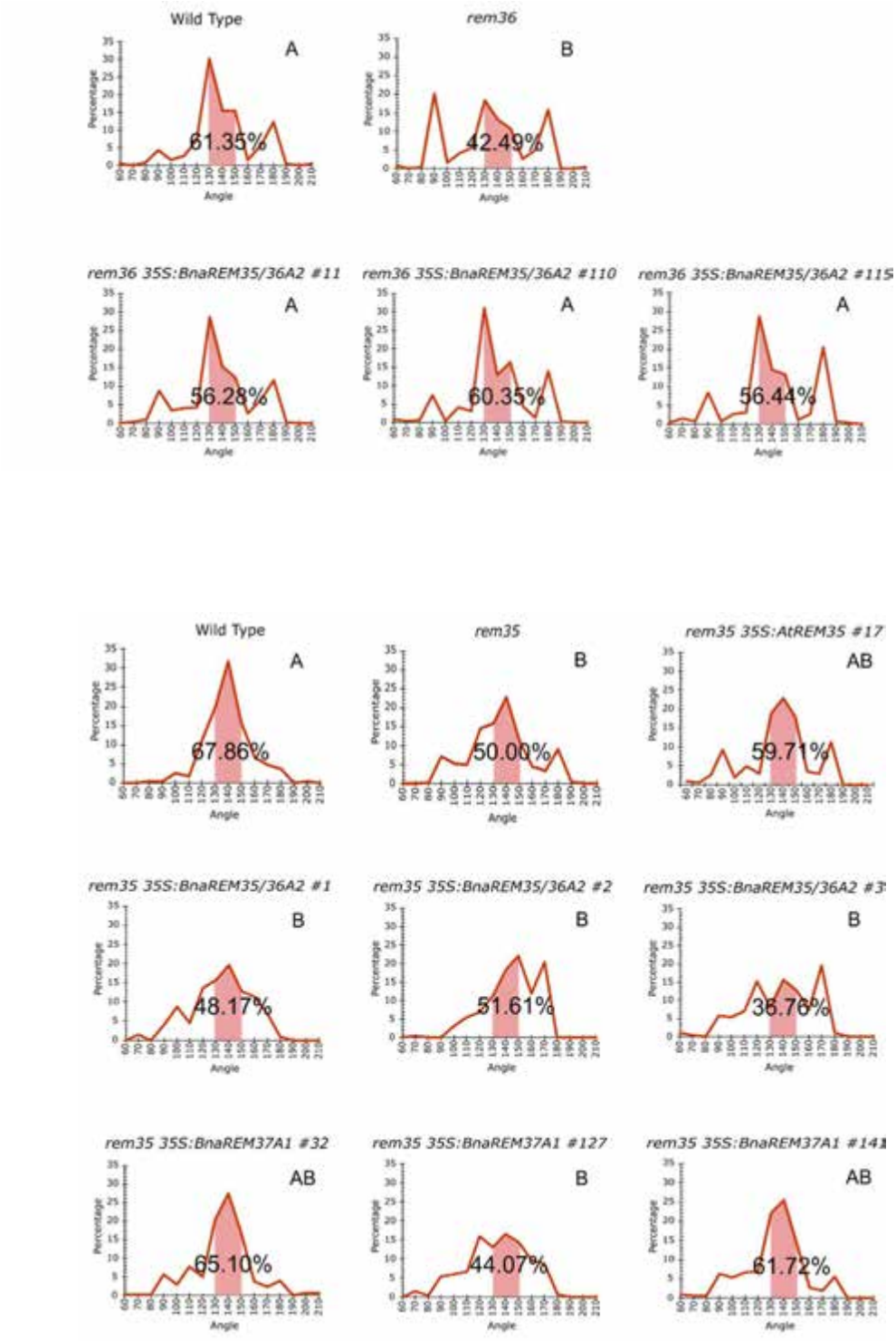

Fig. 21. Complementation test, REM35-36-37 group. The graphs show the distribution of angles between two successive siliques. The range 130°-150°, used to evaluate the phenotype complementation, is highlighted and the percentage is reported. WT, mutants and constitutive expression lines are depicted. *rem35 35S:REM35* is included as an additional control (Caselli et al, under revision). For each *Brassica*'s gene overexpression, 3 independent lines were evaluated. 9-15 plants per genotype were used. Statistical significance was analysed by ANOVA and Dunnett's test in both *rem35* and *rem36* groups analysis ($p<0.05$, according to the normality and homoscedasticity of the data). Different letters are given to significantly different genotypes.

2.4 Evaluation of REM protein complexes in *Brassica napus*

To further characterize the *Brassica* cluster and test the conservation of the protein behaviour, we used the same cloned genes for a Y2H assay.

Some REM-REM interactions have already been described in the literature (Caselli et al., 2019; Manrique et al., 2023; Mendes et al., 2016), possibly depicting a functional feature widely spread in the gene family. As between them there are REM35 homodimers and REM35-REM34 heterodimers, we tested the interactions between *Brassica*'s REMs under study.

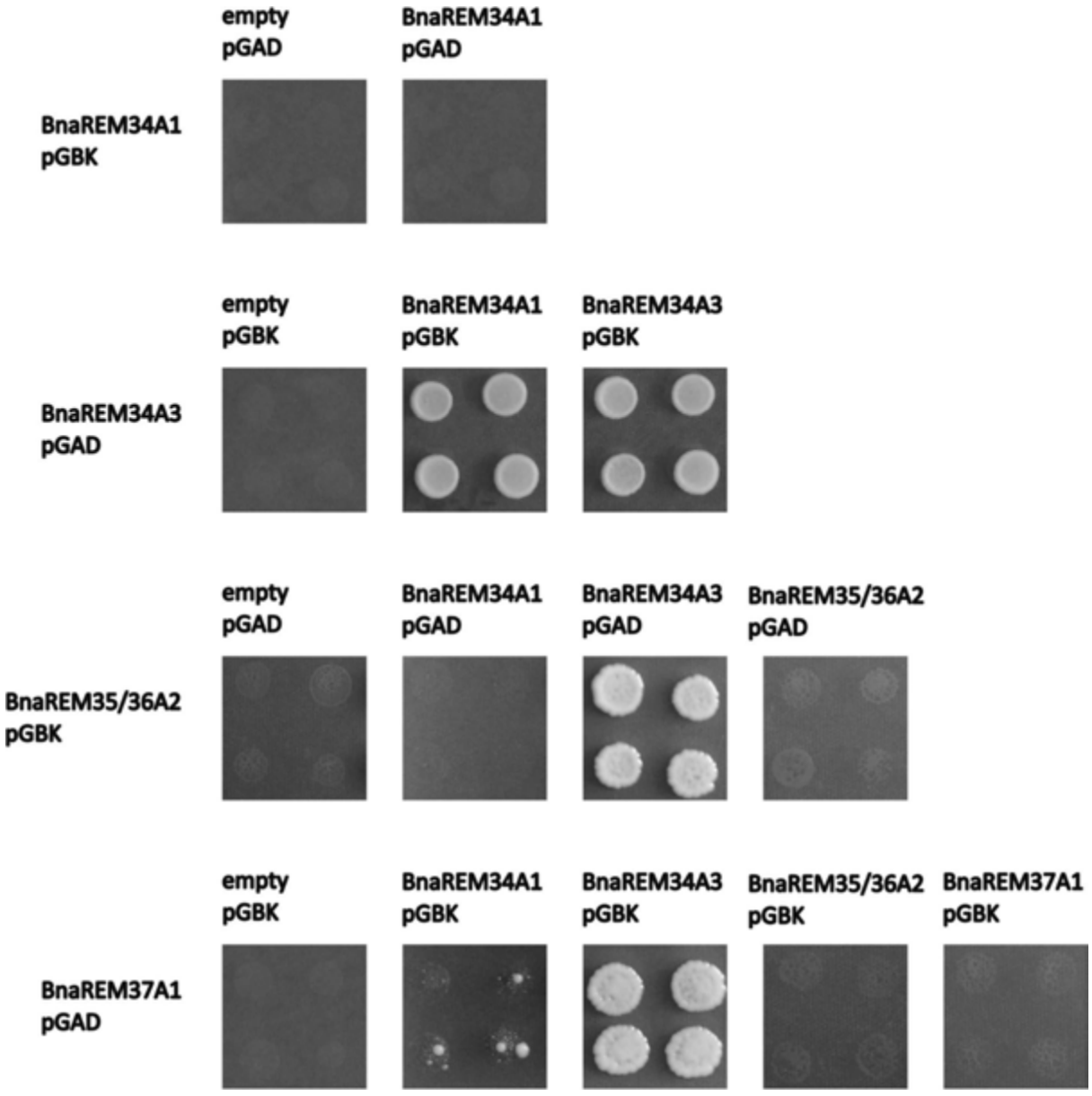

Fig. 22. Y2H between BnaREMs. All the combinations were tested. Selective medium lacking Adenin, Histidine, Tryptophan and Leucin was used to test the interactions. AtREM35-AtREM35 and AtREM34-AtREM34 were used respectively as positive and negative control (Caselli et al, 2019, appendix fig A2).

BnaREM34A1 and BnaREM35/36A2 can't dimerize (Fig 22), behaving similarly to AtREM34 and AtREM36 (Caselli et al., 2019) in heterodimer formation. In the same perspective, BnaREM35/36 doesn't homodimerize (Fig 22), again as AtREM36 (Caselli et al., 2019). Therefore, considering both the interactions tested and the results of the complementation assay, BnaREM35/36 seems to be more related to AtREM36 than to AtREM35.

On the other hand, and differently from AtREM34, BnaREM34A3 is very sticky and presents wide interactions with all the other proteins tested, including itself (Fig 21). According to the numerosity of the BnaREM34 genes, BnaREM34A3 might have accumulated a few mutations that have changed its interaction capabilities. BnaREM37A1, more than with BnaREM34A3, slightly interact with BnaREM34A1 (Fig. 9).

The positive interactions were further confirmed in a plant context by BiFC, supporting the results of the Yeast-2-Hybrid assay (Fig 23).

Overall, some interactions, but not all of them, superimpose with the *Arabidopsis* results and new interactions are pointed out for a *B. napus* environment.

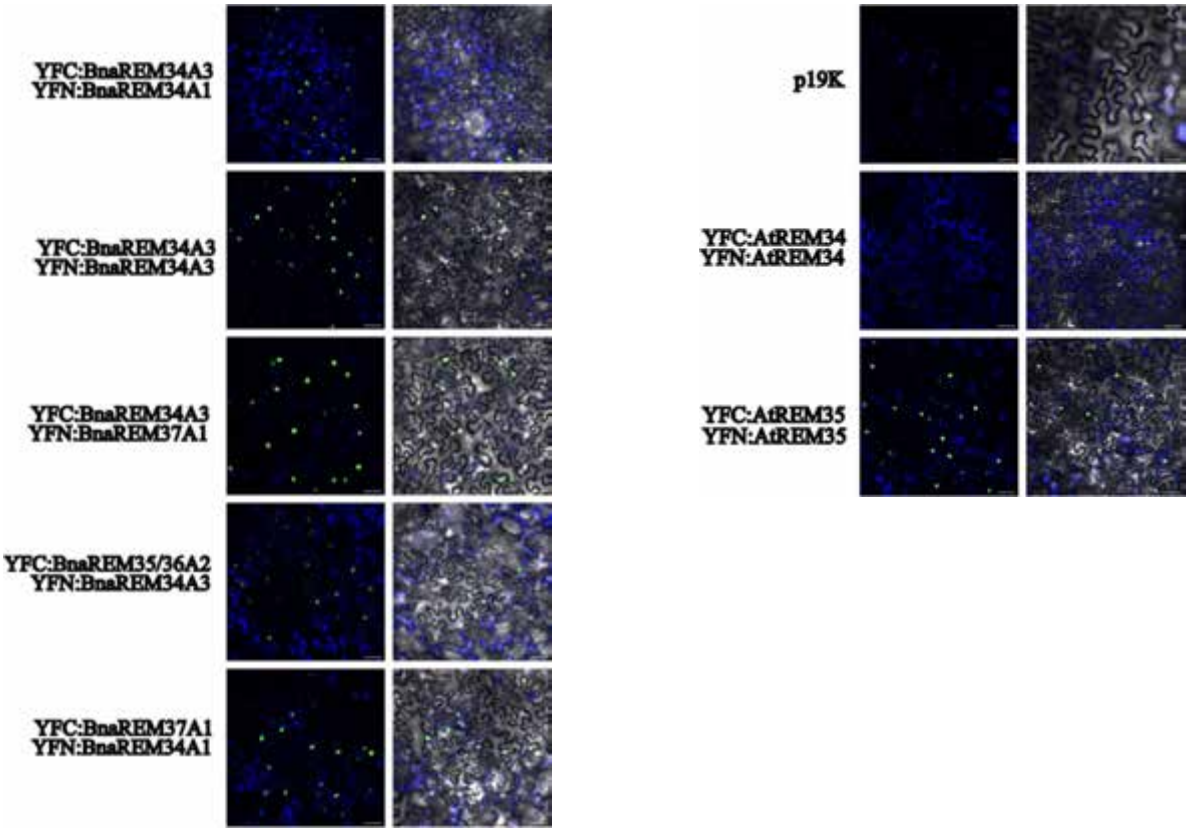

Fig. 23. Confirmation of the positive *Brassica* intraspecific protein interactions by BiFC. The left line shows YFP and Chlorophyll channels and the right line includes the bright field too. p19K was co-infiltrated with the *Brassica* constructs. On the right panel, the controls are depicted (AtREM34 homodimers: negative control, p19K only: negative control, AtREM35 homodimers: positive control; Caselli et al, 2019). Scale bar=50 μm

2.5 BnaREMs possibly interact with the auxin pathway

Since the impact of some of the studied *AtREM* genes on phyllotaxis is related to auxin perception via genetic interaction with AtARF7 and AtARF19, and it is known that AtREM35 can physically interact with these two proteins (Caselli et al, under revision), the interactions between the BnaREMs and AtARF7 and AtARF19 (whose constructs were available in the lab) were tested. Even if intra-specific interactions should be tested for a complete assay, these sets of tests can help clarifying the potential interaction pattern of BnaREMs.

All the BnaREM tested can interact with AtARF19, and BnaREM35/36 can also interact with AtARF7 (Fig. 24). In this case, more than BnaREM34A3, even BnaREM34A1 and BnaREM35/36 partially and completely behave differently from their homologs (Caselli et al, under revision; Caselli's PhD thesis for ARF19 interactions, appendix fig. A3 for ARF7 interactions).

This suggests that the auxin pathway can be related to these REM gene functions in *Brassica napus* and that testing the interaction with the BnaARFs can be of great interest.

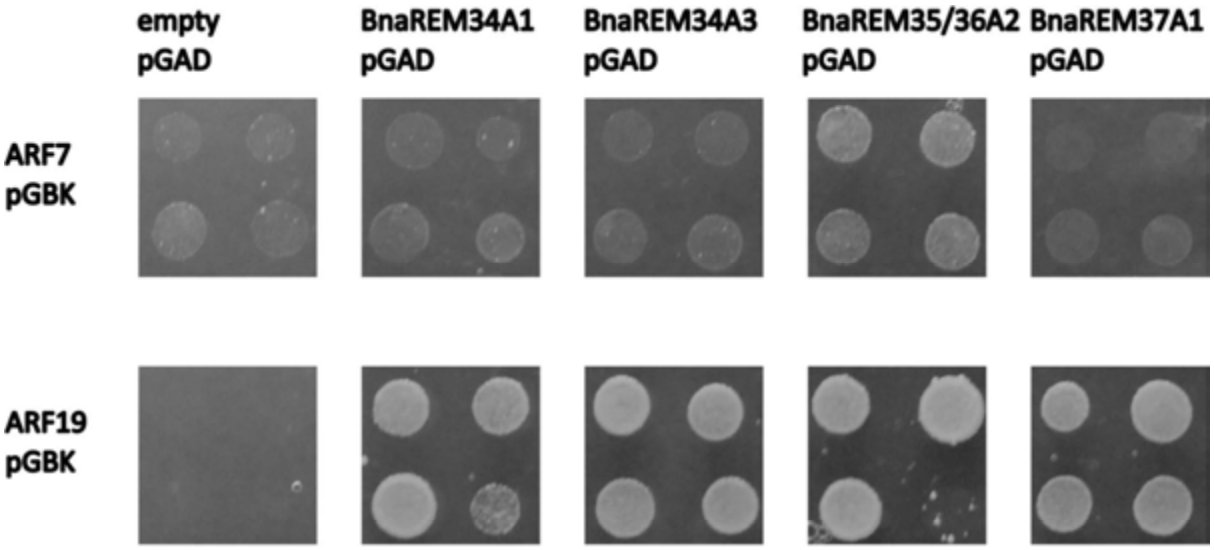

Fig. 24. Y2H between BnaREMs and AtARF7 and AtARF19. All the interspecific combinations were tested. Selective medium lacking Adenin, Histidine, Tryptophan and Leucin, supplemented with 100 mM of 3-At, was used to test the interactions (to counteract ARF autoactivation). AtREM35-AtREM35 and AtREM34-AtREM34 were used respectively as positive and negative control (Caselli et al, 2019; appendix fig A2).

2.6 BnaREM and AtREM interspecific interactions

Last, we analysed the interactions between the BnaREMs and AtREMs under study to understand if the BnaREM interactions with them and/or with the AtARFs could explain the complementation results. We found that all BnaREM can interact with AtREM35 and that all of them but BnaREM37 can interact with AtREM34 (Fig. 25).

Just by these data, we can't explain the phenotype that we observe in the complementation test, witnessing a possible much more complex environment in the molecular determination of phyllotaxis.

Complexes of more than two proteins between the tested proteins can be involved (as detailed in Caselli et al., under revision), as well as many other interactors we don't know about. For example, it is known that AtREM34 not only interacts with AtREM35, but also with AtREM46 (Manrique et al., 2023).

Again, this suggests that the REMs have a wide list of partners in the plant cell and that trying to explain a phenotype just by some of them can be reductive.

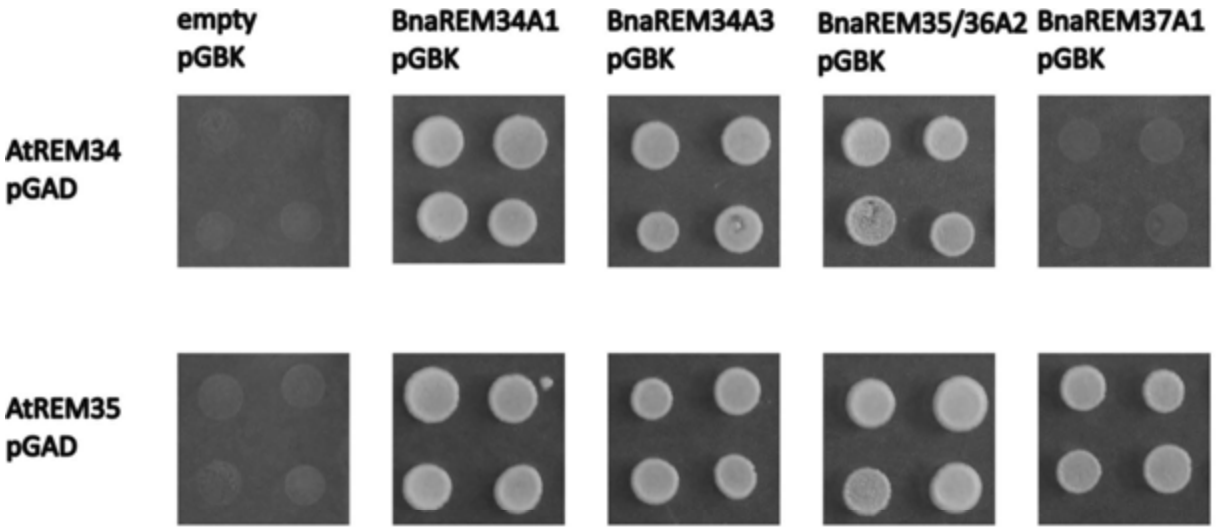

Fig. 25. Y2H between BnaREMs and AtREM34 and AtREM35. Selective medium lacking Adenin, Histidine, Tryptophan and Leucin was used to test the interactions. AtREM35-AtREM35 and AtREM34-AtREM34 were used respectively as positive and negative control (Caselli et al, 2019, Fig appendix A2).

2.7 Summary of the results: cluster characterization

In the first part of this thesis, we demonstrated the yield impact of *REM34*, *REM35* and *REM36* in *Arabidopsis thaliana* and we characterized the homologous genes in *Brassica napus*.

In coherence with the *B. napus* genome and *REM* gene family evolution, we found 6 homologs of *REM34* and 2 homologs of *REM35* and *REM36*. Possibly, the latter have duplicated after the *Brassica-Arabidopsis* clade split. We included in our study the homologs of *REM37*, as it is part of the same phylogenetic group as our target genes, and it is supposed to be highly redundant with them. Indeed, it was not accounted in Arabidopsis as it is almost not expressed in the reproductive meristems of the species, but we can't assume the same for the homologs in *B. napus*. 2 homologs of *REM37* could be found in *Brassica napus*.

The 10 candidate genes, except *BnaREM34C2*, share a very similar expression pattern, being expressed in inflorescence and floral meristems and floral organs at different stages, as their homologs in Arabidopsis.

According to the recent hybridization which gave rise to *B. napus* from the two diploid progenitor *B. rapa* and *oleracea*, the twin genes of the parent genomes are supposed to be highly redundant. Therefore, the protein characterization was performed on 4 genes of the *B. rapa* subgenome. An interspecific complementation test and a Y2H assay were performed.

Regarding the complementation test, BnaREM34A1 and BnaREM34A3 could complement *rem34*, BnaREM35/36 could complement *rem36* but not *rem35* and BnaREM37A1 could partially complement *rem35*, which is the functional mutant of the closest homolog. The results suggest that all the genes can have a function in phyllotaxis determination in *B. napus* and that *BnaREM35/36* is more functionally related to REM36 than to REM35.

The Y2H assays were performed not only between the BnaREMs themselves, but also between BnaREMs and AtARF7 and AtARF19 (known to interact with AtREM35) and BnaREMs and AtREMs. This was meant to investigate a possible involvement of the auxin pathway also in *B. napu*s and to try to explain the results of the complementation assay.

Both conserved and new interactions could be found between the protein tested. In BnaREM-BnaREM test specifically, we pointed out that BnaREM34A1 and BnaREM35/36 behave similar to REM34 and REM36, while BnaREM34A3 is unexpectedly sticky. Moreover, wide interactions could be found with the AtARFs, suggesting a possible involvement of auxin and the need of performing such assay with the intraspecific *Brassica napus* ARFs. Last, we couldn't explain the complementation by these the Brassica- Arabidopsis interactions tested, pointing out that the molecular determination of phyllotaxis possibly involve more complex mechanisms.

3. *Brassica napus* genome editing

Having defined and characterized our genes of interest, we moved to the actual editing in *Brassica napus*.

3.1 gRNAs design and test

To generate the mutants we planned to use the CRISPR Cas9 technology coupled with the Agrobacterium-mediated transformation.

We selected the *Westar* spring variety to work with, as it is the model for *B. napus* transformation (Bhalla & Singh, 2008).

To design the gRNAs, the CRISPOR web tool was used (Concordet & Haeussler, 2018) and the *Brassica napus* v2.0 genome (*Brassica napus* NCBI GCF_000686985.2 - 2017) and SpCas9 were selected.

The gRNAs research was performed on the first exons, bearing in mind the aim of generating KO mutants, as are the ones that were studied in Arabidopsis (Caselli's PhD thesis, Caselli et al, under revision).

To select the gRNAs for every gene, a deep analysis of the off-targets was performed, as they could have been on our other target genes. We selected gRNAs that could have hit our candidate genes in exons with up to 3 mismatches of precision (in this way, other off-targets are predicted to have at least 4 exonic mismatches and, therefore, are very unlikely to be cut). The selected gRNAs have no off-targets without mismatches on non-coding sequences too.

Two other parameters displayed on CRISPOR were accounted in our gRNAs design. Indeed, the tool can predict the efficiency of out-of-frame indels, which is very useful in KO generation, and the predicted efficiency of the U6-driven gRNAs (Doench '16 parameter on CRISPOR, Doench et al., 2016)

We ended up with a list of 9 (perfectly matching on gDNA) gRNAs that have the potential to generate at least 3 cuts on every single *BnaREM34* candidate genes (and 1 cut for *BnaREM34C2*, that is not expressed), and a list of 12 gRNAs that could potentially do the same on *BnaREM35/36*, *BnaREM36* and *BnaREM37* genes.

		n° of gRNA cutting with n mismatches			
		0 mismatches	1 mismatch	2 mismatches	3 mismatches
gene	BnaREM34A1	4	1	2	1
	BnaREM34C1	3	1	2	1
	BnaREM34A2	3	0	2	2
	BnaREM34C2	1	1	1	3
	BnaREM34A3	3	0	0	0
	BnaREM34C3	3	0	0	0

		n° of gRNA cutting with n mismatches			
		0 mismatches	1 mismatch	2 mismatches	3 mismatches
gene	BnaREM35/36A2	3	1	1	0
	BnaREM36C1	3	*1 (intron-exon junction)*	0	*(1 intron)*
	BnaREM37A1	3	2	1	0
	BnaREM37C1	3	3	0	0

Table 4. Number of potential cut sites per gene. *BnaREM34C2* is highlighted as it is not expressed.

The cutting potential also increased considering cuts in loci with up to 3 mismatches.

A summary of the gRNAs designed and their targets, as well as the hypothetic number of cuts, are depicted in Tables 4 and 5.

		protospacer	0 mismatches	1 mismatch	2 mismatches	3 mismatches
			REM34 HOMOLOGS			
gRNA 1	257	TTCACTGTCGTCAGTATCAT	BnaREM34C1 BnaREM34A2 BnaREM34A1 - 3 times	BnaREM34C1		
gRNA 2	144	GCCGTTAGTAATTTCAGCCA	BnaREM34A1		BnaREM34C1	BnaREM34C2
gRNA 3	213	TACTTCAAACTTTCCGAAAG	BnaREM34C1	BnaREM34C2 BnaREM34A1	BnaREM34A2	
gRNA 4	180	TCAGCTAATGGGTTAATCCG	BnaREM34C1 BnaREM34C2		BnaREM34A1	BnaREM34A2
gRNA 5	141	GGTGCATTTAACATCAGACG	BnaREM34A2			
gRNA 6	44	TAAATATATCTCACACGGTT	BnaREM34A2			
gRNA 7	243	TCGTCAGTATCAACCAAGCT	BnaREM34A3 BnaREM34C3			BnaREM34C2
gRNA 8	102	CTAGACGGAAGCAGGCTCGC	BnaREM34A3 BnaREM34C3			BnaREM34A2 BnaREM34A1 BnaREM34C2 BnaREM34C1
gRNA 9	53	AAGGTGTGACACGTGCTCTG	BnaREM34A3 BnaREM34C3		BnaREM34A2 BnaREM34A1 BnaREM34C2 BnaREM34C1	
			REM35/36 - REM37 HOMOLOGS			
gRNA 10	76	TCGACTTAGGCTTGAAGGTG	BnaREM37A1	BnaREM37C1		
gRNA 11	138	GGTCAAGCATTTGTCAGTAA	BnaREM37A1	BnaREM37C1		
gRNA 12	60	ATCTTCATCGTAGATCTGTC	BnaREM37A1	BnaREM37C1		
gRNA 13	35	CTTTGTTTCGAATCACTTAA	BnaREM37C1	BnaREM37A1		
gRNA 14	331	CGACCTGACTTAAACATGTA	BnaREM37C1	BnaREM37A1		
gRNA 15	75	ATCGATCTAAGGAACGAACA	BnaREM37C1		BnaREM37A1	
gRNA 16	118	GCCGGGGATTCGCTGATGGC	BnaREM35/36A2			*BnaREM36C1 intron*
gRNA 17	176	CGACGTTTTGCTTTTCAGAG	BnaREM35/36A2	*BnaREM36C1 intron- exon junction*		
gRNA 18	189	CAGTCCGGACAAGTTCGAAC	BnaREM35/36A2			
gRNA 19	23	GTTATTACCGTCTAAGTGAG	BnaREM36C1			
gRNA 20	139	TAATCTACGCCTGAATCGAG	BnaREM36C1		BnaREM35/36A2	
gRNA 21	124	TCGGCAAAACCTAACAGGGC	BnaREM36C1	BnaREM35/36A2		

Table 5. Complete list of all the designed gRNA according to their potential cut site.

The gRNAs were subsequently tested by a protoplast destructive assay.

The gRNAs were synthesized *in vitro* and purified. Protoplasts were recovered from young leaves of *B. napus* and transfected by a mixture of gRNA and Cas9. 125.000 protoplast were used to test a single gRNA. After 2 days, the DNA was extracted, and the targeted genes were sequenced.

At least one gRNA per gene managed to edit, except for *BnaREM34C3* (fig. 26). The best functional gRNAs were selected to be cloned in the CRISPR constructs, and a new gRNA was designed for *BnaREM34C3* (sgRNA23, table 6, not tested for economic and time constraints).

gRNA16 was discarded according to the presence of an in frame- ATG after the cut site, as it might have had the possibility to be used as an alternative translation start site, while gRNA21 was discarded as containing a 4 T stretch that terminates transcription if it is U3 and U6 driven.

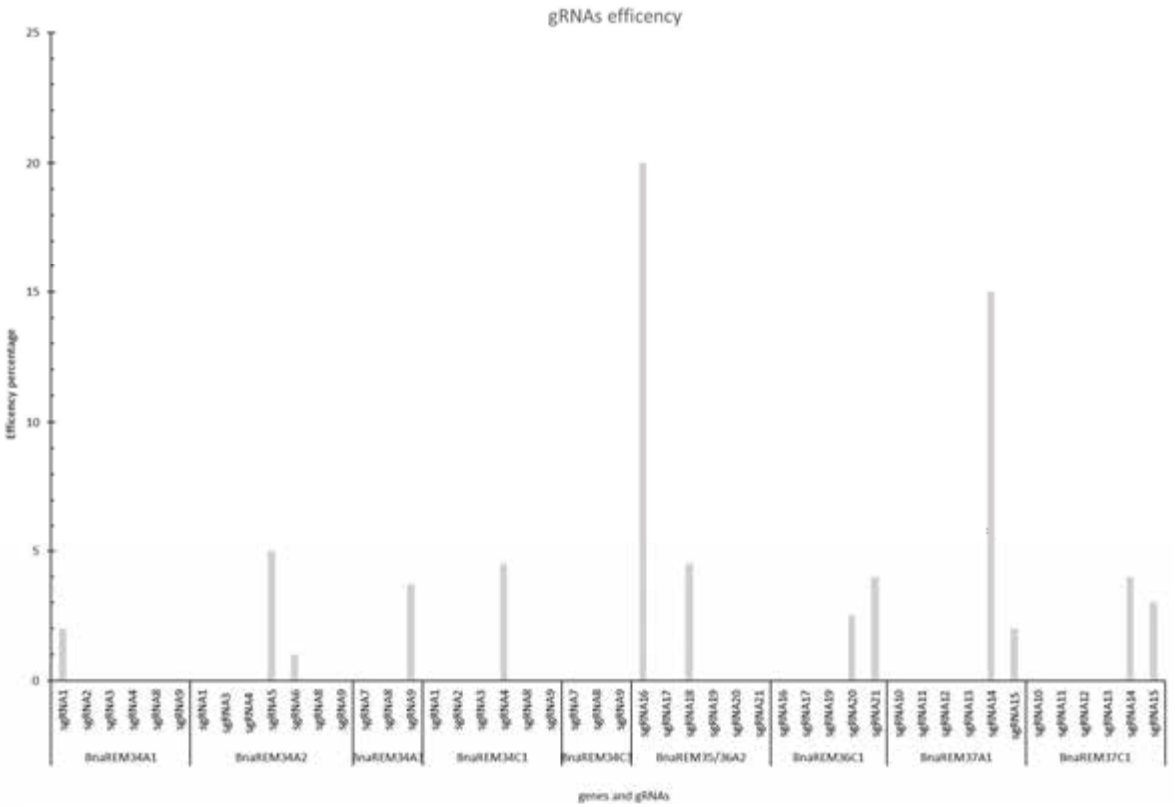

Fig. 26. gRNAs efficiency in protoplast destructive assay

3.2 Strategy and Constructs

In order to get both single homologs (eg. All the *BnaREM34* KO, all the *BnaREM35-36* KO, all *BnaREM37* KO) and higher-order mutants, we designed 3 different constructs. One was meant to edit all the *BnaREM34*, one was meant to edit all the *BnaREM35-36* and *BnaREM37* and one was designed to obtain mutants on the genes in linkage (the genes targeted by each construct are represented in Fig 27).

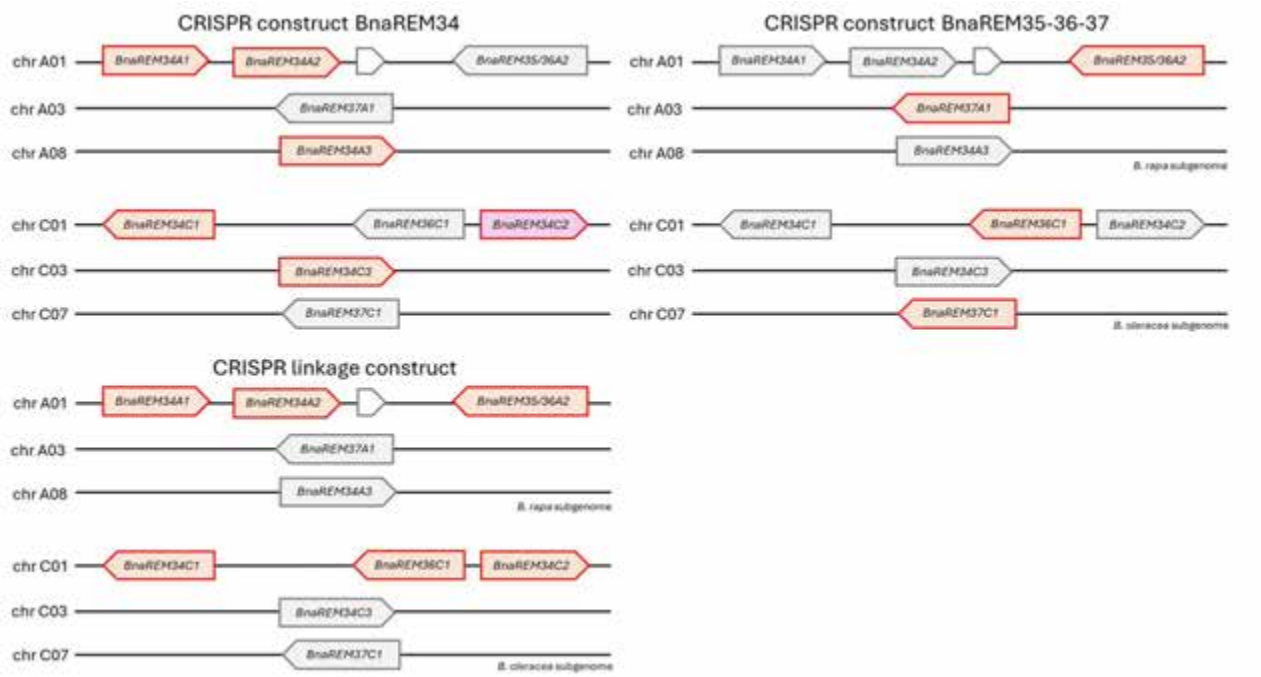

Fig. 27. The genes targeted by the CRISPR constructs are highlighted in red. Left: genes targeted by the *BnaREM34* CRISPR construct (*BnaREM34C2* is in violet as the gRNAs also target this gene, but mutations there are not necessary as the gene is not expressed). Right: genes targeted by the *BnaREM35-36-37* CRISPR construct. Below: genes targeted by the linkage CRISPR construct. Lower order mutants can be generated by backcrossing and higher order mutants by crossing or retransforming according to the genomic position of the genes.

Higher or lower-order mutants could then be obtained by crossing, and if needed, re-transforming.

The BnaREM34 edit construct was designed to contain gRNA1, gRNA4, gRNA5, gRNA9 and the newly designed gRNA23 (sequence: AAGTGAAACTAGACGGAAGC). The BnaREM35-36-37 edit construct contained gRNA18, 20, 14 and 15 and the "linkage construct" would have contained gRNA1, gRNA5, gRNA4, gRNA18, and gRNA20.

The BnaREM34 and the BnaREM35-36-37 poly-tRNA-gRNA (PTG) cassettes were designed and assembled in pUC construct by the GeneWiz service. AtU6p and AtU6t were used to drive gRNAs PTG cassette transcription. Finally, the cassettes were cloned in the CRISPR binary vector by Gateway reaction (pBIN plus backbone).

The CRISPR backbone construct was available in the lab and contained an Arabidopsis codon-optimized Cas9 driven by the *Petroselium crispum Ubiquitin* promoter. This promoter has been found to work very efficiently in *A. thaliana* (reported and patented by Plesch and Ebneth 2011) and other species (Kishi-Kaboshi et al., 2019 in chrysanthemum) and could drive editing in both *A. thaliana* (Fauser et al., 2014) and *B. napus* (Okuzaki et al., 2018). As a selection mark both a kanamycin resistance gene and a *35S:GFP* were present.

The linkage construct was not cloned during this thesis, as we first wanted to test the functionality of the other two constructs.

3.3 *Agrobaterium*-mediated transformation

The constructs were transformed in GV3101 *Agrobacterium tumefaciens* strain (already used in *Brassica napus* transformation by several authors, e.g Braatz et al., 2017; Okuzaki et al., 2018; Sriboon et al., 2020; Xing et al., 2014) and the protocol of Bhalla & Singh, 2008, was selected to be used as it resembled to be one of the simplest, fastest and most efficient between the ones available in literature. A transformation efficiency of 33% is expected in *Westar* (Bhalla & Singh, 2008).

The selected protocol uses the cotyledons as explants to be transformed and involves a direct regeneration of the transformed plants from the edge of the petiole, which just swells, without going through a real callus phase.

60 explants were initially used, and a trial plasmid containing the RFP visual marker was used to easily screen the eventual transformants.

While the control of non-transformed plants showed good results in terms of regeneration efficiency, no transformants were retrieved. Several trials were performed, modifying parameters that could have impacted the transformation efficiency. Specifically, we tested other plasmids and plant selection agents, a different *Agrobacterium* strain, we increased the bacterial OD, added acetosyringone, increased the co-cultivation time and temperature, increased the infection time, and tested other co-cultivation media. In total, we tried to transform around 450 cotyledons, without any success.

Therefore, we decided to test other protocols and we designed a pilot experiment which integrated different conditions, to test multiple parameters simultaneously to increase the probability of finding the right conditions for our environment in the shortest time possible.

We investigated 3 types of protocol: two *in vitro* protocols, working respectively with cotyledons and hypocotyls as starting explants, and a floral dip approach.

The alternative cotyledon method was based on Moloney et al., 1989 (ca 55% transformation efficiency in *Westar* - calculated as a percentage of explants producing at least one transformed plant, so it can be higher if accounting for multiple plants per explant).

We tested:

1) two different constructs
    a. 35S:RFP in pGWB2 backbone
    b. Our CRISPR construct with no gRNAs (the *REM34* CDS was cloned without promoter just to remove the ccdb cassette; pBIN plus vector)
2) Two *Agrobaterium tumefaciens* strains
    a. GV3101
    b. EHA105
3) Different light conditions (before cotyledons excision, the plants were subjected to different light conditions):
    a. Dark (plants were kept in the dark to increase *Agrobacterium* transformation efficiency; Bhalla et al, 2008)
    b. Light (grown in long day conditions, 16/8 h)
4) Different *Agrobacterium* OD (the optical density) of the cultures used for transformation:

    a. 0.2 (GV3101)
    b. 0.6 (EHA105)
5) Different infection time (two different durations of infection were tested during the transformation process):
    a. Instant dip (dip only the base of the petiole)
    b. 1-minute immersion of the full cotyledon

We used a total of 100 cotyledons, in 8 final overall conditions (plus the not-transformed control). No transformants were found in any condition.

It is worth to underline that we lost our not-transformed control (regeneration control) because of contamination. This questions the effectiveness of the protocol in regenerating plants. Indeed, compared to the trial based on Bhalla, the non-transformed bleached regenerants obtained in the selective medium of this trial were very few (plants that regenerate on selection, but are not transformed, are bleached by kanamycin). One reason could be that the Moloney method doesn't use $AgNO_3$ in the regeneration medium, which past studies have shown to improve plant regeneration by inhibiting ethylene pathway as containing silver ions (Maheshwari et al., 2011and many others, first published by Beyer, 1976).

The hypocotyl method was based on Maheshwari et al, 2011 (ca% 30 transformation efficiency reported in *Westar*-calculated as transformed plants per initial explant). Differently from the cotyledons method (Bhalla & Singh, 2008; Moloney et al., 1989), here the regeneration passes through a real stage of callus formation.

Also in this trial plenty of conditions were tested to improve transformation, matching them to test all the combinations. We used a total of 90 plantlets, for a total of 270 explants tested in 32 final conditions (plus the not transformed control).

Specifically, we tested:

1) Two different constructs
    a. 35S:RFP in pGWB2 backbone
    b. Our CRISPR construct with no gRNAs (the *REM34* CDS was cloned without promoter just to remove the ccdb cassette; pBIN plus vector)
2) Two *Agrobacterium* strains:
    a. GV3101
    b. EHA105
3) Included or not a pre-cultivation step: hypocotyl segments were pre-cultured for 72 hours on callus induction media before transformation (according to Cardoza & Stewart, 2003, it improves the transformation of *B. napus* hypocotyls), or not.
4) Light conditions before excision:
    a. plants are grown in the dark
    b. plants are grown in light conditions (long day, 16/8 h)
5) *Agrobacterium* OD600
    a. 0.2
    b. 1
6) Infection duration:
    a. 5 minutes
    b. 30 minutes

7) Explant Age. Hypocotyl explants used for transformation were at the age of:
    a. 7 days
    b. 10 days

The media composition was retrieved from the best conditions found in the reference protocol with minor modifications. Importantly, we removed $AgNO_3$ from co-cultivation media as in the previous trial we noticed that it inhibits *Agrobacterium* growth, as published by Gyves et al., 2010.

Again, we managed to regenerate plants but not to transform them.

In fig. 28 a graphical summary of the results of the different *in vitro* protocols tested can be found.

Even if the actual transformation failed, we used the regeneration control of the Maheshwari trial to optimise the rooting step and the recovery of abnormal plantlets. Indeed, during the *in vitro* transformation, it happens that some regenerants appear vitrified or stumpy, and the rooting is published to be a critical step in *B. napus* transformation (Cardoza & Stewart, 2003). The recovery of vitrified plants was accomplished as suggested by De Block et al., 1989, by culturing them in half MS with no vitamins and reduced sugar, cytokinins and carbenicillin.

To optimize the rooting step, we tested different concentrations of NAA according to Maheshwari and got a good rooting efficiency with 0.1 mg/L of NAA.

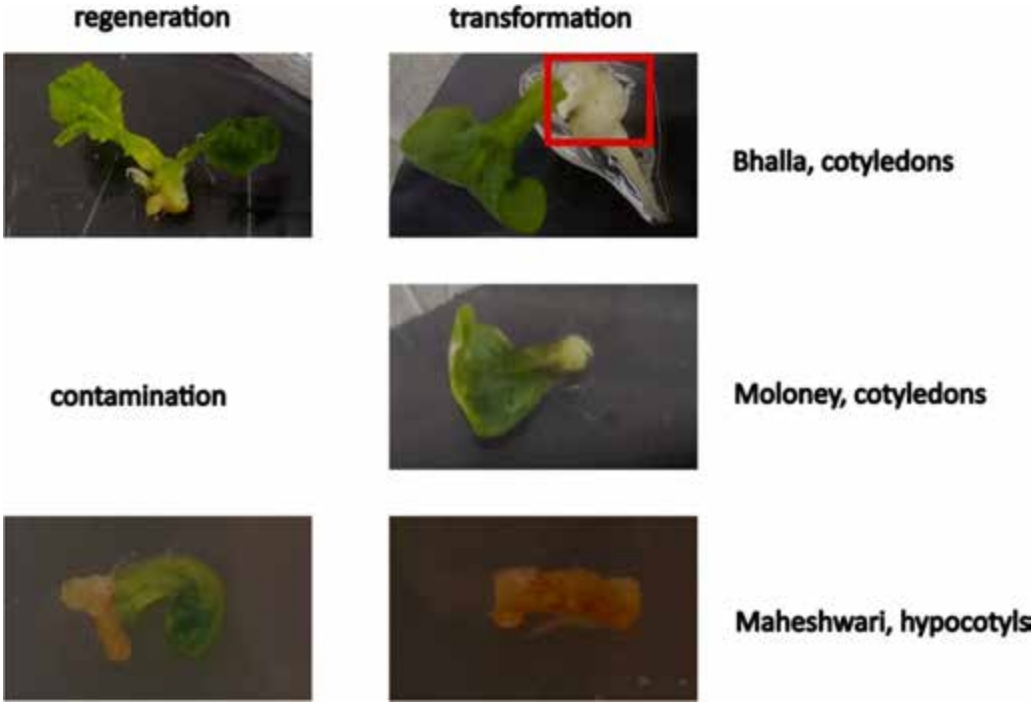

Fig.28. Graphical summary of the results of the different *in vitro* protocols tested. We were able to regenerate plants but not to transform them. In Moleney-based trial, we got very few bleached regenerants compared to Bhalla's one (a bleached regenerant is squared in the picture as an example). This, together with the loss of the regeneration control, questions the efficiency of regeneration of the protocol. The lack of silver ions in the media could indeed be a cause of lower capability of regeneration.

Finally, we tested a floral dip approach (first published by Clough & Bent, 1998, which was proven to work in *B. napus* by some labs: Li Juan et al., 2010; Shaohong et al., 2005; Verma et al., 2008).

First, based on Hu et al., 2019, we performed a morphological analysis at the stereomicroscope to understand the stage of the flowers competent for the transformation. Indeed, in Arabidopsis, it is described as the pistil should be still open at the moment of the transformation in order for *Agrobacterium* to reach the female gametophyte (Desfeux et al., 2000), which is the target of the transformation (Bechtold et al., 2000; Desfeux et al., 2000; Ye et al., 1999).

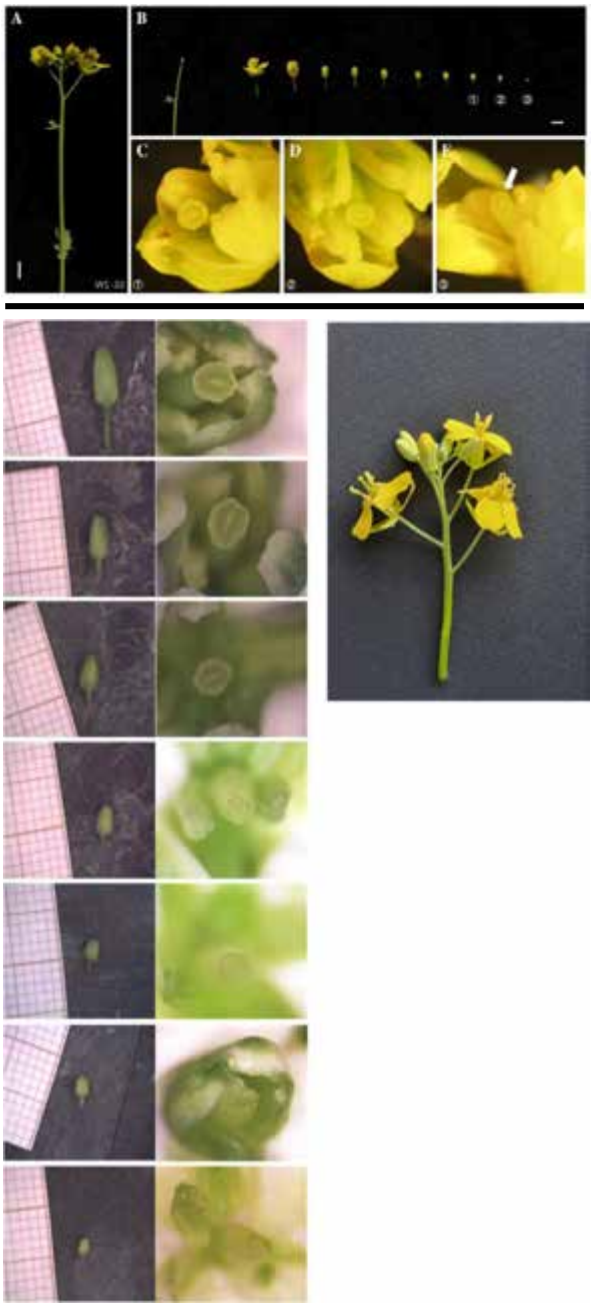

Fig. 29. Microscopical analysis. Above: from Hu et al, 2019, *B. rapa* flower morphology. The arrow points the unsealed carpel. Below: *B. napus* flower morphology. In smaller flowers the carpel is undeveloped, but we couldn't see a clear opening.

During this analysis, we could differentiate various stages of pistil development, but a clear opening at the edge couldn't be detected (Fig. 29). To get better clues, we decided to analyse sections of paraffin-embedded flowers.

By analysing the sections, we could state that the pistil is still open in flowers smaller than 0.5 mm and that therefore this is the size of the flowers where the bacterium can autonomously reach the developing ovule (Fig. 30).

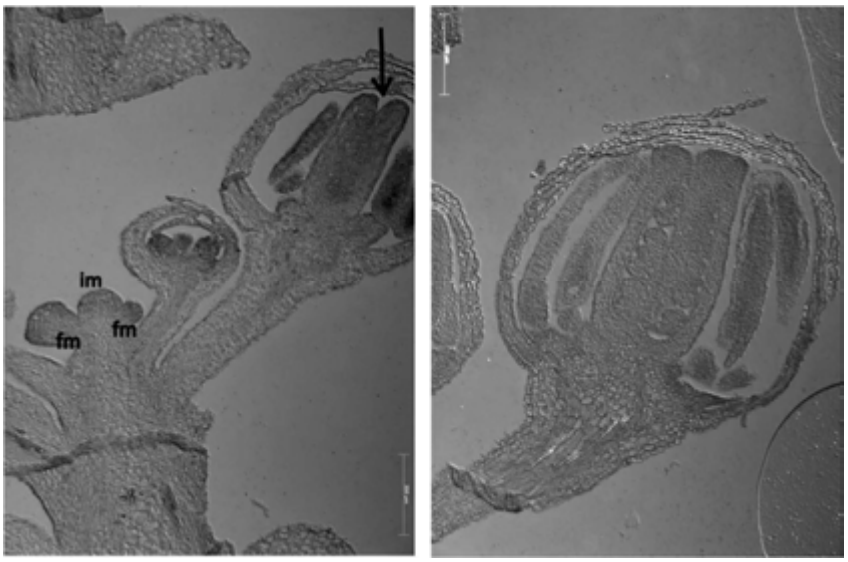

Fig. 30. Analysis of the paraffin included sections. Scale bar 50 µm. Left: unsealed carpel (arrow); right, sealed carpel. IM= inflorescence meristem; FM= floral meristem.

However, as it is also published in *Lisianthus* the possibility of transforming the developed embryo (F. Fang et al., 2018; Xu et al., 2008) and in tomato the obtainment of transformants by injecting *Agrobacterium* directly in the pistil lumen regardless its development stage (Sharada et al., 2017), we decided to target closed flowers both smaller and bigger than 0.5 mm to increase our possibility of success.

Following a deep literature research, we selected the conditions to test the protocol.

Just summarizing the most important steps, we used the GV3101 strain according to Verma et al, 2008; Hu et al, 2019 (plus, it is the strain we routinely use for Arabidopsis floral dip), we composed our transformation buffer according to Verma et al, 2008; Hu et al, 2019 and Shaohong et al, 2008, we kept the transformed flowers humid according to Verma et al, 2008 and we performed multiple transformations every 2-3 days according to Shaohong et al, 2008.

We tried both to pour the *Agrobacterium* suspension on the inflorescences and to directly inject it in closed flowers. Since the carpel is expected to be closed in most of the flowers, during the injection we meant to make a hole in the carpel so that *Agrobacterium* could have reached the ovules.

We tested the 35S:RFP and the CRISPR (no gRNA) plasmids. As a control of the plasmids, we transformed them in Arabidopsis and we successfully got transformants.

The screening for possibly transformed *Brassica* seeds was performed by testing two protocols: seed soaking, according to Juan Li et al., 2010 and *in vitro* screening (Verma et al., 2008 and Shaohong et al., 2008).

For the in vitro screening, different MS (1/2, full MS) and kanamycin concentrations (50-100-150-200 mg/L) were tested. As we didn't have *Brassica*'s positive controls which are resistant to kanamycin, we aimed to select the best condition efficiently selecting WT *Brassica*'s seeds, but avoiding increasing too much the antibiotic selection, to not loose potential transformants (the literature gave hints on the concentration where is reasonable to stop).

Moreover, we used resistant and WT Arabidopsis seeds as an additional control, to get an additional hint of the best conditions. However, what works for Arabidopsis can be not functional in *Brassica napus* and viceversa.

The best condition for the in vitro selection was selected on the response of Arabidopsis WT and resistant plants as well as *Brassica* WT plantlets and selected to be 50-100 mg/L of kanamycin of full MS medium, for 2-4 weeks.

The soaking screening was performed according to Juan li et al., 2010 by a 24 h soaking in 300 mg/L kanamycin. The method was not working for Arabidopsis seeds, which, therefore couldn't be used as positive control.

Both methods resulted in being only partially able to select WT plants and, therefore, would have required handling with escapes. Similar problems in kanamycin screening are reported by Shaohong et al., 2008 in *B. napus* and by Hu et al, 2019 in the close species *B.rapa*. This is even emphasized in our case, as we couldn't compare the WT plants with a positive control.

During the screening of transformed *Brassica* seeds, the non-transformants are supposed to be bleached by kanamycin, while the resistants are supposed to maintain fully green leaves. According to these expected results, the greener plants were analysed for the presence of visual marker (RFP in 35S:RFP transformation trial, GFP in CRISPR plasmid transformation trial) but none of them was transformed.

We tested around 300 seeds with no success. Even if in *B. napus* these numbers should have been high enough to get some transformants, (1.86% transformation efficiency Verma et al, 2008; 1-1.34% Shaohong et al, 2008; 2-3% Juan li et al,2010) more seeds could have been screened for precaution, as for other species the method is published to be less efficient (e.g 0.1% *B. rapa*, Hu et al, 2019; 0.25-0.5% in tomato, Sharada et al 2017; 0.2-2.9% Lisianthus, Fang et al, 2018).

However, given the high amount of work required for screening the dip-derived seeds, the expected low efficiency, and the lack of a control, we decided to focus our attention on the *in vitro* transformation protocol.

As the transformation appeared hard to achieve in our laboratory, we looked for an experienced lab where to learn it. We found support in Robert Sablowski's lab (Jhon Innes Centre-JIC, GB), where *B. oleracea* transformation had already been accomplished once, even if never in *B. napus*. Indeed, often, the same protocols are published to work in both

species. Moreover, a Brassica transformation platform operates in the same institute (BRACT facility, driven by Penny Hundleby), which kindly supplied us with its protocols.

Despite the publications, at the JIC the protocols used for the transformation of the two species are different. B. oleracea transformation is routinely performed with cotyledons (Hundleby Née Sparrow & Irwin, 2015; Hundleby & Chhetry, 2020), while a hypocotyl-based protocol resulted to be more efficient for *B. napus* (even if a *B. napus* internal protocol based on Hundleby and Chhtery, 2020 is available at JIC).

Importantly, at the JIC we could add to our experimental plan a positive control plasmid proved to efficiently work in *B. napus* (pGGG 35S:GUS, kindly supplied by Mark Smedley, BRACT) and scale up the transformation according to the space availability in the growing chamber of the platform. Moreover, they suggested adding an additional control to our transformation, that is, transformed explants but grown in no selection. This, compared to the transformed (and selected) samples and the not transformed (and no selected ones), can differentiate between errors in the media and the effect of the *Agrobacterium* infection.

We tested the transformation of our final PTG BnaREM34 and PTG BnaREM35-36-37 constructs in both *B. napus* (*Westar*; cotyledons and hypocotyl methods) *and B. oleracea* (*DH1012*; cotyledons).

Indeed, we retrieved the *B. oleracea* homolog sequences from Ensembl plants (BOL, INSDC Assembly GCA_000695525.1, May 2014) and revealed that our gRNAs could have efficiently targeted them, too. *B. oleracea* could have been a B plan where to establish the gene function in case we couldn't have had any mutants in *B. napus*. Moreover, as it is diploid and the number of candidates is lower (Fig. 31), the mutants' generation could have been faster.

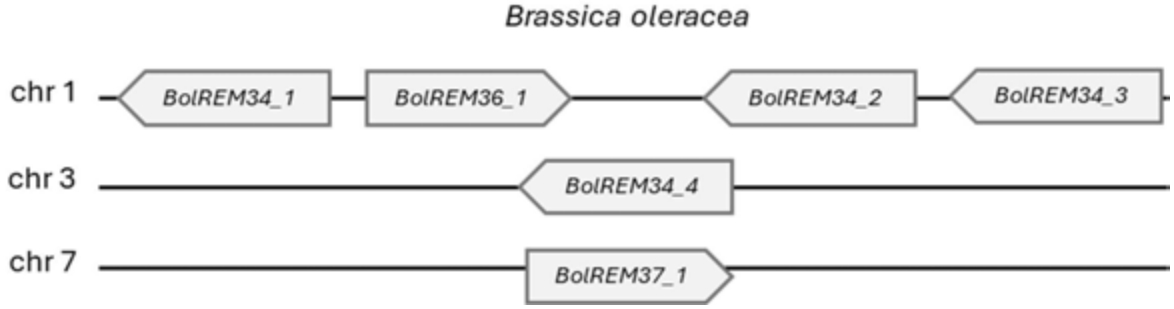

Fig 31. *Brassica oleracea* cluster of *REM34*, *REM35*, *REM36* and *REM37* homologs. Bol, REM, homolog number, successive number.

After having performed several transformation trials, we pointed out that the age of the explants is very critical in the cotyledon method, for both *Brassica napus* and *oleracea*.

Even stratifying the seeds to optimize germination or growing them for 1 day more or in the wrong light conditions can strongly affect the regeneration of the transformed explants.

Plus, the positioning of the explant in the media had to be perfect. Indeed, if the cotyledon itself and not only the petiole touches the medium, it absorbs the medium, just enlarges and doesn't regenerate (as also stated in Hundleby Née Sparrow & Irwin, 2015). Even using

new blades to get the explants is a good suggestion, as it produces more defined cuts (also highlighted in Hundleby Née Sparrow & Irwin, 2015), and reduces the handling time of the explants.

The final conditions by which we got transformants with the GUS control plasmid, were based on Hundleby and Chhtery with some tips. Seeds were stored in the fridge, directly sown on germination media and grown in scattered low light (30 µmol/m^2/s for 4 days for *Bol* and *Bna*). New blades were used to explant the cotyledons and just the petiole was implanted in the media. The right size of the cotyledons, meaning the good one to get regenerants and transformants, is 6-7 mm in width. If the cotyledons fell on the media during the whole culturing process, a lot of attention was kept bringing them back upright in order to not affect the regeneration potential. The cotyledons were cultured in scattered low light during the process (30 µmol/m^2/s).

Under these conditions, we managed to get GUS transformants in both *B. oleracea* and *napus*, but the efficiency was very low. If in *napus,* we were warned about it by the BRACT platform, we expected a transformation percentage of 25% for *oleracea* (on Hundleby and Chhtery, 2020), which we didn't get. This points out that this method is very challenging, and a lot of expertise is needed to achieve good results.

Moreover, no transformants were obtained using our construct, which probably is not as efficient as the plasmid containing GUS that was used as control. A graphical representation of the results obtained in *B. oleracea* and *B. napus* transformed at the JIC by the CRISPR constructs, by the cotyledon method, is depicted in fig. 32.

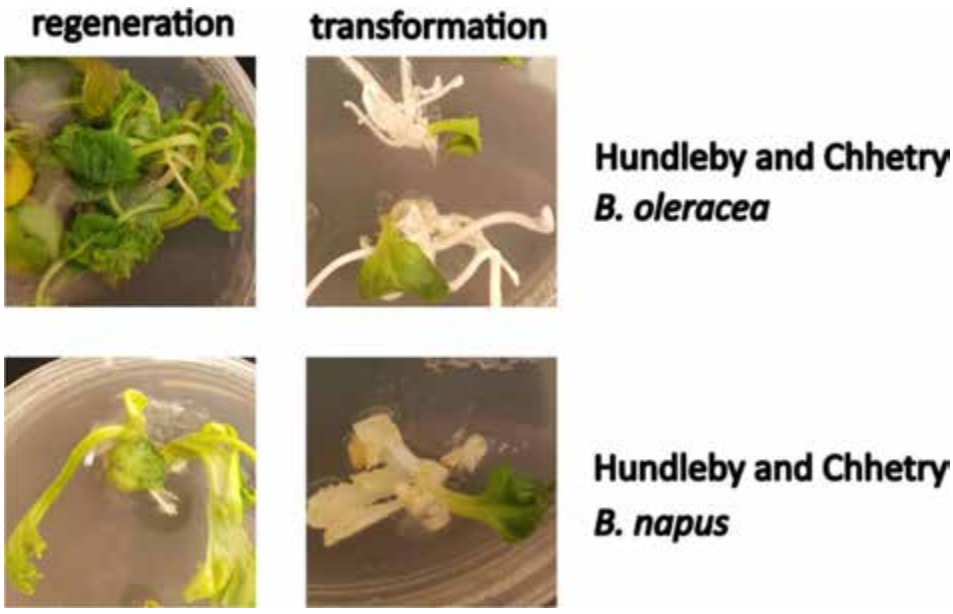

Fig. 32. Graphical summary of the results of the JIC cotyledons transformations by CRISPR constructs. *B. oleracea* and *B. napus* were transformed by a protocol based on Hundleby and Chhtery . We were able to regenerate plants but not to transform them (just bleached, non-transformed regenerants could be observed). Few transformants were obtained by the pGGG:GUS control construct (not shown).

We further tested the hypocotyl protocol for *B. napus* (internal protocol of the BRACT platform, kindly supplied by them). The protocol is based on Liu et al., 2014, with few modifications.

In this case, we just stored the seeds in the fridge and strictly followed the protocol.

After three rounds of regeneration medium (6 weeks, that is from when transformants are expected to show up), in the controls without selection, all the explants showed green calli and 34% of the explants had produced plants (this is, therefore, the regeneration potential we got with this protocol, even if some more plants can emerge later). The growth on the no-selection medium of transformed and not-transformed explants didn't have a difference in the regeneration potential, showing that the explants can recover from the stress of the infection and co-cultivation.

Analysing the transformation itself, in the pGGG:GUS transformed petri 114 explants out of 133 showed green calli (86%), while only 33 out of 406 (8%) and 52 out of 470 (11%) did it in the CRISPR_BnaREM34 and in CRISPR_BnaREM35-36-37 transformed petri. This definitely shows the low efficiency of transformation of our construct compared to the control and the need to work with a high number of explants to get transformants. A graphical representation of the results obtained at the JIC by the hypocotyl protocol can be found in fig. 33.

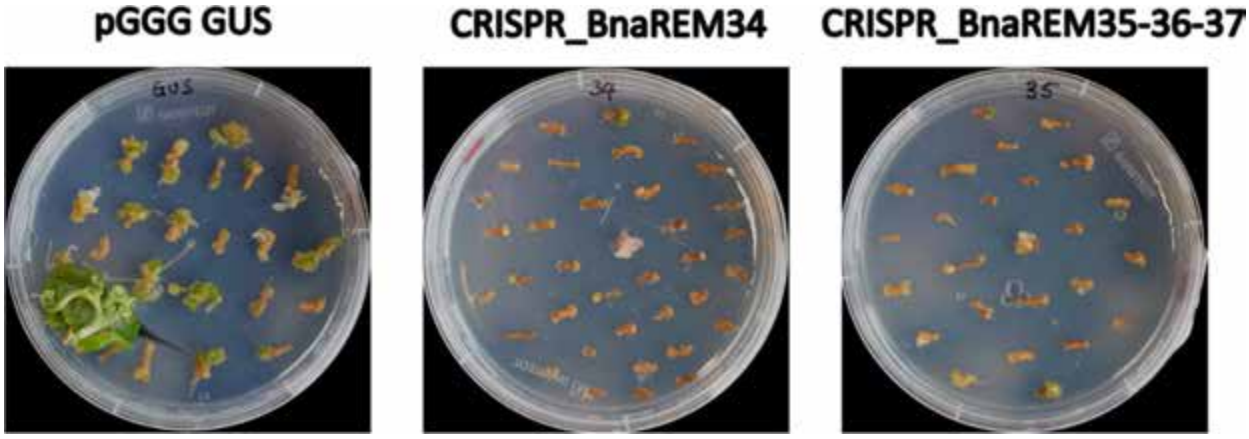

Fig. 33. Graphical summary of the results of the JIC *B. napus* hypocotyls transformation. The amount of green (possibly transformed) calli is representative of the transformation efficiency of the constructs. In the images can be visualized as the pGGG:GUS control construct is much more efficient than the CRISPR one. This points out the need of a high amount of starting material to get transformants by our CRISPR construct.

At the same stage, we could observe 2 green plants (out of 133 explants, 1.15%) in the GUS-transformed explants, 2 in CRISPR_BnaREM34 (out of 406 explants, 0.49%) and 4 in CRISPR_BnaREM35-36-37 (out of 470 explants, 0.85%). This can give an idea of the regeneration potential of the transformed calli, which is quite low in this protocol. However, plants are known to appear from the 6th week of regeneration and possibly continuously emerge for a long time.

At the end of the whole process we got 4 plants transformed by CRISPR_BnaREM34 and 4 by CRISPR_BnaREM35-36-37 (Fig. 34). 2 more plants never made roots and 1 died.

The final efficiency for the CRISPR construct was therefore 1.68% (number of green plants by initial number of explants, efficiency got by combining the 2 CRISPR constructs).

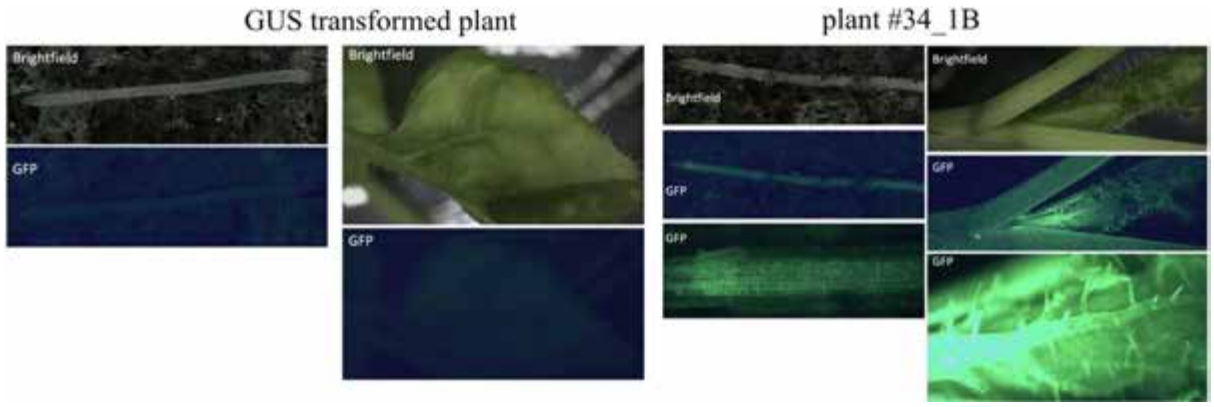

Fig 34. Transformation confirmation. GUS plants was the positive control for the transformation, but is expected to be GFP negative. 34_1B express GFP. Roots and shoot are visualized.

We then screened all the target sequences of the gRNAs cloned in the constructs according to the specificity of the sequence (meaning that the gRNA perfectly matches the genomic DNA, without mismatches). Indeed, if the gRNA didn't edit a specific gene in the protoplast transient assay, it still might have done it in a stable transformant, where the editing machine is constitutively expressed. In total, 10 gRNAs loci were screened for the CRISPR_BnaREM34 transformants, and 4 for CRISPR_BnaREM35-36-37, but no edits were found.

2 loci for the second group, on *BnaREM37A1* gene, could never be amplified neither in WT plants, and new primers should be tested. However, we think that according to the other results, it is not likely that we will find edits there.

The functionality of the editing machine should be tested in planta to understand what can explain these results in order to improve them. For example, the Cas9 and gRNAs cassette expression should be tested first, as well as the gRNAs splicing from the tRNAs in the PTG construct.

Nevertheless, the lack of mutations in our transformants could be just a matter of efficiency, as also in literature, the editing frequency reported is often quite low (eg in Westar 15% edited plants in Huang et al., 2020, who uses PTG system as we are doing; 15-20% in Sriboon et al., 2020; 5% in Okuzaki et al., 2018).

3.4 Summary of the results

In the second part of this thesis, the editing trial we performed with the aim to develop higher yield genotypes by mutating the homologs of *REM34*, *REM35*, *REM36* and *REM37* in *B. napus*, is detailed.

gRNAs were designed and tested by protoplast destructive assay. The most efficient were then cloned in poly t-RNA gRNA constructs according to the mutants we want to obtain and the linkage context of the genes. 3 constructs were designed and 2 of them were cloned and tested during this thesis.

The *Agrobacterium* transformation was selected as the method to develop the mutants, and many published protocols were tested. However, a spread inefficiency and high technical requirements were detected in our experiments.

We were able to get CRISPR transformants by a hypocotyl method based on Liu et al., 2014, even if at a low efficiency. The parallel transformation of a control construct additionally pointed out the inefficiency of our CRISPR construct itself. Among the 8 transformants we successfully regenerated and rooted, unfortunately, none of them was edited.

Conclusion and future perspectives

The sustainable growth of the population without exacerbating humanity's environmental impact stands as a paramount challenge of the century. Addressing the need to enhance food production without expanding agricultural land requires a focus on increasing crop yields.

As a feature of the inflorescence architecture, phyllotaxis can offer a pathway to manipulate that yield.

This thesis reports the reliability of this hypothesis, unclosing novel Arabidopsis genotypes characterized by altered phyllotaxis and a heightened number of siliques. Double mutants in *REM34*, *REM35*, and *REM36* show a remarkable enhancement of the siliques produced on the main stem, yielding approximately 20% more than the wild type.

Importantly, the mutants maintain a consistent number of seeds per silique, indicating their potential to substantially increase seed production.

In the era of the *de-novo* design of varieties, we think that applying translational biology to get similar phenotypes in relevant crops can be of high value.

Brassica napus is phylogenetically close to *Arabidopsis thaliana* and this can make the genetic results easily transferable.

It's the third oil-producing plant in the world following palm and soybean, and it is the first in Europe (oilseed and protein crops production, European Commission, 2022 data; Consumption of vegetable oils worldwide from 2013/14 to 2022/2023, by oil type, M. Shahbandeh, Sep 20, 2023; statista.com). Even if mainly used for food processing, it has many other industrial uses, such as biofuel production, making it a strategic crop for both the food industry and the bioeconomy.

The number of siliques, together with parameters such as the number of seeds per silique and 1000-seed weight, determines the yield in *Brassica napus* (P. Yang et al., 2012). Moreover, considering the current rapeseed high planting density, the yield of the main inflorescence has the main impact, contributing up to 73% of the whole plant yield (Yuan et al., 2022).

For all these reasons, generating *B. napus* mutants similar to those described for Arabidopsis would be of considerable interest.

Applying the workflow described in the introduction, we first used deep phylogenetic analysis to get the high-confidence homologous gene in this species. Then, we studied their conservation by gene expression analysis, interspecific complementation and protein interaction experiments. This analysis was designed to get the final target genes for a multiplex editing strategy. Indeed, by this preliminary analysis, we aimed to uncover possible neo and sub-functionalization as well as expression divergence, to possibly help narrowing down the gene pool to be targeted in *B. napus*.

In detail, we first studied the *REM IX* gene family in the species, highlighting the phylogenetical relationships between *Arabidopsis thaliana, Arabidopsis lyrata, Brassica napus, Brassica rapa* and *Brassica oleracea* homologs. Subsequently, we focused on the

homologs of our genes of interest, expanding the analysis to *REM37* given its phylogenetic proximity and possible redundancy.

We identified six homologous genes for *AtREM34*, two for *AtREM35* and *AtREM36* and two for *AtREM37*. These findings can be explained by accounting for both *Brassica* genome evolution and ploidy, as well as the *REM IX* class recent duplications.

All but one of the 10 candidate genes are expressed in the inflorescence and floral tissues, with a pattern that highly resemble the Arabidopsis one (Caselli et al., 2019; Mantegazza et al., 2014) and is compatible with an involvement in the inflorescence architecture.

The genes of the two sub-genomes code for very similar protein and could be hypothesized to have the same function because the event of hybridization is recent. Therefore, the analysis of the protein function was performed on 4 candidates of the subgenome A.

The interspecific complementation test suggests a functional conservation of the *Brassica* proteins and further support the hypothesis of the involvement of *BnaREM* genes in phyllotaxis determination.

Finally, the protein interaction tests performed revealed conserved as well as new REM dimers formation in *B. napus* and opened the possibility that a REM-ARF interaction can be involved in inflorescence development as it has been recently described in Arabidopsis (Caselli et al, under revision).

Building upon these results, we designed a gene editing strategy to obtain both single and multiple homologs mutants in *B. napus*. We rationalized the gRNAs design to possibly get multiple mutants by the same gRNA, and we tested their functionality in a protoplast assay. Even if it revealed a generally low activity of the machinery in *Brassica napus* protoplast, it enabled us to select at least one gRNA per gene, which proved to be functional *in vivo* but not for *BnaREM34C3*. In this case, a new gRNA was designed.

To obtain the actual mutants we designed poly-tRNA-gRNA cassettes with 4-6 gRNA stacked according to the mutants we want to obtain and the linkage relation of our targets, and we cloned them in a CRISPR vector.

Last, to introduce the editing machinery in the plant, we used an *Agrobacterium* mediated strategy. The results we got point out that this transformation technique is suboptimal in *Brassica napus* and many published protocols require a lot of expertise to be applied successfully.

Moreover, the actual editing often has a low efficiency (in *Westar* variety; this thesis, Huang et al., 2020; Okuzaki et al., 2018; Sriboon et al., 2020), and therefore many transformation trials are needed to obtain mutants.

In our case, we generated 8 viable transformants but no edits were observed. Even if we should check the good expression of the editing machinery *in planta*, we can hypothesize that the number of events we got is just not enough to detect mutations.

Given the polyploidy and high redundancy of the genome in *Brassica napus*, the use of random mutagenesis and natural variation to breed new varieties can be incredibly time-consuming. Therefore, to optimize the tools we have for a reverse genetic approach and rational design of the new genotypes is a milestone.

Specifically, getting transformation protocols of good efficiency that can be genotype independent, as well as optimize the CRISPR-mediated editing in the species, are relevant aspects to be taken into account.

Co-transformation with meristematic genes such as *BBM* and *WUS*, as well as other genes published to impact transformants regeneration as well as editing efficiency (Che et al., 2022; Lee et al., 2022; Lian et al., 2022; Lin et al., 2023; Wang et al., 2023 and reviewed in Z. Chen et al., 2022), have the potential to provide improved results and should be tested in *Brassica napus*. However, given the pleiotropic effects of these genes, strategies to remove them after the obtainment of the transformant already in T0 should be accounted (eg. using inducible promoters to express the "helper genes" only when needed and/or using recombinase or cutting systems to remove them after the regeneration and editing events, or just transiently transforming them).

Overall, this application-driven study describes the impact of some *REM* genes on flower production and studies the possibility of producing similar higher-yield genotypes in the crop *Brassica napus*, in the context of a translational biology approach.

Material and Methods

1. Plant material and growth conditions

Arabidopsis thaliana Col-0 and *Brassica napus* plants were grown under long-day conditions, with 16h of light/8h dark, at 22°C.

Brassica napus transformants at JIC, when completely rooted, were grown in long-day conditions (16/8) at 18 °C/12 °C (day/night).

The conditions of the growing chamber used for the *in vitro* protocols were: in Milan, 22-25°C, long day conditions (16/8), light 20-30 µmol/m^2*s; at the JIC, 22°C, long day (16/8), full light at 45 µmol/ m^2*s light, scattered light at 30 µmol/ m^2*s.

Dim light was applied by wrapping the petri/boxes with dark but partially transparent papers.

rem34, rem35, rem36 and the double mutants were previously generated in the lab. The obtainment of *rem34*, *rem35* and *rem34 rem35* is described in Caselli et al., under revision and Caselli PhD thesis. *rem36* was generated following the protocol published by Fauser et al., 2014. The protospacer sequence (GTGATCTGACGAAAAAAGGT) was selected with the aid of the CRISPR-P 2.0 software (http://crispr.hzau.edu.cn/CRISPR2). The resulting mutation is a T insertion, which falls into the first B3 DNA binding domain, causing a frameshift and the formation of an early stop codon in position aa31. *rem34 rem36* and *rem35 rem36* double mutants were generated by re-transforming single mutants, as the in-linkage position of the genes makes unlikely the generation of higher-order mutants by crossing. The re-transformation gave the same edit obtained in the single mutants.

2. Phyllotactic pattern measurement and yield analysis

The phyllotactic pattern was measured as described before (A Peaucelle et al., 2007, Caselli et al., under revision) on the main inflorescence of 2-month-old plants using a 3D clockwise protractor. The first 3 cm of the stem were not considered because elongation is incomplete in this region. The divergence angle was measured by evaluating the insertion point of the two successive floral pedicels. The clockwise or anticlockwise orientation of the phyllotaxis was determined by following the direction that gives the smallest average divergence angle.

The yield analysis was performed by counting the number of siliques produced on the main inflorescence of completely developed plants (spent IM).

The number of seeds per silique was counted in green but completely elongated siliques. The siliques were opened by a needle following the replum and maturing seeds were counted by aid of a stereomicroscope.

Kruskal-Wallis and Dunn's post hoc test were used to evaluate the significance of the results, according to the normality and homoscedasticity of the data (GraphPad Prism).

3. Bioinformatic analysis

3.1 Homology and phylogenetic analysis

The homologous sequence identification was performed by querying proteomes databases from Ensembl plants by Jackhmmer, and the resultant sequences were filtered to retain only those with a minimum sequence identity of 40%. Specifically, for the *REM IX* clade homology

analysis, all the *REM IX* Arabidopsis genes were used to query the *Brassica napus* proteome. To narrow down and fine tune the results, then *AtREM34, AtREM35, AtREM36* and *AtREM37* were used to query *Arabidopsis lyrata*, *Brassica oleracea, Brassica rapa* and *Brassica napus* proteomes.

The homologous sequences obtained were aligned by Clustal Omega 1.2.4 (default parameters) and their phylogenetic relationships were inferred by RAxML-NG with the WAG+G substitution model (50 bootstrap replicates).

The conserved protein motifs were identified by MEME tool and integrated in the phylogenetic tree, visualized by ETE toolkit.

3.2 Protein identity and similarity analysis

The *Arabidopsis* protein sequences were recovered from TAIR (Araport11_genome_release), and the *napus* ones from Ensembl plants, *Brassica napus* genome annotation AST_PRJEB5043_v1, INSDC Assembly GCA_000751015.1, Sep 2014.

To get the protein sequence similarity, a multiple sequence alignment was performed by BLAST. The gap cost was lowered to a minimum to permit the whole protein alignment.

4. Gene expression analysis in *Brassica napus*

4.1 qPCR

RNA was extracted from *Brassica napus* tissues using the LiCl method (Verwoerd et al., 1989). For each sample, 500 ng of RNA was retro-transcribed using iScript kit (BioRad). qRT-PCR assay was performed using iTaq Universal SYBR Green supermix (BioRad) in a Bio-Rad iCycler iQ Optical System (software version 3.0a). Three biological replicates, with three technical replicates for each sample, were analysed.

The relative transcript enrichment of the targets of interest was calculated by normalizing the amount of mRNA against the *ACTIN-7* transcript (NCBI reference sequence NM_001316010.1). The expression of the genes was calculated using the $2^{-\Delta\Delta Ct}$ method. The primers employed for qPCR are listed in appendix table 1.

4.2 *In situ* hybridization

The apical part of the inflorescences, containing the reproductive meristems and early stages of flower development, were fixed in FAA (50% ethanol, 5% acetic acid, 3.7% formaldehyde) under vacuum for 15 min, dehydrated in ethanol and bioclear (Bioptica) and embedded in Paraplast Plus (Sigma-Aldrich). *In situ* hybridization was performed as previously described (Coen et al., 1990) with slight modifications. Digoxigenin-labelled antisense probes were synthesized with T7 RNA polymerase (Promega) and tested by dot blot.

The specificity of the signal was assessed by hybridizing the same type of tissues with the sense probe (Appendix Fig A1).

Slides were imaged with the aid of a Zeiss Axiophot® microscope equipped with differential interference contrast (DIC) optics.

Primers employed for probe synthesis are listed in appendix.

5. Complementation test

The CDS of 4 of the *Brassica napus* candidate genes were cloned from *Brassica napus* cDNA samples in p207 pDONR vector by BP Gateway reaction and were subsequently cloned in the pDEST vector pB2GW7 by LR Gateway reaction.

The constructs were transformed in *Agrobacterium tumefaciens* GV3101 and subsequently in the homolog Arabidopsis mutants by floral dip. The expression of the construct was tested in T1 inflorescences. RNA extraction and qPCR were performed as described above. Relative transcript enrichment of the targets of interest was calculated by normalizing the amount of mRNA against the *RCE1* ubiquitin-like transcript (*AT4G36800*). Expression of the genes was calculated using the $2^{-\Delta\Delta Ct}$ method, using the Wild Type as a normalizer.

The T2 was used for the phenotype complementation analysis, after having applied a BASTA (phosphinothricin) selection to remove the WT segregating plants. The phyllotactic pattern, specifically the percentage of angles falling in the 130°-150° range (around the golden angle, according to the precision of the instrument used), was analysed to evaluate the phenotype complementation.

ANOVA and post-hoc tests were run by GraphPad Prism and were used to evaluate the statistical significance of the results ($p<0.05$). Specifically, according to the normality and homoscedasticity of the data, ANOVA and Dunnett's test were used for the *rem35* and *rem36* complementation, and Kruskall Wallis and Dunn's test for *rem34* one. The post hoc test was run vs the WT and vs the *rem* mutant of control.

The primers used for cloning and for the expression analysis are listed in Appendix.

6. Protein interaction test

6.1 Yeast-2-Hybrid (Y2H)

The coding sequences of the genes of interest were cloned in the GAL4 system Gateway vectors (pGADT7 and pGBKT7; Clontech Laboratories, Inc.) by LR recombination (from the p207-derived Entry vector described above). The Y2H constructs for AtREM34, AtREM35, AtARF19 and AtARF7 were already available in the lab (Caselli et al, under revision).

The pGADT7 derived vectors were transformed in the AH109 strain, and the pGBKT7 derived ones in the Y187 strain. Yeast transformation was performed as described by de Folter & Immink, 2011. Mating between the two strains produced diploid genotypes producing both the proteins.

The protein-protein interaction assays were performed on selective yeast synthetic dropout medium lacking Leu, Trp, His and Ade and if needed, supplemented with different concentrations of 3-aminotriazole (3-At; 0-100 mM). Plates were grown for 3-5 days at 28°C.

AtREM35-AtREM35 and AtREM34-AtREM34 were used respectively as positive and negative controls (Caselli et al, 2019).

6.2 Bimolecular fluorescence complementation (BiFC)

The same CDS used for Y2H were cloned from the p207 derived entry vectors in pYFPN43 and pYFPC43 by LR gateway reaction and the resulting constructs were transformed *in Agrobacterium tumefaciens* GV3101. The interactions were tested by co-infiltrating the

abaxial surface of *Nicotiana benthamiana* leaves with the viral suppressor p19K construct. After 3 days, interactions were visualized by Laser Scanning Confocal Microscope Nikon A1 (laser emission 488 nm, YFP fluorescence collection between 500 and 550 nm, chlorophyll autofluorescence collection 660-740 nm). As positive control, AtREM35 homodimerization was tested, while AtREM34 homodimerization was used as negative control (Caselli et al, 2019), coupled with p19K only infiltration.

7. Editing design and transformation

7.1 gRNA design

To design the gRNAs, the CRISPOR web tool was used (Concordet and Haeussler, 2018) and the *Brassica napus* v2.0 (*Brassica napus* NCBI GCF_000686985.2 - 2017) and SpCas9 were selected.

To get KO, the gRNAs were designed on the first exons, and the predicted efficiency of the gRNA when U6 driven and the probability it has to generate indels were accounted (data found on CRISPOR).

At least 3 gRNAs possibly editing each (expressed) gene with no mismatches, were designed. Some gRNAs presented as off-targets the genes of interest, even increasing the probability of generating mutants. gRNAs possibly editing more than one of our genes of interest were considered of relevant value, as they could open the possibility of generating not-that-cumbersome poly-tRNA-gRNA cassettes.

7.2 gRNA test by protoplast destructive assay

7.2.1 gRNA synthesis

The sgRNAs were synthesized by the EnGen sgRNA Synthesis Kit, S. pyogenes Protocol (NEB#E3322). After DNase I treatment, the resulting sgRNAs were purified following the RNeasy kit - RNA cleanup procedure from Qiagen.

7.2.2 Protoplast destructive assay

Protoplast transfection by RNPs was performed according to Murovec et al., 2018 with slight modifications.

B. napus protoplasts were recovered from leaf mesophyll cells. They were released by a O/N enzymatic digestion of the cell wall (no vacuum applied, incubation in dark) and filtered by a 50 µm sieve. After that, they were washed by three subsequent centrifugation and resuspension steps in W5 medium (2 mM MES pH 5.7, 154 mM NaCl, 125 mM CaCl2, 5 mM KCl) and then purified by a density gradient centrifugation according to the protocol.

Viable protoplasts were recovered from the interface layer and resuspended W5 medium. Their density was calculated by a haemocytometer and adjusted to 0.5×10^6 /ml.

For each gRNA the RNP suspension was prepared by mixing 4 µg of sgRNA with 10 µg of Cas9 from *S. pyogenes* (NEB #M0386T) (in a 3.74 molar ratio) 1X NEBuffer™ r3.1. The mix was incubated 15 min before the use, according to the protocol.

125000 protoplasts per transfection were moved to a tube and resuspended by MMG solution, keeping the same protoplast concentration.

PEG solution and DNA were added (40 µg of a GFP reporter as a positive control, 4 µg of oligos + 10 µg Cas9) and mixed well. After 20 min incubation, 1 volume of W5 solution was added twice to stop the reaction. The protoplasts were centrifuged, resuspended in CPP medium and incubated in the dark.

After O/N incubation, the fluorescence of the reporter was analysed to check the transfection efficiency. After 2 O/N, DNA was recovered and subsequently analysed. The surroundings of the gRNAs target sites were amplified by specific primers and sequenced. The ratio between the mutated reads and the total aligned reads gave the gRNAs editing efficiency.

7.3 CRISPR construct cloning

The gRNA cassette was designed to contain an AtU6 promoter, a poly-tRNA-gRNA structure with 4-6 gRNAs, and a U6 terminator. Moreover, attL Gateway-compatible tails were designed at the borders. The cassette synthesis was accomplished by GeneWiz (Azenta). The company furnishes the cassette cloned in pUC vector. The cassette was cloned in the CRISPR construct by LR recombination (Gateway system).

7.4 *Brassica* transformation

7.4.1 Plasmids and bacterial strains

During the optimization of the *Brassica* transformation, the following plasmids were used: 35S:RFP in pGWB2 backbone (kanamycin resistance both in bacterium and in planta); DII:VENUS in pIPK0002 backbone (kindly provided from Dr. Raffaella Battaglia, CREA, spectinomycin resistance in bacterium, hygromycin in planta), our CRISPR/Cas9-vector (pBIN plus derived; kanamycin resistance both in bacterium and in planta); pGGG 35S:GUS plasmid (kindly provided from the BRACT platform, JIC, Norwich; kanamycin resistance both in bacterium and in planta). pGGG 35S:GUS needs co-transformation with pSOUP in *Agrobacterium*. The CRISPR vector gave very low bacterial growth, which was improved in Agrobacterium by pSOUP co-transformation. Therefore, co-transformed colonies were used in plant transformations.

Specifically, in Bhalla, Moloney and Maheshwari based trials, we used the base CRISPR vector with no gRNAs cloned, but only REM34 CDS with no promoter just to remove the ccdB cassette. In JIC trials, the final CRISPR vector including the gRNA cassette was ready and therefore was used for the transformation.

During the transformation trials, several *Agrobacterium* strains were used: GV3101, EHA105 and AGL1.

7.4.2 Bhalla trial

The first trial of transformation and regeneration was performed according to Bhalla & Singh, 2008.

In the case of the transformation, 35S:RFP, DII:VENUS and CRISPR constructs were tested in GV3101 or EHA105 *Agrobacterium* strain.

Minor modifications were applied to the protocol. We sterilized the seeds with washes in EtOH 70% and SDS 0.1% (10 min, shaking) and EtOH 100% (10 min, shaking). We stratified the seeds for 2 days and then grew them in dim light for 6 days. A complete overview of the media and timings used can be found in Table A1.

7.4.3 Moleney-based trial

The protocol used was based on Moloney et al., 1989 with branched conditions as detailed in the main text.

Additional minor modifications were applied. Sterilization was performed as described above (Bhalla trial); to facilitate excision and to reduce plant stress, we germinated the seeds in Magenta boxes and we added acetosyringone 200 µM in *Agrobacterium* resuspension media and co-cultivation media to boost infection.

During the plant regeneration steps, we used surgical tape to cover the plates and we transferred the explants to fresh media every 2 weeks to maintain the antibiotic selection pressure (Bhalla et al, 2008).

A complete overview of the media and timings used can be found in Table A1.

7.4.4 Maheshwari trial

The protocol used was based on the best conditions published by Maheshwari et al., 2011. We introduced the same modifications described above (Moloney-based trial) and removed $AgNO_3$ from co-cultivation media as it inhibits *Agrobacterium* growth (Gyves et al., 2010).

A complete overview of the media and timings used can be found in Table A1.

7.4.5 Optimization of vitrification recovery and rooting

The recovery of vitrified plants was accomplished as suggested by De Block et al, 1989, by culturing them in half MS with no vitamins and reduced sugar, cytokinins and carbenicillin (1,1 g/L MS without vitamins, 1% sucrose, 0.5% phytoagar, 2.5 µg/L BAP, 100 mg/L carbenicillin, as in table A1).

To optimize the rooting step, we tested different concentrations of NAA according to Maheshwari and got good rooting efficiency from 0.1 mg/L of NAA. The complete rooting medium is depicted in Table A1.

7.4.6 Floral dip

The protocol was set up after a deep literature analysis and was applied as follows.

Multiple colonies of transformed GV3101 were cultured in LB supplied with antibiotics for 24 h at 28°C. The culture was refreshed and cultured O/N (the OD reached values between 0.6 and 4). Cells were pelleted for 15 min at 4000 rpm and resuspended in 5% sucrose, 1.1 g/L MS without vitamins, 0.05% Silwet-77, and 200 µM acetosyringone (Hu et al., 2019; Shaohong et al., 2005; Verma et al., 2008) to reach an OD between 0.8 and 2(Hu et al., 2019; Verma et al., 2008).

Open flowers were removed, and transformation was performed by two methods.

Method 1: around 300 µl of Agrobacterium suspension were poured on the inflorescences and a delicate massage was performed to facilitate the entry of the solution into the floral tissues.

Method 2: The transformation suspension was injected into closed flowers using a fine needle. Since the carpel was expected to be closed in most of the flowers, during injection

we meant to make a hole in the carpel, so that Agrobacterium could have reached the ovules.

After the transformation, the treated inflorescences were immediately bagged with stretch film to maintain moisture (Verma et al., 2008). The plastic cover was removed the day after.

The procedure was repeated every 2-3 days (Shaohong et al., 2005) till competent inflorescences were present on the plants for a maximum of 4 times per inflorescence. We transformed the main inflorescence and the three upper secondary inflorescences.

To differentiate between the two transformation methods (to determine the most efficient one), the inflorescences were tagged by a thread.

7.4.7 Seeds screening

The seed soaking was performed by shaking the seeds for 24 h in a 300 mg/L kanamycin solution according to Li Juan et al., 2010.

The best condition for in vitro screening was selected to be sowing seeds on full MS (2.2 g/L MS including vitamins, Duchefa, 1% sucrose, 0.6% gelrite) supplied by 50-100 mg/L of kanamycin and growing them for 2-4 weeks in long-day conditions (16/8h), 22-25°C.

7.4.8 JIC-based trials

7.4.8.1 Cotyledon method

Brassica oleracea and *Brassica napus* cotyledons were transformed according to Hundleby & Chhetry, 2020. Some important tips are detailed in the main text.

Slight modifications were applied for *B. napus* according to the BRACT suggestions (described here below).

Germination media: 4.71 g/L MS with vitamins, sucrose 30 g/L pH 5.8, 8 g/L bactoagar.

Co-coltivation medium: MS with vitamins 4.71 g/L, sucrose 30 g/L, BAP 4 mg/L, gelrite 2.5 g/L, pH 5.8.

Selection: MS with vitamins 4.71 g/L, sucrose 30 g/L, BAP 4 mg/L, MES 500 mg/L, bactoagar 8 g/L, pH 5.8, 160 mg/L timentin.

Regeneration medium: 4.71 g/L MS with vitamins, 3% sucrose, 500 mg/L MES, pH 5.8, 4 mg/L BAP, 8 g/L bactoagar, 160 mg/L timentin, 15 mg/L kanamycin.

As no plants transformed by the CRISPR construct were obtained, we didn't root them.

A complete overview of the media and timings used can be found in Table A1.

7.4.8.2 Hypocothyl method

B. napus transformation by hypocotyl method was set up according to the BRACT internal protocol, which is based on Liu et al., 2014 with slight modifications. Seeds were sterilized by washing them in 70% EtOH for 2 min, followed by a 20 min wash in 1.5% bleach (15 ml of 10% NaClO solution, 85 ml sterile water, drop of Tween-20), shaking. Seeds were rinsed 3 times in sterile water (10 min each) before sowing. Seeds were sown in high boxes (Phytatray II), in germination medium (4.4 g/L MS with vitamins, 10 g/L glucose, 0.6 g MES, 10 g/L bactoagar, pH 5.7). 30 seeds for each box were used. They were stratified in cold and dark O/N and then germinated 6 days in dark at 22°C to allow hypocotyl elongation. Agrobacterium preparation was performed according to Hundleby & Chhetry, 2020, by inoculating 50 µL of stock previously prepared in 10 ml of MGL medium without antibiotics

and growing the culture O/N at 28°, shaking (MGL medium: Peptone from casein 5 g/L; Yeast extract 2.5 g/L;NaCl 0.1 g/L; Mannitol 5 g/L; L-glutamic acid sodium salt 1 g/L; KH2PO4 0.25 g/L; $MgSO_4$ x 7H20 0.1 g/L; Biotin (0.01 g/100 ml) 1 ml; pH 7). The bacteria were pelleted by 10 min centrifuge at 3000 rpm and resuspended in liquid MS (4.4 g/L MS, 3% sucrose pH 5.8), supplied with 100 µM acetosyringone. Hypocotyls were cut in ca 7 mm pieces in a large petri dish containing MS+3% sucrose to keep moisture. The hypocotyl explants were transferred to the Agrobacterium suspension in a deep petri, it was closed by micropore tape and shaked for 30 min. The liquid media was removed by pipetting and the explants were blot dried. When dried (but they shouldn't be left withering), they were put on co-cultivation medium for 2 days in the dark (4.4 g MS + vitamins, 3% sucrose, 1.8%mannitol, 0.6 g/L MES hydrate, pH 5.8, agarose low EEO, 1 mg/L 2.4 D, 0.3mg/L kinetin, acetosyringone 100 um), 23°C. 50 explants per high petri can be placed. After co-cultivation, the explants were moved on selection media (4.4 g MS+vitamins, 3% sucrose, 1.8%mannitol, 0.6 g/L MES hydrate, pH 5.8, agarose 7.5 g/L , 1 mg/L 2.4 D, 0.3mg/L kinetin, 20 mg/L kanamycin, 320 mg/L timentin, 150 µl/L STS (30 µL $AgNO_3$ 0.1 M + 120 µL $Na_2S_2O_3$ 0.1 M), where they were grown for 3 weeks at 23°C; long day (16/8), 45 µmol/m^2*s (from now on ca 30 explants per petri are placed). The explants were then moved to regeneration medium (4.4 g MS+vitamins, 10 g/L glucose, 0.25 g/L xylose, 0.6 g/L MES hydrate, pH 5.8, agarose 7.5, zeatin 2 mg/L, 0.1 mg/L IAA, kanamycin 25 mg/L, timentin 320 mg/L) and sub-cultured every 2 weeks for at least 3 times. In regeneration 2 the explants were cut in halves to increase the number of explants. Usually, regenerants start to appear from the end of regeneration 3. Further subcultures can bring additional regenerants.

The regenerants were moved to rooting (Gamborg's B5 medium with vitamins 3.16g/L, 1% sucrose, pH 5.8, kanamycin 25 mg/L, timentin 160 mg/L, IBA 1 mg/L) in sterile jars, previously having removed the callus material and the base of the plantlet. Roots appear in 3 weeks or longer (subcultures needed). Plants were carefully moved to the soil in closed sterile magenta before moving to the greenhouse.

A complete overview of the media and timings used can be found in Table A1. During the whole procedure, high petri dishes and micropore tape are used.

8. Microscopical analysis of *Brassica napus* flower

Before performing the floral dip, *Brassica napus* inflorescences were recovered and single flowers were dissected in order to observe if the two valves of the carpel were sealed. The carpel was observed at the stereomicroscope.

9. GUS staining

To verify the transformation by the pGGG GUS plasmid, the GUS staining was performed on calli and pieces of the leaf of the regenerants.

Tissues were fixed in 90% cold acetone, 2 h at -20°C. Acetone was removed and tissues were rinsed with 50 mM $NaPO_4$ pH 7.2, 0.5 mM $K_3Fe(CN)_6$, 0.5 mM $K_4Fe(CN)_6$ before being immersed in a staining solution. It is the same as the rinse solution added by 2mM X-Gluc (stock 100 mM in N,N Dimethylformamide). They were incubated at least O/N at 37°C. If the GUS stain was visible, the reaction was stopped, and the tissues were cleared from chlorophyll by EtOH series 15%, 30%, 50%, 70%. Prior to imaging, chloral hydrate or lactic acid clearing was performed.

10. GFP screening

To check the transformation of the plants by the CRISPR construct, they were analysed for GFP expression when they were ready to be moved to soil (in order to not contaminate them during the in vitro culture). Roots and SAM region were analysed.

The microscope used for the screening was a Leica MZIII fitted with a CoolLED pE-300 white LED Replacement Fluorescence light Source CLD300W, GFP3 (GFP for plants) filter.

Supplementary

***Brassica REMs in situ* negative control**

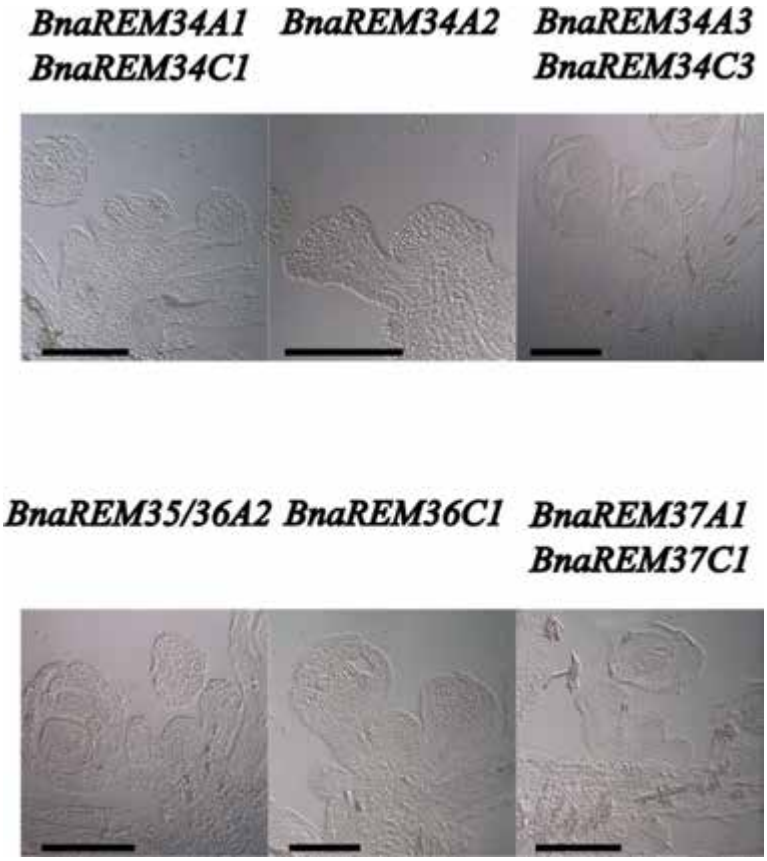

Fig. A1. *In situ* hybridization with sense probes on *Brassica napus* IM and floral tissues. Scale bar 200 µm. The absence of signal witnesses the specificity of the antisense probes.

Y2H controls

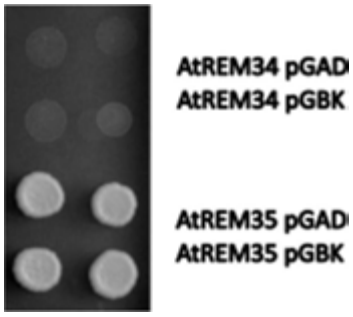

Fig. A2. Y2H controls. Selective medium lacking Adenin, Histidine, Tryptophan and Leucin. AtREM35-AtREM35 and AtREM34-AtREM34 homodimers presence and absence as in Caselli et al, 2019.

AtARF7 interactions with the REMs under investigation

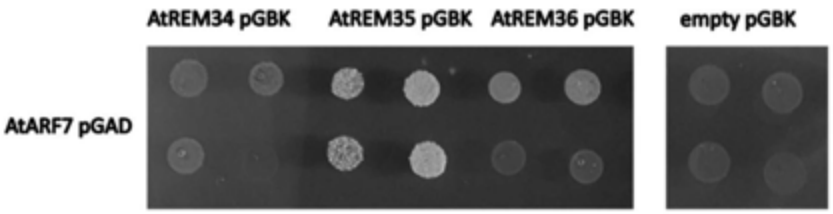

Fig. A3. AtARF7 interactions. Selective medium lacking Adenin, Histidine, Tryptophan and Leucin, 15 mM 3-At. Data from Caselli.

Transformation media and times

Table A1.1

	MEDIA					
	Bhalla based trail	**Moloney based trail**	**JIC based trail* cotyledons B.na**	**JIC based trail* cotyledons B. ol**	**Maheshwari based trail**	**JIC hypocotyl method**
explant type	napus cotyledons	napus cotyledons	napus cotyledons	oleracea cotyledons	napus hypocotyls	napus hypocotyls
Germination	1% sucrose, 2.2 g/L MS with vitamins, pH 6, 0.6% gelrite	1% sucrose, 2.2 g/L MS with vitamins, pH 6, 0.6% gelrite	4.71 g/L MS with vits, sucrose 30 g/L pH 5.8, 8 g/L bactoagar	4.41 g/L MS with vits, glucose 1%, 500 mg/L MES, pH 5.7, 10 g/L Difco bactoagar	1% sucrose, 2.2 g/L MS with vitamins, pH 6, 0.6% gelrite	4.4 g/L MS with vits, glucose 10 g/L , MES hydrate 0.6 g/L pH 5.7, 10 g/L bactoagar
Agrobacterium suspension medium	2% sucrose, 2.2 g/L MS with vitamins, pH 5.8	2.2 g/L MS with vitamins, 3% sucrose, pH 5.8, 200 uM AS	4.3 g/L MS without vitamins, 3% sucrose, pH 5.7	4.3 g/L MS without vitamins, 3% sucrose, pH 5.7	2,2, g/L MS with vitamins, 3% sucrose, pH 5.6, AS 200 um	4.4 g/L MS with vits, sucrose 30 g/L , pH 5.8, acetosyringone 100 uM
pre-coltivation medium					2,2, g/L MS with vitamins, 3% sucrose, 0.1% myo inositol, 0.25 % MES, pH 5.8, 0.8% phytoagar, 1 mg/L 2.4D, 5 mg/L AgNO3	
Co-coltivation	2.2 g/L MS with vitamins, CaCl2 1 mM, 2% sucrose, pH 5.8, 5 mg/L AgNO3, 0,75 mg/L BAP, NAA 200 ug/L, GA3 10 ug/L, gelrite 4 g/L	2.2 g/L MS with vitamins, 3% sucrose, pH 5.8, 20 uM BAP (4.5 mg/L), 0.7% phytoagar, 200 uM AS	4.71 g/L MS with vitamins, 3% sucrose, pH 5.8, 4 mg/L BAP, 2.5 g/L gelrite	4.3 g/L MS with vitamins, 3% sucrose, 500 mg/L MES, pH 5.7, 2 mg/L BAP, 8 g/L phytoagar	2,2, g/L MS with vitamins, 3% sucrose, 0.1% myo inositol, 0.25 % MES, pH 5.8, 0.8% phytoagar, 1 mg/L 2.4D, 200 uM AS (NO AgNO3)	4.4 g MS+vits, 3% sucrose, 1.8%mannitol, 0.6 g/L MES hydrate, pH 5.8, agarose low EEO, 1 mg/L 2.4 D, 0.3mg/L kinetin, acetosyringone 100 um
Callus induction	2.2 g/L MS with vitamins, CaCl2 1 mM, 2% sucrose, pH 5.8, carbenicillin 500 mg/L, NO KANA, 5 mg/L AgNO3, 0,75 mg/L BAP, NAA 200 ug/L, 10 ug/L GA3, gelrite 4 g/L				2,2, g/L MS with vitamins, 3% sucrose, 0.1% myo inositol, 0.25 % MES, pH 5.8, 0.8% phytoagar, 1 mg/L 2.4D, 5 mg/L AgNO3, 500 mg/L carbenicillin	4.4 g MS+vits, 3% sucrose, 1.8%mannitol, 0.6 g/L MES hydrate, pH 5.8, agarose 7.5 g/L , 1 mg/L 2.4 D, 0.3mg/L kinetin, 20 mg/L kana, 320 mg/L timentin, 150 ul/L STS (30 ul AgNO3 0.1 M + 120 ul Na2S2O3 0.1 M)
Regeneration (shoot indution)	2.2 g/L MS with vitamins, CaCl2 1 mM, pH 5.8, carbenicillin 500 mg/L, kana 25 mg/L, 5 mg/L AgNO3, 3 mg/L BAP, NAA 200 ug/L, 10 ug/L GA3, gelrite 4 g/L	2.2 g/L MS with vitamins, 3% sucrose, pH 5.8, 20 uM BAP (4.5 mg/L) , 500 mg/L carbenicillin, 15 mg/L kana , 0.7% phytoagar	4.71 g/L MS with vitamins, 3% sucrose, 500 mg/L MES, pH 5.8, 4 mg/L BAP, 8 g/L bactoagar, 160 mg/L timentin, 15 mg/L kana	4.3 g/L MS with vitamins, 3% sucrose, 500 mg/L MES, pH 5.7, 2 mg/L BAP, 8 g/L phytoagar, 160 mg/L timentin, 15 mg/L kana	2,2, g/L MS with vitamins, 3% sucrose, 0.1% myo inositol, 0.25 % MES, pH 5.8, 0.8% phytoagar,5 mg/L BAP, 5 mg/L AgNO3, kana 50 mg/L, carbenicillin 500 mg/L	4.4 g MS+vits, 10 g/L glucose, 0.25 g/L xylose, 0.6 g/L MES hydrate, pH 5.8, agarose 7.5, zeatin 2 mg/L, 0.1 mg/L IAA, kana 25 mg/L, timentin 320 mg/L
Shoot outgrowth	2.2 g/L MS with vitamins, CaCl2 1 mM, 2% sucrose, 40 mg/L adenine hemisulfate, 500 mg/L PVP 40.000, pH 5.8, carbenicillin 500 mg/L, kana 25 mg/L, 1.25 ug/L BAP, gelrite 4 g/L	2.2 g/L MS with vitamins, 3% sucrose, pH 5.8, (NO BAP) , 500 mg/L carbenicillin, 15 mg/L kana , 0.7% phytoagar			2,2, g/L MS with vitamins, 3% sucrose, 0.1% myo inositol, 0.25 % MES, pH 5.8, 0.8% phytoagar, 0,05 mg/L BAP, kana 50 mg/L, carbenicillin 500 mg/L	
transformant selection (escapes pruning)	2.2 g/L MS with vitamins, CaCl2 1 mM, 1%sucrose, 40 mg/L adenine hemisulfate, 500 mg/L PVP 40.000, pH 5.8, carbenicillin 500 mg/L, kana 50 mg/L, 1.25 ug/L BAP, gelrite 4 g/L					
vitrification recovery	not tested in this trial	not tested in this trial	not tested in this trial		1,1 g/L MS without vitamins, 1% sucrose, 0.5% phytoagar, 2.5 ug/L BAP, 100 mg/L carbenicillin	
rooting	not tested in this trial	not tested in this trial	not tested in this trial	not tested in this trial	2,2, g/L MS with vitamins, 3% sucrose, 0.1% myo inositol, 0.25 % MES, pH 5.8, 0.8% phytoagar, 0.1 mg/L NAA, 100 mg/L carbenicillin	Gamborg's B5 medium with vitamins 3.16g/L, 1% sucrose, pH 5.8, kana 25 mg/L, timentin 160 mg/L, IBA 1 mg/L

Table A1.1. Summary of the transformation trials media. The actual methods used are reported (in some case they have slight differences compared to the original protocol). The modifications reported in the main text refers to the protocols depicted here. All sterilization processes if not performed at the JIC were performed as follow: EtOH 70% and SDS 0.1% (10 min, shaking), EtOH 100% (10 min, shaking). The JIC sterilization method is detailed in the main text. The no transformation control wasn't infected and was cultured on the same media of the transformants, but without kanamycin. At the JIC a further control was included, with explants that were infected but grown without kanamycin selection. * Specifics that managed to give GUS transformants

Table A1.2

	TIMING					
	Bhalla based trail	**Moloney based trail**	**JIC based trail* cotyledons B.na**	**JIC based trail* cotyledons B. ol**	**Maheshwari based trail**	**JIC hypocotyl method**
explant type	napus cotyledons	napus cotyledons	napus cotyledons	oleracea cotyledons	napus hypocotyls	napus hypocotyls
Germination	stratify seeds 2 days, then grow 6d, dim light	stratify 2 days, grow 5d, full light/ dark according to the branched scheme	no stratification, 4 d. If too small, leave for other 24 h (protocol is highly stage dependent)	no stratification, 4 d	stratify seeds 2 days, grow in light/darkfor 7/10 days according to the branched scheme	1 day stratification, 6 d at dark
infection in Agrobacterium suspension and OD 600	dip petiol base; OD 0.05	dip petiol base/ 1 min full immersion of the cotyledon , OD 0.2-0.6 according to the branched scheme	dip petiol base, OD 0.1-0.3	dip petiol base, OD 0.1-0.3	5/30 min, OD 0.2-1, according to the branched scheme	30 min, OD 0.1-0.3
pre-coltivation					0/72 h, according to the branched scheme	
Co-coltivation	dim light, 2 days	3 days, light	3 days, scattered light	3 days, scattered light	3 days, dim light	2 days, dark
Callus induction	dim light, 1 week				2 weeks	3 weeks, full light
Regeneration (shoot indution)	minimum 4 weeks, subcolture every 2 weeks	minimum 2-3 weeks, till shoots emerge	minimum 4-5 weeks, subcolture every 2 weeks. scattered light	minimum 3 weeks, subcolture every 2-3 weeks. scattered light	4-6 weeks, till buds are observed. Then move the whole explant (with callus, no cuts)	minimum 6 weeks, cut in halves after 2 weeks. full light
Shoot outgrowth	2-4 weeks	1-2 weeks to establish apical dominance according to Moloney et al. Not tested as no transformed plants were recovered			minimum 2 weeks, till plants are 2-3 cm	
transformant selection (escapes pruning)	dim-light 2-3 weeks					
vitrification recovery	not tested in this trial	not tested in this trial			till recovery (minimum 2-3 weeks), light	
rooting	not tested in this trial	not tested in this trial	not tested in this trial	not tested in this trial	3-4 weeks minimum, light	3 weeks minimum, full light

Table A1.2. Summary of the transformation trials timings. The actual methods used are reported (in some case they have slight differences compared to the original protocol). The modifications reported in the main text refers to the protocols depicted here. All sterilization processes if not performed at the JIC were performed as follow: EtOH 70% and SDS 0.1% (10 min, shaking), EtOH 100% (10 min, shaking). The JIC sterilization method is detailed in the main text. The no transformation control wasn't infected and was cultured on the same media of the transformants, but without kanamycin. At the JIC a further control was included, with explants that were infected but grown without kanamycin selection. * Specifics that managed to give GUS transformants

Primers list

ID	sequence	gene ID	gene code and notes
Bna1	TAATTTCAGCCACGGAGACG	BnaREM34A1	BnaA01g34820 fw RT-PCR, sequencing gRNA1 BnaA01g34820 edits fw
Bna2	CTGCTTCTGGTTTCTCACTC	BnaREM34A1	BnaA01g34820 rv RT-PCR, sequencing gRNA1 BnaA01g34820 edits rv
Bna3	GAATGACTCATTCGTGTTGGAG	BnaREM34C1	BnaC01g06860 fw RT-PCR
Bna4	CTGTTTGAAACCCTAGTGCATC	BnaREM34C1	BnaC01g06860 rv RT-PCR
Bna5	TCTAGCCTCATCGATGATCG	BnaREM34A2	BnaA01g34830 fw RT-PCR
Bna6	CAGCCTCGTCTGATGTTAAATG	BnaREM34A2	BnaA01g34830 rv RT-PCR
Bna7	TCCAGTGACATACAACACGC	BnaREM34C2	BnaC01g06840 fw RT-PCR, sequencing gRNA4 BnaC01g06840 (not expressed) edits fw
Bna8	TCTCACACGGTTTATTGTGC	BnaREM34C2	BnaC01g06840 rv RT_PCR
Bna9	TGTATCTGTGTCCCCTCGGT	Bna34REMA3	BnaA08g30700 fw RT-PCR
Bna10	GTCATCCTCTCCTCCATCGTC	Bna34REMA3	BnaA08g30700 rv RT-PCR, sequencing gRNA23 BnaA08g30700 edits rv
Bna11	TGCTGTGAGTGATGATGAATC	BnaREM34C3	BnaC03g77300 fw RT-PCR, sequencing gRNA9 BnaC03g77300 edits fw
Bna12	GCTCATTAAACGACACAACAG	BnaREM34C3	BnaC03g77300 rv RT-PCR, sequencing gRNA9 BnaC03g77300 edits rv
Bna13	AGAGATTCGCCCGTGGATG	BnaREM37C1	BnaC07g43390 fw RT-PCR
Bna14	TCTGCTGAGTGAATCTGCGT	BnaREM37C1	BnaC07g43390 rv RT-PCR
Bna21	GGAAGCTCCTGGAATCCATGAGA	BnaACT7	actin-7 fw RT-PCR
Bna22	TCTTTGCTCATACGGTCAGCAATTCC	BnaACT7	actin-7 rv RT-PCR
Bna23	TGAAAGATGGCCGATGGTGA	BnaACT7	actin-7 fw RT-PCR + intron
Bna24	GTGCCTAGGACGACCAACAA	BnaACT7	actin-7 rv RT-PCR + intron
Bna25	CAATCTTCATCGTAGATCTGTCCG	BnaREM37A1	BnaA03g51640 fw RT-PCR new, sequencing gRNA15 BnaA03g51640 * edits fw
Bna26	ACCGAAGCGTCTGAAGTCAG	BnaREM37A1	BnaA03g51640 rv RT-PCR new
Bna27	ACGCTCACTGTCTTCGAAACG	BnaREM35/36A2	BnaA01g34850 fw RT-PCR new
Bna28	CTCAAATCTGAAACTTTGTCCCATG	BnaREM35/36A2	BnaA01g34850 rv RT-PCR new
Bna29	CAAAACCTAACAGGGCAGGC	BnaREM36C1	BnaC01g06850 fw RT-PCR new
Bna30	ATGCATGAGTACGGCGAGAG	BnaREM36C1	BnaC01g06850 rv RT-PCR new
Bna34	GGGGACAAGTTTGTACAAAAAAGCAGGCTTCATGGTGGTTCCTCCTCCAAAAC	BnaREM34A1	BnaA01g34820 fw GW for Nterm fusion
Bna35	GGGGACCACTTTGTACAAGAAAGCTGGGTCTAAACCAGATTATTGTTGAG	BnaREM34A1	BnaA01g34820 rv GW with STOP
Bna36	GGGGACAAGTTTGTACAAAAAAGCAGGCTtcATGGCGACTTCTCCAAAATCG	BnaREM35/36A2	BnaA01g34850D fw GW for Nterm fusion
Bna37	GGGGACCACTTTGTACAAGAAAGCTGGGTTTACTTGAAGAATTTGTTGAC	BnaREM35/36A2	BnaA01g34850D rv GW with STOP
Bna38	GGGGACAAGTTTGTACAAAAAAGCAGGCTtcATGGTGGATCCAGTTATGGC	BnaREM37A1	BnaA03g51640D fw GW for Nterm fusion
Bna39	GGGGACCACTTTGTACAAGAAAGCTGGGTTTAGACTTGATTGATGTTGAAG	BnaREM37A1	BnaA03g51640D rv GW with STOP
Bna40	GGGGACAAGTTTGTACAAAAAAGCAGGCTtcATGACTATTCCTCCTACATTTTC	BnaREM34A3	BnaA08g30700D fw GW for Nterm fusion, sequencing gRNA23 BnaA08g30700D edits fw
Bna41	GGGGACCACTTTGTACAAGAAAGCTGGGTTTACACCaGATTATTGTTGAG	BnaREM34A3	BnaA08g30700D rv GW with STOP
Bna42	TAATACGACTCACTATAGGG ACACCAACTCTTGTGCAGTCC	BnaREM35/36A2	BnaA01g34850D rv +T7 in situ (fw Bna27)
Bna43	TAATACGACTCACTATAGGG ACCGAAGCGTCTGAAGTCAG	BnaREM37A1	BnaA03g51640D rv +T7 in situ (fw Bna25)
Bna45	TAATACGACTCACTATAGGG TCTGCTGAGTGAATCTGCGT	BnaREM37C1	BnaC07g43390D rv +T7 in situ (fw Bna13)
Bna46	TAATACGACTCACTATAGGG CTGTTTGAAACCCTAGTGCATC	BnaREM34_1 C/A rv	BnaA01g34820/BnaC01g06860 + T7 in situ (FW Bna3)
Bna47	GAATGACTCATTCGTGTTGGAG	BnaREM34A2 fw	BnaA01g34830 fw in situ
Bna48	TAATACGACTCACTATAGGG CTGTTTAAAACCCTAGCGTGTC	BnaREM34A2 rv	BnaA01g34830 rv + T7 in situ (FW Bna47)
Bna49	TAATACGACTCACTATAGGG GTCATCCTCTCCTCCATCGTC	BnaREM34_3 A/C rv	BnaA08g30700/BnaC03g77300 + T7 in situ (FW Bna9)
Bna50	ATGGCGACTTCTCCAAAATCG	BnaREM35/36A2	BnaA01g34850D fw cloning for Nterm fusion
Bna51	TTACTTGAAGAATTTGTTGAC	BnaREM35/36A2	BnaA01g34850D rv cloning with STOP
Bna38_bis	ATGGTGGATCCAGTTATGGC	BnaREM37A1	BnaA03g51640D fw cloning for Nterm fusion
Bna39_bis	TTAGACTTGATTGATGTTGAAG	BnaREM37A1	BnaA03g51640D cloning GW with STOP
Bna52	TAATACGACTCACTATAGGG ACAGACGGCCATGTTCCTCC	BnaREM36C1	BnaC01g06850D rv +T7 in situ new (fw Bna29)
Bna54	CAATGTGAGATCGATCTAAG	BnaREM37A1	BnaA03g51640D fw internal primer
Bna55	CCAGCCATTACTGACAAATGC	BnaREM37A1	BnaA03g51640D rv internal primer
Bna61	TGGAAGCGGAAGACCTCG	BnaREM34_C/A fw	C03g77300 fw in situ - 34C3/A3 probe n2
Bna62	TAATACGACTCACTATAGGG GAATGCTCAGCTTCACGTTAG	BnaREM34_C/A rv	C03g77300 rv in situ + T7 tail (bna58 fw) 34C3/A3 probe n2
Bna63	GTCGGATGATGTAGAAGACGAAG	BnaREM34A2	BnaA01g34830D in situ probe2 fw
Bna64	TAATACGACTCACTATAGGG ACGACATAACCTTAAAATCCTC	BnaREM34A2	BnaA01g34830D in situ probe2 rv
bna68	TAATACGACTCACTATAGGG GTCGGATGATGTAGAAGACGAAG	BnaREM34_C/A2	BnaA01g34830D in situ SENSE probe2
bna69	ACGACATAACCTTAAAATCCTC	BnaREM34_C/A2	BnaA01g34830D in situ SENSE probe2
bna70	TAATACGACTCACTATAGGG TGGAAGCGGAAGACCTCG	BnaREM34_C/A3	C03g77300 fw SENSE in situ - 34C3/A3 probe n2 fw
bna71	GAATGCTCAGCTTCACGTTAG	BnaREM34_C/A3	C03g77300 rv SENSE in situ 34C3/A3 probe n2 rv
bna72	TAATACGACTCACTATAGGG GAATGACTCATTCGTGTTGGAG	BnaREM34A2	BnaA01g34830 fw SENSE in situ
bna73	CTGTTTAAAACCCTAGCGTGTC	BnaREM34A2	BnaA01g34830 rv SENSE in situ
bna74	TAATACGACTCACTATAGGG TGTATCTGTGTCCCCTCGGT	BnaREM34_C/A3	BnaA08g30700/BnaC03g77300 SENSE fw in situ
bna75	GTCATCCTCTCCTCCATCGTC	BnaREM34_C/A3	BnaA08g30700/BnaC03g77300 SENSE rv in situ
bna76	TAATACGACTCACTATAGGG GAATGACTCATTCGTGTTGGAG	BnaREM34_C/A1	BnaA01g34820/BnaC01g06860 SENSE fw in situ
bna77	CTGTTTGAAACCCTAGTGCATC	BnaREM34_C/A1	BnaA01g34820/BnaC01g06860 SENSE rv in situ
bna78	TAATACGACTCACTATAGGG ACGCTCACTGTCTTCGAAACG	BnaREM35/36A2	BnaA01g34850D SENSE fw in situ
bna79	ACACCAACTCTTGTGCAGTCC	BnaREM35/36A2	BnaA01g34850D SENSE rv in situ
bna80	TAATACGACTCACTATAGGG AGAGATTCGCCCGTGGATG	BnaREM37C1	BnaC07g43390D SENSE fw in situ
bna81	TCTGCTGAGTGAATCTGCGT	BnaREM37C1	BnaC07g43390D SENSE rv in situ
bna82	TAATACGACTCACTATAGGG CAAAACCTAACAGGGCAGGC	BnaREM36C1	BnaC01g06850D SENSE fw in situ
bna83	ACAGACGGCCATGTTCCTCC	BnaREM36C1	BnaC01g06850D SENSE rv in situ
RT 147	CTGTTCACGGAACCCAATTC	RCE1 (RUB1 CONJUGATING ENZYME 1) - UBIQUITIN L	AT4G36800 housekeeping for qPCR fw (Pribil et al, 2010; https://doi.org/10.1371/journal.pbio.1000288)
RT 148	GGAAAAAGGTCTGACCGACA	RCE1 (RUB1 CONJUGATING ENZYME 1) - UBIQUITIN L	AT4G36800 housekeeping for qPCR rv (Pribil et al, 2010; https://doi.org/10.1371/journal.pbio.1000288)
22_08288	/5AmMC6/gcagtcgaacatgtagctgactcaggtcacGGTGTACAGAGTGTAGTCC	BnaREM34A1	genomic amplification in protoplast assay
22_08306	/5AmMC6/tggatcacttgtgcaagcatcacatcgtagCCGATGAAAGCATTGAAATATAC	BnaREM34A1	genomic amplification in protoplast assay
22_08290	/5AmMC6/gcagtcgaacatgtagctgactcaggtcacTCATCTTAGGCCTCTAAAACTC	BnaREM34A2	genomic amplification in protoplast assay
22_08308	/5AmMC6/tggatcacttgtgcaagcatcacatcgtagCCGATGAAATAGTCTGATTCATG	BnaREM34A2	genomic amplification in protoplast assay
22_08297	/5AmMC6/gcagtcgaacatgtagctgactcaggtcacCCAATATGGACAGTGAGCTC	BnaREM34A3	genomic amplification in protoplast assay
22_08315	/5AmMC6/tggatcacttgtgcaagcatcacatcgtagTGCATCTGCTTCAAGGC	BnaREM34A3	genomic amplification in protoplast assay
22_08300	/5AmMC6/gcagtcgaacatgtagctgactcaggtcacTCCATCATTGTCCAGCAG	BnaREM34C1	genomic amplification in protoplast assay
22_08318	/5AmMC6/tggatcacttgtgcaagcatcacatcgtagCTACTCAGCTCTGCTCTG	BnaREM34C1	genomic amplification in protoplast assay
22_08302	/5AmMC6/gcagtcgaacatgtagctgactcaggtcacGATCCCATACTAAGACTAGACC	BnaREM34C3	genomic amplification in protoplast assay
22_08320	/5AmMC6/tggatcacttgtgcaagcatcacatcgtagGTTCATGAACTTACTAGCTGC	BnaREM34C3	genomic amplification in protoplast assay
22_08292	/5AmMC6/gcagtcgaacatgtagctgactcaggtcacGGCCTTGGAGAAGAACTG	BnaREM35/36A2	genomic amplification in protoplast assay
22_08310	/5AmMC6/tggatcacttgtgcaagcatcacatcgtagCGTCACATTATATACTATTGCTCTC	BnaREM35/36A2	genomic amplification in protoplast assay
22_08299	/5AmMC6/gcagtcgaacatgtagctgactcaggtcacCGTCTTCTCCATCAGGTTAG	BnaREM36C1	genomic amplification in protoplast assay
22_08317	/5AmMC6/tggatcacttgtgcaagcatcacatcgtagCTGTCTTGACTTGAGCATG	BnaREM36C1	genomic amplification in protoplast assay
22_08294	/5AmMC6/gcagtcgaacatgtagctgactcaggtcacGAAGATATGGTTTGGAAGTAGATG	BnaREM37A1	genomic amplification in protoplast assay
22_08312	/5AmMC6/tggatcacttgtgcaagcatcacatcgtagTGGAGCAGATCTTGAGAATAG	BnaREM37A1	genomic amplification in protoplast assay
22_08304	/5AmMC6/gcagtcgaacatgtagctgactcaggtcacGAGATGACCAGTCGCTG	BnaREM37C1	genomic amplification in protoplast assay
22_08322	/5AmMC6/tggatcacttgtgcaagcatcacatcgtagCGTGACGCTTGAATCATC	BnaREM37C1	genomic amplification in protoplast assay
22_01728	TGG AGT TCA GAC GTG TGC TCT TCC GAT CTG ATG AGT TCA TAA GTA GTC ACA C	BnaREM34C1	sequencing gRNA1 BnaC01g06860 edits fw in transformants
22_01725	ACT CTT TCC CTA CAC GAC GCT CTT CCG ATC TCT ACT GTC CCC TGC AAT C	BnaREM34C1	sequencing gRNA1 BnaC01g06860 edits rv in transformants
bna67	TCAGTGACGGAGACGTCTTG	BnaREM34A2	sequencing gRNA1 and gRNA5 BnaREM34A2 edits fw in transformants
22_1634	GTC ATG ACT ACA TCC TCC TAA TC	BnaREM34A2	sequencing gRNA1 BnaA01g34830 edits rv in transformants
22_01651	TCC ATC ATT GTC CAG CAG	BnaREM34C1	sequencing gRNA4 BnaC01g06860 edits fw in transformants
22_01730	TGG AGT TCA GAC GTG TGC TCT TCC GAT CTA TCT CAA GTG GTG CGT TC	BnaREM34C1	sequencing gRNA4 BnaC01g06860 edits rv in transformants
22_01630	GTC TTG AAA CGG CTT GGT	BnaREM34C2	sequencing gRNA4 BnaC01g06840 (not expressed) edits rv in transformants
22_1634	GTC ATG ACT ACA TCC TCC TAA TC	BnaREM34A2	sequencing gRNA5 BnaA01g34830 edits rv in transformants
24_00118	ACATAAGTCACCACGCGTC	BnaREM34A3	sequencing gRNA9 BnaA08g30700 edits fw in transformants
24_00119	AACCCATTAGCGGAGCAGA	BnaREM34A3	sequencing gRNA9 BnaA08g30700 edits rv in transformants
24_00120	GGTGATGGGTTGTTTGATCGTT	BnaREM34C3	sequencing gRNA23 BnaC03g77300 edits fw in transformants
22_01738	TGG AGT TCA GAC GTG TGC TCT TCC GAT CTC TTA CCT GCG TCG TCA TC	BnaREM34C3	sequencing gRNA23 BnaC03g77300 edits rv in transformants
22_01743	ACT CTT TCC CTA CAC GAC GCT CTT CCG ATC TTG TCG AAG AAG AGA GCA AG	BnaREM37C1	sequencing gRNA14 and gRNA15 BnaC07g43390 edits fw in transformants
24_00109	AGCTCACGTCCCTTCATGTT	BnaREM37C1	sequencing gRNA14 and gRNA15 BnaC07g43390 edits rv in transformants
22_01642	CAA CTT TCT TTA TGC CAT TGG	BnaREM37A1	sequencing gRNA14 BnaA03g51640 edits fw and *gRNA15 BnaA03g51640 rv* in transformants
22_01699	ACT CTT TCC CTA CAC GAC GCT CTT CCG ATC TGT GAG ATC GAT CTA AGA GAC G	BnaREM37A1	sequencing gRNA14 BnaA03g51640 edits rv in transformants
22-01692	TGG AGT TCA GAC GTG TGC TCT TCC GAT CTT CAG GAT TAT ATG CGT GGT G	BnaREM35/36A2	sequencing gRNA18 BnaA01g34850Dedits fw in transformants
22_01695	ACT CTT TCC CTA CAC GAC GCT CTT CCG ATC TCA TGT AAG GCT TCA AGG TTA C	BnaREM35/36A2	sequencing gRNA18 BnaA01g34850D edits rv in transformants
22_01721	ACT CTT TCC CTA CAC GAC GCT CTT CCG ATC TTC ACC GAA GAA GAG ATC AAG	BnaREM36C1	sequencing gRNA20 BnaC01g06850 edits fw in transformants
24_00113	CCTGACCAGTCCCTTTGTT	BnaREM36C1	sequencing gRNA20 BnaC01g06850 edits rv in transformants

* managed to amplify the WT genomic DNA once, but the PCR needs to be oprimized as often failed. New primers design is recommended

Bibliography

Adler, I., Barabe, D., & J E A N †, R. V. (1997). A History of the Study of Phyllotaxis. In *Annals of Botany* (Vol. 80).

Babula-Skowrońska, D., Ludwików, A., Cieśla, A., Olejnik, A., Cegielska-Taras, T., Bartkowiak-Broda, I., & Sadowski, J. (2015). Involvement of genes encoding ABI1 protein phosphatases in the response of Brassica napus L. to drought stress. *Plant Molecular Biology*, *88*(4–5), 445–457. https://doi.org/10.1007/S11103-015-0334-X/FIGURES/9

Bainbridge, K., Guyomarc'h, S., Bayer, E., Swarup, R., Bennett, M., Mandel, T., & Kuhlemeier, C. (2008). Auxin influx carriers stabilize phyllotactic patterning. *Genes & Development*, *22*(6), 810–823. https://doi.org/10.1101/GAD.462608

Barabé, D., & Lacroix, C. (2020). Phyllotactic patterns: A multidisciplinary approach. *Phyllotactic Patterns: A Multidisciplinary Approach*, 1–273. https://doi.org/10.1142/11571/ASSET/18EE2C74-0218-E2C7-4021-EE2C7440218E/11571.COVER.JPG

Bartlett, M. E., & Thompson, B. (2014). Meristem identity and phyllotaxis in inflorescence development. *Frontiers in Plant Science*, *5*(OCT), 1–11. https://doi.org/10.3389/fpls.2014.00508

Bartrina, I., Otto, E., Strnad, M., Werner, T., & Schmülling, T. (2011). Cytokinin regulates the activity of reproductive meristems, flower organ size, ovule formation, and thus seed yield in Arabidopsis thaliana. *Plant Cell*, *23*(1), 69–80. https://doi.org/10.1105/tpc.110.079079

Bechtold, N., Jaudeau, B., Jolivet, S., Maba, B., Vezon, D., Voisin, R., & Pelletier, G. (2000). The maternal chromosome set is the target of the T-DNA in the in planta transformation of Arabidopsis thaliana. *Genetics*, *155*(4), 1875–1887. https://doi.org/10.1093/genetics/155.4.1875

Besnard, F., Refahi, Y., Morin, V., Marteaux, B., Brunoud, G., Chambrier, P., Rozier, F., Mirabet, V., Legrand, J., Lainé, S., Thévenon, E., Farcot, E., Cellier, C., Das, P., Bishopp, A., Dumas, R., Parcy, F., Helariutta, Y., Boudaoud, A., … Vernoux, T. (2014). Cytokinin signalling inhibitory fields provide robustness to phyllotaxis. *Nature*, *505*(7483), 417–421. https://doi.org/10.1038/nature12791

Beyer, E. M. (1976). A potent inhibitor of ethylene action in plants. *Plant Physiology*, *58*(3), 268–271. https://doi.org/10.1104/PP.58.3.268

Bhalla, P. L., & Singh, M. B. (2008). Agrobacterium-mediated transformation of Brassica napus and Brassica oleracea. *Nature Protocols*, *3*(2), 181–189. https://doi.org/10.1038/nprot.2007.527

Bichet, A., Desnos, T., Turner, S., Grandjean, O., & Höfte, H. (2001). BOTERO1 is required for normal orientation of cortical microtubules and anisotropic cell expansion in Arabidopsis. *The Plant Journal : For Cell and Molecular Biology*, *25*(2), 137–148. https://doi.org/10.1046/J.1365-313X.2001.00946.X

Bowers, J. E., Chapman, B. A., Rong, J., & Paterson, A. H. (2003). Unravelling angiosperm genome evolution by phylogenetic analysis of chromosomal duplication events. *Nature*, *422*(6930), 433–438. https://doi.org/10.1038/NATURE01521

Braatz, J., Harloff, H. J., Mascher, M., Stein, N., Himmelbach, A., & Jung, C. (2017). CRISPR-Cas9 Targeted Mutagenesis Leads to Simultaneous Modification of Different Homoeologous Gene Copies in Polyploid Oilseed Rape (Brassica napus). *Plant Physiology*, *174*(2), 935. https://doi.org/10.1104/PP.17.00426

Braybrook, S. A., & Peaucelle, A. (2013). Mechano-Chemical Aspects of Organ Formation in Arabidopsis thaliana: The Relationship between Auxin and Pectin. *PLOS ONE*, *8*(3), e57813. https://doi.org/10.1371/JOURNAL.PONE.0057813

Burk, D. H., & Ye, Z. H. (2002). Alteration of oriented deposition of cellulose microfibrils by mutation of a katanin-like microtubule-severing protein. *The Plant Cell*, *14*(9), 2145–2160. https://doi.org/10.1105/TPC.003947

Cardoza, V., & Stewart, C. N. (2003). Increased Agrobacterium-mediated transformation and rooting efficiencies in canola (Brassica napus L.) from hypocotyl segment explants. *Plant Cell Reports*, *21*(6), 599–604. https://doi.org/10.1007/s00299-002-0560-y

Caselli, F., Beretta, V. M., Mantegazza, O., Petrella, R., Leo, G., Guazzotti, A., Herrera-Ubaldo, H., de Folter, S., Mendes, M. A., Kater, M. M., & Gregis, V. (2019). REM34 and REM35 Control Female and Male Gametophyte Development in Arabidopsis thaliana. *Frontiers in Plant Science*, *10*(October), 1–17. https://doi.org/10.3389/fpls.2019.01351

Caselli, F., Zanarello, F., Kater, M. M., Battaglia, R., & Gregis, V. (2020). Crop reproductive meristems in the genomic era: A brief overview. *Biochemical Society Transactions*, *48*(3), 853–865. https://doi.org/10.1042/BST20190441

Cavell, A. C., Lydiate, D. J., Parkin, I., Dean, C., & Trick, M. (1998). Collinearity between a 30-centimorgan segment of Arabidopsis thaliana chromosome 4 and duplicated regions within the Brassica napus genome. *Https://Doi.Org/10.1139/G97-097*, *41*(1), 62–69. https://doi.org/10.1139/G97-097

Chalhoub, B., Denoeud, F., Liu, S., Parkin, I. A. P., Tang, H., Wang, X., Chiquet, J., Belcram, H., Tong, C., Samans, B., Corréa, M., Da Silva, C., Just, J., Falentin, C., Koh, C. S., Le Clainche, I., Bernard, M., Bento, P., Noel, B., … Wincker, P. (2014). Early allopolyploid evolution in the post-neolithic Brassica napus oilseed genome. *Science*, *345*(6199), 950–953. https://doi.org/10.1126/science.1253435

Che, P., Wu, E., Simon, M. K., Anand, A., Lowe, K., Gao, H., Sigmund, A. L., Yang, M., Albertsen, M. C., Gordon-Kamm, W., & Jones, T. J. (2022). Wuschel2 enables highly efficient CRISPR/Cas-targeted genome editing during rapid de novo shoot regeneration in sorghum. *Communications Biology 2022 5:1*, *5*(1), 1–11. https://doi.org/10.1038/s42003-022-03308-w

Chen, M. K., Wilson, R. L., Palme, K., Ditengou, F. A., & Shpak, E. D. (2013). ERECTA family genes regulate auxin transport in the shoot apical meristem and forming leaf

primordia. *Plant Physiology*, *162*(4), 1978–1991. https://doi.org/10.1104/PP.113.218198

Chen, X., Tong, C., Zhang, X., Song, A., Hu, M., Dong, W., Chen, F., Wang, Y., Tu, J., Liu, S., Tang, H., & Zhang, L. (2021). A high-quality Brassica napus genome reveals expansion of transposable elements, subgenome evolution and disease resistance. *Plant Biotechnology Journal*, *19*(3), 615–630. https://doi.org/10.1111/PBI.13493

Chen, Z., Debernardi, J. M., Dubcovsky, J., & Gallavotti, A. (2022). Recent advances in crop transformation technologies. *Nature Plants 2022 8:12*, *8*(12), 1343–1351. https://doi.org/10.1038/s41477-022-01295-8

Cheng, Y., Dai, X., & Zhao, Y. (2007). Auxin Synthesized by the YUCCA Flavin Monooxygenases Is Essential for Embryogenesis and Leaf Formation in Arabidopsis. *The Plant Cell*, *19*(8), 2430–2439. https://doi.org/10.1105/TPC.107.053009

Clough, S. J., & Bent, A. F. (1998). Floral dip: A simplified method for Agrobacterium-mediated transformation of Arabidopsis thaliana. *Plant Journal*, *16*(6), 735–743. https://doi.org/10.1046/j.1365-313X.1998.00343.x

Coen, E. S., Romero, J. M., Doyle, S., Elliott, R., Murphy, G., & Carpenter, R. (1990). floricaula: A homeotic gene required for flower development in antirrhinum majus. *Cell*, *63*(6), 1311–1322. https://doi.org/10.1016/0092-8674(90)90426-F

Concordet, J. P., & Haeussler, M. (2018). CRISPOR: intuitive guide selection for CRISPR/Cas9 genome editing experiments and screens. *Nucleic Acids Research*, *46*(W1), W242–W245. https://doi.org/10.1093/NAR/GKY354

Conti, L. (2017). Hormonal control of the floral transition: Can one catch them all? *Developmental Biology*, *430*(2), 288–301. https://doi.org/10.1016/J.YDBIO.2017.03.024

Cui, R., Feng, Y., Yao, J., Shi, L., Wang, S., & Xu, F. (2023). The transcription factor BnaA9.WRKY47 coordinates leaf senescence and nitrogen remobilization in Brassica napus. *Journal of Experimental Botany*, *74*(18), 5606–5619. https://doi.org/10.1093/JXB/ERAD282

De Block, M., De Brouwer, D., & Tenning, P. (1989). Transformation of Brassica napus and Brassica oleracea Using Agrobacterium tumefaciens and the Expression of the bar and neo Genes in the Transgenic Plants . *Plant Physiology*, *91*(2), 694–701. https://doi.org/10.1104/pp.91.2.694

de Folter, S., & Immink, R. G. H. (2011). Yeast Protein–Protein Interaction Assays and Screens. In *Methods in molecular biology (Clifton, N.J.)* (Vol. 754, pp. 145–165). https://doi.org/10.1007/978-1-61779-154-3_8

Delourme, R., Falentin, C., Fomeju, B. F., Boillot, M., Lassalle, G., André, I., Duarte, J., Gauthier, V., Lucante, N., Marty, A., Pauchon, M., Pichon, J. P., Ribière, N., Trotoux, G., Blanchard, P., Rivière, N., Martinant, J. P., & Pauquet, J. (2013). High-density SNP-based genetic map development and linkage disequilibrium assessment in Brassica napus L. *BMC Genomics*, *14*(1), 1–18. https://doi.org/10.1186/1471-2164-14-120

Desfeux, C., Clough, S. J., & Bent, A. F. (2000). Female reproductive tissues are the primary target of Agrobacterium-mediated transformation by the Arabidopsis floral-dip method. *Plant Physiology*, *123*(3), 895–904. https://doi.org/10.1104/pp.123.3.895

Doench, J. G., Fusi, N., Sullender, M., Hegde, M., Vaimberg, E. W., Donovan, K. F., Smith, I., Tothova, Z., Wilen, C., Orchard, R., Virgin, H. W., Listgarten, J., & Root, D. E. (2016). Optimized sgRNA design to maximize activity and minimize off-target effects of CRISPR-Cas9. *Nature Biotechnology 2015 34:2*, *34*(2), 184–191. https://doi.org/10.1038/nbt.3437

Douady, S., & Couder, Y. (1992). Phyllotaxis as a physical self-organized growth process. *Physical Review Letters*, *68*(13), 2098. https://doi.org/10.1103/PhysRevLett.68.2098

Douady, S., & Couder, Y. (1996a). Phyllotaxis as a Dynamical Self Organizing Process Part I: The Spiral Modes Resulting from Time-Periodic Iterations. *Journal of Theoretical Biology*, *178*(3), 255–273. https://doi.org/10.1006/JTBI.1996.0024

Douady, S., & Couder, Y. (1996b). Phyllotaxis as a Dynamical Self Organizing Process Part II: The Spontaneous Formation of a Periodicity and the Coexistence of Spiral and Whorled Patterns. *Journal of Theoretical Biology*, *178*(3), 275–294. https://doi.org/10.1006/JTBI.1996.0025

Douady, S., & Couder, Y. (1996c). Phyllotaxis as a Dynamical Self Organizing Process Part III: The Simulation of the Transient Regimes of Ontogeny. *Journal of Theoretical Biology*, *178*(3), 295–312. https://doi.org/10.1006/JTBI.1996.0026

Duarte, J. M., Cui, L., Wall, P. K., Zhang, Q., Zhang, X., Leebens-Mack, J., Ma, H., Altman, N., & DePamphilis, C. W. (2006). Expression pattern shifts following duplication indicative of subfunctionalization and neofunctionalization in regulatory genes of Arabidopsis. *Molecular Biology and Evolution*, *23*(2), 469–478. https://doi.org/10.1093/MOLBEV/MSJ051

Fang, F., Oliva, M., Ehi-Eromosele, S., Zaccai, M., Arazi, T., & Oren-Shamir, M. (2018). Successful floral-dipping transformation of post-anthesis lisianthus (Eustoma grandiflorum) flowers. *Plant Journal*, *96*(4), 869–879. https://doi.org/10.1111/tpj.14076

Fang, J. (2024). Breeding 4.0: The Breeding Revolution of Genetic Information Integration and Editing. *Molecular Plant Breeding*, *15*(0), 15–26. https://doi.org/10.5376/MPB.2024.15.0003

Fauser, F., Schiml, S., & Puchta, H. (2014a). Both CRISPR/Cas-based nucleases and nickases can be used efficiently for genome engineering in Arabidopsis thaliana. *Plant Journal*, *79*(2), 348–359. https://doi.org/10.1111/tpj.12554

Fauser, F., Schiml, S., & Puchta, H. (2014b). Both CRISPR/Cas-based nucleases and nickases can be used efficiently for genome engineering in Arabidopsis thaliana. *Plant Journal*, *79*(2), 348–359. https://doi.org/10.1111/tpj.12554

Franco-Zorrilla, J. M., Cubas, P., Jarillo, J. A., Fernández-Calvín, B., Salinas, J., & Martínez-Zapater, J. M. (2002). AtREM1, a member of a new family of B3 domain-

containing genes, is preferentially expressed in reproductive meristems. *Plant Physiology*, *128*(2), 418–427. https://doi.org/10.1104/pp.010323

Franco-Zorrilla, J. M., López-Vidriero, I., Carrasco, J. L., Godoy, M., Vera, P., & Solano, R. (2014). DNA-binding specificities of plant transcription factors and their potential to define target genes. *Proceedings of the National Academy of Sciences of the United States of America*, *111*(6), 2367–2372. https://doi.org/10.1073/pnas.1316278111

Friml Jiri, Yang Xiong, Michniewicz Marta, Weijers Dolf, Q. A. and T. O. (2004). *A PINOID-dependent binary switch in apical-basal PIN polar targeting directs auxin efflux*. Science(Vol. 306, Issue 5697). https://doi.org/10.1126/science.1100618

Galvan-Ampudia, C. S., Cerutti, G., Legrand, J., Brunoud, G., Martin-Arevalillo, R., Azais, R., Bayle, V., Moussu, S., Wenzl, C., Jaillais, Y., Lohmann, J. U., Godin, C., & Vernoux, T. (2020). Temporal integration of auxin information for the regulation of patterning. *ELife*, *9*, 1–65. https://doi.org/10.7554/eLife.55832

Gälweiler, L., Guan, C., Müller, A., Wisman, E., Mendgen, K., Yephremov, A., & Palme, K. (1998). Regulation of polar auxin transport by AtPIN1 in Arabidopsis vascular tissue. *Science (New York, N.Y.)*, *282*(5397), 2226–2230. https://doi.org/10.1126/SCIENCE.282.5397.2226

Giulini, A., Wang, J., & Jackson, D. (2004). Control of phyllotaxy by the cytokinin-inducible response regulator homologue ABPHYL1. *Nature*, *430*(7003), 1031–1034. https://doi.org/10.1038/NATURE02778

Godin, C., Golé, C., & Douady, S. (2020). Phyllotaxis as geometric canalization during plant development. *Development (Cambridge)*, *147*(19). https://doi.org/10.1242/dev.165878

Gomes, G. L. B., & Scortecci, K. C. (2021). Auxin and its role in plant development: structure, signalling, regulation and response mechanisms. *Plant Biology*, *23*(6), 894–904. https://doi.org/10.1111/PLB.13303

Gómez-Campo, C., & Prakash, S. (1999). 2 Origin and domestication. *Developments in Plant Genetics and Breeding*, *4*(C), 33–58. https://doi.org/10.1016/S0168-7972(99)80003-6

Gómez-Mena, C., de Folter, S., Costa, M. M. R., Angenent, G. C., & Sablowski, R. (2005). Transcriptional program controlled by the floral homeotic gene AGAMOUS during early organogenesis. *Development*, *132*(3), 429–438. https://doi.org/10.1242/DEV.01600

Gregis, V., Andrés, F., Sessa, A., Guerra, R. F., Simonini, S., Mateos, J. L., Torti, S., Zambelli, F., Prazzoli, G. M., Bjerkan, K. N., Grini, P. E., Pavesi, G., Colombo, L., Coupland, G., & Kater, M. M. (2013). Identification of pathways directly regulated by SHORT VEGETATIVE PHASE during vegetative and reproductive development in Arabidopsis. *Genome Biology 2013 14:6*, *14*(6), 1–26. https://doi.org/10.1186/GB-2013-14-6-R56

Guilfoyle, T. J., & Hagen, G. (2007). Auxin response factors. *Current Opinion in Plant Biology*, *10*(5), 453–460. https://doi.org/10.1016/J.PBI.2007.08.014

Gulden, R. H., Warwick, S. I., & Thomas, A. G. (2008). The Biology of Canadian Weeds. 137. Brassica napus L. and B. rapa L. *Canadian Journal of Plant Science*, *71*(3), 885–886. https://doi.org/10.4141/cjps91-129

Gyves, E. M., Enea, M., & Fabrizio, P. (2010). Inhibition of Agrobacterium tumefaciens Growth by Silver Nitrate. *Int J Plant Dev Biol*, *4*(1), 64–67.

Henchion, M., Moloney, A. P., Hyland, J., Zimmermann, J., & McCarthy, S. (2021). Review: Trends for meat, milk and egg consumption for the next decades and the role played by livestock systems in the global production of proteins. *Animal*, *15*, 100287. https://doi.org/10.1016/j.animal.2021.100287

Heo, J. B., Sung, S., & Assmann, S. M. (2012). Ca2+-dependent GTPase, Extra-large G Protein 2 (XLG2), Promotes Activation of DNA-binding Protein Related to Vernalization 1 (RTV1), Leading to Activation of Floral Integrator Genes and Early Flowering in Arabidopsis. *The Journal of Biological Chemistry*, *287*(11), 8242. https://doi.org/10.1074/JBC.M111.317412

Hofmeister W. (1868). Allgemeine morphologie der gewachse. In *Bary A, Irmisch TH, Sachs J (eds) Handbuch der physiologischen botanik*. (p. pp 405–664). https://books.google.it/books?hl=it&lr=&id=9sY_AAAAYAAJ&oi=fnd&pg=PA405&ots=mTzrGv0Iy2&sig=Z5G1u3V6vSrgaAatgZuzSoQP2xI&redir_esc=y#v=onepage&q&f=false

Hu, D., Bent, A. F., Hou, X., & Li, Y. (2019). Agrobacterium-mediated vacuum infiltration and floral dip transformation of rapid-cycling Brassica rapa. *BMC Plant Biology*, *19*(1), 1–9. https://doi.org/10.1186/s12870-019-1843-6

Huang, H., Cui, T., Zhang, L., Yang, Q., Yang, Y., Xie, K., Fan, C., & Zhou, Y. (2020). Modifications of fatty acid profile through targeted mutation at BnaFAD2 gene with CRISPR/Cas9-mediated gene editing in Brassica napus. *Theoretical and Applied Genetics*, *133*(8), 2401–2411. https://doi.org/10.1007/s00122-020-03607-y

Hundleby Née Sparrow, P. A. C., & Irwin, J. A. (2015). Brassica oleracea and B. napus. *Methods in Molecular Biology (Clifton, N.J.)*, *1223*, 287–297. https://doi.org/10.1007/978-1-4939-1695-5_23

Hundleby, P., & Chhetry, M. (2020). Brassica oleracea Transformation. In *Genetic Transformation in Crops*. IntechOpen. https://doi.org/10.5772/INTECHOPEN.93570

Ikeda, K., Nagasawa, N., & Nagato, Y. (2005). ABERRANT PANICLE ORGANIZATION 1 temporally regulates meristem identity in rice. *Developmental Biology*, *282*(2), 349–360. https://doi.org/10.1016/J.YDBIO.2005.03.016

Ikeda-Kawakatsu, K., Maekawa, M., Izawa, T., Itoh, J. I., & Nagato, Y. (2012). ABERRANT PANICLE ORGANIZATION 2/RFL, the rice ortholog of Arabidopsis LEAFY, suppresses the transition from inflorescence meristem to floral meristem through interaction with APO1. *The Plant Journal : For Cell and Molecular Biology*, *69*(1), 168–180. https://doi.org/10.1111/J.1365-313X.2011.04781.X

Itoh, J. I., Hibara, K. I., Kojima, M., Sakakibara, H., & Nagato, Y. (2012). Rice DECUSSATE controls phyllotaxy by affecting the cytokinin signaling pathway. *The Plant Journal*, *72*(6), 869–881. https://doi.org/10.1111/J.1365-313X.2012.05123.X

Jacobs, M., & Ray, P. M. (1976). Rapid Auxin-induced Decrease in Free Space pH and Its Relationship to Auxin-induced Growth in Maize and Pea. *Plant Physiology*, *58*(2), 203. https://doi.org/10.1104/PP.58.2.203

Kaufmann, K., Wellmer, F., Muiño, J. M., Ferner, T., Wuest, S. E., Kumar, V., Serrano-Mislata, A., Madueño, F., Kraiewski, P., Meyerowitz, E. M., Angenent, G. C., & Riechmann, J. L. (2010). Orchestration of floral initiation by APETALA1. *Science (New York, N.Y.)*, *328*(5974), 85–89. https://doi.org/10.1126/SCIENCE.1185244

Ki, D., Sasayama, D., & Cho, H. T. (2016). The M3 Phosphorylation Site Is Required for Trafficking and Biological Roles of PIN-FORMED1, 2, and 7 in Arabidopsis. *Frontiers in Plant Science*, *7*(September2016). https://doi.org/10.3389/FPLS.2016.01479

Kishi-Kaboshi, M., Aida, R., & Sasaki, K. (2019). Parsley ubiquitin promoter displays higher activity than the CaMV 35S promoter and the chrysanthemum actin 2 promoter for productive, constitutive, and durable expression of a transgene in Chrysanthemum morifolium. *Breeding Science*, *69*(3), 536. https://doi.org/10.1270/JSBBS.19036

Klepikova, A. V., Kasianov, A. S., Gerasimov, E. S., Logacheva, M. D., & Penin, A. A. (2016). A high resolution map of the Arabidopsis thaliana developmental transcriptome based on RNA-seq profiling. *The Plant Journal : For Cell and Molecular Biology*, *88*(6), 1058–1070. https://doi.org/10.1111/TPJ.13312

Křeček, P., Skůpa, P., Libus, J., Naramoto, S., Tejos, R., Friml, J., & Zažímalová, E. (2009). The PIN-FORMED (PIN) protein family of auxin transporters. *Genome Biology*, *10*(12), 1–11. https://doi.org/10.1186/GB-2009-10-12-249/FIGURES/8

Landry, B. S., Hubert, N., Etoh, T., Harada, J. J., & Lincoln, S. E. (2011). A genetic map for Brassica napus based on restriction fragment length polymorphisms detected with expressed DNA sequences. *Https://Doi.Org/10.1139/G91-084*, *34*(4), 543–552. https://doi.org/10.1139/G91-084

Lee, B. H., Johnston, R., Yang, Y., Gallavotti, A., Kojima, M., Travençolo, B. A. N., Costa, L. D. F., Sakakibara, H., & Jackson, D. (2009). Studies of aberrant phyllotaxy1 Mutants of Maize Indicate Complex Interactions between Auxin and Cytokinin Signaling in the Shoot Apical Meristem. *Plant Physiology*, *150*(1), 205–216. https://doi.org/10.1104/PP.109.137034

Lee, K., Kim, J. H., Park, O. S., Jung, Y. J., & Seo, P. J. (2022). Ectopic expression of WOX5 promotes cytokinin signaling and de novo shoot regeneration. *Plant Cell Reports*, *41*(12), 2415–2422. https://doi.org/10.1007/S00299-022-02932-4

Leibfried, A., To, J. P. C., Busch, W., Stehling, S., Kehle, A., Demar, M., Kieber, J. J., & Lohmann, J. U. (2005). WUSCHEL controls meristem function by direct regulation of cytokinin-inducible response regulators. *Nature*, *438*(7071), 1172–1175. https://doi.org/10.1038/NATURE04270

Levy, Mesnage, Mylne, Gendall, D. (2002). *Multiple roles in Arabidopsis VRN1 in bernalization and flowering time*. science.

Li, F., Ma, C., Wang, X., Gao, C., Zhang, J., Wang, Y., Cong, N., Li, X., Wen, J., Yi, B., Shen, J., Tu, J., & Fu, T. (2011). Characterization of Sucrose transporter alleles and

their association with seed yield-related traits in Brassica napus L. *BMC Plant Biology*, *11*(1), 1–14. https://doi.org/10.1186/1471-2229-11-168/FIGURES/7

Li, H., Li, J., Song, J., Zhao, B., Guo, C., Wang, B., Zhang, Q., Wang, J., King, G. J., & Liu, K. (2019). An auxin signaling gene BnaA3.IAA7 contributes to improved plant architecture and yield heterosis in rapeseed. *The New Phytologist*, *222*(2), 837–851. https://doi.org/10.1111/NPH.15632

Li Juan, Tan Xiaoli, Zhu Fuge, & Guo Jingjing. (2010). A Rapid and Simple Method for Brassica Napus Floral-Dip Transformation and Selection of Transgenic Plantlets. *International Journal of Biology*, *2*(1), 127–131. http://www.ccsenet.org/journal/index.php/ijb/article/view/4778/4022

Li, Y. J., Yu, Y., Liu, X., Zhang, X. S., & Su, Y. H. (2021). The Arabidopsis MATERNAL EFFECT EMBRYO ARREST45 protein modulates maternal auxin biosynthesis and controls seed size by inducing AINTEGUMENTA. *Plant Cell*, *33*(6), 1907–1926. https://doi.org/10.1093/plcell/koab084

Lian, Z., Nguyen, C. D., Liu, L., Wang, G., Chen, J., Wang, S., Yi, G., Wilson, S., Ozias-Akins, P., Gong, H., & Huo, H. (2022). Application of developmental regulators to improve in planta or in vitro transformation in plants. *Plant Biotechnology Journal*, *20*(8), 1622–1635. https://doi.org/10.1111/PBI.13837

Lin, Z., Chen, L., Tang, S., Zhao, M., Li, T., You, J., You, C., Li, B., Zhao, Q., Zhang, D., Wang, J., Shen, Z., Song, X., Zhang, S., & Cao, X. (2023). Efficient CRISPR/Cas9-mediated genome editing in sheepgrass (Leymus chinensis). *Journal of Integrative Plant Biology*, *65*(11), 2416–2420. https://doi.org/10.1111/JIPB.13567

Liu, F., Xiong, X., Wu, L., Fu, D., Hayward, A., Zeng, X., Cao, Y., Wu, Y., Li, Y., & Wu, G. (2014). BraLTP1, a lipid transfer protein gene involved in epicuticular wax deposition, cell proliferation and flower development in Brassica napus. *PLoS ONE*, *9*(10), 1–12. https://doi.org/10.1371/journal.pone.0110272

Lu, K., Wei, L., Li, X., Wang, Y., Wu, J., Liu, M., Zhang, C., Chen, Z., Xiao, Z., Jian, H., Cheng, F., Zhang, K., Du, H., Cheng, X., Qu, C., Qian, W., Liu, L., Wang, R., Zou, Q., … Li, J. (2019). Whole-genome resequencing reveals Brassica napus origin and genetic loci involved in its improvement. *Nature Communications*. https://doi.org/10.1038/s41467-019-09134-9

Lysak, M. A., Koch, M. A., Pecinka, A., & Schubert, I. (2005). Chromosome triplication found across the tribe Brassiceae. *Genome Research*, *15*(4), 516–525. https://doi.org/10.1101/GR.3531105

Lyu, J., Guo, Y., Du, C., Yu, H., Guo, L., Liu, L., Zhao, H., Wang, X., & Hu, S. (2022). BnERF114.A1, a Rapeseed Gene Encoding APETALA2/ETHYLENE RESPONSE FACTOR, Regulates Plant Architecture through Auxin Accumulation in the Apex in Arabidopsis. *International Journal of Molecular Sciences*, *23*(4). https://doi.org/10.3390/IJMS23042210

Maheshwari, P., Selvaraj, G., & Kovalchuk, I. (2011). Optimization of Brassica napus (canola) explant regeneration for genetic transformation. *New Biotechnology*, *29*(1), 144–155. https://doi.org/10.1016/j.nbt.2011.06.014

Manrique, S., Caselli, F., Matías-Hernández, L., Franks, R. G., Colombo, L., & Gregis, V. (2023). Assessing the role of REM13, REM34 and REM46 during the transition to the reproductive phase in Arabidopsis thaliana. *Plant Molecular Biology*, *112*(3), 179–193. https://doi.org/10.1007/s11103-023-01357-1

Mantegazza, O., Gregis, V., Mendes, M. A., Morandini, P., Alves-Ferreira, M., Patreze, C. M., Nardeli, S. M., Kater, M. M., & Colombo, L. (2014). Analysis of the arabidopsis REM gene family predicts functions during flower development. *Annals of Botany*, *114*(7), 1507–1515. https://doi.org/10.1093/aob/mcu124

Matias-Hernandez, L., Battaglia, R., Galbiati, F., Rubes, M., Eichenberger, C., Grossniklaus, U., Kater, M. M., & Colombo, L. (2010). VERDANDI is a direct target of the MADS domain ovule identity complex and affects embryo sac differentiation in Arabidopsis. *Plant Cell*, *22*(6), 1702–1715. https://doi.org/10.1105/tpc.109.068627

McCarty, D. R., Hattori, T., Carson, C. B., Vasil, V., Lazar, M., & Vasil, I. K. (1991). The Viviparous-1 developmental gene of maize encodes a novel transcriptional activator. *Cell*, *66*(5), 895–905. https://doi.org/10.1016/0092-8674(91)90436-3

Mendes, M. A., Guerra, R. F., Castelnovo, B., Silva-Velazquez, Y., Morandini, P., Manrique, S., Baumann, N., Groß-Hardt, R., Dickinson, H., & Colombo, L. (2016). Live and let die: A REM complex promotes fertilization through synergid cell death in Arabidopsis. *Development (Cambridge)*, *143*(15), 2780–2790. https://doi.org/10.1242/dev.134916

Mitchell, P. J., & Tjian, R. (1989). Transcriptional regulation in mammalian cells by sequence-specific DNA binding proteins. *Science (New York, N.Y.)*, *245*(4916), 371–378. https://doi.org/10.1126/SCIENCE.2667136

Moloney, M. M., Walker, J. M., & Sharma, K. K. (1989). High efficiency transformation of Brassica napus using Agrobacterium vectors. *Plant Cell Reports*, *8*(4), 238–242. https://doi.org/10.1007/BF00778542

Mun, J. H., Kwon, S. J., Yang, T. J., Seol, Y. J., Jin, M., Kim, J. A., Lim, M. H., Kim, J. S., Baek, S., Choi, B. S., Yu, H. J., Kim, D. S., Kim, N., Lim, K. B., Lee, S. I., Hahn, J. H., Lim, Y. P., Bancroft, I., & Park, B. S. (2009). Genome-wide comparative analysis of the Brassica rapa gene space reveals genome shrinkage and differential loss of duplicated genes after whole genome triplication. *Genome Biology*, *10*(10), 1–18. https://doi.org/10.1186/GB-2009-10-10-R111/FIGURES/6

Murovec, J., Guček, K., Bohanec, B., Avbelj, M., & Jerala, R. (2018). DNA-free genome editing of brassica oleracea and B. Rapa protoplasts using CRISPR-cas9 ribonucleoprotein complexes. *Frontiers in Plant Science*, *871*(November), 1–9. https://doi.org/10.3389/fpls.2018.01594

Nagaharu, U. (1935). *Genome Analysis in Brassica with Special Reference to the Experimental Formation of B. Napus and Peculiar Mode of Fertilization*. Japanese

Journal of Botany, 7. https://www.scirp.org/reference/referencespapers?referenceid=2043664

Okabe, T. (2016). The riddle of phyllotaxis: Exquisite control of divergence angle. In *Acta Societatis Botanicorum Poloniae* (Vol. 85, Issue 4). Polskie Towarzystwo Botaniczne. https://doi.org/10.5586/asbp.3527

Okada, K., Ueda, J., Komaki, M. K., Bell, C. J., & Shimura, Y. (1991). Requirement of the Auxin Polar Transport System in Early Stages of Arabidopsis Floral Bud Formation. *The Plant Cell*, *3*(7), 677. https://doi.org/10.1105/TPC.3.7.677

Okuzaki, A., Ogawa, T., Koizuka, C., Kaneko, K., Inaba, M., Imamura, J., & Koizuka, N. (2018). CRISPR/Cas9-mediated genome editing of the fatty acid desaturase 2 gene in Brassica napus. *Plant Physiology and Biochemistry*, *131*(April), 63–69. https://doi.org/10.1016/j.plaphy.2018.04.025

O'Shea, E. K., Rutkowski, R., & Kim, P. S. (1989). Evidence that the leucine zipper is a coiled coil. *Science (New York, N.Y.)*, *243*(4890), 538–542. https://doi.org/10.1126/SCIENCE.2911757

Park, J. Y., Koo, D. H., Hong, C. P., Lee, S. J., Jeon, J. W., Lee, S. H., Yun, P. Y., Park, B. S., Kim, H. R., Bang, J. W., Plaha, P., Bancroft, I., & Lim, Y. P. (2005). Physical mapping and microsynteny of Brassica rapa ssp. pekinensis genome corresponding to a 222 kbp gene-rich region of Arabidopsis chromosome 4 and partially duplicated on chromosome 5. *Molecular Genetics and Genomics : MGG*, *274*(6), 579–588. https://doi.org/10.1007/S00438-005-0041-4

Parkin, I. A. P., Gulden, S. M., Sharpe, A. G., Lukens, L., Trick, M., Osborn, T. C., & Lydiate, D. J. (2005). Segmental structure of the Brassica napus genome based on comparative analysis with Arabidopsis thaliana. *Genetics*, *171*(2), 765–781. https://doi.org/10.1534/genetics.105.042093

Peaucelle, A., Braybrook, S. A., Le Guillou, L., Bron, E., Kuhlemeier, C., & Höfte, H. (2011). Pectin-induced changes in cell wall mechanics underlie organ initiation in Arabidopsis. *Current Biology : CB*, *21*(20), 1720–1726. https://doi.org/10.1016/J.CUB.2011.08.057

Peaucelle, A., Louvet, R., Johansen, J. N., Höfte, H., Laufs, P., Pelloux, J., & Mouille, G. (2008). Arabidopsis Phyllotaxis Is Controlled by the Methyl-Esterification Status of Cell-Wall Pectins. *Current Biology*, *18*(24), 1943–1948. https://doi.org/10.1016/J.CUB.2008.10.065

Pinon, V., Prasad, K., Grigg, S. P., Sanchez-Perez, G. F., & Scheres, B. (2013). Local auxin biosynthesis regulation by PLETHORA transcription factors controls phyllotaxis in Arabidopsis. *Proceedings of the National Academy of Sciences of the United States of America*, *110*(3), 1107–1112. https://doi.org/10.1073/pnas.1213497110

Prasad, K., Grigg, S. P., Barkoulas, M., Yadav, R. K., Sanchez-Perez, G. F., Pinon, V., Blilou, I., Hofhuis, H., Dhonukshe, P., Galinha, C., Mähönen, A. P., Muller, W. H., Raman, S., Verkleij, A. J., Snel, B., Reddy, G. V., Tsiantis, M., & Scheres, B. (2011). Arabidopsis

PLETHORA transcription factors control phyllotaxis. *Current Biology*, *21*(13), 1123–1128. https://doi.org/10.1016/j.cub.2011.05.009

Prusinkiewicz, P., Erasmus, Y., Lane, B., Harder, L. D., & Coen, E. (2007). Evolution and development of inflorescence architectures. *Science (New York, N.Y.)*, *316*(5830), 1452–1456. https://doi.org/10.1126/SCIENCE.1140429

Ranftl, Q. L., Bastakis, E., Klermund, C., & Schwechheimer, C. (2016). LLM-Domain Containing B-GATA Factors Control Different Aspects of Cytokinin-Regulated Development in Arabidopsis thaliana. *Plant Physiology*, *170*(4), 2295. https://doi.org/10.1104/PP.15.01556

Reinhardt, D. (2005). Regulation of phyllotaxis. *International Journal of Developmental Biology*, *49*(5–6), 539–546. https://doi.org/10.1387/ijdb.041922dr

Reinhardt, D., Mandel, T., & Kuhlemeier, C. (2000). Auxin regulates the initiation and radial position of plant lateral organs. *The Plant Cell*, *12*(4), 507–518. https://doi.org/10.1105/TPC.12.4.507

Reinhardt, D., Pesce, E. R., Stieger, P., Mandel, T., Baltensperger, K., Bennett, M., Traas, J., Friml, J., & Kuhlemeier, C. (2003). Regulation of phyllotaxis by polar auxin transport. *Nature*, *426*(6964), 255–260. https://doi.org/10.1038/nature02081

Richter, R., Kinoshita, A., Vincent, C., Martinez-Gallegos, R., Gao, H., van Driel, A. D., Hyun, Y., Mateos, J. L., & Coupland, G. (2019). Floral regulators FLC and SOC1 directly regulate expression of the B3-type transcription factor TARGET of FLC and SVP 1 at the Arabidopsis shoot apex via antagonistic chromatin modifications. *PLoS Genetics*, *15*(4), 1–27. https://doi.org/10.1371/journal.pgen.1008065

Ritchie, H., Rodés-Guirao, L., Mathieu, E., Gerber, M., Ortiz-Ospina, E., Hasell, J., & Roser, M. (2024). Population Growth. *Our World in Data*. https://ourworldindata.org/population-growth

Romanel, E. A. C., Schrago, C. G., Couñago, R. M., Russo, C. A. M., & Alves-Ferreira, M. (2009). Evolution of the B3 DNA binding superfamily: New insights into REM family gene diversification. *PLoS ONE*, *4*(6). https://doi.org/10.1371/journal.pone.0005791

R.V. Jean, D. B. (1998). Symmetry in Plants. In *World Scientific Publishing Co. Pte. Ltd.: Vol. Series in*. Urban & Fischer. https://doi.org/10.1016/S0176-1617(00)80062-0

Ryu, M. Y., Cho, S. K., & Kim, W. T. (2009). RNAi suppression of RPN12a decreases the expression of type-A ARRs, negative regulators of cytokinin signaling pathway, in Arabidopsis. *Molecules and Cells*, *28*(4), 375–382. https://doi.org/10.1007/S10059-009-0132-X

S. Smith, R., Kuhlemeier, C., & Prusinkiewicz, P. (2006). *Inhibition fields for phyllotactic pattern formation: a simulation study*. Canadian Journal of Biology.

Sassi, M., Ali, O., Boudon, F., Cloarec, G., Abad, U., Cellier, C., Chen, X., Gilles, B., Milani, P., Friml, J., Vernoux, T., Godin, C., Hamant, O., & Traas, J. (2014). An auxin-mediated shift toward growth isotropy promotes organ formation at the shoot

meristem in Arabidopsis. *Current Biology : CB*, *24*(19), 2335–2342. https://doi.org/10.1016/J.CUB.2014.08.036

Schiessl, S. (2020). Regulation and Subfunctionalization of Flowering Time Genes in the Allotetraploid Oil Crop Brassica napus. *Frontiers in Plant Science*, *11*, 605155. https://doi.org/10.3389/FPLS.2020.605155/BIBTEX

Schiessl, S., Williams, N., Specht, P., Staiger, D., & Johansson, M. (2019). Different copies of SENSITIVITY to RED LIGHT REDUCED 1 show strong subfunctionalization in Brassica napus. *BMC Plant Biology*, *19*(1), 1–12. https://doi.org/10.1186/S12870-019-1973-X/FIGURES/6

Schwarz, I., Scheirlinck, M. T., Otto, E., Bartrina, I., Schmidt, R. C., & Schmülling, T. (2020a). Cytokinin regulates the activity of the inflorescence meristem and components of seed yield in oilseed rape. *Journal of Experimental Botany*, *71*(22), 7146–7159. https://doi.org/10.1093/jxb/eraa419

Schwarz, I., Scheirlinck, M. T., Otto, E., Bartrina, I., Schmidt, R. C., & Schmülling, T. (2020b). Cytokinin regulates the activity of the inflorescence meristem and components of seed yield in oilseed rape. *Journal of Experimental Botany*, *71*(22), 7146–7159. https://doi.org/10.1093/JXB/ERAA419

Shah, S., Karunarathna, N. L., Jung, C., & Emrani, N. (2018). An APETALA1 ortholog affects plant architecture and seed yield component in oilseed rape (Brassica napus L.). *BMC Plant Biology*, *18*(1), 1–12. https://doi.org/10.1186/S12870-018-1606-9/FIGURES/5

Shaohong, F. U., Xianya, W. E. I., Yingze, N. I. U., & Shixing, G. U. O. (2005). Transformation of Brassica napus with the method of floral-dip. *BIOTECHNOLOGY: Genomics and Its Applications*, 45–49.

Sharada, M. S., Kumari, A., Pandey, A. K., Sharma, S., Sharma, P., Sreelakshmi, Y., & Sharma, R. (2017). Generation of genetically stable transformants by Agrobacterium using tomato floral buds. *Plant Cell, Tissue and Organ Culture*, *129*(2), 299–312. https://doi.org/10.1007/s11240-017-1178-7

Snow Mary and Snow Robert. (1932a). I. Experiments on Phyllotaxis. I. - The effect of isolating a Primordium. *Philosophical Transactions of the Royal Society of London. Series B, Containing Papers of a Biological Character*, *221*(474–482), 1–43. https://doi.org/10.1098/RSTB.1932.0001

Snow Mary and Snow Robert. (1932b). IX. Experiments on Phyllotaxis. II. — The effect of displacing a primordium. *Philosophical Transactions of the Royal Society of London. Series B, Containing Papers of a Biological Character*, *222*(483–493), 353–400. https://doi.org/10.1098/RSTB.1932.0019

Snow Mary and Snow Robert. (1935). II - Experiments on Phyllotaxis - Part III - Diagonal splits through Decussate Apices. *Philosophical Transactions of the Royal Society of London. Series B, Biological Sciences*, *225*(519), 63–94. https://doi.org/10.1098/RSTB.1935.0007

Snow Mary and Snow Robert. (1947). ON THE DETERMINATION OE LEAVES. *New Phytologist*, *46*(1), 5–19. https://doi.org/10.1111/J.1469-8137.1947.TB05068.X

Snow Mary and Snow Robert. (1962). A theory of the regulation of phyllotaxis based on Lupinus albus. *Philosophical Transactions of the Royal Society of London. Series B, Biological Sciences*, *244*(717), 483–513. https://doi.org/10.1098/RSTB.1962.0003

Song, J. M., Guan, Z., Hu, J., Guo, C., Yang, Z., Wang, S., Liu, D., Wang, B., Lu, S., Zhou, R., Xie, W. Z., Cheng, Y., Zhang, Y., Liu, K., Yang, Q. Y., Chen, L. L., & Guo, L. (2020). Eight high-quality genomes reveal pan-genome architecture and ecotype differentiation of Brassica napus. *Nature Plants*, *6*(1), 34–45. https://doi.org/10.1038/s41477-019-0577-7

Sriboon, S., Li, H., Guo, C., Senkhamwong, T., Dai, C., & Liu, K. (2020). Knock-out of TERMINAL FLOWER 1 genes altered flowering time and plant architecture in Brassica napus. *BMC Genetics*, *21*(1), 1–13. https://doi.org/10.1186/s12863-020-00857-z

Steeves, T. A., & Sussex, I. M. (1989). Patterns in Plant Development. *Patterns in Plant Development*. https://doi.org/10.1017/CBO9780511626227

Swaminathan, K., Peterson, K., & Jack, T. (2008). The plant B3 superfamily. *Trends in Plant Science*, *November*, 647–655. https://doi.org/10.1016/j.tplants.2008.09.006

Tan, Z., Han, X., Dai, C., Lu, S., He, H., Yao, X., Chen, P., Yang, C., Zhao, L., Yang, Q. Y., Zou, J., Wen, J., Hong, D., Liu, C., Ge, X., Fan, C., Yi, B., Zhang, C., Ma, C., … Zhao, H. (2024). Functional genomics of Brassica napus: Progresses, challenges, and perspectives. *Journal of Integrative Plant Biology*, *66*(3), 484–509. https://doi.org/10.1111/JIPB.13635/SUPPINFO

Town, C. D., Cheung, F., Maiti, R., Crabtree, J., Haas, B. J., Wortman, J. R., Hine, E. E., Althoff, R., Arbogast, T. S., Tallon, L. J., Vigouroux, M., Trick, M., & Bancroft, I. (2006). Comparative genomics of Brassica oleracea and Arabidopsis thaliana reveal gene loss, fragmentation, and dispersal after polyploidy. *Plant Cell*, *18*(6), 1348–1359. https://doi.org/10.1105/tpc.106.041665

Traas, J. (2013). Phyllotaxis. *Development (Cambridge)*, *140*(2), 249–253. https://doi.org/10.1242/dev.074740

Verma, S., Chinnusamy, V., & Bansal, K. C. (2008). Short Communication A Simplified Floral Dip Method for Transformation of Brassica napus. *J. Plant Biochemistry & Biotechnology*, *17*(2), 197–200.

Vernoux, T., Kronenberger, J., Grandjean, O., Laufs, P., & Traas, J. (2000). PIN-FORMED 1 regulates cell fate at the periphery of the shoot apical meristem. *Development*, *127*(23), 5157–5165. https://doi.org/10.1242/DEV.127.23.5157

Wallace, J. G., Rodgers-Melnick, E., & Buckler, E. S. (2018). On the road to breeding 4.0: Unraveling the good, the bad, and the boring of crop quantitative genomics. *Annual Review of Genetics*, *52*(Volume 52, 2018), 421–444. https://doi.org/10.1146/ANNUREV-GENET-120116-024846/CITE/REFWORKS

Waltner, J. K., Peterson, F. C., Lytle, B. L., & Volkman, B. F. (2005). Structure of the B3 domain from Arabidopsis thaliana protein At1g16640 . *Protein Science*, *14*(9), 2478–2483. https://doi.org/10.1110/ps.051606305

Wang, N., Ryan, L., Sardesai, N., Wu, E., Lenderts, B., Lowe, K., Che, P., Anand, A., Worden, A., van Dyk, D., Barone, P., Svitashev, S., Jones, T., & Gordon-Kamm, W. (2023). Leaf transformation for efficient random integration and targeted genome modification in maize and sorghum. *Nature Plants 2023 9:2*, *9*(2), 255–270. https://doi.org/10.1038/s41477-022-01338-0

Wang, X., Torres, M. J., Pierce, G., Lemke, C., Nelson, L. K., Yuksel, B., Bowers, J. E., Marler, B., Xiao, Y., Lin, L., Epps, E., Sarazen, H., Rogers, C., Karunakaran, S., Ingles, J., Giattina, E., Mun, J. H., Seol, Y. J., Park, B. S., … Paterson, A. H. (2011). A physical map of Brassica oleracea shows complexity of chromosomal changes following recursive paleopolyploidizations. *BMC Genomics*, *12*. https://doi.org/10.1186/1471-2164-12-470

Wang, Y., Deng, D., Zhang, R., Wang, S., Bian, Y., & Yin, Z. (2012). Systematic analysis of plant-specific B3 domain-containing proteins based on the genome resources of 11 sequenced species. *Molecular Biology Reports*, *39*(5), 6267–6282. https://doi.org/10.1007/S11033-012-1448-8

Wardlaw, C. W. (1949). Phyllotaxis and Organogenesis in Ferns. *Nature 1949 164:4161*, *164*(4161), 167–169. https://doi.org/10.1038/164167a0

Wellmer, F., Alves-Ferreira, M., Dubois, A., Riechmann, J. L., & Meyerowitz, E. M. (2006). Genome-wide analysis of gene expression during early Arabidopsis flower development. *PLoS Genetics*, *2*(7), 1012–1024. https://doi.org/10.1371/journal.pgen.0020117

Wu, X., Liang, Y., Gao, H., Wang, J., Zhao, Y., Hua, L., Yuan, Y., Wang, A., Zhang, X., Liu, J., Zhou, J., Meng, X., Zhang, D., Lin, S., Huang, X., Han, B., Li, J., & Wang, Y. (2021). Enhancing rice grain production by manipulating the naturally evolved cis-regulatory element-containing inverted repeat sequence of OsREM20. *Molecular Plant*, *14*(6), 997–1011. https://doi.org/10.1016/J.MOLP.2021.03.016/ATTACHMENT/7AA37CAF-2980-43D1-850C-55933121941D/MMC3.PDF

Wuest, S. E., O'Maoileidigh, D. S., Rae, L., Kwasniewska, K., Raganelli, A., Hanczaryk, K., Lohan, A. J., Loftus, B., Graciet, E., & Wellmer, F. (2012). Molecular basis for the specification of floral organs by APETALA3 and PISTILLATA. *Proceedings of the National Academy of Sciences of the United States of America*, *109*(33), 13452–13457. https://doi.org/10.1073/pnas.1207075109

Xing, H. L., Dong, L., Wang, Z. P., Zhang, H. Y., Han, C. Y., Liu, B., Wang, X. C., & Chen, Q. J. (2014). A CRISPR/Cas9 toolkit for multiplex genome editing in plants. *BMC Plant Biology*, *14*(1). https://doi.org/10.1186/S12870-014-0327-Y

Xu, H., Wang, X., Zhao, H., & Liu, F. (2008). An intensive understanding of vacuum infiltration transformation of pakchoi (Brassica rapa ssp. chinensis). *Plant Cell Reports*, *27*(8), 1369–1376. https://doi.org/10.1007/s00299-008-0564-3

Yan, G., Li, S., Ma, M., Quan, C., Tian, X., Tu, J., Shen, J., Yi, B., Fu, T., Ma, C., Guo, L., & Dai, C. (2023). The transcription factor BnaWRKY10 regulates cytokinin dehydrogenase BnaCKX2 to control cytokinin distribution and seed size in Brassica

napus. *Journal of Experimental Botany*, *74*(17), 4994–5013. https://doi.org/10.1093/JXB/ERAD201

Yang, F., Bui, H. T., Pautler, M., Llaca, V., Johnston, R., Lee, B. H., Kolbe, A., Sakai, H., & Jackson, D. (2015). A Maize Glutaredoxin Gene, Abphyl2, Regulates Shoot Meristem Size and Phyllotaxy. *The Plant Cell*, *27*(1), 121–131. https://doi.org/10.1105/TPC.114.130393

Yang, M., Yang, Q., Fu, T., & Zhou, Y. (2011). Overexpression of the Brassica napus BnLAS gene in Arabidopsis affects plant development and increases drought tolerance. *Plant Cell Reports*, *30*(3), 373–388. https://doi.org/10.1007/S00299-010-0940-7

Yang, P., Shu, C., Chen, L., Xu, J., Wu, J., & Liu, K. (2012). Identification of a major QTL for silique length and seed weight in oilseed rape (Brassica napus L.). *Theoretical and Applied Genetics*, *125*(2), 285–296. https://doi.org/10.1007/S00122-012-1833-7/FIGURES/3

Ye, G. N., Stone, D., Pang, S. Z., Creely, W., Gonzalez, K., & Hinchee, M. (1999). Arabidopsis ovule is the target for Agrobacterium in planta vacuum infiltration transformation. *Plant Journal*, *19*(3), 249–257. https://doi.org/10.1046/j.1365-313X.1999.00520.x

Yin, X. (2021). Phyllotaxis: from classical knowledge to molecular genetics. *Journal of Plant Research*, *134*(3), 373–401. https://doi.org/10.1007/s10265-020-01247-3

Yu, Y., Qiao, L., Chen, J., Rong, Y., Zhao, Y., Cui, X., Xu, J., Hou, X., & Dong, C. H. (2020). Arabidopsis REM16 acts as a B3 domain transcription factor to promote flowering time via directly binding to the promoters of SOC1 and FT. *Plant Journal*, *103*(4), 1386–1398. https://doi.org/10.1111/tpj.14807

Yuan, D., Zhang, Y., Wang, Z., Qu, C., Zhu, D., Wan, H., & Liang, Y. (2022). BnKAT2 Positively Regulates the Main Inflorescence Length and Silique Number in Brassica napus by Regulating the Auxin and Cytokinin Signaling Pathways. *Plants*, *11*(13). https://doi.org/10.3390/plants11131679

Zhang, K., Nie, L., Cheng, Q., Yin, Y., Chen, K., Qi, F., Zou, D., Liu, H., Zhao, W., Wang, B., & Li, M. (2019). Effective editing for lysophosphatidic acid acyltransferase 2/5 in allotetraploid rapeseed (Brassica napus L.) using CRISPR-Cas9 system. *Biotechnology for Biofuels*, *12*(1), 1–18. https://doi.org/10.1186/s13068-019-1567-8

Zhang, K., Zhang, H., Pan, Y., Niu, Y., Guo, L., Ma, Y., Tian, S., Wei, J., Wang, C., Yang, X., Fu, Y., Qu, P., Liu, L., Zhang, Y., Sun, H., Bai, Z., Dong, J., Li, C., & Liu, X. (2022). Cell- and noncell-autonomous AUXIN RESPONSE FACTOR3 controls meristem proliferation and phyllotactic patterns. *Plant Physiology*, *190*(4), 2335–2349. https://doi.org/10.1093/plphys/kiac370

Zhang, Q., Chen, H., He, M., Zhao, Z., Cai, H., Ding, G., Shi, L., & Xu, F. (2017). The boron transporter BnaC4.BOR1;1c is critical for inflorescence development and fertility under boron limitation in Brassica napus. *Plant, Cell & Environment*, *40*(9), 1819–1833. https://doi.org/10.1111/PCE.12987

Zhao, F., Chen, W., Sechet, J., Martin, M., Bovio, S., Lionnet, C., Long, Y., Battu, V., Mouille, G., Monéger, F., & Traas, J. (2019). Xyloglucans and Microtubules Synergistically Maintain Meristem Geometry and Phyllotaxis. *Plant Physiology*, *181*(3), 1191–1206. https://doi.org/10.1104/PP.19.00608

Zhao, Y. (2012). Auxin Biosynthesis: A Simple Two-Step Pathway Converts Tryptophan to Indole-3-Acetic Acid in Plants. *Molecular Plant •*, *5*(2), 334–338. https://doi.org/10.1093/mp/ssr104

Zhao, Z., Andersen, S. U., Ljung, K., Dolezal, K., Miotk, A., Schultheiss, S. J., & Lohmann, J. U. (2010). Hormonal control of the shoot stem-cell niche. *Nature 2010 465:7301*, *465*(7301), 1089–1092. https://doi.org/10.1038/nature09126

Zheng, M., Zhang, L., Tang, M., Liu, J., Liu, H., Yang, H., Fan, S., Terzaghi, W., Wang, H., & Hua, W. (2020). Knockout of two BnaMAX1 homologs by CRISPR/Cas9-targeted mutagenesis improves plant architecture and increases yield in rapeseed (Brassica napus L.). *Plant Biotechnology Journal*, *18*(3), 644–654. https://doi.org/10.1111/PBI.13228

Appendix

During my thesis I focused my attention on plant architecture. I was involved in projects aimed to unveil the molecular basis of the phyllotaxis and its link to the yield, and to characterize the role of strigolactones in plant architecture and other plant processes.

Phyllotaxis and yield – a translational study between *Arabidopsis thaliana* and *Brassica napus*

Ferrario C. [1]; Caselli F. [1]; Davlatboeva S. [1]; Bloom E.[2]; Bundock P.[2]; Van Tunen A.[2]; Gregis V. [1], Kater M[1].

[1] University of Milan, Department of Biosciences, Via Celoria 26, 20133 Milan, Italy

[2] Keygene Company, Agrobusiness Park 90, Wageningen, Gelderland: 6701 AA, Netherlands

In preparation

In this paper the yield impact of mutations in *AtREM34*, *AtREM35* and *AtREM36* is described, and the homologous gene cluster in *Brassica napus* is deeply studied to identify the best targets to develop similar higher yield genotypes in the species.

I contributed to this paper by performing most of the experiments and writing the manuscript.

Phyllotaxis and yield – a translational study between *Arabidopsis thaliana* and *Brassica napus*

Carlotta Ferrario[1], Francesca Caselli[1], Shokhsanam Davlatboeva[1,3], Evert-Jan Bloom[2], Arjen van Tunen[2], Veronica Gregis[1], Martin Kater[1*]

[1] University of Milan, Department of Biosciences, Via Celoria 26, 20133 Milan, Italy

[2] Keygene Company, Agrobusiness Park 90, Wageningen, Gelderland: 6701 AA, Netherlands

[3] Present address: Johannes Gutenberg-Universität Mainz, Saarstraße 21, 55122 Mainz, Germania

*Corresponding author: martin.kater@unimi.it

Abstract

In a world that is continuously growing and developing, it is crucial to enhance agricultural yields to ensure an adequate food supply for the population while minimizing the environmental impact. Plant yield is influenced by a range of factors, among which inflorescence architecture and its geometrical organization, known as phyllotaxis. Despite centuries of studies, the mechanism behind phyllotactic patterning is still partially unknown, especially in non-model plant species. Furthermore, the impact of phyllotaxis on yield is not well understood.

This paper addresses these gaps by characterizing different combinations of Arabidopsis mutants belonging to the *REM* gene family with a permutated phyllotaxis and an increased yield.

The research also investigates the possibility of exploiting the knowledge derived from Arabidopsis to identify functional orthologous in the economically important crop *Brassica napus*, commonly known as rapeseed. Indeed, we were able to identify a set of homologous *BnaREM* genes that are expressed in *Brassica napus* reproductive tissues and can influence phyllotaxis in *Arabidopsis*, suggesting a retained role between these two species. The mechanisms may involve an interaction with the auxin pathway.

This application-driven study unveils novel genes associated with phyllotaxis and yield in the *Brassicaceae* family, contributing to our understanding of plant architecture and offering insights into sustainable strategies for improving crop productivity.

Introduction

The global population is steadily increasing and is expected to reach 10 billion people by 2060 (Ritchie *et al.*, 2024). This, together with the expected increase in meat and dairy consumption (Henchion *et al.*, 2021) points out the imperative to enhance crop production (Schwarz *et al.*, 2020).

Expanding agricultural land is not a sustainable solution, as preserving wild environments is crucial to prevent biodiversity erosion and avoid further greenhouse gas emissions associated with land-use change. Alternatively, boosting crop yield allows for increased food production within the existing cultivated areas.

The number of fruits and seeds that a plant can bear is linked to the architecture of its inflorescence and, specifically, to its length, branching potential and phyllotaxis, which is the geometrical arrangement of the organs around the stem.

The phyllotaxis is determined by the spatio-temporal regulation of primordia emergence from the inflorescence meristem (IM), and consequently by the divergence angle between primordia of successive emergence events. Understanding and manipulating these factors can contribute to optimizing crop yield and addressing the pressing challenge of global food security.

Different phyllotactic patterns can be observed in nature, among which the most common is described by the Fibonacci spiral. Observable in different model dicots, such as tobacco, tomato and *Arabidopsis* (Reinhardt, 2005), it is characterized by consecutive angles which diverge one from each other by a 137.5° angle, the so-called “golden angle”.

This precise patterning has attracted the attention of mathematicians, physicists and biologists for centuries, who developed models and theories trying to explain such a regularity (Adler, Barabe and J E A N †, 1997; Okabe, 2016; Barabé and Lacroix, 2020; Yin, 2021).

The current model identifies the phytohormone auxin as the primary regulator of the phyllotaxis. In the inflorescence meristem, the growing primordium, whose growth and differentiation is triggered by this hormone, acts as an auxin sink. Auxin is therefore depleted in the primordium surroundings, creating an area in which organogenesis is inhibited (e.g. Galvan-Ampudia et al., 2016; Traas, 2013; Yin, 2021).

The spatial distribution of auxin depends both on its biosynthesis and transport, and there are evidences in *Arabidopsis* that mutants in genes related to such processes have a defective phyllotactic pattern or can’t develop primordia at all (Okada *et al.*, 1991; Bennett *et al.*, 1995; Okal *et al.*, 1999; Reinhardt *et al.*, 2003; Heisler *et al.*, 2005; Prasad *et al.*, 2011; Pinon *et al.*, 2013; Bhatia *et al.*, 2016; Shi and Vernoux, 2019; Yin, 2021). Moreover, similar mutated patterns can be observed in genotypes where auxin is correctly distributed but not perceived, as the *arf* mutants (Przemeck *et al.*, 1996; Sessions *et al.*, 1997; Nemhauser, Feldman and Zambryski, 2000; Simonini *et al.*, 2017; Zhang *et al.*, 2022).

However, there’s not only auxin. As the interest on the topic is increasing, more and more studies are revealing the complexity of the biological mechanism, pointing out the involvement of cytokinins, cell cycle-regulating factors, meristem size, cytoskeletal factors and cell wall synthesis (Heisler *et al.*, 2005; Peaucelle *et al.*, 2007; Besnard *et al.*, 2014; Landrein *et al.*, 2015; Shi and Vernoux, 2019; Yin, 2021).

Even if probably we are just revealing the top of the iceberg and we still need a lot of research to understand the mechanism governing the phyllotactic pattern specification, it can be

hypothesized that manipulating these patterns can yield agricultural benefits. For instance, it was published as Arabidopsis *arf3*, as well as *ckx3 ckx5* mutants present a mutated phyllotaxis, an increased shoot or inflorescence apical meristem (SAM or IM) area and an increase in flowers and siliques production (Bartrina *et al.*, 2011; Zhang *et al.*, 2022).

In our laboratory, we have generated and studied *Arabidopsis* mutants, belonging to the *Reproductive Meristem (REM)* family, displaying mutated phyllotaxis and increased IM area (Caselli et al, under revision). This led us to explore whether these mutations could also have an impact on flower and silique production. Thus, the first aim of the present work has been to investigate the impact on yield resulting from mutations in selected *REM* genes : *REM34*, *REM35* and *REM36*.

The *REM* (REproductive Meristem) genes belong to the B3 DNA binding domain superfamily together with the *ARF, ABI3/VP1*, *HIS* (High-level expression of Sugar Inducible gene), and *RAV* (Related to Abi3/Vp1) families (Swaminathan, Peterson and Jack, 2008; Romanel *et al.*, 2009). In the *Arabidopsis* genome, there are 87 B3 proteins, among which 45 are classified as belonging to the *REM* family, making it the most numerous and divergent within this superfamily (Romanel et al., 2009). Phylogenetically, the *REMs* can be divided into subclasses according to the phylogeny of the domains they contain (Romanel *et al.*, 2009).

Despite being the most abundant, the *REM* genes are the least characterized among the B3 superfamily. However, recent studies have been uncovering their involvement in several developmental processes related to the regulation of flowering time, inflorescence and gametes development (Caselli et al, under revision, Levy, Mesnage, Mylne, Gendall, 2002; Gómez-Mena et al., 2005; Matias-Hernandez et al., 2010; Heo, Sung and Assmann, 2012; Mendes et al., 2016; Richter et al., 2019; Yu et al., 2020; Li et al., 2021; Wu et al., 2021; Manrique et al., 2023).

Mantegazza et al. (2014) identified a cluster of *REM* genes —*REM34*, *REM35*, and *REM36* – which was considered particularly interesting for studying its potential impact on *Arabidopsis* flower and inflorescence development due to its expression pattern and the presence of floral integrator binding motifs in its regulatory elements. The three genes are located on chromosome 4 and placed in tandem within a wider cluster of phylogenetically related *REM* genes, subclass IX. Indeed, 9 out of the *15 REM IX* are placed there, while almost all the others are part of a duplication on chromosome 2 (Romanel *et al.*, 2009; Mantegazza *et al.*, 2014).

The three genes are expressed in the inflorescence and floral meristems (Mantegazza *et al.*, 2014), as well as in reproductive organs and petals at different stages (Caselli *et al.*, 2019) and are direct target of important MADS factors as AP1 (Kaufmann *et al.*, 2009), AP3 and PI (Wuest *et al.*, 2012) and SVP (Gregis *et al.*, 2013). *REM34* and *REM35* are known to play various role in plant development, as they are involved in gametophyte development (Caselli *et al.*, 2019) regulate both SAM and IM dimensions and impact phyllotaxis possibly genetically interacting with some ARF proteins (Caselli et al, under revision, Manrique et al., 2023).

In this study, we describe a new phenotype observed in various combinations of double mutants involving *REM34*, *REM35*, and *REM36*, showing an increase in silique production.

After having determined the yield impact of *REM* mutations, we wanted to explore the potential for generating similar mutants in an economically important crop through translational biology.

Brassica napus, as *Arabidopsis thaliana*, is part of the *Brassicaceae* family, and the close genetic relationship between them allows using comparative genetics to predict orthologous genes (Parkin *et al.*, 2005).

Brassica napus (or rapeseed) is a young allotetraploid, born 7500 years ago from the interspecific hybridization between *Brassica rapa* and *Brassica oleracea* (Chalhoub *et al.*, 2014).

It is cultivated mainly for its seeds, from which is produced approximately 13–16% of the world vegetable oil (Consumption of vegetable oils worldwide from 2013/14 to 2022/2023, by oil type, M. Shahbandeh, Sep 20, 2023; statista.com; Yuan et al., 2022), which is used both for food production and industrial processes. Getting *Brassica napus* genotypes of increased yield could therefore be of great economic value.

Overall, this application-driven study describes the impact of different *REM* genes on *Arabidopsis* flower production and emphasizes the possibility of precisely individuating orthologues genes which are likely to give similar higher yield phenotypes if mutated in *Brassica napus*.

Material and Methods

Plant material and growth conditions

Arabidopsis thaliana Col-0 and *Brassica napus* plants were grown under long day conditions, with 16h of light/8h dark, at 22°C.

rem34, rem35 and *rem34 rem35* mutants were previously generated and described (Caselli et al, under revision). *rem36* was generated following the protocol published by Fauser et al., 2014. The protospacer sequence (GTGATCTGACGAAAAAAGGT) was selected with the aid of the CRISPR-P 2.0 software (http://crispr.hzau.edu.cn/CRISPR2). The resulting mutation is a T insertion which falls into the first B3 DNA binding domain, causing a frameshift and the formation of an early stop codon in position aa31 (Supplementary figure S1). *rem34 rem36* and *rem35 rem36* double mutants were generated by re-transforming single mutants, as the in-linkage position of the genes makes unlikely the generation of higher order mutants by crossing. Different transformation events always gave the same mutation.

Phyllotactic pattern measurement and yield analysis

The phyllotactic pattern was measured as described before (A Peaucelle et al., 2007, Caselli et al, under revision) on the main inflorescence of 2-month-old plants using a 3D clockwise protractor. The first 3 cm of the stem was not considered because elongation is incomplete in this region. The divergence angle was measured by considering the insertion point of the two successive floral pedicels. The clockwise or anticlockwise orientation of the phyllotaxis was determined by following the direction that gives the smallest average divergence angle.

The yield analysis was performed by counting the number of siliques produced on the main inflorescence of completely developed plants (spent IM).

The number of seeds per silique was counted in green but completely elongated siliques. The siliques were opened by a needle following the replum and maturing seeds were counted by the aid of a stereomicroscope.

Kruskal-Wallis and Dunn's post hoc test were used to evaluate the significance of the results, according to the normality and homoscedasticity of the data (GraphPad Prism).

Bioinformatic analysis

Homology and phylogenetic analysis

The homologous sequence identification was performed by querying proteomes databases from Ensembl plants by Jackhmmer, and resultant sequences were filtered to retain only those with a minimum sequence identity of 40%. Specifically, for the *REM IX* clade homology analysis, all *the REM IX Arabidopsis* genes were used to query the *Brassica napus* proteome. To narrow down and fine-tune the results, then *AtREM34, AtREM35, AtREM36* and *AtREM37* were used to query *Arabidopsis lyrata*, *Brassica oleracea, Brassica rapa* and *Brassica napus* proteomes.

The homologous sequences obtained were aligned by Clustal Omega 1.2.4 (default parameters) and their phylogenetic relationships were inferred by RAxML-NG with the WAG+G substitution model (50 bootstrap replicates).

The conserved protein motifs were identified by MEME tool and integrated into the phylogenetic tree, visualized by ETE toolkit.

Protein identity and similarity analysis

The *Arabidopsis* protein sequences were recovered from TAIR (Araport11_genome_release), and the *B. napus* ones from Ensembl plants, brassica genome annotation AST_PRJEB5043_v1.

To get the protein sequences similarity, a multiple sequence alignment was performed by BLAST. The gap cost was lowered at minimum to permit the whole protein alignment.

Gene expression analysis in Brassica napus

qPCR

RNA was extracted from *Brassica napus* tissues using the LiCl method (Verwoerd et al., 1989). For each sample, 500 ng of RNA was retro-transcribed using iScript kit (BioRad). qRT-PCR assay was performed using iTaq Universal SYBR Green supermix (BioRad) in a Bio-Rad iCycler iQ Optical System (software version 3.0a). Three biological replicates, with three technical replicates for each sample, were analysed.

Relative transcript enrichment of the targets of interest was calculated by normalizing the amount of mRNA against the *ACTIN-7* transcript (NCBI reference sequence NM_001316010.1). Expression of genes was calculated using the $2^{-\Delta\Delta Ct}$ method. The primers employed for qPCR are listed in Supplementary primers Table.

In situ hybridization

IM enriched tissues were fixed in FAA (50% ethanol, 5% acetic acid, 3.7% formaldehyde) under vacuum for 15 min, dehydrated in ethanol and bioclear (Bioptica) and embedded in Paraplast Plus (Sigma-Aldrich). *In situ* hybridization was performed as previously described (Coen *et al.*, 1990) with slight modifications. Digoxigenin-labelled antisense probes were synthesized with T7 RNA polymerase (Promega) and tested by dot blot.

The specificity of the signal was assessed by hybridizing the same type of tissues with the sense probe (Supplementary figure S6).

Slides were imaged with the aid of a Zeiss Axiophot® microscope equipped with differential interference contrast (DIC) optics.

Primers employed for probe synthesis are listed in Supplementary primers Table.

Complementation test

The CDS of 4 of the *Brassica napus* candidate genes were cloned from *Brassica napus* cDNA samples in p207 pDONR vector by Gateway and reaction and were subsequently cloned in the pDEST vector pB2GW7.

For some genes, the amplification of half of them was necessary. Then the halves were merged by PCR and cloned in the pDONR as described above.

The constructs were transformed in *Agrobacterium tumefaciens* GV3101 and subsequently in the homolog *Arabidopsis* mutants by floral dip (Clough and Bent, 1998). The expression of the construct was tested in T1 inflorescences. RNA extraction and qPCR were performed as described above. Relative transcript enrichment of the targets of interest was calculated by normalizing the amount of mRNA against the *UBIQUITIN* transcript (Pribil *et al.*, 2010). Expression of the genes was calculated using the $2^{-\Delta\Delta Ct}$ method, using the Wild Type as normalizer.

The T2 was used for the phenotype complementation analysis, after having applied a BASTA (phosphinothricin) selection to remove the Wild Type segregating plants. The phyllotactic pattern, specifically the percentage of angles falling in the 130°-150° range (range around the golden angle, according to the precision of the instrument used), was analyzed to evaluate the phenotype complementation.

ANOVA and post-hoc tests were run by GraphPad Prism and were used to evaluate the statistical significance of the results ($p<0.05$). Specifically, according to the normality and homoscedasticity of the data, ANOVA and Dunnett's test were used for the rem35 and rem36 complementation, and Kruskall Wallis and Dunn's test for rem34 one. The post hoc test was run versus the WT and the *rem* mutant of control.

The primers used for cloning and for the expression analysis are listed in Supplementary primers Table.

Yeast-2-Hybrid (Y2H)

The coding sequences of the genes of interest were cloned in the GAL4 system Gateway vectors (pGADT7 and pGBKT7; Clontech Laboratories, Inc.) by LR recombination (from the p207-derived Entry vector described above). The Y2H constructs for AtARF19 and AtARF7 were already available in the lab (Caselli et al, under revision).

The pGADT7 derived vectors were transformed in AH109 strain, and the pGBKT7 derived ones in the Y187 strain. Yeast transformation was performed as described by de Folter & Immink, 2011. Mating between the two strains produced diploid genotypes producing both the two proteins.

The protein-protein interaction assays were performed on selective yeast synthetic dropout medium lacking Leu, Trp, His and Ade, in some cases supplemented with different concentrations of 3-aminotriazole (3-At; 0-100 mM). Plates were grown for 3-5 days at 28°C.

AtREM35-AtREM35 and AtREM34-AtREM34 were used respectively as positive and negative controls (Caselli et al, 2019, supplementary figure S9).

Bimolecular fluorescence complementation (BiFC)

The same CDS used for Y2H were cloned from the p207 derived entry vectors in pYFPN43 and pYFPC43 by Gateway LR reaction and the resulting constructs were transformed in Agrobacterium tumefaciens GV3101. The interactions were tested by co-infiltrating the abaxial surface of *Nicotiana benthamiana* leaves with the viral suppressor p19K construct. After 3 days, interactions were visualized by Laser Scanning Confocal Microscope Nikon A1 (laser emission 488 nm, YFP fluorescence collection between 500 and 550 nm, chlorophyll autofluorescence collection 660-740 nm). As positive control, AtREM35 homodimerization was tested, while AtREM34 homodimerization was used as negative control (Caselli et al, 2019), coupled with p19K only infiltration.

Results

Multiple mutants in *AtREM34*, *AtREM35* and *AtREM36* can produce more siliques on the main inflorescence

To investigate *REM34*, *REM35* and *REM36* gene function, single and double mutants were generated by CRISPR-Cas9 technology (Caselli et al, under revision for *REM34* and *REM35,* this paper for *REM36* and related double mutants). Both single and double mutants show an aberrant phyllotactic pattern, with angles that frequently diverge from the golden angle and often cluster around 90° and 180° (this paper, paragraph complementation test for *rem36*; supplementary fig. S2 for *rem34 rem36* and *rem35 rem36*; Caselli et al, under revision, for *rem34*, *rem35* and *rem34 rem35*).

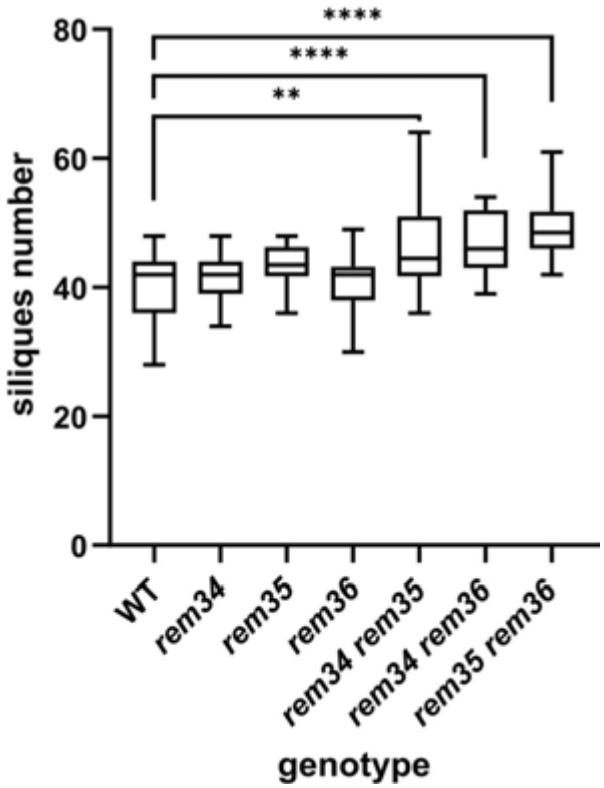

Fig. 1. Siliques on primary stem. >20 plants per genotype were analysed (30 Wild type, 29 *rem34*, 30 *rem35*, 23 *rem36*, 26 *rem34 rem35*, 29 *rem34 rem36*, 21 *rem35 rem36*). Statistical significance was calculated by Kruskal-Wallis and Dunn's *post hoc* test according to the normality and homoscedasticity of the data ($p<0.05$, compared to WT).

We evaluated the impact of such structural changes on the yield of the plant by counting the siliques produced on the main inflorescence. Interestingly, the double mutants show an increase in the number of siliques (Fig. 1). Specifically, compared to an average number of 40.65 in the Wild Type, the single mutants produce a similar amount of siliques (of 41.46 in *rem34*; 43.54 in *rem35* and 40.86 in *rem36*), while the double mutants produce approximately 20% more. Indeed we observe an average of siliques on the main stem of 46.23 in *rem34 rem35*, 46.59 in *rem34 rem36*, and 49.25 in *rem35 rem36.*

Importantly, as the mutants maintain a consistent number of seeds per silique (supplementary fig. S3), they potentially could increase seed production.

The observation of the phyllotactic phenotype for single mutants, but the yield phenotype only in the doubles, suggests that the genes under study have a partial redundant function in the inflorescence development.

We studied the conservation of the gene cluster in *Brassica napus*, one of the main oil crops. In this species, genetic knowledge and results can be easily transferred from *Arabidopsis*, given their phylogenetic proximity.

Study of the cluster conservation in *Brassica napus*

To get the homologous and study the phylogenetic conservation of our genes of interest, we performed a phylogenetic analysis on the *REM* IX subclass on *Brassica napus* (Supplementary fig. S4).

The proteome of *B. napus* was queried by all the *Arabidopsis* proteins belonging to the *REM IX* family (REM28-REM42, Romanel et al., 2009) using JackHmmer and a minimum sequence identity of 40% was applied. The homologous sequences retrieved were alligned by ClustalO and a phylogeny was inferred by RAxML-NG, WAG+G substitution model.

As *B. napus* is an allotetraploid and both the parental diploids underwent genome triplication after the *Brassica-Arabidopsis* clades split (14-24 million years ago, Bowers et al., 2003; Lysak et al., 2005; Wang et al., 2012), 6 genes are theoretically expected for every gene in *Arabidopsis*. However, it is known that a genome average of 4 is observed as a consequence of fractionation and pseudogenization (Park *et al.*, 2005; Town *et al.*, 2006).

This is not what we observe for the *REM IX* class, supporting the evidence that this class underwent recent duplication events in Arabidopsis, as reported by Romanel et al, 2009.

Focusing on the homologs of our genes of interest, we observe 6 *REM34* homologs, and 2 genes which are homologs of *REM35* and *REM36* (Fig.2) . These latter therefore probably duplicated after the clade split. Indeed, the estimated age of duplication of AtREM35 and AtREM36 is 14 Millions years ago (Romanel *et al.*, 2009), that's similar to the age of the Brassica-Arabidopsis clade split (Bowers *et al.*, 2003; Lysak *et al.*, 2005; Wang *et al.*, 2012). The original gene might have been more similar to *AtREM36*, as both the two homologs are more similar to *REM36* than to *REM35*. In REM36C1 this is more pronounced, while BnaREM35/36A2 sets more in the middle (see protein identity and similarity in supplementary fig. S5)

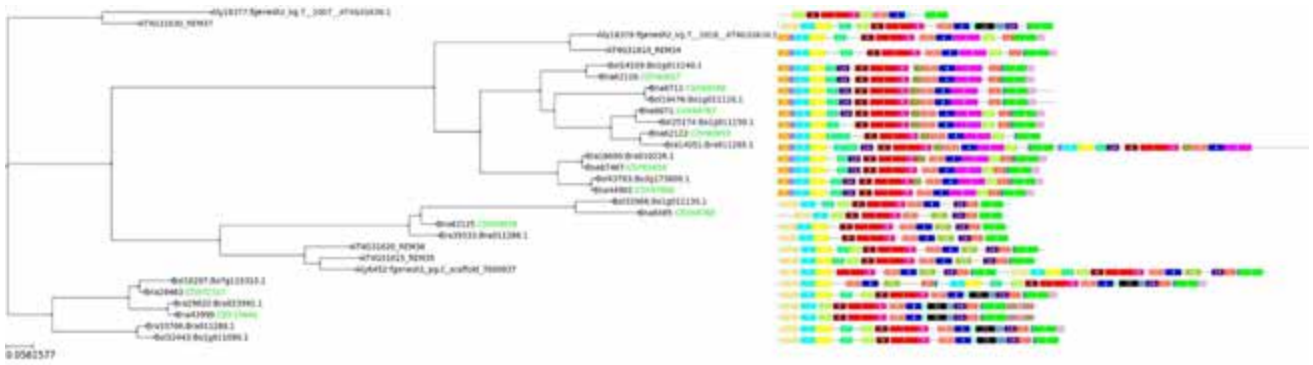

Fig. 2. *REM34, REM35, REM36* and *REM37 Brassica napus* homologs. *Brassica oleracea* and *rapa* proteins, as well as *Arabidopsis lyrata* ones, are included to provide more sound phylogenetic evidence. Distance as aminoacid substitution per site. Different protein motifs as determined by MEME suite are displayed by different number and colors.

As *REM37* clusters in the same phylogenetic group of our genes of interest (Romanel et al, 2009; supplementary fig S4), we decided to include it in our study too. Indeed, it was not previously characterized in *Arabidopsis* as it is not expressed there (Mantegazza *et al.*, 2014), but we can't assume the same for the *B. napus* homologs.

In the idea of producing edited lines of increased yield and knowing that the phenotype can be hindered by redundancy (as shown in fig 1), identifying all the good-confidence redundant genes is of paramount interest. 2 *B. napus* homologs are reported for *AtREM37*.

To simplify the nomenclature we here name our genes as *BnaREM*, a number according to the *REM* homolog in *Arabidopsis*, A or C according to the *rapa* or *oleracea* subgenome, and a successive number (Table 1).

protein code	gene code	gene name in this article
CDY60855	*BnaA01g34820D*	*BnaREM34A1*
CDY60857	*BnaA01g34830D*	*BnaREM34A2*
CDX68767	*BnaC01g06860D*	*BnaREM34C1*
CDX68769	*BnaC01g06840D*	*BnaREM34C2*
CDY65658	*BnaA08g30700D*	*BnaREM34A3*
CDY57886	*BnaC03g77300D*	*BnaREM34C3*
CDY13446	*BnaA03g51640D*	*BnaREM37A1*
CDX72317	*BnaC07g43390D*	*BnaREM37C1*
CDY60859	*BnaA01g34850D*	*BnaREM35/36A2*
CDX68768	*BnaC01g06850D*	*BnaREM36C1*

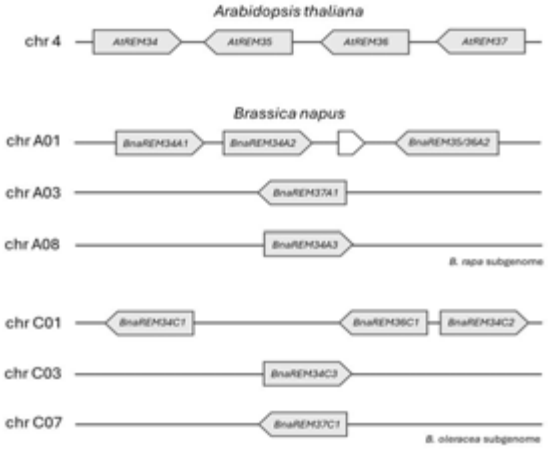

Table 1. Proteins and genes codes translation. Fig. 3. Chromosomic location of the genes studied.

Further analysis revealed the chromosome positioning of the *napus* homologs. The linkage context observed in *thaliana* is at least partially maintained in both the diploid subgenomes, with the *BnaREM37* genes that on the other hand are moved to a different chromosome (in *Arabidopsis* all the clade is linked), as an additional copy of *BnaREM34* (Fig. 3).

The coded homolog proteins have high sequence similarity with the *Arabidopsis* counterpart (supplementary figure S5), and are very similar one to the other. Especially the proteins coded by the twin genes of the two diploid subgenomes show poor divergence, as would be expected in a recent hybridization between related species (Chalhoub *et al.*, 2014). The BnaREM34s display between 70 and 91% of protein similarity, the BnaREM37 display the 80%, while BnaREM35/36A2 and Bna36C1 have diverged more, having a 68% of protein similarity (supplementary figure S4).

BnaREM34, _BnaREM35-36_ and _BnaREM37_ expression pattern is conserved

Retrieved our candidate genes, their expression profile was deeply studied by qPCR and *in situ* hybridization.

We sampled vegetative tissues including roots, cotyledons, leaves, hypocotyl and SAM-enriched apex, as well as reproductive ones, as IM-enriched apex (containing also small developing flowers), developed flowers and young siliques. Despite the high sequence identity between the gene sequences, specific primers were successfully designed for each candidate gene to be studied by qPCR.

The genes are mainly restricted in the reproductive tissues, as expected for *REM* genes (Mantegazza *et al.*, 2014).

The *REM34* homologs share an almost identical expression pattern, excluding *BnaREM34C2* whose mRNA was almost not detected in any of the tested tissues (Fig. 4).

In particular, they exhibit high expression in the inflorescence apex and in developed flowers, with a robust presence also in the shoot apical meristem enriched sample, consistent with the findings of (Franco-Zorrilla et al., 2002; Manrique et al., 2023). Among the six *AtREM34* homologues, *REM34A3* has a broader expression profile compared to the others, as it is also present in siliques and leaves (Fig. 4).

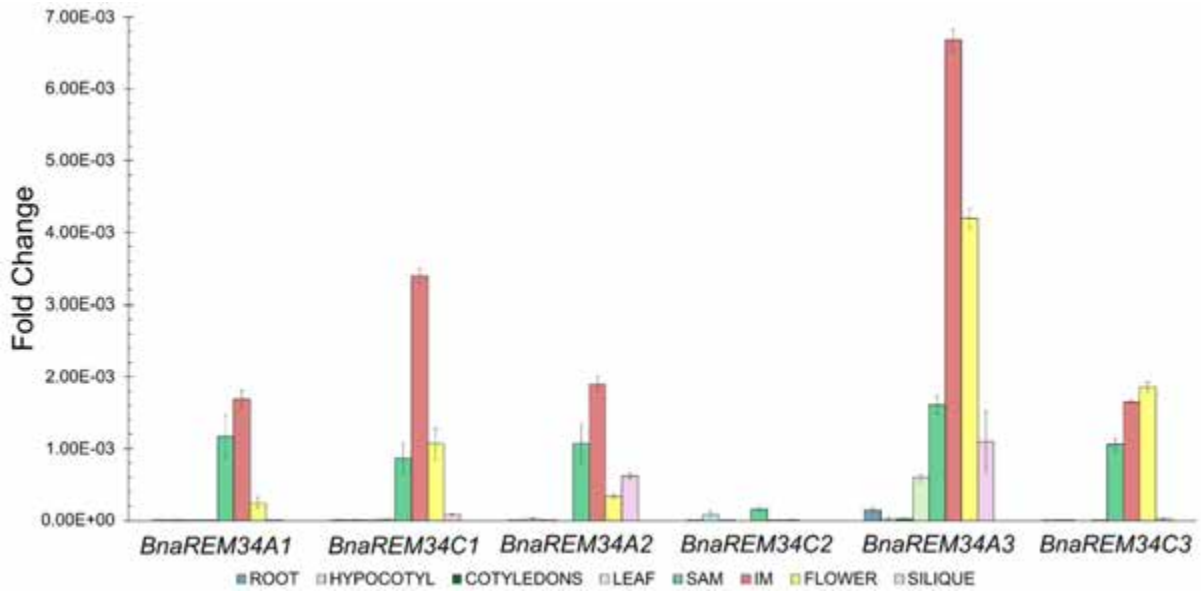

Fig. 4. *REM34* homologs expression. Average +/- Std error is displayed. The graph shows one representative biological replica out of 3. The fold change is calculated compared to the housekeeping gene *BnaACTIN-7* by the $2^{-\Delta Ct}$ method.

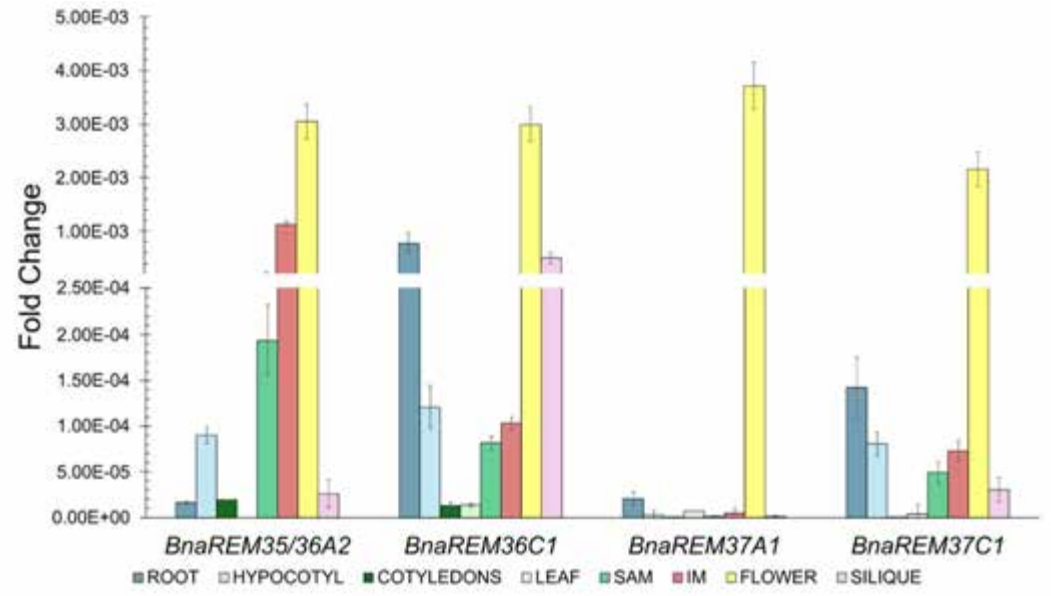

Fig. 5. *BnaREM35-36* and *BnaREM37* homologs expression. Average +/- Std error is displayed. The graph shows one representative biological replica out of 3. The fold change is calculated compared to the housekeeping gene *BnaACTIN-7* by the $2^{-\Delta Ct}$ method.

The *REM35-36* and *REM37* homologs display the highest expression in floral tissues. *REM35/36A2* show similarity to the *REM34* group, as it is expressed also in the IM- and slightly in the SAM- enriched samples, while *REM36C1* is modestly expressed also in roots and siliques (Fig. 5).

Some mild expression is visible in other tissues also for *BnaREM37s*. Given the similar results we got for the two *BnaREM37* genes, we speculate that the expression of the homolog was lost in *Arabidopsis* genre, and not re-acquired in the *Brassica* ones, after the clade split.

Subsequently, to study the precise localization of the gene expression during the first phases of floral development, we performed an *in situ* hybridization analysis on the *Brassica napus* inflorescences.

For this purpose, given the length of the probe and the high CDS sequence identity, each probe targets the twin genes of the two diploid progenitors, except for *REM35-36* twins, which diverged more (sense probe results presented in supplementary figure S6).

The expression pattern of all the genes under investigation is highly consistent with the one of their *Arabidopsis* homologs (Franco-Zorrilla *et al.*, 2002; Mantegazza *et al.*, 2014; Caselli *et al.*, 2019), suggesting a possible conservation of their biological role. *BnaREM37s* pattern is superimposable with the one of the other genes under study.

For all the genes the probes signal strongly localizes in the floral meristems and in the inflorescence meristem dome. Across the floral development, the expression is excluded from the first floral whorl and restrict to petals, anthers, pistil and nectary glands of different developmental stages. Later, the signal is clearly visible also in developing ovules (Fig. 6).

Given the results of the *in situ* hybridization we can state that all the *BnaREM* under investigation show expression in IM and FM and might therefore have a role in the phyllotaxis determination.

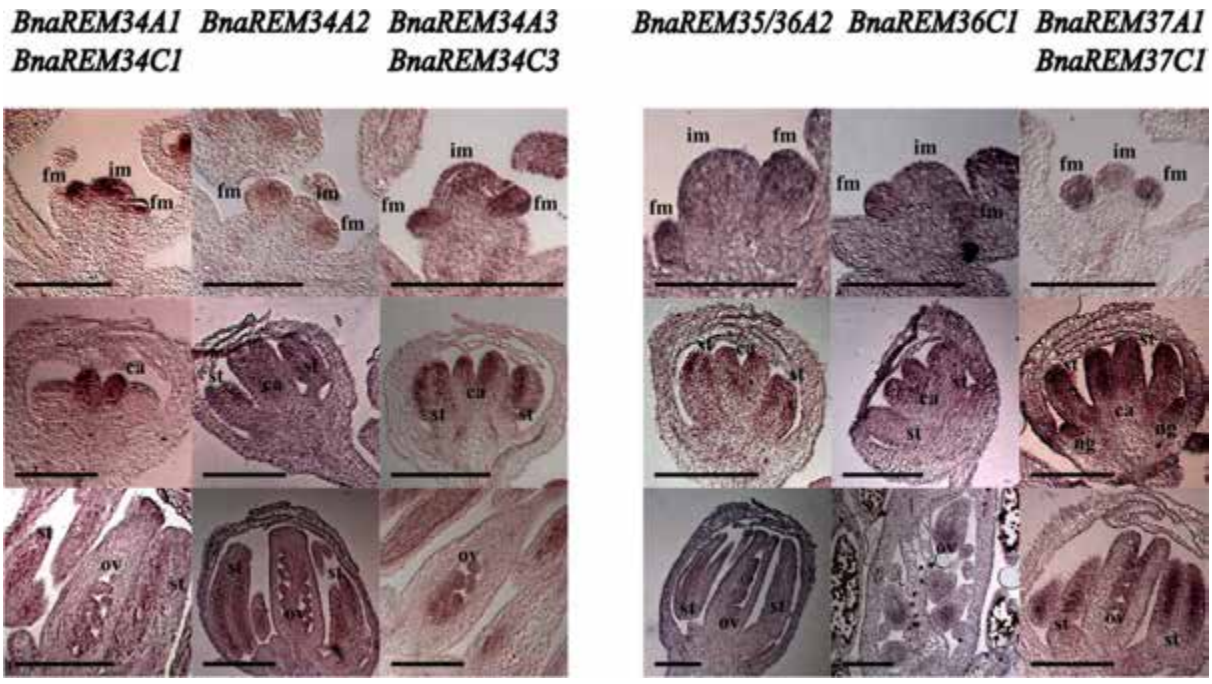

Fig. 6. *In situ* hybridization. The *REM34*, *REM35*, *REM36* and *REM37* homologs are expressed in the floral meristems (fm) and in the inflorescence dome im). Following the flower development, the expression restricts in the inner floral whorls (carpel=ca; stamen=st) and nectary glands (ng) and is excluded from sepals. Scale bar 200 µm.

BnaREMs are possibly involved in phyllotaxis determination

To analyse the interspecific functional conservation of the genes we set up a complementation test in the homolog Arabidopsis single mutants.

Since the twin genes of the two subgenomes of *Brassica napu*s are predicted to code for proteins with very high percentages of similarity (supplementary figure S5) we focused on a single subgenome (subgenome A, *Brassica rapa* derived). We therefore cloned under the 35S constitutive promoter *BnaREM34A1*, *BnaREM34A3*, *BnaREM35/36A2* and *BnaREM37A1*. We excluded *BnaREM34A2* as the protein that codes is similar to BnaREM34A1 (supplementary figure S5).

The Arabidopsis homolog mutants were transformed by floral dip and the phenotypical complementation was analysed evaluating the percentage of angles falling around the golden angle (130-150° range).

Specifically, *BnaREM34A1* and *BnaREM34A3* constructs were transformed in *rem34* mutant and *BnaREM35/36A2* was transformed in both *rem35* and *rem36* mutants. As we couldn't evaluate the functional conservation of *BnaREM37* by the same method (missing *AtREM37* expression and, therefore, a functional mutant), we decided to try to transform *BnaREM37A1* construct in the Arabidopsis mutant of the closest homolog. In this case, *rem35* was selected according to the protein similarity (supplementary figure S7). We hypothesized that if *BnaREM37A1* has a role in the phyllotaxis establishment, we could have observed some kind of perturbation in the pattern of the background mutant by constitutively expressing the gene. Moreover, if some important protein motif is conserved, maybe at least a partial complementation could have been observed.

For each *Brassica*'s gene constitutive expression, 3 independent lines showing different degrees of expression of the transgene (supplementary figure S8) were evaluated. We included *rem34 35S:REM34* and *rem35 35S:REM35* lines (Caselli et al, under revision) as a control for the effect of the constitutive expression of homologous *REMs* genes.

All the lines expressing *BnaREM34A1* (line 2; 68.54% - line 5; 67.74% - line 6; 68.11% of angles in the 130°-150° range), as well as the lines expressing *BnaREM34A3* (line 1; 62.58% - line 9; 66.24% - line 11; 61.07%), complement the Arabidopsis *rem34* mutant (45.13%), bringing the percentage of angles around the golden angle back to a WT situation (67.47%) and suggesting a functional conservation of the proteins coded (Fig 7).

The expression of *BnaREM35/36A2* can complement *rem36* mutant but not *rem35*. Indeed, observing a WT golden angle percentage of 61.35% and a *rem36* one of 42.49%, *rem36 35S:BnaREM35/36A2* #11, 110 and 115 presented respectively percentages of 56.28%; 60.35% and 56.44%, which are statistically equal to the WT percentage (Fig. 8). On the other hand, compared to a WT percentage of 67.86% and a *rem35* one of 50%, *rem35 35S:BnaREM35/36A2* #1, 2 and 3 presented percentages of 48.17%, 51.61% and 36.76%, equal to the *rem35* mutant (Fig. 8). This suggest the conservation of AtREM36 and BnaREM35/36A2 protein function and support the hypothesis that REM36 was the original gene in Arabidopsis and that REM35 is the result of a recent duplication and divergence. However, it is suggested to analyse the phylogeny of these REMs in other *Brassica* species to get further support to this hypothesis.

Finally, the phenotype of the *rem35 35S:BnaREM37A1* lines suggests a role of this gene in the phyllotaxis determination and the possible presence of some protein motifs similar to the ones of AtREM35. Indeed, compared to a WT ratio of golden angles of again 67.86% and *rem35* of 50%, line #32 and #141 partially complemented the mutant displaying 65.10% and 61.72% of golden angles,

behaving like the *rem35 35S:AtREM35* expression line, and #127 didn't complement, displaying 44.07% of golden angles, similarly to the *rem35* mutant (Fig. 8).

According to the results, it can be speculated that some relevant protein motifs are partially shared between BnaREM37A1 and AtREM35. The phenotype of line #127 could be due or to the T-DNA location in the genome or to the lower level expression of the construct (supplementary figure S8), and more lines should be analysed to state it.

Overall, we can conclude that an interspecific conservation of the protein function exists and that possibly *Brassica*'s genes are involved in phyllotaxis determination.

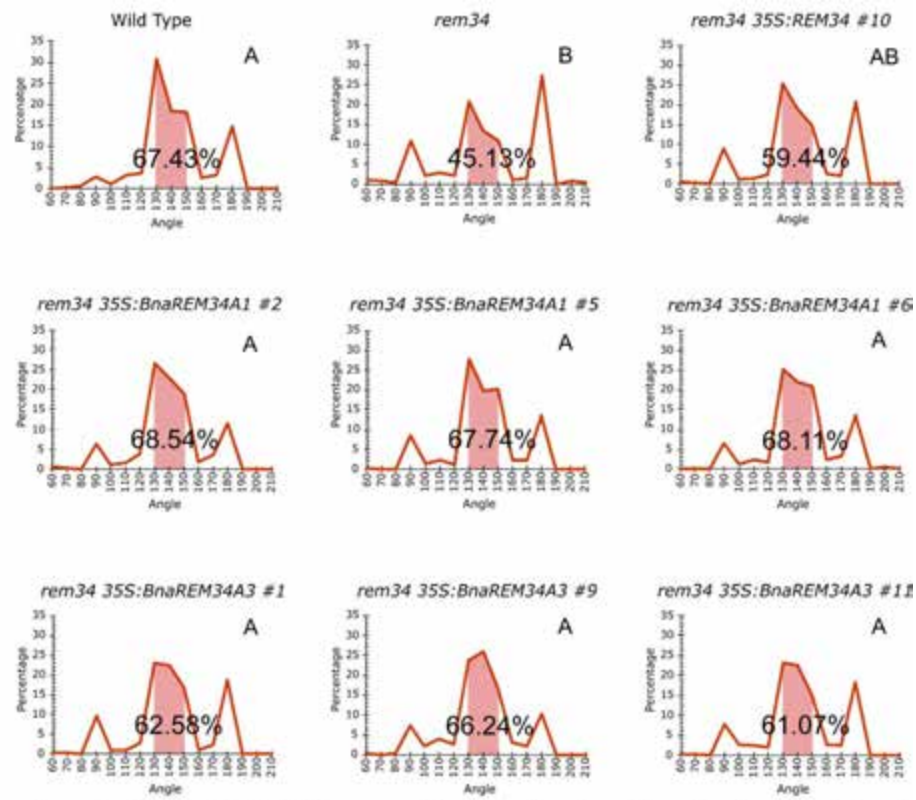

Fig. 7. Complementation test, *REM34* group. The graphs show the distribution of angles between two successive siliques. The range 130°-150°, used to evaluate the phenotype complementation, is highlighted and the percentage is reported. WT, mutants and constitutive expression lines are depicted. *rem34 35S:AtREM34* is included as an additional control. For each *Brassica*'s gene constitutive expression, 3 independent lines were evaluated. 12-15 plants per genotype were used (12 Wild Type – 390 angles, 13 *rem34*– 277 angles, 14 *rem34 35S:REM34#10*– 466 angles, 15 *rem34 35S:BnaREM34A1* #2– 410 angles, 13 *rem34 35S:BnaREM34A1* #5– 341 angles, 15 *rem34 35S:BnaREM34A1* #6– 392 angles, 15 *rem34 35S:BnaREM34A3* #1– 465 angles, 14 *rem34 35S:BnaREM34A3* #9– 388 angles, 15 *rem34 35S:BnaREM34A3* #11– 447 angles) . For *35S:AtREM34* a low expression of the protein was observed; this might be the cause of the partial complementation observed. Statistical significance was analysed by Kruskal-Wallis and Dunn's test ($p<0.05$, tests according to the normality and homoscedasticity of the data). Different letters are given to significantly different genotypes.

392

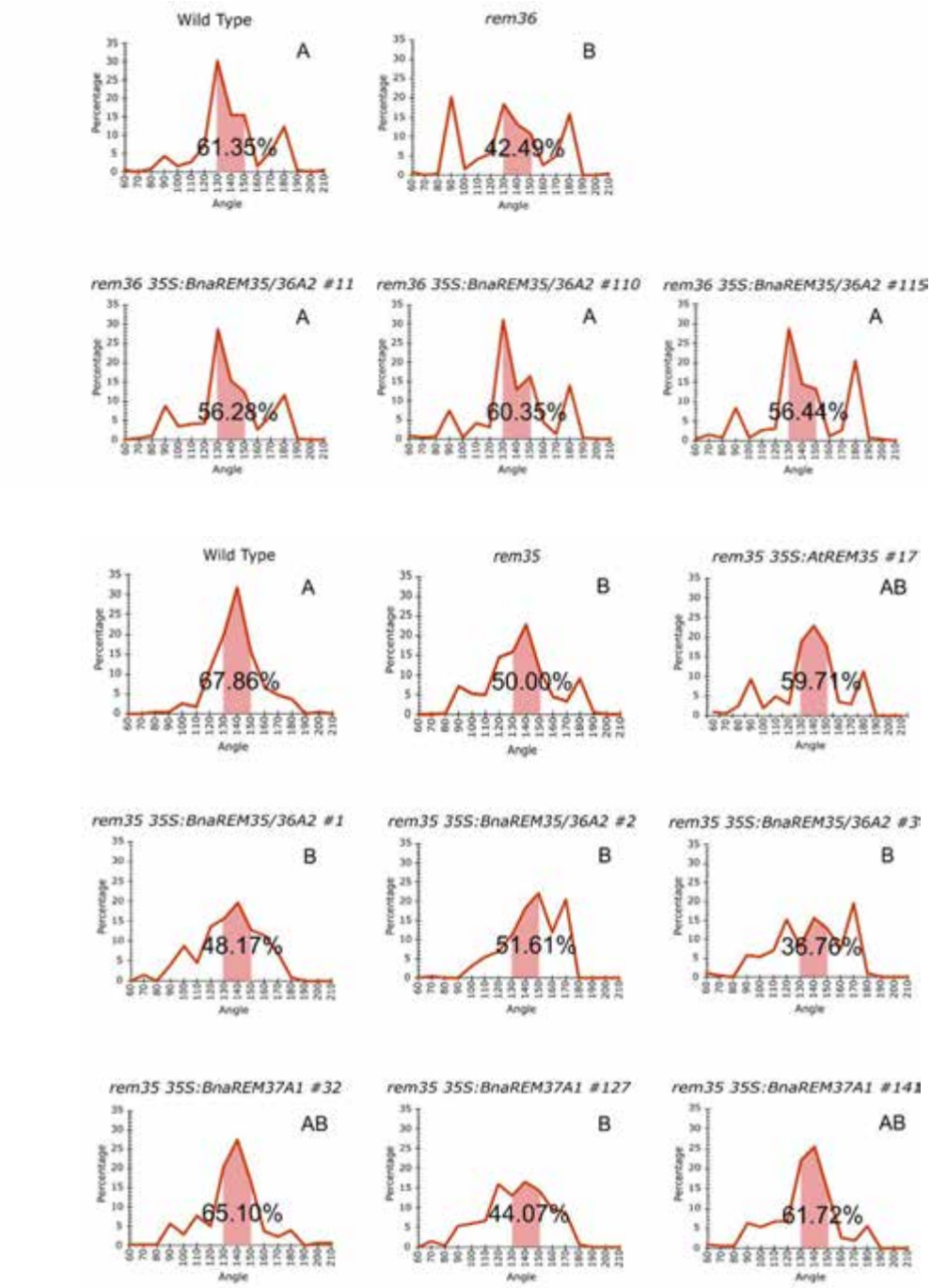

Fig. 8. Complementation test, *REM35-36-37* group. The graphs show the distribution of angles between two successive siliques. The range 130°-150°, used to evaluate the phenotype complementation, is highlighted and the percentage is reported. WT, mutants and constitutive expression lines are depicted. *rem35 35S:REM35* is included as an additional control (Caselli et al, under revision). For each *Brassica*'s gene overexpression, 3 independent lines were evaluated. 9-10 plants per genotype were used in rem35 complementation (9 Wild Type-280 angles, 10 *rem35*-324 angles, 10 *rem35 35S:REM35* #17-206 angles, 9 *rem35 35S:BnaREM35/36A2* #1-218 angles, 9 *rem35 35S:BnaREM35/36A2* #2-186 angles, 10 *rem35 35S:BnaREM35/36A2* #3-185 angles, 9 *rem35 35S:BnaREM37A1* #32-298 angles, 10 *rem35 35S:BnaREM37A1* #127-236 angles, 9 *rem35 35S:BnaREM37A1* #141-303 angles), 9-15 plants in rem36 complementation (10 Wild Type-251 angles, 9 *rem36*-233 angles, 14 *rem36 35S:BnaREM35/36A2* #11-414 angles, 15 *rem36 35S:BnaREM35/36A2* #110-454 angles, 10 *rem36 35S:BnaREM35/36A2* #115-264 angles) . Statistical significance was analysed by ANOVA and Dunnett's test in both *rem35* and *rem36* groups analysis ($p<0.05$, according to the normality and homoscedasticity of the data). Different letters are given to significantly different genotypes.

393 **Evaluation of REM protein complexes in *Brassica napus***

394 To further characterize the *Brassica* cluster and test the conservation of the protein behaviour, we used
395 the same cloned genes for a Y2H assay.

396 Some REM-REM interactions have already been described in the literature (Mendes *et al.*, 2016;
397 Caselli *et al.*, 2019; Manrique *et al.*, 2023), possibly depicting a functional feature widely spread in
398 the gene family. As between them there are REM35 homodimers and REM35-REM34 heterodimers,
399 we tested the interactions among the *Brassica*'s REMs under study.

400

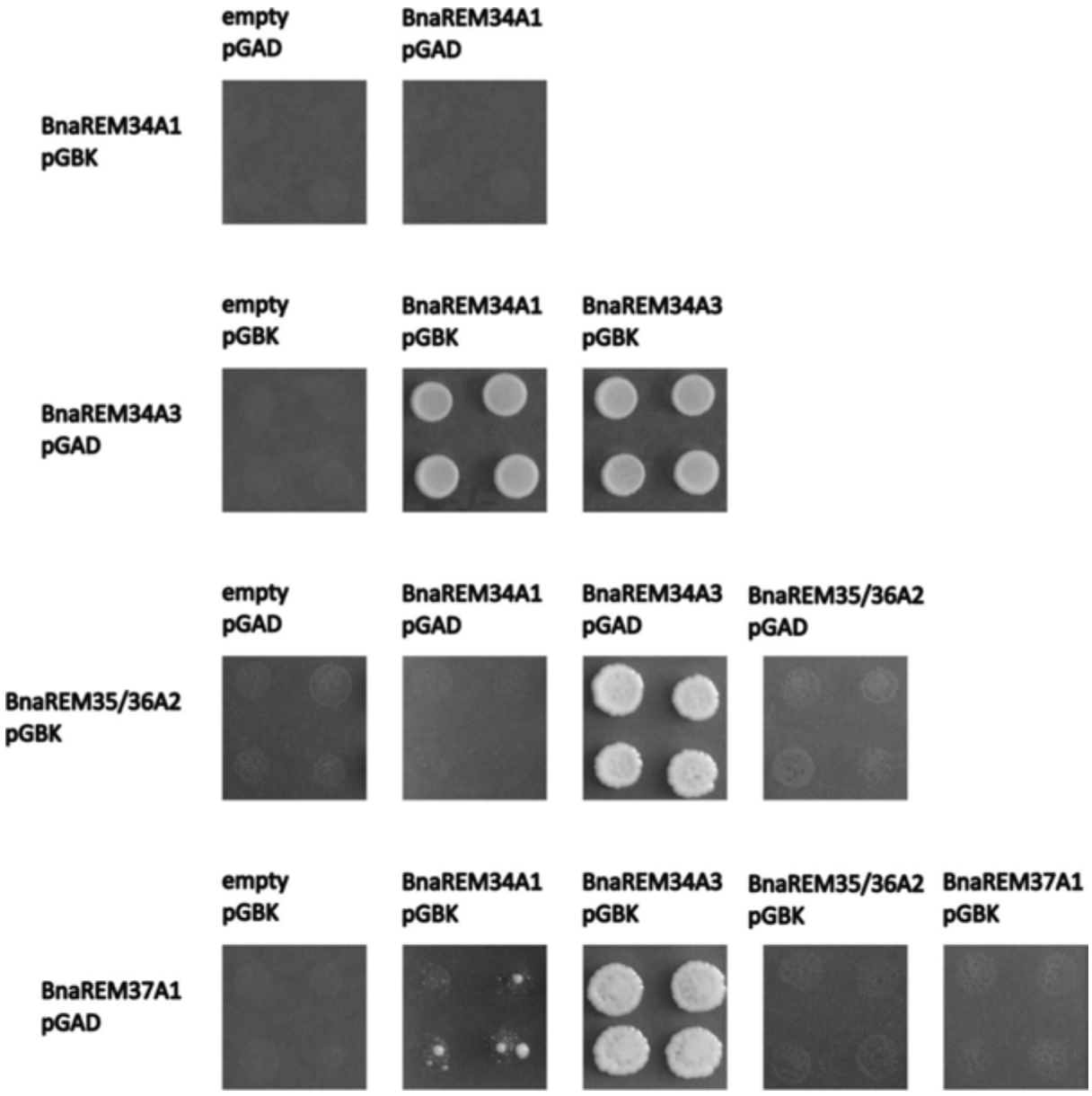

Fig. 9. Y2H between BnaREMs. All the combinations were tested. Selective medium lacking Adenin, Histidine, Tryptophan and Leucin was used to test the interactions. AtREM35-AtREM35 and AtREM34-AtREM34 were used respectively as positive and negative control (Caselli et al, 2019, supplementary figure S8).

BnaREM34A1 and BnaREM35/36A2 can't dimerize (Fig 9), behaving similarly to AtREM34 and AtREM36 (Caselli *et al.*, 2019) in heterodimer formation. In the same perspective, BnaREM35/36 doesn't homodimerize (Fig 9), again as AtREM36 (Caselli *et al.*, 2019). Therefore, considering both the interactions tested and the results of the complementation assay, BnaREM35/36 seems to be more related to AtREM36 than to AtREM35.

On the other hand, and differently from AtREM34, BnaREM34A3 is very sticky and presents wide interactions with all the other proteins tested, including itself (Fig 9). According to the numerosity of the BnaREM34 genes, BnaREM34A3 might have accumulated a few mutations that have changed its interaction capabilities. BnaREM37, more than with BnaREM34A3, slightly interact with BnaREM34A1 (Fig. 9).

The positive interactions were further confirmed in a plant context by BiFC (supplementary figure S10), supporting the results obtained in the Yeast-2-Hybrid.

Overall, some interactions, but not all of them, superimpose with the *Arabidopsis* results and new interactions are pointed out for a *B. napus* environment.

BnaREMs possibly interact with the auxin pathway

Since the impact of some of the studied *AtREM* genes on phyllotaxis is related to auxin perception via genetic interaction with AtARF7 and AtARF19, and it is known that AtREM35 can physically interact with these two proteins (Caselli et al, under revision), the interactions between the BnaREMs and AtARF7 and AtARF19 (the constructs were available in the laboratory) were tested. Even if intra-specific interactions should be tested for a complete assay, these sets of tests can help clarifying the potential interaction pattern of BnaREMs.

All the BnaREM tested can interact with AtARF19, and BnaREM35/36 can also interact with AtARF7 (Fig. 10). In this case, more than BnaREM34A3, even BnaREM34A1 and BnaREM35/36 partially and

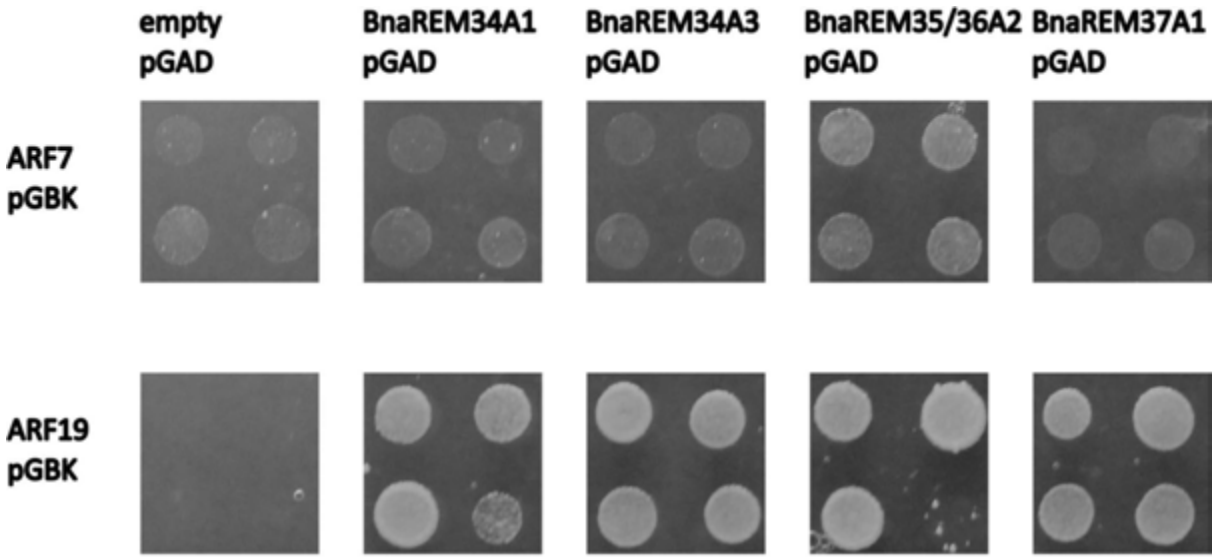

Fig. 10. Y2H between BnaREMs and AtARF7 and AtARF19. All the interspecific combinations were tested. Selective medium lacking Adenin, Histidine, Tryptophan and Leucin, supplemented with 100 mM of 3-At, was used to test the interactions (to counteract ARF autoactivation). AtREM35-AtREM35 and AtREM34-AtREM34 were used respectively as positive and negative control (Caselli et al, 2019; supplementary figure S8).

completely behave differently from their homologs (Caselli et al, under revision for ARF19 interactions, supplementary figure S11 for ARF7 interactions).

This suggests that the auxin pathway can be related to these REM gene functions in *Brassica napus* and that testing the interaction with the BnaARFs can be of great interest.

Discussion

The sustainable growth of the population without exacerbating humanity's environmental impact stands as a paramount challenge of the century. Addressing the need to enhance food production without expanding agricultural land requires a focus on increasing crop yields.

As a feature of the inflorescence architecture, phyllotaxis can offer a pathway to manipulate that yield.

This study reports the reliability of this hypothesis, unclosing novel *Arabidopsis* genotypes characterized by altered phyllotaxis and a heightened number of siliques. Double mutants in *REM34*, *REM35*, and *REM36* show a remarkable enhancement of the siliques produced on the main stem, yielding approximately 20% more than the wild type.

Importantly, the mutants maintain a consistent number of seeds per silique, indicating their potential to substantially increase seed production. Building upon this discovery, we further investigated the potential functional conservation of these genes in the closely related crop *Brassica napus*, aiming to explore the feasibility o f a translational approach.

Brassica napus is the third oil crop in the world following palm and soybean, and it is the first in Europe (Consumption of vegetable oils worldwide from 2013/14 to 2022/2023, by oil type, M. Shahbandeh, Sep 20, 2023; statista.com; oilseed and protein crops production, European commission, 2022 data).

Its primary use in food processing holds the largest share, accounting for 72.6% of the global revenue in 2018 (Rapeseed Oil Market Size, Share & Trends Analysis Report By Application (Food Processing, Bio-fuel, Personal Care, By Region (North America, Europe, APAC, CSA, MEA), And Segment Forecasts, 2019 - 2025)), but it is also used as ingredient for personal care products and for biofuel production (as well as inks, plastics, adhesive, bioplastics and sealants, canolacouncil.org). Notably, the 16% of the global biodiesel production stems form rapeseed oil (UFOP Chart of the week (50 2019), press release, 2019-12).

Increase yield in rapeseed would therefore be of high value, serving both as a vital food source and as a resource for the bioeconomy.

The number of siliques, together with parameters as the number of seeds per silique and 1000-seed weight, determine the yield in *Brassica napus* (Yang *et al.*, 2012). Moreover, considering the current rapeseed high planting density, the yield of the main inflorescence has the main impact, contributing up to 73% of the whole plant yield (Yuan *et al.*, 2022). Consequently, generating *B. napus* mutants similar to those described for *Arabidopsis* would be of considerable interest.

Given the evolution of the genome and its ploidy, the complexity expected in working with *B. napus* genome is not low and getting functional mutants can be long and difficult, especially targeting genes part of a big redundant family as the *REM*s are. Therefore, we think that is of paramount importance to well establish the candidate genes before pursuing mutants' generation.

In order to identify the soundest candidates to be mutated for producing higher yield genotypes, we performed the study you are reading of.

We first studied the *REM IX* gene family in the species, highlighting the phylogenetical relationships between *Arabidopsis thaliana, Brassica napus, Brassica rapa* and *Brassica oleracea* homologs. Subsequently we focused on the homologs of our genes of interest, expanding the analysis to *REM37* given is phylogenetic proximity.

We identified six homologous genes for *AtREM34*, two for *AtREM35* and *AtREM36* and two for *AtREM37.* This finding can be explained accounting for both *Brassica* genome evolution and ploidy, as well as the *REM IX* class recent duplications.

All but one of the 10 candidate genes are expressed in the inflorescence and floral tissues, with a pattern that highly resemble the *Arabidopsis* one (Mantegazza *et al.*, 2014; Caselli *et al.*, 2019) and is compatible with an involvement in the inflorescence architecture.

The genes of the two subgenomes code for very similar protein and are hypothesized to have the same function because the event of hybridization is recent.

Therefore, the analysis of protein function was performed on 4 candidates of the subgenome A. The interspecific complementation test suggests a functional conservation of the *Brassica* proteins and further support the hypothesis of the involvement of *BnaREM* genes in phyllotaxis determination.

Finally, the protein interaction tests performed reveal conserved as well as new REM dimers formation in *B. napus* and open the possibility that a REM-ARF interaction can be involved in inflorescence development as it has been recently described in *Arabidopsis*. Cloning and interaction testing of the BnaARFs is therefore of great relevance.

Concluding, this study underscores the significance of *Arabidopsis thaliana* as a model system for investigating crucial agronomic traits and reveal candidate genes that knocked-out could produce *Brassica napus* genotypes of increased yield.

Given the multitude of genes, expected redundancy and genomic positions, we think that modern editing approaches offer enhanced efficiency compared to traditional mutagenesis methods (also stated in Braatz et al., 2017; Tian et al., 2022) and would therefore be the best choice to produce those kinds of mutants.

Supplementary materials

***REM36* gene structure and mutant**

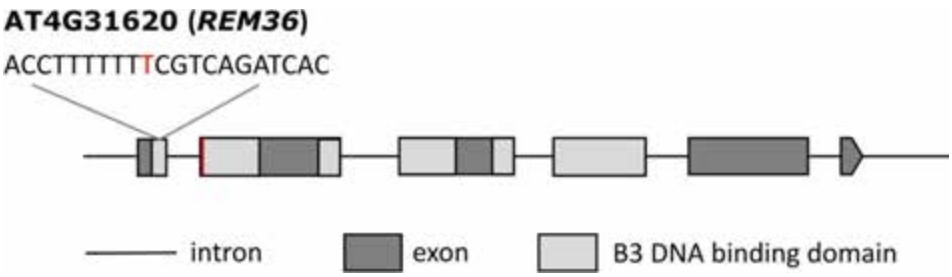

Figure S1. Schematic representation of the structure of *REM36* gene and *rem36* mutant. Boxes: exons, lines: introns. The gene is characterized by three repetitions of the B3 DNA binding domain (light grey boxes), as *REM34* and *REM35* (Caselli et al, under revision). The protospacer used to generate *rem36* mutant is reported, as well as the nucleotide insertion (red T) and the location of the premature stop codon (red line at the beginning of the second exon) generated by the genome editing.

***rem34 rem36* and *rem34 rem36* phyllotaxis**

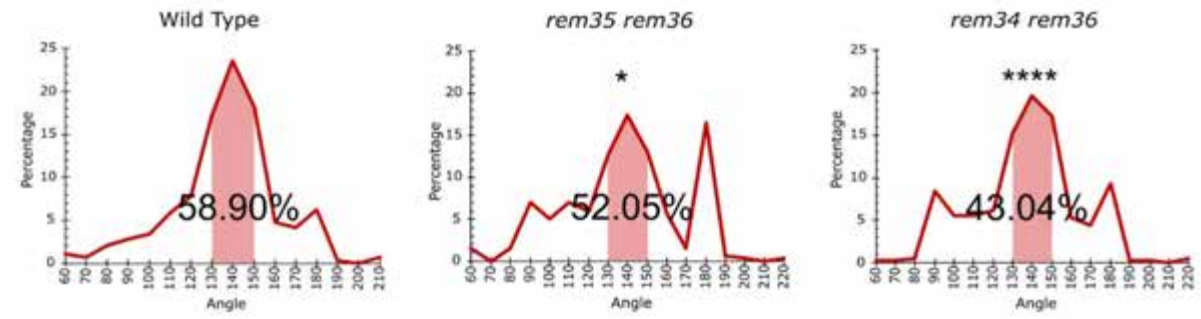

Figure S2. The graphs show the distribution of angles between two successive siliques. The range 130°-150° is highlighted and the percentage is reported. 11-12 plants per genotype were used (11 Wild Type, 292 angles, 12 *rem34 rem36* 342 angles, 11 *rem35 rem36* 316 angles). Statistical significance was analysed by ANOVA and Dunnett's post hoc tests ($p<0.05$; <0.0001)

Number of seeds per silique of *Atrems* mutants

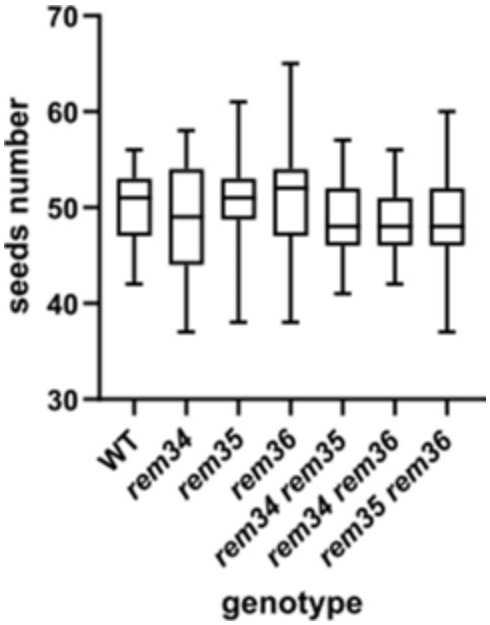

Figure S3. Number of seed per silique in *Atrem* mutants. 11 plants per genotype, 5 siliques each plant (55 Wild Type, 54 *rem34*, 47 *rem35*, 55 *rem36*, 48 *rem34 rem35*, 55 *rem34 rem36*, 55 *rem35 rem36*). No significant differences from WT (Kruskal Wallis – Dunn's post hoc test).

499 ***Brassica napus REM* IX clade phylogeny**

500

Figure S4. Phylogenesis of the *Brassica napus REM* IX class and their *Arabidopsis* counterparts. Distance as aminoacid substitution per site. Different protein motifs as determined by MEME suite are displayed by different number and colors.

Protein identity and similarity

	BnaREM34A1	BnaREM34A2	BnaREM34A3	BnaREM34C1	BnaREM34C2	BnaREM34C3
AtREM34 identity	50	51	54	50	53	53
AtREM34 similarity	63	62	68	63	65	66

	BnaREM35/36A2	BnaREM36C1
AtREM35 identity	49	36
AtREM35 similarity	61	50
AtREM36 identity	52	42
AtREM36 similarity	64	54

	BnaREM37A1	BnaREM37C1
AtREM37 identity	51	59
AtREM37 similarity	61	72

	BnaREM34A1	BnaREM34A2	BnaREM34A3	BnaREM34C1	BnaREM34C2
BnaREM34A2	77				
BnaREM34A3	69	70			
BnaREM34C1	90	79	71		
BnaREM34C2	78	78	73	80	
BnaREM34C3	70	72	91	71	74

	BnaREM35/36A2
BnaREM36C1	68

	BnaREM37A1
BnaREM37C1	80

Figure S5. Similarity and identity between the *Arabidopsis* and *Brassica* proteins and within *Brassica* proteins. A color code is given to the *BnaREM34* table to simplify the reading (conditional colour from green to red)

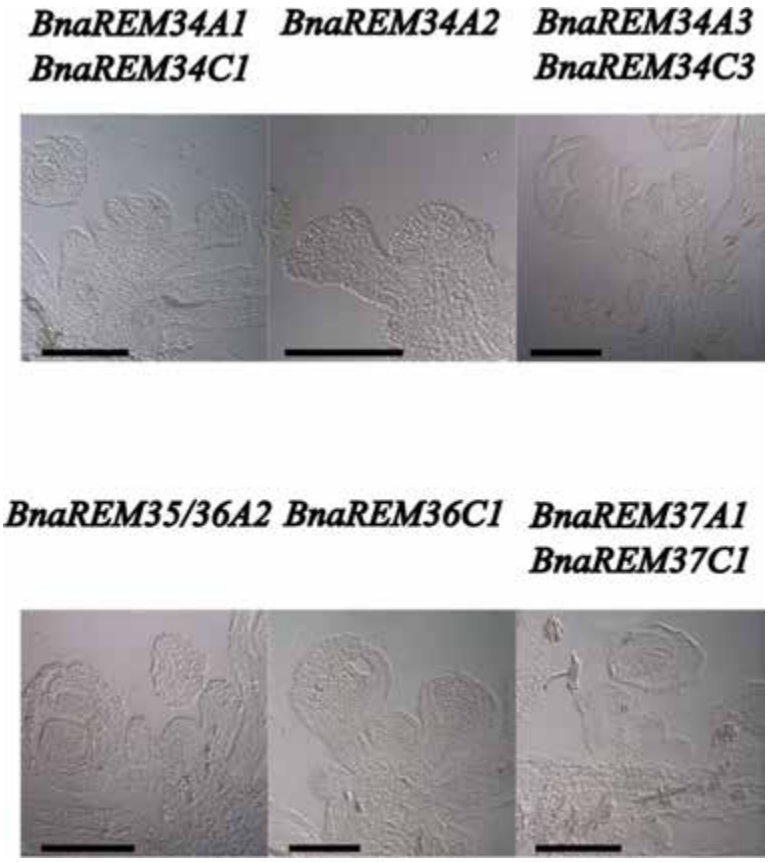

Figure S6. *In situ* hybridization with sense probes on *Brassica napus* IM and floral tissues. Scale bar 200 µm. The absence of signal witnesses the specificity of the antisense probes.

503 **BnaREM37 identity and similarity to AtREMs**

	BnaREM37A1	BnaREM37C1
AtREM34 identity	155/491(32%)	191/549(35%)
AtREM34 similarity	225/491(45%)	281/549(51%)
AtREM35 identity	218/489(45%)	245/526(47%)
AtREM35 similarity	286/489(58%)	327/526(62%)
AtREM36 identity	210/496(42%)	243/528(46%)
AtREM36 similarity	279/496(56%)	323/528(61%)
AtREM37 identity	267/520(51%)	311/526(59%)
AtREM37 similarity	320/520(61%)	378/526(71%)

Figure S7. Identity and similarity of BnaREM37 to the AtREM included in this study. Excluding AtREM37, AtAtREM35 gets the best results.

504

505

506 ***Bna* genes overexpression levels in *Arabidopsis* complementation lines, generation T1**

507

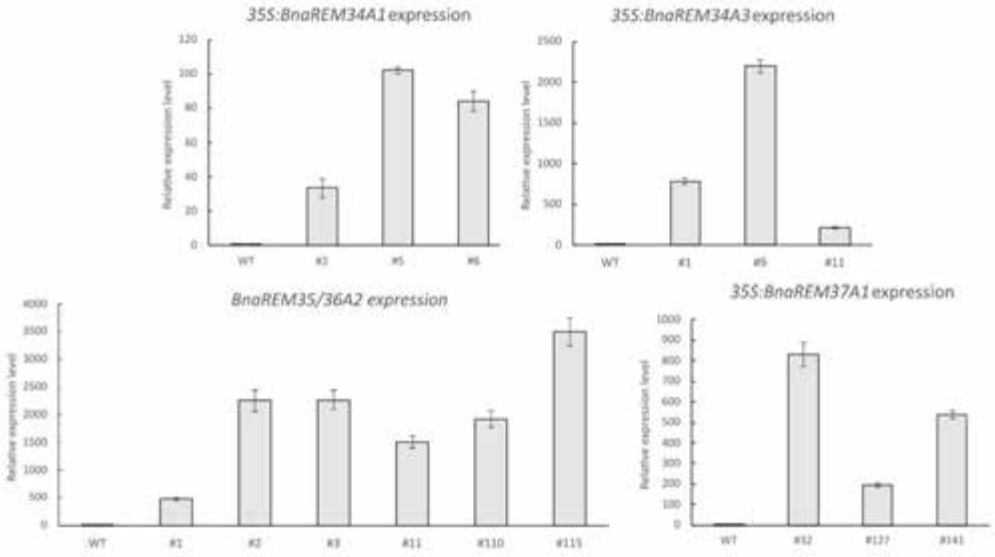

Fig. S8. Relative expression levels of *Brassica* genes in *Arabidopsis* complementation lines, generation T1. The expression in the WT is manually set at 1. For conciseness, only the number of the line is depicted. The *35S:BnaREM34A1* and *35S:BnaREM34A3* constructs are in a *rem34* background, *35S:BnaREM37A1* construct is in a *rem35* background and 35S:BnaREM35/36A2 construct is in *rem35* background for lines #1, 2, 3 and in *rem36* background for #11, 110, 115 respectively. The lines selected for the phenotype complementation have different levels of expression of the transgene. Mean +/- standard error is displayed. 3 technical replicas per line were used.

508

509 **Y2H controls**

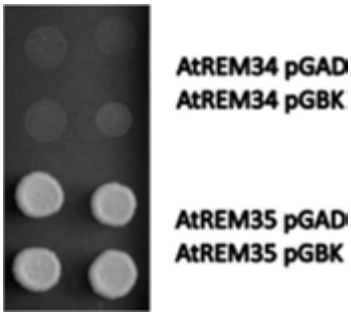

Figure S9. Y2H controls. Selective medium lacking Adenin, Histidine, Tryptophan and Leucin. AtREM35-AtREM35 and AtREM34-AtREM34 homodimers presence and absence as in Caselli et al, 2019.

510

511 **Bimolecular Fluorescence Complemennatation (BIFC)**

512

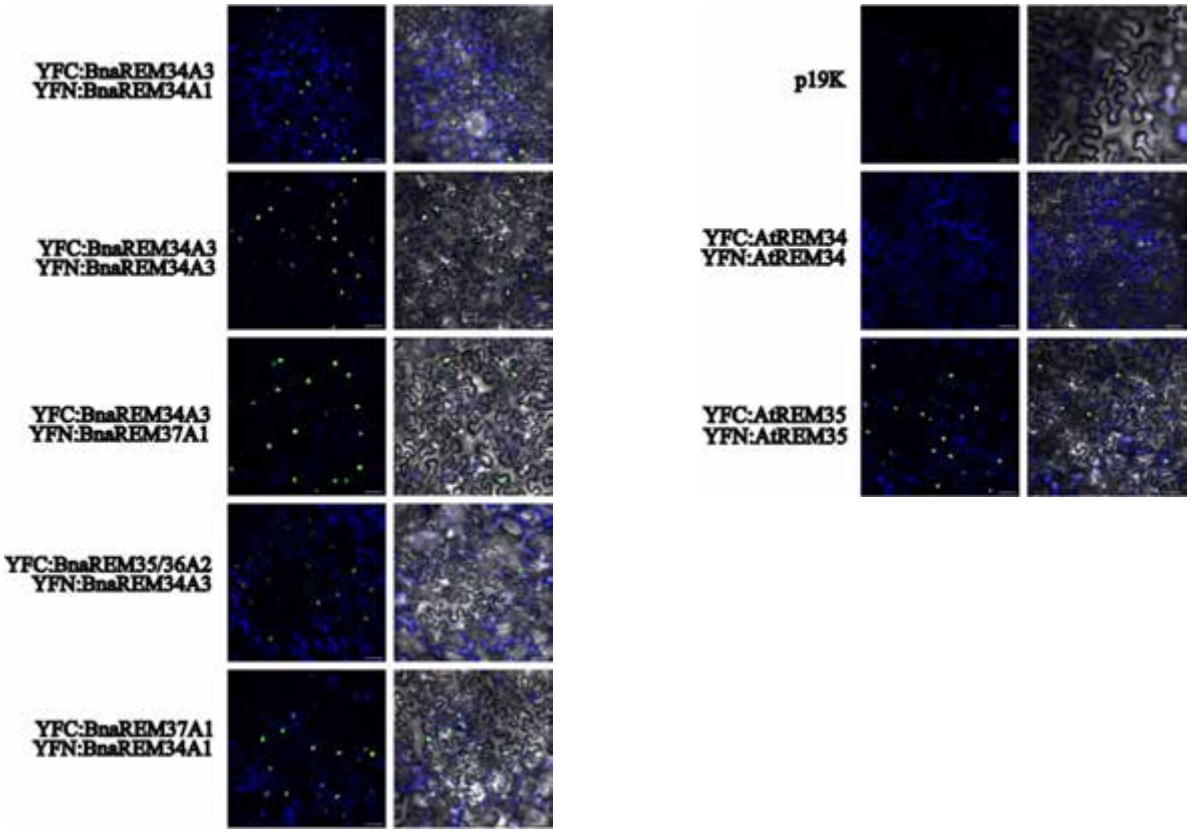

Figure S10. Confirmation of the positives *Brassica* intraspecific protein interaction by BiFC. The left line shows YFP and Chl channels, the right line includes the bright field too. p19K was co-infiltrated with the *Brassica* constructs. On the right panel the controls are depicted (AtREM34 homodimers: negative control, p19K only: negative control, AtREM35 homodimers: positive control; Caselli et al, 2019). Scale bar=50 µm

513 **AtARF7 interactions with the AtREMs under investigation**

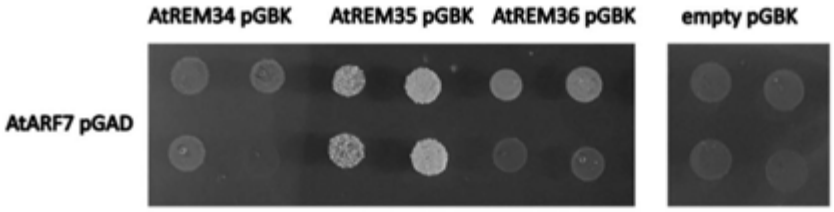

Figure S11. AtARF7 interactions. Selective medium lacking Adenin, Histidine, Tryptophan and Leucin, 15 mM 3-At. Data from Caselli.

514

Primers list

ID	sequence	amplified gene ID	target gene code and notes
Bna1	TAATTTCAGCCACGGAGACG	BnaREM34A1	BnaA01g34820 fw RT-PCR
Bna2	CTGCTTCTGGTTTCTCACTC	BnaREM34A1	BnaA01g34820 rv RT-PCR
Bna3	GAATGACTCATTCGTGTTGGAG	BnaREM34C1	BnaC01g06860 fw RT-PCR
Bna4	CTGTTTGAAACCCTAGTGCATC	BnaREM34C1	BnaC01g06860 rv RT-PCR
Bna5	TCTAGCCTCATCGATGATCG	BnaREM34A2	BnaA01g34830 fw RT-PCR
Bna6	CAGCCTCGTCTGATGTTAAATG	BnaREM34A2	BnaA01g34830 rv RT-PCR
Bna7	TCCAGTGACATACAACACGC	BnaREM34C2	BnaC01g06840 fw RT-PCR
Bna8	TCTCACACGGTTTATTGTGC	BnaREM34C2	BnaC01g06840 rv RT_PCR
Bna9	TGTATCTGTGTCCCCTCGGT	Bna34REMA3	BnaA08g30700 fw RT-PCR
Bna10	GTCATCCTCTCCTCCATCGTC	Bna34REMA3	BnaA08g30700 rv RT-PCR
Bna11	TGCTGTGAGTGATGATGAATC	BnaREM34C3	BnaC03g77300 fw RT-PCR
Bna12	GCTCATTAAACGACACAACAG	BnaREM34C3	BnaC03g77300 rv RT-PCR
Bna13	AGAGATTCGCCCGTGGATG	BnaREM37C1	BnaC07g43390 fw RT-PCR
Bna14	TCTGCTGAGTGAATCTGCGT	BnaREM37C1	BnaC07g43390 rv RT-PCR
Bna21	GGAAGCTCCTGGAATCCATGAGA	BnaACT7	actin-7 fw RT-PCR
Bna22	TCTTTGCTCATACGGTCAGCAATTCC	BnaACT7	actin-7 rv RT-PCR
Bna23	TGAAAGATGGCCGATGGTGA	BnaACT7	actin-7 fw RT-PCR + intron
Bna24	GTGCCTAGGACGACCAACAA	BnaACT7	actin-7 rv RT-PCR + intron
Bna25	CAATCTTCATCGTAGATCTGTCCG	BnaREM37A1	BnaA03g51640 fw RT-PCR
Bna26	ACCGAAGCGTCTGAAGTCAG	BnaREM37A1	BnaA03g51640 rv RT-PCR
Bna27	ACGCTCACTGTCTTCGAAACG	BnaREM35/36A2	BnaA01g34850 fw RT-PCR
Bna28	CTCAAATCTGAAACTTTGTCCCATG	BnaREM35/36A2	BnaA01g34850 rv RT-PCR
Bna29	CAAAACCTAACAGGGCAGGC	BnaREM36C1	BnaC01g06850 fw RT-PCR
Bna30	ATGCATGAGTACGGCGAGAG	BnaREM36C1	BnaC01g06850 rv RT-PCR
Bna34	GGGGACAAGTTTGTACAAAAAAGCAGGCTTCATGGTGGTTCCTCCTCCAAAAC	BnaREM34A1	BnaA01g34820 fw GW for Nterm fusion
Bna35	GGGGACCACTTTGTACAAGAAAGCTGGGTCTAAACCAGATTATTGTTGAG	BnaREM34A1	BnaA01g34820 rv GW with STOP
Bna36	GGGGACAAGTTTGTACAAAAAAGCAGGCTtcATGGCGACTTCTCCAAAATCG	BnaREM35/36A2	BnaA01g34850D fw GW for Nterm fusion
Bna37	GGGGACCACTTTGTACAAGAAAGCTGGGTTTACTTGAAGAATTTGTTGAC	BnaREM35/36A2	BnaA01g34850D rv GW with STOP
Bna38	GGGGACAAGTTTGTACAAAAAAGCAGGCTtcATGGTGGATCCAGTTATGGC	BnaREM37A1	BnaA03g51640D fw GW for Nterm fusion
Bna39	GGGGACCACTTTGTACAAGAAAGCTGGGTTTAGACTTGATTGATGTTGAAG	BnaREM37A1	BnaA03g51640D rv GW with STOP
Bna40	GGGGACAAGTTTGTACAAAAAAGCAGGCTtcATGACTATTCCTCCTACATTTTC	BnaREM34A3	BnaA08g30700D fw GW for Nterm fusion
Bna41	GGGGACCACTTTGTACAAGAAAGCTGGGTTTACACCaGATTATTGTTGAG	BnaREM34A3	BnaA08g30700D rv GW with STOP
Bna42	TAATACGACTCACTATAGGG ACACCAACTCTTGTGCAGTCC	BnaREM35/36A2	BnaA01g34850D rv +T7 in situ (fw Bna27)
Bna45	TAATACGACTCACTATAGGG TCTGCTGAGTGAATCTGCGT	BnaREM37C1	BnaC07g43390D/BnaA03g51640 rv +T7 in situ (fw Bna13)
Bna46	TAATACGACTCACTATAGGG CTGTTTGAAACCCTAGTGCATC	BnaREM34_1 C/A	BnaA01g34820/BnaC01g06860 rv + T7 in situ (FW Bna3)
Bna47	GAATGACTCATTCGTGTTGGAG	BnaREM34A2	BnaA01g34830 fw in situ
Bna48	TAATACGACTCACTATAGGG CTGTTTAAAACCCTAGCGTGTC	BnaREM34A2	BnaA01g34830 rv + T7 in situ (FW Bna47)
Bna49	TAATACGACTCACTATAGGG GTCATCCTCTCCTCCATCGTC	BnaREM34_3 A/C	BnaA08g30700/BnaC03g77300 rv + T7 in situ (FW Bna9)
Bna50	ATGGCGACTTCTCCAAAATCG	BnaREM35/36A2	BnaA01g34850D fw cloning for Nterm fusion
Bna51	TTACTTGAAGAATTTGTTGAC	BnaREM35/36A2	BnaA01g34850D rv cloning with STOP
Bna38_bis	ATGGTGGATCCAGTTATGGC	BnaREM37A1	BnaA03g51640D fw cloning for Nterm fusion
Bna39_bis	TTAGACTTGATTGATGTTGAAG	BnaREM37A1	BnaA03g51640D rv cloning with STOP
Bna52	TAATACGACTCACTATAGGG ACAGACGGCCATGTTCCTCC	BnaREM36C1	BnaC01g06850D rv +T7 in situ (fw Bna29)
Bna54	CAATGTGAGATCGATCTAAG	BnaREM37A1	BnaA03g51640D fw internal primer
Bna55	CCAGCCATTACTGACAAATGC	BnaREM37A1	BnaA03g51640D rv internal primer
Bna61	TGGAAGCGGAAGACCTCG	BnaREM34_3 C/A	C03g77300 fw in situ - 34C3/A3 probe n2
Bna62	TAATACGACTCACTATAGGG GAATGCTCAGCTTCACGTTAG	BnaREM34_3 C/A	C03g77300 rv in situ + T7 tail (bna58 fw) 34C3/A3 probe n2
Bna63	GTCGGATGATGTAGAAGACGAAG	BnaREM34A2	BnaA01g34830D in situ probe n2 fw
Bna64	TAATACGACTCACTATAGGG ACGACATAACCTTAAAATCCTC	BnaREM34A2	BnaA01g34830D in situ probe n2 rv
bna68	TAATACGACTCACTATAGGG GTCGGATGATGTAGAAGACGAAG	BnaREM34_2 C/A	BnaA01g34830D in situ SENSE probe n2
bna69	ACGACATAACCTTAAAATCCTC	BnaREM34_2 C/A	BnaA01g34830D in situ SENSE probe n2
bna70	TAATACGACTCACTATAGGG TGGAAGCGGAAGACCTCG	BnaREM34_3 C/A	C03g77300 fw SENSE in situ - 34C3/A3 probe n2 fw
bna71	GAATGCTCAGCTTCACGTTAG	BnaREM34_3 C/A	C03g77300 rv SENSE in situ- 34C3/A3 probe n2 rv
bna72	TAATACGACTCACTATAGGG GAATGACTCATTCGTGTTGGAG	BnaREM34A2	BnaA01g34830 fw SENSE in situ
bna73	CTGTTTAAAACCCTAGCGTGTC	BnaREM34A2	BnaA01g34830 rv SENSE in situ
bna74	TAATACGACTCACTATAGGG TGTATCTGTGTCCCCTCGGT	BnaREM34_3 C/A	BnaA08g30700/BnaC03g77300 SENSE fw in situ
bna75	GTCATCCTCTCCTCCATCGTC	BnaREM34_3 C/A	BnaA08g30700/BnaC03g77300 SENSE rv in situ
bna76	TAATACGACTCACTATAGGG GAATGACTCATTCGTGTTGGAG	BnaREM34_1 C/A	BnaA01g34820/BnaC01g06860 SENSE fw in situ
bna77	CTGTTTGAAACCCTAGTGCATC	BnaREM34_1 C/A	BnaA01g34820/BnaC01g06860 SENSE rv in situ
bna78	TAATACGACTCACTATAGGG ACGCTCACTGTCTTCGAAACG	BnaREM35/36A2	BnaA01g34850 SENSE fw in situ
bna79	ACACCAACTCTTGTGCAGTCC	BnaREM35/36A2	BnaA01g34850 SENSE rv in situ
bna80	TAATACGACTCACTATAGGG AGAGATTCGCCCGTGGATG	BnaREM37C1	BnaC07g43390/BnaA03g51640 SENSE fw in situ
bna81	TCTGCTGAGTGAATCTGCGT	BnaREM37C1	BnaC07g43390/BnaA03g51640 SENSE rv in situ
bna82	TAATACGACTCACTATAGGG CAAAACCTAACAGGGCAGGC	BnaREM36C1	BnaC01g06850D SENSE fw in situ
bna83	ACAGACGGCCATGTTCCTCC	BnaREM36C1	BnaC01g06850D SENSE rv in situ
RT 147	CTGTTCACGGAACCCAATTC	AtUBIQUITIN	houskeeping for qPCR fw (Pribil et al, 2010)
RT 148	GGAAAAAGGTCTGACCGACA	AtUBIQUITIN	houskeeping for qPCR rv (Pribil et al, 2010)

Bibliography

Adler, I., Barabe, D. and J E A N †, R. V (1997) *A History of the Study of Phyllotaxis*, *Annals of Botany*.

Barabé, D. and Lacroix, C. (2020) 'Phyllotactic patterns: A multidisciplinary approach', *Phyllotactic Patterns: A Multidisciplinary Approach*, pp. 1–273. Available at: https://doi.org/10.1142/11571/ASSET/18EE2C74-0218-E2C7-4021-EE2C7440218E/11571.COVER.JPG.

Bartrina, I. *et al.* (2011) 'Cytokinin regulates the activity of reproductive meristems, flower organ size, ovule formation, and thus seed yield in Arabidopsis thaliana', *Plant Cell*, 23(1), pp. 69–80. Available at: https://doi.org/10.1105/tpc.110.079079.

Bennett, S.R.M. *et al.* (1995) *Morphogenesis in pinoid mutants of Arabidopsis thaliana*, *The Plant Journal*.

Besnard, F. *et al.* (2014) 'Cytokinin signalling inhibitory fields provide robustness to phyllotaxis', *Nature*, 505(7483), pp. 417–421. Available at: https://doi.org/10.1038/nature12791.

Bhatia, N. *et al.* (2016) 'Auxin Acts through MONOPTEROS to Regulate Plant Cell Polarity and Pattern Phyllotaxis', *Current Biology*, 26(23), pp. 3202–3208. Available at: https://doi.org/10.1016/j.cub.2016.09.044.

Bowers, J.E. *et al.* (2003) 'Unravelling angiosperm genome evolution by phylogenetic analysis of chromosomal duplication events', *Nature*, 422(6930), pp. 433–438. Available at: https://doi.org/10.1038/NATURE01521.

Braatz, J. *et al.* (2017) 'CRISPR-Cas9 Targeted Mutagenesis Leads to Simultaneous Modification of Different Homoeologous Gene Copies in Polyploid Oilseed Rape (Brassica napus)', *Plant Physiology*, 174(2), p. 935. Available at: https://doi.org/10.1104/PP.17.00426.

Caselli, F. *et al.* (2019) 'REM34 and REM35 Control Female and Male Gametophyte Development in Arabidopsis thaliana', *Frontiers in Plant Science*, 10(October), pp. 1–17. Available at: https://doi.org/10.3389/fpls.2019.01351.

Chalhoub, B. *et al.* (2014) 'Early allopolyploid evolution in the post-neolithic Brassica napus oilseed genome', *Science*, 345(6199), pp. 950–953. Available at: https://doi.org/10.1126/science.1253435.

Clough, S.J. and Bent, A.F. (1998) 'Floral dip: A simplified method for Agrobacterium-mediated transformation of Arabidopsis thaliana', *Plant Journal*, 16(6), pp. 735–743. Available at: https://doi.org/10.1046/j.1365-313X.1998.00343.x.

Coen, E.S. *et al.* (1990) 'floricaula: A homeotic gene required for flower development in antirrhinum majus', *Cell*, 63(6), pp. 1311–1322. Available at: https://doi.org/10.1016/0092-8674(90)90426-F.

Fauser, F., Schiml, S. and Puchta, H. (2014) 'Both CRISPR/Cas-based nucleases and nickases can be used efficiently for genome engineering in Arabidopsis thaliana', *Plant Journal*, 79(2), pp. 348–359. Available at: https://doi.org/10.1111/tpj.12554.

de Folter, S. and Immink, R.G.H. (2011) 'Yeast Protein–Protein Interaction Assays and Screens', in *Methods in molecular biology (Clifton, N.J.)*, pp. 145–165. Available at: https://doi.org/10.1007/978-1-61779-154-3_8.

Franco-Zorrilla, J.M. *et al.* (2002) 'AtREM1, a member of a new family of B3 domain-containing genes, is preferentially expressed in reproductive meristems', *Plant Physiology*, 128(2), pp. 418–427. Available at: https://doi.org/10.1104/pp.010323.

Galvan-Ampudia, C.S. *et al.* (2016) 'Phyllotaxis: from patterns of organogenesis at the meristem to shoot architecture', *Wiley Interdisciplinary Reviews: Developmental Biology*, 5(4), pp. 460–473. Available at: https://doi.org/10.1002/wdev.231.

Gómez-Mena, C. *et al.* (2005) 'Transcriptional program controlled by the floral homeotic gene AGAMOUS during early organogenesis', *Development*, 132(3), pp. 429–438. Available at: https://doi.org/10.1242/DEV.01600.

Gregis, V. *et al.* (2013) 'Identification of pathways directly regulated by SHORT VEGETATIVE PHASE during vegetative and reproductive development in Arabidopsis', *Genome Biology 2013 14:6*, 14(6), pp. 1–26. Available at: https://doi.org/10.1186/GB-2013-14-6-R56.

Heisler, M.G. *et al.* (2005) 'Patterns of Auxin Transport and Gene Expression during Primordium Development Revealed by Live Imaging of the Arabidopsis Inflorescence Meristem', *Current Biology*, 15(21), pp. 1899–1911. Available at: https://doi.org/10.1016/J.CUB.2005.09.052.

Henchion, M. *et al.* (2021) 'Review: Trends for meat, milk and egg consumption for the next decades and the role played by livestock systems in the global production of proteins', *Animal*, 15, p. 100287. Available at: https://doi.org/10.1016/j.animal.2021.100287.

Heo, J.B., Sung, S. and Assmann, S.M. (2012) 'Ca2+-dependent GTPase, Extra-large G Protein 2 (XLG2), Promotes Activation of DNA-binding Protein Related to Vernalization 1 (RTV1), Leading to Activation of Floral Integrator Genes and Early Flowering in Arabidopsis', *The Journal of Biological Chemistry*, 287(11), p. 8242. Available at: https://doi.org/10.1074/JBC.M111.317412.

586 Kaufmann, K. *et al.* (2009) 'Target Genes of the MADS Transcription Factor SEPALLATA3:
587 Integration of Developmental and Hormonal Pathways in the Arabidopsis Flower', *PLoS*
588 *Biology*, 7(4), pp. 0854–0875. Available at:
589 https://doi.org/10.1371/JOURNAL.PBIO.1000090.

590 Landrein, B. *et al.* (2015) 'Meristem size contributes to the robustness of phyllotaxis in
591 Arabidopsis', *Journal of Experimental Botany*, 66(5), pp. 1317–1324. Available at:
592 https://doi.org/10.1093/jxb/eru482.

593 Levy, Mesnage, Mylne, Gendall, D. (2002) 'Multiple roles in Arabidopsis VRN1 in
594 bernalization and flowering time'. science.

595 Li, Y.J. *et al.* (2021) 'The Arabidopsis MATERNAL EFFECT EMBRYO ARREST45 protein
596 modulates maternal auxin biosynthesis and controls seed size by inducing
597 AINTEGUMENTA', *Plant Cell*, 33(6), pp. 1907–1926. Available at:
598 https://doi.org/10.1093/plcell/koab084.

599 Lysak, M.A. *et al.* (2005) 'Chromosome triplication found across the tribe Brassiceae',
600 *Genome research*, 15(4), pp. 516–525. Available at:
601 https://doi.org/10.1101/GR.3531105.

602 Manrique, S. *et al.* (2023) 'Assessing the role of REM13, REM34 and REM46 during the
603 transition to the reproductive phase in Arabidopsis thaliana', *Plant Molecular Biology*,
604 112(3), pp. 179–193. Available at: https://doi.org/10.1007/s11103-023-01357-1.

605 Mantegazza, O. *et al.* (2014) 'Analysis of the arabidopsis REM gene family predicts
606 functions during flower development', *Annals of Botany*, 114(7), pp. 1507–1515.
607 Available at: https://doi.org/10.1093/aob/mcu124.

608 Matias-Hernandez, L. *et al.* (2010) 'VERDANDI is a direct target of the MADS domain
609 ovule identity complex and affects embryo sac differentiation in Arabidopsis', *Plant Cell*,
610 22(6), pp. 1702–1715. Available at: https://doi.org/10.1105/tpc.109.068627.

611 Mendes, M.A. *et al.* (2016) 'Live and let die: A REM complex promotes fertilization
612 through synergid cell death in Arabidopsis', *Development (Cambridge)*, 143(15), pp.
613 2780–2790. Available at: https://doi.org/10.1242/dev.134916.

614 Nemhauser, J.L., Feldman, L.J. and Zambryski, P.C. (2000) 'Auxin and ETTINin
615 Arabidopsisgynoecium morphogenesis Jennifer', *Development* [Preprint].

616 Okabe, T. (2016) 'The riddle of phyllotaxis: Exquisite control of divergence angle', *Acta*
617 *Societatis Botanicorum Poloniae*. Polskie Towarzystwo Botaniczne. Available at:
618 https://doi.org/10.5586/asbp.3527.

619 Okada, K. *et al.* (1991) 'Requirement of the Auxin Polar Transport System in Early Stages
620 of Arabidopsis Floral Bud Formation.', *The Plant Cell*, 3(7), p. 677. Available at:
621 https://doi.org/10.1105/TPC.3.7.677.

Okal, M. *et al.* (1999) 'Auxin Polar Transport and Flower Formation in Arabidopsis thaliana Transformed with Indoleacetamide Hydrolase (iaaH) Gene', *Plant and Cell Physiology*, 40(2), pp. 231–237. Available at: https://doi.org/10.1093/OXFORDJOURNALS.PCP.A029532.

Park, J.Y. *et al.* (2005) 'Physical mapping and microsynteny of Brassica rapa ssp. pekinensis genome corresponding to a 222 kbp gene-rich region of Arabidopsis chromosome 4 and partially duplicated on chromosome 5', *Molecular genetics and genomics : MGG*, 274(6), pp. 579–588. Available at: https://doi.org/10.1007/S00438-005-0041-4.

Parkin, I.A.P. *et al.* (2005) 'Segmental structure of the Brassica napus genome based on comparative analysis with Arabidopsis thaliana', *Genetics*, 171(2), pp. 765–781. Available at: https://doi.org/10.1534/genetics.105.042093.

Peaucelle, A. *et al.* (2007) 'Plants expressing a miR164-resistant CUC2 gene reveal the importance of post-meristematic maintenance of phyllotaxy in Arabidopsis', *Development*, 134(6), pp. 1045–1050. Available at: https://doi.org/10.1242/dev.02774.

Pinon, V. *et al.* (2013) 'Local auxin biosynthesis regulation by PLETHORA transcription factors controls phyllotaxis in Arabidopsis', *Proceedings of the National Academy of Sciences of the United States of America*, 110(3), pp. 1107–1112. Available at: https://doi.org/10.1073/pnas.1213497110.

Prasad, K. *et al.* (2011) 'Arabidopsis PLETHORA transcription factors control phyllotaxis', *Current Biology*, 21(13), pp. 1123–1128. Available at: https://doi.org/10.1016/j.cub.2011.05.009.

Pribil, M. *et al.* (2010) 'Role of plastid protein phosphatase TAP38 in LHCII dephosphorylation and thylakoid electron flow', *PLoS Biology*, 8(1). Available at: https://doi.org/10.1371/journal.pbio.1000288.

Przemeck, G.K.H. *et al.* (1996) 'Studies on the role of the Arabidopsis gene MONOPTEROS in vascular development and plant cell axialization', *Planta*, 200(2), pp. 229–237. Available at: https://doi.org/10.1007/BF00208313.

Reinhardt, D. *et al.* (2003) 'Regulation of phyllotaxis by polar auxin transport', *Nature*, 426(6964), pp. 255–260. Available at: https://doi.org/10.1038/nature02081.

Reinhardt, D. (2005) 'Regulation of phyllotaxis', *International Journal of Developmental Biology*, 49(5–6), pp. 539–546. Available at: https://doi.org/10.1387/ijdb.041922dr.

Richter, R. *et al.* (2019) 'Floral regulators FLC and SOC1 directly regulate expression of the B3-type transcription factor TARGET of FLC and SVP 1 at the Arabidopsis shoot apex via antagonistic chromatin modifications', *PLoS Genetics*, 15(4), pp. 1–27. Available at: https://doi.org/10.1371/journal.pgen.1008065.

Ritchie, H. *et al.* (2024) 'Population Growth', *Our World in Data* [Preprint]. Available at: https://ourworldindata.org/population-growth (Accessed: 25 September 2024).

Romanel, E.A.C. *et al.* (2009) 'Evolution of the B3 DNA binding superfamily: New insights into REM family gene diversification', *PLoS ONE*, 4(6). Available at: https://doi.org/10.1371/journal.pone.0005791.

Schwarz, I. *et al.* (2020) 'Cytokinin regulates the activity of the inflorescence meristem and components of seed yield in oilseed rape', *Journal of Experimental Botany*, 71(22), pp. 7146–7159. Available at: https://doi.org/10.1093/jxb/eraa419.

Sessions, A. *et al.* (1997) 'ETTIN patterns the Arabidopsis floral meristem and reproductive organs', *Development*, 124(22), pp. 4481–4491. Available at: https://doi.org/10.1242/dev.124.22.4481.

Shi, B. and Vernoux, T. (2019) 'Patterning at the shoot apical meristem and phyllotaxis', *Current Topics in Developmental Biology*, 131, pp. 81–107. Available at: https://doi.org/10.1016/bs.ctdb.2018.10.003.

Simonini, S. *et al.* (2017) 'Auxin-induced modulation of ETTIN activity orchestrates gene expression in arabidopsis', *Plant Cell*, 29(8), pp. 1864–1882. Available at: https://doi.org/10.1105/tpc.17.00389.

Swaminathan, K., Peterson, K. and Jack, T. (2008) 'The plant B3 superfamily', *Trends in Plant Science*, (November), pp. 647–655. Available at: https://doi.org/10.1016/j.tplants.2008.09.006.

Tian, Q. *et al.* (2022) 'Application of CRISPR/Cas9 in Rapeseed for Gene Function Research and Genetic Improvement', *Agronomy*. MDPI. Available at: https://doi.org/10.3390/agronomy12040824.

Town, C.D. *et al.* (2006) 'Comparative genomics of Brassica oleracea and Arabidopsis thaliana reveal gene loss, fragmentation, and dispersal after polyploidy', *Plant Cell*, 18(6), pp. 1348–1359. Available at: https://doi.org/10.1105/tpc.106.041665.

Traas, J. (2013) 'Phyllotaxis', *Development (Cambridge)*, 140(2), pp. 249–253. Available at: https://doi.org/10.1242/dev.074740.

Wang, Y. *et al.* (2012) 'Systematic analysis of plant-specific B3 domain-containing proteins based on the genome resources of 11 sequenced species', *Molecular biology reports*, 39(5), pp. 6267–6282. Available at: https://doi.org/10.1007/S11033-012-1448-8.

Wu, X. *et al.* (2021) 'Enhancing rice grain production by manipulating the naturally evolved cis-regulatory element-containing inverted repeat sequence of OsREM20', *Molecular Plant*, 14(6), pp. 997–1011. Available at: https://doi.org/10.1016/J.MOLP.2021.03.016/ATTACHMENT/7AA37CAF-2980-43D1-850C-55933121941D/MMC3.PDF.

Wuest, S.E. *et al.* (2012) 'Molecular basis for the specification of floral organs by APETALA3 and PISTILLATA', *Proceedings of the National Academy of Sciences of the United States of America*, 109(33), pp. 13452–13457. Available at: https://doi.org/10.1073/pnas.1207075109.

Yang, P. *et al.* (2012) 'Identification of a major QTL for silique length and seed weight in oilseed rape (Brassica napus L.)', *Theoretical and Applied Genetics*, 125(2), pp. 285–296. Available at: https://doi.org/10.1007/S00122-012-1833-7/FIGURES/3.

Yin, X. (2021) 'Phyllotaxis: from classical knowledge to molecular genetics', *Journal of Plant Research*, 134(3), pp. 373–401. Available at: https://doi.org/10.1007/s10265-020-01247-3.

Yu, Y. *et al.* (2020) 'Arabidopsis REM16 acts as a B3 domain transcription factor to promote flowering time via directly binding to the promoters of SOC1 and FT', *Plant Journal*, 103(4), pp. 1386–1398. Available at: https://doi.org/10.1111/tpj.14807.

Yuan, D. *et al.* (2022) 'BnKAT2 Positively Regulates the Main Inflorescence Length and Silique Number in Brassica napus by Regulating the Auxin and Cytokinin Signaling Pathways', *Plants*, 11(13). Available at: https://doi.org/10.3390/plants11131679.

Zhang, K. *et al.* (2022) 'Cell- and noncell-autonomous AUXIN RESPONSE FACTOR3 controls meristem proliferation and phyllotactic patterns', *Plant Physiology*, 190(4), pp. 2335–2349. Available at: https://doi.org/10.1093/plphys/kiac370.

Behind phyllotaxis, within the meristem: a REM-ARF complex shapes inflorescence in *Arabidopsis thaliana*

Caselli F,[1]. Ferrario C. C. [1], Beretta V. M[1], Tondepu S. [1] , Dumas R.[2] , Herrera-Ubaldo H. [3], de Folter S. [4]; Kater M. [1], Gregis V. [1]

[1]Università degli Studi di Milano, Department of Biosciences

[2]cnrs, pcv/irtsv/cea

[3]Cinvestav UGA-Langebio

[4]Centro de Investigacion y de Estudios Avanzados del Instituto Politecnico Nacional, Unidad de Genómica Avanzada (Langebio)

Resubmitted after revision on December 2024, The Plant Journal

In this paper REM34 and REM35 are deeply characterized, unveiling the protein expression pattern, protein interactions and role in phyllotaxis determination. Specifically, the functional interaction with the auxin responsive factors ARF7 and ARF19 is highlighted and the mechanisms underpinning REM34 and REM35 functions are described in both cellular and molecular perspective.

I contributed to this paper by performing the *in situ hybridization* on *H4*, marker for dividing cells, on the *rem34 rem35,* and *arf7 arf19* mutants and on the WT and by performing some of the phyllotaxis analysis depicted in the manuscript.

Behind phyllotaxis, within the meristem: a REM-ARF complex shapes inflorescence in *Arabidopsis thaliana*

Francesca Caselli[1], Carlotta Ferrario[1], Veronica Beretta[1], Sri Amarnadh Gupta Tondepu[1,4], Renaud Dumas[2], Humberto Herrera-Ubaldo[3,5], Stefan de Folter[3,] Martin M. Kater[1], Veronica Gregis[1,*]

[1] Dipartimento di Bioscienze, Università degli Studi di Milano, Milano 20133, Italy
[2] Laboratoire Physiologie Cellulaire et Végétale, Université Grenoble Alpes, Centre national de la recherche scientifique, Commissariat à l'énergie atomique et aux énergies alternatives, Institut national de recherche pour l'agriculture, l'alimentation et l'environnement, Département de Biologie Structurale et Cellulaire intégrée, Grenoble F-38054, France
[3] Unidad de Genómica Avanzada (UGA-Langebio), Centro de Investigación y de Estudios Avanzados del Instituto Politécnico Nacional, Irapuato, Mexico.
[4] Present address: Department of Biology and Biotechnology "L. Spallanzani", University of Pavia, Via Adolfo Ferrata 9, 27100 Pavia, Italy.
[5] Present address: Department of Plant Sciences, University of Cambridge, Cambridge CB2 3EA, UK

* Corresponding author: veronica.gregis@unimi.it

Abstract

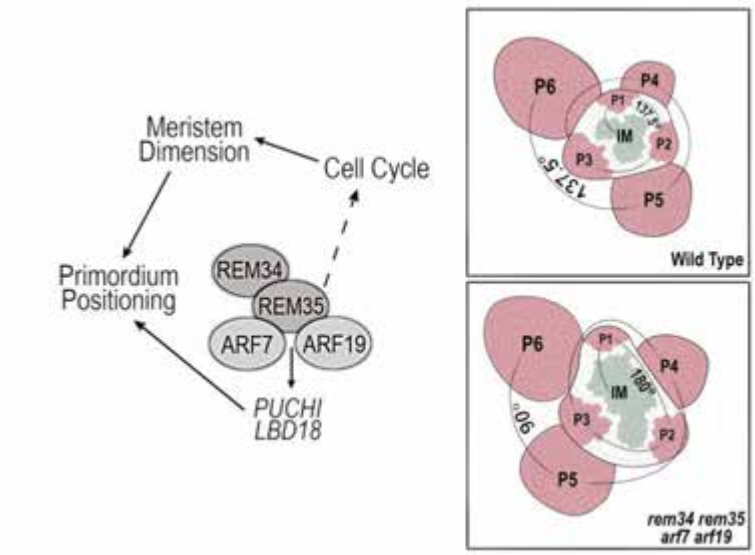

Inflorescence architecture is established during the early stages of reproductive development and depends on the activity and identity of meristems. In *Arabidopsis thaliana*, the floral meristems, which will develop into flowers, arise with precise spatiotemporal regulation from the inflorescence meristem. The outcome of this process is a geometrically organized structure characterized by a reiterated pattern called phyllotaxis, in which successive organs arise at specific divergence angles of 137.5°.

Here we show that REM34 and REM35 transcription factors control phyllotactic patterning through cooperative interaction with ARF7 and ARF19, influencing the cell cycle rate and thus the inflorescence meristem dimension.

Our proposed model suggests that ARF7 and ARF19, whose activity is triggered by auxin accumulation, interact with REM34 and REM35 to regulate two auxin-induced genes, LBD18 and PUCHI whose mutants phenocopy the permutated phyllotactic pattern of rem34 rem35 and arf7 arf19. This complex also restricts cell cycling activity to specific areas of the meristem, indirectly determining its dimension, and ultimately establishing floral meristem positioning and phyllotaxis.

Reiterative patterns are found in morphogenetic processes of complex organisms and phyllotaxis has been employed to understand the mechanisms behind this regularity. Our research broads the knowledge on this mechanism which is also strictly correlated with yield.

Significance statement

We showed that REM34 and REM35, cooperating with ARF7 and ARF19, regulate phyllotaxis establishment in Arabidopsis, by the transcriptional control of a common set of genes and by influencing cell cycle. This fundamental research study adds knowledge on the complex programs that drive inflorescence development, such as cell division, growth, and differentiation, which are tightly connected to agricultural relevant traits such as fruit and seed production.

Key words

Reproductive meristems, REproductive Meristem (REM), Auxin Response Factors (ARFs), morphogenic processes, phyllotaxis, cell cycle, inflorescence architecture, *Arabidopsis thaliana*, transcriptional regulation.

Introduction

Throughout their life cycle, plants continuously produce new organs from pools of stem cell niches localized in the center of meristems. During reproductive development, the meristem gives rise to the inflorescence, the reproductive structure of the plant, which bears flowers, fruits and seeds.

Flowering plants are characterized by a striking variety of inflorescence architectures, which differ mainly as a consequence of their different branching abilities. The branching potential of the different species derives from the balance between the proliferation of the indeterminate stem cell niche and the differentiation of these cells into determinate structures (Prusinkiewicz *et al.*, 2007; Somssich *et al.*, 2016; Caselli *et al.*, 2020). Furthermore, the positioning of lateral organs on the main stem, which is called phyllotaxis, is a self-organizing process that follows strict geometrical constraints. During reproductive development in flowering plants, the floral primordia, which will develop into flowers, arise with a precise spatiotemporal pattern from the inflorescence meristem (IM), resulting in regular arrangements of organs around the main axis of the plant. The spiral phyllotactic pattern is the most diffused in nature and is characterized by organs arising at constant divergence angles from one another, often following the Fibonacci sequence (Galvan-Ampudia *et al.*, 2016; Azpeitia *et al.*, 2021). The prevalence in nature of this pattern might be linked to advantages in light capturing as well as the consequence of developmental constraints (Strauss *et al.*, 2020). In-depth studies of the molecular genetic programs underlying inflorescence development are highly significant, not only for gaining a deeper comprehension of the mechanisms governing cell division, growth, and differentiation but also because they are related to agricultural traits like fruit and seed production. Consequently, unraveling the underlying mechanisms could prove helpful for enhancing yield per hectare, an important goal for feeding the world population.

At the molecular level, floral meristem (FM) initiation on the inflorescence meristem is driven by the action of the phytohormone auxin, which is distributed in gradients across the meristems and acts as a morphogenic agent, triggering organ formation in the loci of its maximum accumulation. Indeed, auxin is synthesized in the center of the meristem and is then polarly transported in the periphery of the stem cell niche, where the new primordium will arise. The area surrounding this new meristem will be depleted in auxin and will act as inhibitory fields, setting the spacing between successive organ initiations (Benková *et al.*, 2003; Vernoux *et al.*, 2011; Kierzkowski *et al.*, 2013; Galvan-Ampudia *et al.*, 2020). As reiterative processes driven by the perception of morphogenic signals are common phenomena in the development of different organisms (Marcon and Sharpe, 2012; Shyer *et al.*, 2013; Corson *et al.*, 2017), understanding how phyllotaxis is established in Arabidopsis is useful to clarify the general mechanism behind such pathways (Guédon *et al.*, 2013; Refahi *et al.*, 2016).

The auxin signaling pathway has been deeply studied in the model species *Arabidopsis thaliana* and relies on the action of Auxin Response Factors (ARFs), which belong to the B3 DNA binding domain transcription factor superfamily. The classical model that explains the ARF function suggests that ARFs are bound to the Auxin

Responsive Elements (AuxREs) in the promoter of their target genes where, at low auxin concentrations, their transcriptional activity is inhibited through the interaction with Aux/IAA repressors, which keep the chromatin of the ARF target genes in a repressive state (Szemenyei, Hannon and Long, 2008; Wang, Kim and Somers, 2013). At high auxin concentrations, the Aux/IAA repressors are degraded by the 26S proteasome allowing the activation of the ARF transcription factors, which can regulate the expression of genes downstream of auxin response (Gray *et al.*, 2001).

Although auxin is considered to be sufficient to promote organogenesis at the meristem by shaping the spiral phyllotactic pattern, changes in the meristem size can also affect the organization of this pattern. Specifically, plants with larger meristems show a higher rate of permutation events at the level of the phyllotaxis while smaller meristems display a more robust phyllotactic pattern (Landrein *et al.*, 2015a).

To characterize new components involved in the regulation of lateral primordia development in the inflorescence meristem, we focused our studies on two members of the *REM* (*REproductive Meristem*) gene family. *REM* genes belong to a family of plant-specific transcription factors, characterized by the presence of multiple B3 DNA binding domains, phylogenetically related to the ARF transcription factors and preferentially expressed during the reproductive phase of the Arabidopsis plant's life cycle (Swaminathan, Peterson and Jack, 2008; Mantegazza *et al.*, 2014). Even if the functional characterization of these genes is strenuous, due to the abundance of possibly redundant members of this family, an increasing number of studies is disclosing the involvement of *REM* genes in several key developmental processes, spacing from flowering time regulation to gametophytic development (Levy *et al.*, 2002; Matias-Hernandez *et al.*, 2010; Heo, Sung and Assmann, 2012; Mendes *et al.*, 2016; Caselli *et al.*, 2019; Richter *et al.*, 2019; Yu *et al.*, 2020; Manrique *et al.*, 2023). While several REMs were shown to homo- and/or hetero-dimerize with other members of this family, no interactions with proteins belonging to different families have been reported so far. Furthermore, it is still not clear whether REM factors can bind the DNA in a sequence-specific way. Indeed, while VRN1 (REM39) was reported to bind DNA in a nonspecific way (Levy *et al.*, 2002), a consensus sequence for REM34 was identified *in vitro* (Franco-Zorrilla *et al.*, 2014). Interestingly, this binding motif differs from the ones described for other members of the B3 superfamily, suggesting divergence in DNA-binding affinities among members of this superfamily.

Among the different members of this family, the study presented by (Mantegazza *et al.*, 2014) identified a cluster of highly homologous genes that are likely to play a role in Arabidopsis reproductive development. This cluster includes *REM34* and *REM35*, which gene products were later shown to be able to homo and heterodimerize (Caselli *et al.*, 2019).

In this study, we investigated the role of *REM34* and *REM35* in the control of Arabidopsis inflorescence development. We revealed that their function in this developmental process is established through the interaction with ARF7 and ARF19. Our data disclose a novel gene regulatory network that connects B3 superfamily members to auxin signaling, cell cycle regulation and meristem patterning to establish inflorescence phyllotaxis in Arabidopsis.

Results

REM34 and REM35 are involved in the establishment of the phyllotactic pattern

A *rem34* insertional mutant was previously identified and characterized in our laboratory (Mantegazza *et al.*, 2014; Manrique *et al.*, 2023). However, no suitable mutant lines were available for *REM35.* Furthermore, the tight genetic linkage of *REM34* and *REM35* prevented the isolation of a double mutant through crosses. Therefore, the CRISPR/Cas9 genome editing system was employed to generate *rem34* and *rem35* single and double mutants.

REM34 and REM35 can homo and heterodimerize (Caselli *et al.*, 2019) and their proteins share a similar structure, characterized by the repetition in tandem of three B3 DNA binding domains. AlphaFold modeling of REM34 and REM35 indicates that both proteins have a C-terminal amphipathic alpha-helix. The models, corroborated by a yeast-2-hybrid experiment, suggest that the C-terminal helix of REM35 interacts strongly with that of REM34/35 via an interface composed of ionic bonds on one side and hydrophobic interactions on the other (Supplementary Fig. 1).

To disrupt their function for each *REM* gene a single-guide RNA (sgRNA) was designed to target the first of the DNA-binding domains. Both *rem* mutants that were obtained are characterized by the insertion of a single nucleotide which causes a frameshift in the coding sequence (CDS), inducing the formation of a premature stop codon at the beginning of the first B3 domain (Supplementary Fig. 2A-C). The same protospacers were employed for the generation of the *rem34 rem35* double mutant, which carries the same mutations as the single mutants.

While wild-type Arabidopsis plants are characterized by a spiral phyllotactic pattern, in which successive siliques arise at an angle of 137.5°, in the *rem34* and *rem35* single mutants and the *rem34 rem35* double mutant, flowers arise at non-canonical divergence angles (Fig 1A). In particular, in wild-type plants 60.38% of the siliques are separated by an angle between 130° and 150°, which is considered the range of the canonical angles (Fig. 1B). In the *rem34* and *rem35* mutants, we registered a decrease in the percentage of canonical angles, which were 45.97% and 49.32% respectively (Fig. 1C-D). The *rem34 rem35* double mutant also displays a lower percentage of canonical angles, accounting for 45.54% of the measured siliques. Interestingly, the majority of the non-canonical angles registered in the *rem34 rem35* double mutant are not randomly distributed but fall into two distinct intervals, 80°-100° and 170°-190°, suggesting a shift in the phyllotactic pattern (Fig. 1E). A similar three peaks distribution is visible, although not statistically significant, in *rem35*, but not in *rem34*, suggesting that REM35 might play a more prominent role in the control of phyllotaxis stability, relative to REM34.

To exclude a possible off-target contribution to the observed phenotype, both *rem34* and *rem35* single mutants were successfully complemented with two transgenes carrying the promoter (-538 bp from the ATG for *REM34*, and -564 for *REM35*), the genomic region (exons and introns) of the corresponding gene and a fluorescent tag (Supplementary Fig. 2D).

Both *REM34* and *REM35* expression in the inflorescence meristem (Mantegazza *et al.*, 2014) and the phenotypical alteration of *rem34 rem35* mutants indicate that these genes play a role in primordia positioning and phyllotaxis establishment.

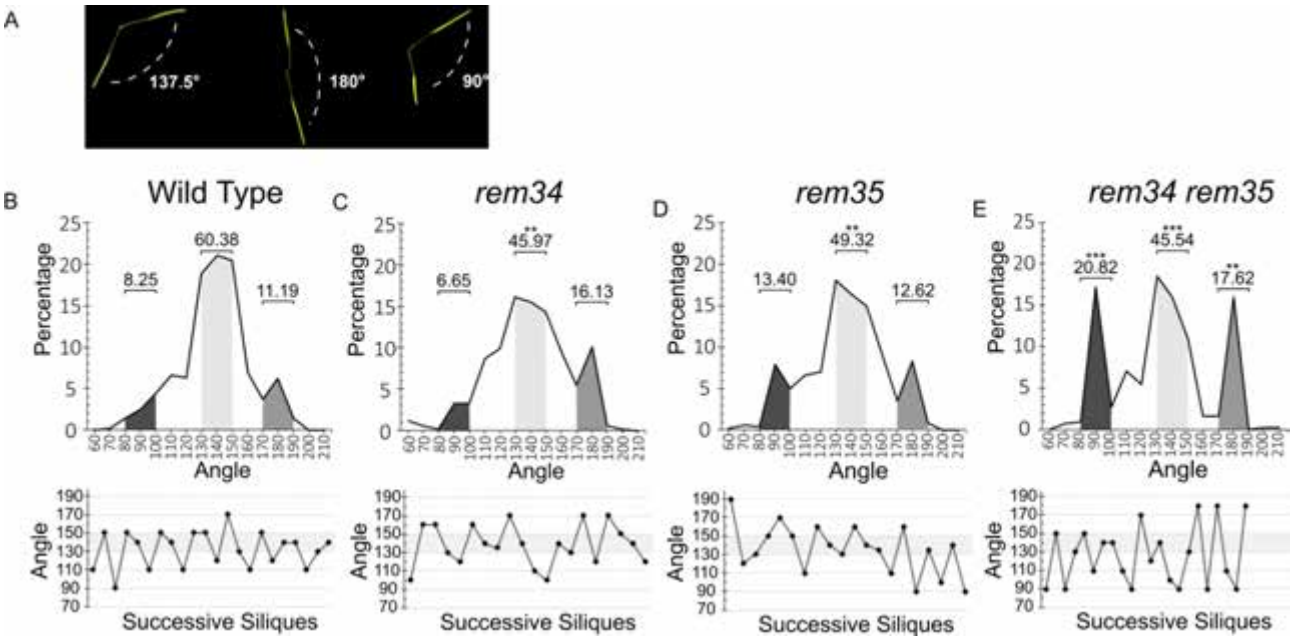

Figure 1. *rem34* and *rem35* single and double mutant analysis. (A) View from the top of different sections of Arabidopsis stem, showing a canonical divergence angle (137.5°, left) and two non-canonical angles (180°, center; 90°, right) between successive siliques. (B) Top: Distribution of the divergence angles between successive siliques in wild type Arabidopsis plants, on the x-axis the values of the divergence angle are indicated, while on the y-axis the percentage for each value is shown (30 plants, 679 angles), Bottom: graph showing a representative phyllotactic pattern of a single wild type plant, the canonical interval (130°-150°) is highlighted in light gray. The same analysis was performed on (C) *rem34* (20 plants, 496 angles), (D) *rem35* (20 plants, 515 angles), and (E) *rem34 rem35* (20 plants, 437 angles). The dark, light, and medium gray areas represent the percentages of angles falling within the ranges of 80°-100°, 130°-150°, and 170°-190°, respectively. The numbers above each area indicate the total percentage of angles within each range. A t-test was used to assess the statistical significance of differences between the wild type and mutants for each of these angle intervals (** p<0.01; *** p<0.001).

REM35 interacts with two members of the ARF family

To better understand the molecular mechanism by which REM34 and REM35 perform their functions, we conducted a Yeast-2-Hybrid (Y2H) screening to study their interactions with transcription factors that are expressed in the Arabidopsis inflorescence. *REM34* and *REM35* were cloned in bait vector (pDEST32, Invitrogen) and tested against a set of transcription factors cloned in pray vectors (pDEST22, Invitrogen) (Supplementary Fig. 3). Through this analysis, we discovered that REM35 (but not REM34) can interact with a member of the Auxin Response Factor family, named ARF19.

Since ARF19 is closely related to ARF7, which was not present in the employed Y2H library, we repeated the Y2H experiment and combined these analyses with a Bimolecular fluorescence complementation (BiFC) assay to include an alternative approach as confirmation of our observations. All the possible interactions between REM34, REM35, ARF7, and ARF19 were tested (Fig. 2 A-D). The results of this experiment showed that REM35 can interact with both ARF7 and ARF19.

ARFs are characterized by a complex structure in which three different functional domains can be identified: the N-terminal B3 DNA binding domain (DBD), a middle region (MR), whose aminoacidic composition differs between activators and repressors, and a C-terminal PB1 protein-interaction domain, which mediates the ARF-ARF and ARF-Aux/IAA binding. The B3 DBD is often flanked by dimerization domains, which are involved in the cooperative DNA binding of these transcription factors (Boer *et al.*, 2014).

To assess which of the ARF domains mediate the interaction with REM35, four truncated versions of ARF19, ARF19^{B3} ARF19$^{B3\text{-}MR}$ ARF19$^{MR\text{-}BP1}$ and ARF19^{PB1}, were tested through a Y2H assay against the full-length REM35 protein. The REM35-ARF19 interaction was conserved in the two ARF19 truncated versions containing the B3 DBD domain, while it was abolished in the two versions (ARF19$^{MR\text{-}BP1}$ and ARF19^{PB1}) lacking this domain (Fig. 2E), suggesting that the B3 domain of the ARFs is necessary for the REM-ARF dimerization.

Previously it has been shown that ARF7 and ARF19 work together to control lateral root emergence and development (Okushima, Paul J Overvoorde, *et al.*, 2005). Our protein-protein interaction data hinted that ARF7 and ARF19 could also be involved, together with REM34 and REM35, in the control of primordia formation and phyllotaxy establishment in the Arabidopsis inflorescence meristem. We thus analyzed the distribution of angles between successive siliques in the *arf7-1* and *arf19-1* insertional mutants, as well as in the *arf7-1 arf19-1* double mutant. The phyllotaxy of *arf7-1*, *arf19-1* and *arf7-1 arf19-1* showed similar permutations to the one observed in the *rem* knock-out lines, as the successive angles between siliques were distributed around three main intervals: 80°-100°, 130°-150° and 170°-190°. The strongest effect was detected in the *rem34 rem35 arf7-1 arf19-1* quadruple mutant. These plants were smaller compared to the wild type and with a highly perturbed phyllotactic pattern, with on average only 28.57% of angles distributed around the golden angle (Fig. 2F-J and Supplementary Fig. 4).

The evidence showing that REM35 can physically interact with ARF7 and ARF19, combined with the phenotypical characterization of the *rem* and *arf* single and multiple mutants, suggests that the members of these two transcriptional factor families may work together to regulate primordia positioning in the inflorescence meristem of Arabidopsis.

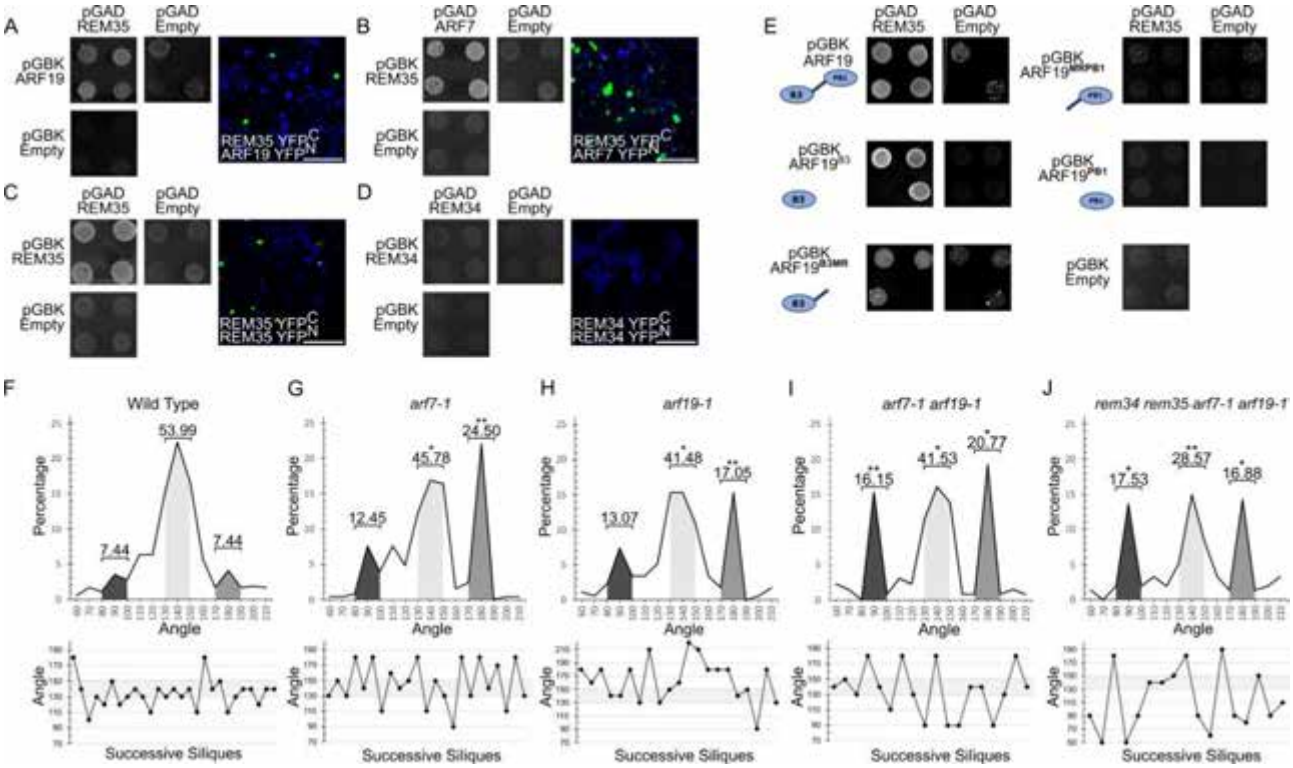

Figure 2 REM-ARF interactions. (A-B) Y2H and BiFC showing the positive interaction between REM35 and ARF19 (A); REM35 and ARF7 (b); (C-D) REM35 and REM35 (C), and REM34 and REM34 (D) were used as positive and negative controls respectively. For the Y2H, 4 independent colonies harboring both pGAD and pGBK constructs of interest were plated on media lacking Leu, Trp and His, with increasing concentrations of 3AT. The pGAD T7 Empty and pGBK T7 REM35 combination is shown in both figures B and C, as it was employed as a control for any REM35 autoactivation activity and the two interactions were tested simultaneously on the same plate. Scale bar=100 µm. (E) Y2H showing the interactions between REM35 and four truncated versions of ARF19 (ARF19^{B3} ARF19$^{B3\text{-}MR}$ ARF19$^{MR\text{-}BP1}$ and ARF19^{PB1}). To test for positive interactions four independent colonies carrying both the pGAD and pGBK vectors of interest were plated on media lacking Leu, Trp and His, with increasing concentrations of 3AT. As a positive control, the interaction between REM35 and the full-length ARF19 was also tested. (F-J) The cumulative phyllotactic pattern of wild type (19 plants, 363 angles), *arf7-1* (10 plants, 249 angles), *arf19-1* (9 plants, 176 angles), *arf7-1 arf19-1* (8 plants, 130 angles) and *rem34 rem35 arf7-1 arf19-1* (10 plants, 154 angles) was assessed. The dark, light, and medium gray areas represent the percentages of angles falling within the ranges of 80°-100°, 130°-150°, and 170°-190°, respectively. The numbers above each area indicate the total percentage of angles within each range. A t-test was used to assess the statistical significance of differences between the wild type and mutants for each of these angle intervals (*<0.05, **<0.01). Below each graph, the phyllotactic pattern of a single representative plant for all the analyzed genotypes is reported, and the canonical divergence angle range is highlighted in light gray.

REM34, REM35, ARF7 and ARF19 expression overlaps in the boundary regions

To better define the expression pattern of both REM34 and REM35 proteins, we evaluated the expression of the tagged proteins crossing the *pREM34:REM34-GFP* and *pREM35:REM35-mCherry* transgenic lines that were used for the complementation experiments. REM34-GFP accumulates in the meristem central zone, which contains the stem cells niche, in the tunica (L1 and L2) and corpus (L3), in the peripheral zone, and in the boundary region between the IM and the youngest primordium (Fig. 7 schematizes the structure of the inflorescence meristem and its zones). REM35-mCherry also accumulated in the tunica, especially in the L1, and boundary regions, and it was present in the developing flower primordia as well. The two proteins co-localized in the boundaries and the tunica, suggesting that REM34 and REM35 might cooperate in these regions to control phyllotaxis establishment (Fig. 3A).

The expression domains of REM34 and REM35 were compared to the ones of *ARF7* and *ARF19*, introgressing the already characterized *pARF7:mVenus* and *pARF19:mVenus* reporters into the newly developed *pREM35:REM35-mCherry* (Truskina *et al.*, 2021). The *ARF7* promoter activity was observed in the whole IM, while *ARF19* appeared to be restricted to the incipient primordia, in the L1 and L2 and the boundary region between the IM and flower primordia (Fig. 3B-C). In both cases, there was a strong overlap with the REM35 domain of expression.

Overall, the expression of the four players of interest overlapped in the boundary region and the L1 and L2 layers of the inflorescence meristem suggesting that they might work there as a complex, influencing primordia positioning and thus phyllotaxis.

Finally, a Y3H experiment showed that REM35 can act as a bridge between REM34 and ARF7 and between ARF7 and ARF19, but not between REM34 and ARF19 (Fig. 3 D-F). This observation is consistent with the expression patterns characterized above, as ARF7 and REM34 are both expressed in the same meristematic districts and can thus form a complex together with REM35. The overlap between REM34 and ARF19, instead, appears to be minimal, making it unlikely that these proteins might work in the same complex.

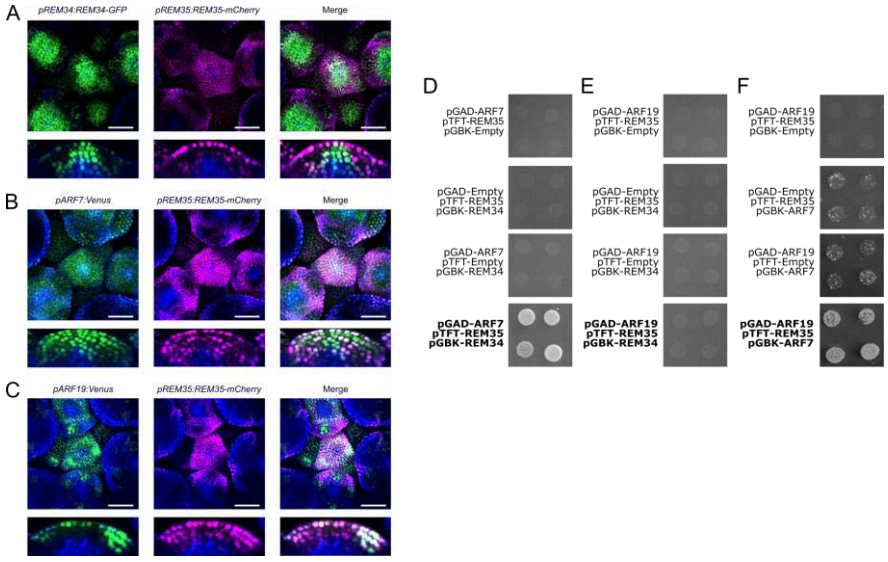

Figure 3. REM34, REM35, *ARF7* and *ARF19* coexpression analysis Confocal microscopy analysis of inflorescence meristems carrying (A) *pREM34:REM34-GFP* and *pREM35:REM35-mCherry* (*B*) *pARF7:Venus* and *pREM35:REM35-mCherry* and (C) *pARF19:Venus* and *pREM35:REM35-mCherry.* The first column shows the expression profile of REM34, *pARF7* and *pARF19* respectively (green) and ClhPh-B (blue), the second column displays the pattern of expression of REM35 (magenta) and ClhPh-B (blue), while in the third column is displayed the merge between the three channels. Meristems were imaged from the top and transversal sections were reconstructed from the z-stack. Scale bar = 50 µm. (D-F) Y3H showing the formation of ARF7-REM35-REM34 and ARF19-REM35-ARF7 trimers. ARF19-REM35-REM34 trimer formation was not detected. Yeast colonies harboring the pGAD, pGBK and pTFT vectors of interest were plated on media lacking Leu, Trp, Ade and His with increasing concentrations of 3AT to detect positive interactions.

IM area and cell cycle rate increase in the rem34 rem35 and arf7-1 arf19-1 mutants

As REM34, REM35, *ARF7* and *ARF19* expression overlaps in the boundary region and knock-out mutants of these genes showed defects in primordia positioning in the IM, we investigated in detail the *rem34 rem35* and *arf7-1 arf19-1* meristem morphology.

In comparison with the wild type, the meristem of both double mutants did not exhibit macroscopical defects (Fig. 4A). However, the IM area was found to be significatively enlarged in *rem34 rem35* and *arf7-1 arf19-1* mutants (Fig. 4B). The increase in the meristem dimension observed in these two genetic backgrounds agrees well with their mutated phyllotactic pattern, as a wider IM correlates with a less organized phyllotaxis (Landrein *et al.*, 2015).

REM34, in complex with a subset of other REMs, was shown to be involved in the control of the size of the shoot apical meristem by regulating the cell cycle rate during the floral transition (Manrique *et al.*, 2023). We, therefore, decided to assess whether this transcription factor retains a similar role during Arabidopsis reproductive development together with *REM35, ARF7* and *ARF19.* To investigate cell-cycle activity, cells expressing the S-phase marker *Histone4 (H4)* were visualized via mRNA *in situ* hybridization (Fig. 4C). In the wild-type IM, the cells expressing this marker were found to be mainly localized in the peripheral zone, where cells are recruited for new organ formation. In *arf7-1 arf19-1,* as well as in *rem34 rem35,* the *H4* mRNA is detectable not only in the peripheral zone but also in the central zone. This may suggest that the increase in the IM area measured in these two double mutants could be linked to an expansion of the meristematic domain in which cells divide.

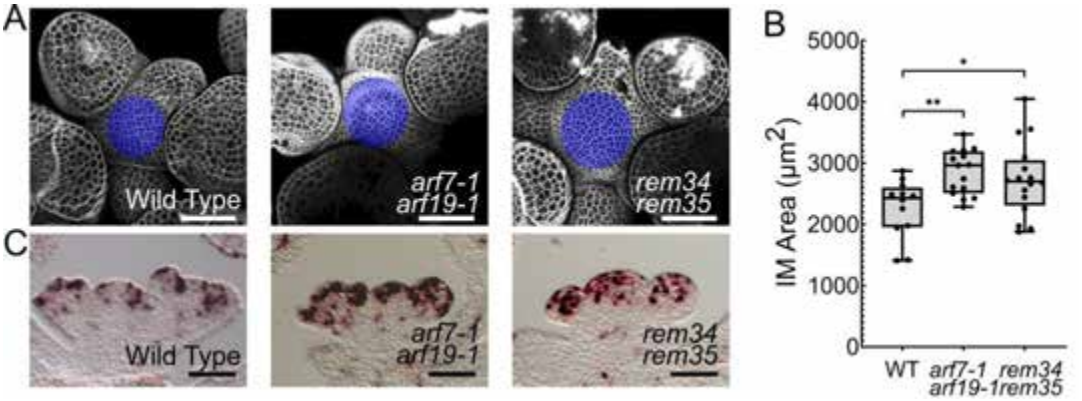

Figure 4. Analysis of the meristem morphology in *rem34 rem35* and *arf7-1 arf19-1* double mutants. (A) Primary inflorescence meristem of wild type, *arf7-1 arf19-1* and *rem34 rem35* double mutant plants. The cell wall was stained with PI (gray), Scale bar = 50 µm. L1 was extracted from Z-stacks with the aid of Fiji's plugin SurfCut (Erguvan et al., 2019)(Erguvan et al., 2019), the meristematic dome is indicated in blue (B) Meristem area was measured for 12 wild type, 15 *arf7-1 arf19-1* and 16 *rem34 rem35* plants, with the aid of Fiji. Statistical significance was determined with ANOVA followed by Dunnett's multiple comparison test (*p<0.05, **p<0.01). (C) *in situ* hybridization showing *H4* mRNA accumulation in wild type, *arf7-1 arf19-1* and *rem34 rem35* inflorescence meristems. Compared to wild-type plants, both mutants showed an enlargement in the expression domain of the *H4* mRNA, which is symptomatic of an increased number of cells in the S phase of the cell cycle. Scale bar = 50 µm.

REM35 overexpression alters both inflorescence and root morphology

To better elucidate how *REM34* and *REM35* contribute to inflorescence architecture determination, we measured the IM area of the two single mutants. Interestingly, while both *rem34* and *rem35* show similar phyllotactic pattern defects (Fig. 1B-D), only *rem35* exhibited an enlarged IM compared to the wild type (Fig. 5B). Y2H and Y3H assays suggest that REM35 is responsible for mediating the interaction between REM and ARF. The changes in the meristem dimensions observed in *rem35*, together with the knowledge gained from the protein-protein interaction assays, suggest that REM35, through its interaction with ARF7 and ARF19, plays a more prominent role in the control of reproductive meristems development.

To clarify the role of REM35, within the inflorescence meristem, transgenic lines overexpressing *REM35* under the *35S* constitutive promoter in the *rem35* mutant background were generated (Fig. 5A). We assessed meristem dimensions in two of these lines and found that overexpression of REM35 reduces the IM area to a size comparable to or smaller than that observed in the wild type (Fig. 5B). While these lines also also showed an increase in the percentage of angles falling into the canonical interval, compared to *rem35,* their phyllotactic pattern was still not wild type-like (Fig. 5 C-F). This partial complementation obtained in these lines cannot be linked to the presence of the RFP at the N-terminal of REM35, in the overexpressing construct, as the chimeric REM35-mCherry protein expressed under the control of the native *REM35* promoter was able to fully complement the mutant (Supplementary Fig.2D).

In roots, ARF7 and ARF19 are known to mediate lateral root development and their mutation leads to the absence of lateral roots (Okushima, Paul J. Overvoorde, *et al.*, 2005). To assess the effect of *REM35* overexpression in this contest we analyzed the root architecture of the *REM35* overexpressing lines. These lines are indeed characterized by a strong expression of *REM35* in the roots, where this protein is normally absent (Fig. 5 G-H). Interestingly, all the lines overexpressing *REM35* showed a decreased ability to produce lateral roots, while no changes were detected in the primary root length (Fig.5 I-J).

Since REM34 does not directly interact with ARF7 and ARF19 in the absence of REM35, its overexpression in roots alone should not impair the ARFs contribution to LR development. To exclude that the observed root phenotype in the *35S:REM35-RFP* lines is due to the overexpression of REMs per se, we also generated different Arabidopsis lines overexpressing *REM34.* As expected, in these lines, the LR number is similar to the wild type, showing that REM34 cannot interfere with LR formation (Supplementary Fig. 5).

Altogether, these analyses clearly showed that the ectopic expression of *REM35* causes alterations in both shoot and root architecture, suggesting that this gene can influence the developmental processes behind organ outgrowth and positioning. As, at least in roots, it is known that the transcriptional activator activity of ARF7 and ARF19 is fundamental for the correct specification of lateral root emergence, it is possible to speculate that REM35 might influence this pathway through its interaction with ARF7 and ARF19.

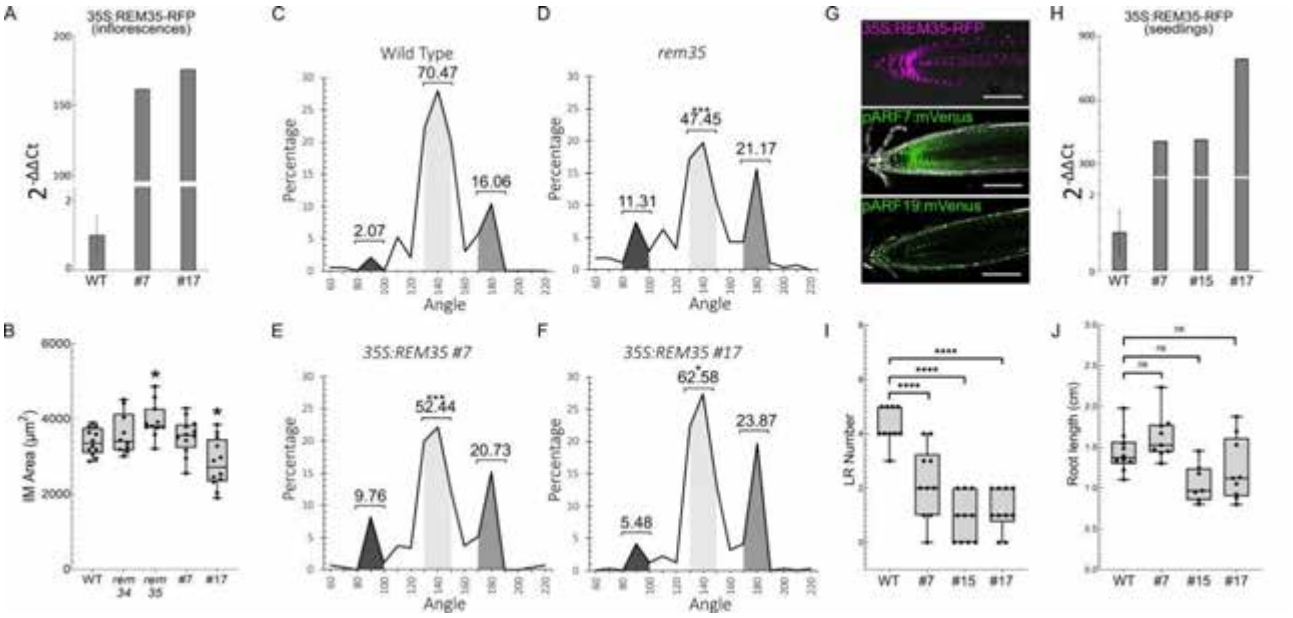

Figure 5. REM35 overexpression effect on shoot and root architecture (A) Levels of expression of *REM35,* determined by qRT-PCR, in the inflorescences of two independent *35S:REM35-RFP* lines, in the *rem35* mutant background. The experiment was performed in triplicates on two biological replicas. (B) Boxplot showing IM area, measured on wild type (n=12), *rem34* (n=10), *rem35* (n=12), *35S:REM35-RFP #7* (n=11) and *35S:REM35-RFP #7* (n=12). *rem35* mutants are characterized by a significantly larger meristem compared to the wild type. In the two lines overexpressing *REM35,* instead, the meristem area was found to be similar or smaller than the wild type. Statistical significance was determined with ANOVA followed by Dunnett's multiple comparison test (*p<0.05). (C-F) Analysis of the distribution of the divergence angles between successive siliques in the *35S:REM35-RFP* lines. The dark, light, and

medium gray areas represent the percentages of angles falling within the ranges of 80°-100°, 130°-150°, and 170°-190°, respectively. The numbers above each area indicate the total percentage of angles within each range. A t-test was used to assess the statistical significance of differences between the wild type and mutants for each of these angle intervals (*<0.05, ***<0.001).In *rem35* (10 plants; 274 angles) 47.45% of successive siliques are separated by an angle falling in the canonical range, while this percentage reaches 70.47% in the wild type (8 plants, 193 angles). The two overexpressing lines show a partial, but not significative, increase in the angles falling into this range (*35S:REM35-RFP #7:* 9 plants, 246 angles; *35S:REM35-RFP #17:* 13 plants, 310 angles), suggesting that the ectopic expression of *REM35* in the whole meristem is only able to partially rescue the mutant phenotype. (G) Confocal images showing the ectopic expression of REM35 (magenta), under the control of the 35S CaMV promoter (top) and the expression domains of *ARF7 (*green, middle) and *ARF19* (green, bottom). Cell walls were stained with PI (gray). Scale bars= 100 µm. (H) Levels of overexpression of *REM35* in the seedling of three independent *35s:REM35-RFP* lines, compared to the wild type. (I_J) LR number and primary root length in wild type and three *35S:REM35-RFP* lines (n=10). Statistical significance was determined with ANOVA followed by Dunnett's multiple comparison test (****p<0.0001, ns non-significative).

REM34 and REM35 directly regulate PUCHI and LBD18

Among several other genes, ARF7 and ARF19 control lateral organ development in the roots, by regulating the expression of their targets *PUCHI* and *LBD18* (Kang, Lee and Kim, 2013). These two genes are also expressed in the inflorescence meristem and, in particular, in the boundary regions, where the expression of REM34, REM35, *ARF7* and *ARF19* overlaps (Fig. 6D-E).

Furthermore, the promoter region of *PUCHI* and *LBD18* share a similar structure, with an AuxRE-enriched region (*pPUCHI II* and *pLBD18 II*) within the first 500 bp from the ATG and a region containing both one AuxRE motif and two putative REM34 binding sites located roughly at -1500 bp/ -2300 bp from the ATG (*pPUCHI I* and *pLBD18 I*) (Fig. 6A).

For both genes, the two regions were tested for direct binding of REM34 and REM35 through ChIP, using the *pREM34:REM34-GFP* and *35S:REM35-RFP* lines. This analysis showed that REM34-GFP and REM35-RFP directly bound the *pPUCHI I* and *pLBD18 I* promoter regions, which contain REM34 putative binding sites, while no enrichment was measured in the *pPUCHI II* and *pLBD18 II* regions (Fig. 6B-C). The experiments indicate that REM34 and REM35 can bind the promoter of their targets in a sequence-specific way and that the binding site is spatially distinct from the AuxRE-enriched region, likely to be bound by ARFs.

LBD18 expression, in the IM, is restricted to the boundary region and the incipient primordia. *In situ* hybridization of subsequent transversal sections of the IM of *rem34 rem35, arf7 arf19* and *rem34 rem35 arf7 arf19* revealed that in these mutants *LBD18* transcript is not confined into the boundaries but appears to be more broadly distributed throughout the meristematic dome(Fig. 6D). *PUCHI*, on the other hand, is expressed only in a few cells in the adaxial side of each floral primordia, where it is involved in floral meristem identity determination (Karim *et al.*, 2009; Rieu *et al.*, 2024). In all the mutants instead, the positional expression of this gene was altered: while in the wild type all the primordia showed a clearly detectable signal, in these mutants only a few primordia were expressing *PUCHI* mRNA (Fig. 6E).

Finally, to verify the involvement of both PUCHI and LBD18 in inflorescence architecture determination downstream of REM34, REM35, ARF7 and ARF19, the phyllotactic pattern of *lbd18-I* and *puchi-I* was measured. In both mutants, a significant decrease in siliques distributed around the canonical interval (130°-150°) was detected, suggesting that indeed these two genes have a role in the gene regulatory network that controls phyllotaxis establishment (Fig. 6F).

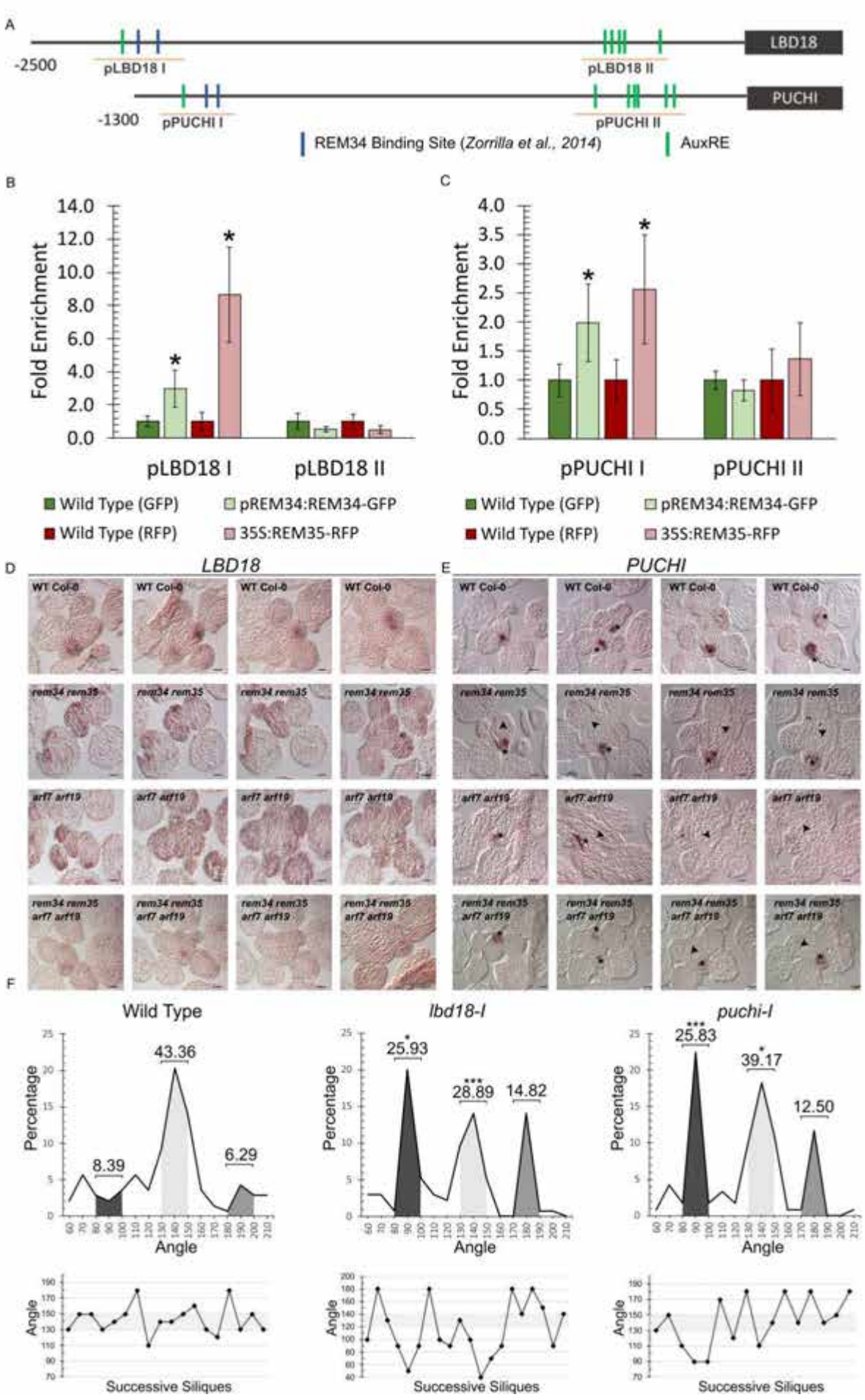
A
-2500
pLBD18 I
pLBD18 II
LBD18
-1300
pPUCHI I
pPUCHI II
PUCHI
REM34 Binding Site (Zorrilla et al., 2014)
AuxRE
B
Fold Enrichment
pLBD18 I
pLBD18 II
C
pPUCHI I
pPUCHI II
Wild Type (GFP)
pREM34:REM34-GFP
Wild Type (RFP)
35S:REM35-RFP
D
LBD18
E
PUCHI
WT Col-0
rem34 rem35
arf7 arf19
rem34 rem35 arf7 arf19
F
Wild Type
lbd18-l
puchi-l
Percentage
Angle
43.36
8.39
6.29
25.93
28.89
14.82
25.83
39.17
12.50
Successive Siliques

Figure 6. *PUCHI* and *LBD18* are targets of REM34, REM35, ARF7 and ARF19 (A) Diagram showing the promoter structure of *LBD18* and *PUCHI,* blue boxes indicate putative *REM34* binding sites (*Zorrilla et al., 2014),* green boxes indicate AuxRE motifs. In both promoters the regions tested via ChIP are underlined in orange. (B-B) ChIP real time PCR on *pLBD18 I* and *pLBD18 II* (b) and *pPUCHI I* and *pPUCHI II* (C)*,* showing a fold enrichment in region I in both *pREM34:REM34-GFP* and *35S:REM35-RFP* compared to wild type chromatin immunoprecipitated with anti-GFP and anti-RFP antibodies, respectively. No enrichment was detected in region II, which does not include REM34 binding sites. Graphs show mean fold enrichment and error of at least two biological replicates, statistical significance was calculated with a t-test (*<0.05) (D) *LBD18 in situ* hybridization on progressive transversal sections of inflorescence meristems of wild type, *rem34 rem35, arf7-1 arf19-1, rem34 rem35 arf7 arf19* plants. Compared to the wild type, where the expression of *LBD18* was strongly confined to the developing floral meristems, in the two double mutants as well as in the quadruple mutant the pattern of expression of *LBD18* appeared both weaker and wider. The specificity of the *LBD18* probe was tested employing a sense probe, as shown in Supplementary Fig. 5. Scale bar = 50 µm. (E) *in situ* hybridization of *PUCHI* in wild type, *rem34 rem35, arf7 arf19, rem34 rem35 arf7 arf19* transversal sections of the inflorescence meristems. Compared to wild type plants, where *PUCHI* was expressed in all of the boundary regions between the IM and FM, both mutants showed several incipient floral meristems in which the boundaries were not marked by *PUCHI* expression. Primordia expressing *PUCHI* in the boundaries are marked with an asterisk, while arrowheads indicate primordia without *PUCHI* signal. Scale bar = 50 µm. (F) Phyllotaxis analysis of *lbd18-1* and *puchi-1* mutants. Compared to the wild type (7 plants, 109 angles), *lbd18-1* (8 plants, 135 angles) and *puchi-1* (8 plants, 120 angles) showed a significant decrease in the number of canonical phyllotactic angles. The dark, light, and medium gray areas represent the percentages of angles falling within the ranges of 80°-100°, 130°-150°, and 170°-190°, respectively. The numbers above each area indicate the total percentage of angles within each range. A t-test was used to assess the statistical significance of differences between the wild type and mutants for each of these angle intervals (*<0.05, ***<0.001). Below each graph, the phyllotactic pattern of a single representative plant for all the analyzed genotypes is reported, and the canonical divergence angle range is highlighted in light gray.

Discussion

Inflorescence development is a key process during the life cycle of plants, as it represents the first step of plant reproduction, and is of great agronomical value because it determines the number of fruits/seeds that the plant will produce. Furthermore, it represents an intriguing developing tissue that can be used as a model to study important processes such as stem cell differentiation and maintenance, organogenesis and morphogenic mechanisms. In the dicot model species *Arabidopsis thaliana*, the indeterminate inflorescence meristem (IM) produces on its flanks determinate flower meristems (FMs), whose destiny unequivocally leads to flower formation and the depletion of the FM undifferentiated cell niches. Organogenesis at the inflorescence level is a very complex process that requires high spatiotemporal regulation and gives rise to a precise geometrical pattern, called phyllotaxis, in which successive primordia are positioned along the main axis following the Fibonacci sequence with a divergence angle of 137.5°.

With the aim of identifying new players involved in the genetic control of inflorescence development, we focused on the characterization of *REM34* and *REM35.* Based on their expression profile these genes were thought to be involved in inflorescence development (Mantegazza *et al.*, 2014), however, their role in this process remained unclear. The phenotypical analysis of the different single and double mutant combinations allowed a deeper understanding of their function and indicated that both *REM34* and *REM35* play a role in the control of the correct phyllotactic pattern establishment.

Among the characterized members of the REM family, many were shown to act as homo- and hetero-dimers (Mendes *et al.*, 2016; Manrique *et al.*, 2023). Similarly, REM35 can homodimerize and heterodimerize with REM34 (Caselli *et al.*, 2019). Here we reported a novel interaction between REM35, ARF7 and ARF19, two Auxin Responsive Factors belonging to the B3 superfamily of transcriptional factors which also includes the REMs, whose role during the reproductive phase of Arabidopsis was still mostly unclear.

We show that the *arf7-1* and *arf19-1* single and *arf7-1 arf19-1* double mutants were characterized by permutations in the phyllotactic sequence, similar to the ones found in the *rem34* and *rem35* mutants. The quadruple *rem34 rem35 arf7 arf19* mutant exhibits the most drastic reduction of canonical angles, suggesting that these four genes are only partially redundant in the control of phyllotaxis establishment. Furthermore, we measured an enlargement of the IM area in the two double mutants *rem34 rem35* and *arf7 arf19*, compared to the wild type, which correlates nicely with the phyllotactic defects observed in these lines.

Our data clearly show that ARFs can play a direct role in orchestrating the inflorescence meristem development, a conclusion further supported by the recent characterization of ARF3 involvement in the control of meristem size and regular spacing between new floral primordia initiation (Zhang *et al.*, 2022a). Moreover, we disclosed a cooperative function between REMs and ARFs during this crucial developmental process.

High-throughput yeast-2-hybrid interaction assays showed that many ARFs are able to homo- and heterodimerize and this interaction is thought to modulate the cell sensitivity to auxin and to increase the different cell-specific effects that auxin triggers in different tissues (Hardtke *et al.*, 2004; Muto *et al.*, 2006; Farcot, Lavedrine and Vernoux, 2015). These interactions are thought to be mediated both by the PB1 dimerization domain and by a second protein-protein dimerization domain, localized near the B3 DNA binding domain (Boer *et al.*, 2014).

Besides from ARF-ARF interactions, evidence highlighted that these proteins are sometimes required to heterodimerize with proteins belonging to other families. For instance, it is known that the interaction between MYB77 and the C-terminal of ARF7 is fundamental for the correct regulation of lateral root growth (Shin *et al.*, 2007). Recently, it was shown that LBD18 can interact with the PB1 domain of ARF7, competing with the IAA14 repressor and thus regulating ARF7 activity as a transcriptional activator (Pandey *et al.*, 2018; Nguyen, Pandey and Kim, 2023).

Here we showed that ARF7 and ARF19 can interact with REM35, through the N-terminal part of the protein, which includes the B3 DNA binding domain. We also found that REM34 and REM35, which were already reported to interact with each other, can control the expression of two auxin-induced genes (*PUCHI* and *LBD18*), directly binding their promoters. As the REM-bound sequence in both *pPUCHI* and *pLBD18* were found to be upstream from the AuxRE enriched sequences, which is the motif bound by the ARFs, it is possible to speculate that the simultaneous binding of an ARF7/ARF19 and REM34/REM35 complex to the promoters of *PUCHI* and *LBD18* can influence the formation of specific chromatin configurations, which in turn regulate the expression of these genes.

Interestingly, analysis of the *cis*-regulatory sequences associated with AuxRE-enriched promoters revealed a significant enrichment of putative REM binding sites, suggesting a possible recurrent mechanism in which different members of these two families of transcription factors cooperatively control the expression of a shared set of genes (Cherenkov *et al.*, 2018).

The REM35, ARF7 and ARF19 expression patterns do not completely overlap, suggesting that their interaction is restricted to a specific set of cells, mainly located in the boundaries (Fig. 3A-C). We observed that overexpressing *REM35* in the *rem35* background partially reverses the mutated phenotypes (i.e. meristem size and phyllotactic pattern). As in these lines, REM35-ARF7/ARF19 interaction can be extended to the whole meristem, it is possible to speculate that these ectopic interactions prevent the *REM35* overexpressing lines from reverting to a fully wild type-like phenotype. Furthermore, the presence of REM35 in roots, where it is normally absent, causes a partial impairment in lateral root development. This process is known to be coordinated by ARF7 and ARF19, which directly control the expression of *PUCHI* and *LBD18.* We showed that REM35 directly binds to the promoters of these genes, and it is also able to interact with ARF7 and ARF19.

Collectively, these observations suggest an intricated relationship between REM34/REM35 and ARF7/ARF19. One possible explanation is that, since these four interacting proteins exhibit partially overlapping yet partially distinct expression patterns, their functions may vary depending on the cells in which they are expressed and the presence or absence of their interaction partners. For instance, the REM35-ARF7/ARF19 interaction can normally occur only in the boundaries, and it appears to be deleterious in other tissues (i.e. roots). An additional layer of complexity is given by the knowledge that ARF7 and ARF19 activity, in root, is regulated by their ability to condense in cytoplasmatic bodies in low auxin responsiveness areas (Powers et al., 2019; Jing et al., 2022). It would be of high interest to try to elucidate whether the REM-ARF interaction in the shoot,

which takes place in the auxin-depleted boundaries, contributes to this nucleus-cytoplasmatic partitioning regulatory mechanism.

The morphological analysis of *rem34 rem35* and *arf7-1 arf19-1* double mutants' meristems revealed a significant increase in their dimensions compared to the wild type, which was probably due to the deregulation of the cell-cycle as evidenced by the higher number of cells in the S-phase detected in these genetic backgrounds. *ARF7* and *ARF19* promoter activity and REM34 and REM35 proteins were found to be co-localized in the L1/L2 layers of the IM and the boundary regions between the IM and the incipient FMs, the same regions in which the *H4* signal was enhanced in the mutants. Taken together, these data suggest that ARF7, ARF19, REM34 and REM35 regulate meristem size, which is correlated with phyllotaxis establishment, by modulating cell-cycle rate in the IM. Interestingly, REM34's role in the regulation of the cell-cycle was already proposed for both gametophytes' development and floral transition (Caselli *et al.*, 2019; Manrique *et al.*, 2023).

In all eukaryotic organisms, cell cycle progression is subjected to two main checkpoints, which regulate the switch between the G1 and S phases, allowing the cells to enter the mitotic cycle, and between the G2/M transition, before the mitotic division. The G1/S transition is generally controlled by the activation of the Cyclin-Dependent Kinase (CDK) A/Cyclin D complex, which causes the hyperphosphorylation and inactivation of retinoblastoma-related protein (RB), releasing its inhibition of the E2F/DPa complex, which activates S-phase genes.

In Arabidopsis roots, auxin is known to positively regulate lateral root development by inducing the G1/S phase transition of the cell cycle (Himanen *et al.*, 2002). This process is partially dependent on the action of ARF7 and ARF19, which are considered the main regulators of lateral root initiation, and which positively influence the expression of *LBD18* (Lee *et al.*, 2009; Kang, Lee and Kim, 2013; Lavenus *et al.*, 2015). LBD18 can subsequently induce the expression of *E2Fa* and of the CDKs necessary to initiate cell cycling (Berckmans *et al.*, 2011; Lee, Cho and Kim, 2015). In addition, recently, a direct role for ARF7 and ARF19 in the maintenance of the distal stem cells in the root meristem, through the transcriptional regulation of DPa, was demonstrated (Wang *et al.*, 2023). In the inflorescence meristem, an additional layer of complexity arises from the necessity to accurately position lateral organs, specifically the floral primordia, around the main axis. This is driven by the specification of boundary regions between the inflorescence meristem and fast-cycling cells of the incipient primordia. Auxin polar distribution in the inflorescence is partially responsible for these differences in cell cycle rate (Žádníková and Simon, 2014).

Here we showed that the loss-of-function of *REM34* and *REM35*, and *ARF7* and *ARF19* permutates the balance between slow and fast cycling zones of the meristem, leading to an enlargement of the inflorescence meristem. Since meristem dimensions highly correlate with the precise spatiotemporal regulation of new primordia formation (Landrein *et al.*, 2015a), it is likely that in the *rem34 rem35* and the *arf7 arf19* mutants the altered phyllotactic pattern arises because of their changes in their meristem size. As *LBD18* is a known regulator of the cell cycle in roots, it is tempting to hypothesize that its downregulation and partial misexpression in *rem34 rem35* and *arf7 arf19* inflorescences*,* caused the defects in the cell cycling rate registered in these mutants.

Indeed, it has been long known that meristem size can influence phyllotactic pattern in Arabidopsis, independently of the analyzed genotype; in particular, plants with a larger meristem are usually characterized by a more disorganized phyllotactic pattern (Landrein *et al.*, 2015). In accordance with this observation, mutants in the ERECTA/CLAVATA pathway, which is fundamental to ensure the correct rate of cell differentiation and proliferation within the meristem, are characterized by larger IM and permutated phyllotaxis (Steven et al, 1993; Mandel et al., 2016). Independently from the WUS/CLV pathway, auxin produced from lateral organs was found to act as a negative regulator of the meristem dimension (Shi *et al.*, 2018). Perturbation of auxin perception trough the mutation of *ARF3,* which contributes to the regulation of

boundary-specific genes, causes an enlargement of the IM and, consequently, permutations of the phyllotactic pattern (Zhang *et al.*, 2022). Cytokinin homeostasis is also fundamental to ensure the correct shaping and organization of the IM. Mutants in the cytokinin degradation pathway are for instance characterized by larger inflorescence meristems and permutated phyllotaxis (Bartrina *et al.*, 2011). Similarly, the correct expression of the cytokinin signaling inhibitor ARABIDOPSIS HISTIDINE PHOSPHOTRANSFER PROTEIN 6 guarantees the correct temporal regulation of primordia formation (Besnard *et al.*, 2014)This study provides insights into this complex gene regulatory network that shapes the precise geometrical organization of inflorescences. We unraveled the crucial cooperative role of a REM-ARF complex in the frame of this developmental process, directly correlating the auxin signaling pathway with cell cycle control and meristem dimension. Our proposed model (Fig. 7) suggests that ARF7 and ARF19, whose activity is triggered by auxin accumulation, interact with REM34 and REM35 to regulate two auxin-induced genes, LBD18 and PUCHI, for which we demonstrated their involvement in the same process. This complex also restricts cell cycling activity to specific areas of the meristem, indirectly determining its dimension, and ultimately establishing floral meristem positioning and phyllotaxis.

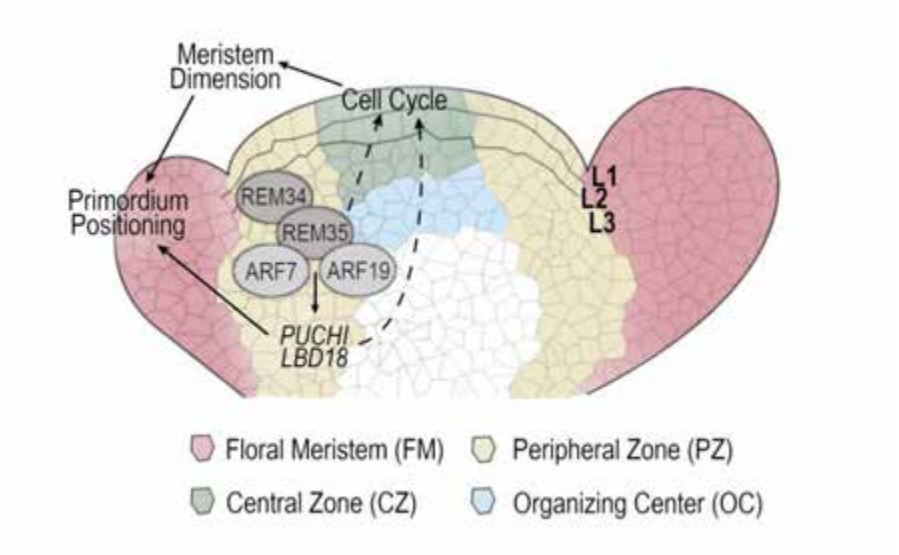

Figure 7. Working model. Arabidopsis inflorescence meristem can be divided into a peripheral zone (PZ), which harbors the boundaries between IM and FM and in which cells rapidly divide, and a central zone (CZ), where the niche of stem cell resides. The organizing center below is responsible for stem cell maintenance. The two outermost cell layers (L1 and L2) of the meristematic dome form the tunica, while the L3 is called corpus. REM34, REM35, ARF7 and ARF19 modulate the phyllotactic pattern directly regulating the expression of both *PUCHI* and *LBD18,* two boundaries-expressed genes whose mutants are also characterized by a permutated phyllotaxis pattern. Furthermore, this REM-ARF complex is involved in the modulation of the cell cycle rate in the CZ of the meristem, as indicated by the dotted lines in the model. As a consequence of the cell cycle misregulation, the *rem34 rem35* and *arf7-1 arf19-1* mutant meristems are larger compared to the wild type and are thus characterized by a permutated phyllotactic pattern.

Experimental Procedures

Plant material and growth conditions

Arabidopsis thaliana Col-0 and *Nicotiana benthamiana* plants were grown under long-day conditions, with 16h of light/8h dark, at 22°C. *arf7-1* (SALK_040394)*, arf19-1* (N24617)*, arf7-1 arf19-1* (N24629) and *lbd18-1* (SALK_038125.28.70.x) seeds were obtained from NASC while *puchi-1* seeds were kindly provided by Tom Beeckman. Primers employed for genotyping are listed in Supplementary Table 1.

The *pARF7:Venus* and *pARF19:Venus* lines were kindly provided by Teva Vernoux. The *pREM34:REM34-GFP* line was obtained by cloning the genomic locus (-538 bp to +2138 from ATG) in frame with GFP, in the *pGREENII* binary vector. The *pREM35:REM35-mCherry* line was obtained by cloning the genomic locus (-564 bp to +1895 from ATG), in the *pH7m34GW* binary vector.

The *35S:REM34-GFP* and *35S:REM35-RFP* overexpressing lines were obtained by cloning the CDS of the genes in frame with the corresponding fluorophore in the pB7FWG2 and *pGWB2* binary vectors, respectively.

CRISPR/Cas9 genome editing

rem34, rem35 and *rem34 rem35* were generated following the protocol published by (Fauser, Schiml and Puchta, 2014) The two protospacers were selected with the aid of the CRISP-P 2.0 software (http://crispr.hzau.edu.cn/CRISPR2) and are: *REM34* TTT CAG CAA AAA TTT CGT AC; *REM35* C TTC GTC ATA GTT CTT CA. As *REM34* and *REM35* are located in linkage in a 5300 bp region on chromosome 4, it was unlikely to obtain the double mutant by crossing. To overcome this difficulty, *rem34* single mutant was transformed with the CRISPR/Cas9 construct for the editing of *REM35,* with the same gRNA employed to obtain the single *rem35* mutant. We were in this way able to generate a *rem34 rem35* double mutant carrying the same mutations of the two single mutants. A schematic representation of the mutated lines, as well as the alignments between the wild type and edited genomic and protein sequences are shown in Supplementary Figure 2A-C. *rem34* and *rem35* single mutants were successfully complemented with the *pREM34:REM34-GFP* and *pREM35:REM35-mCherry* transgenes, respectively (Supplementary Fig. 2D). Primers employed for genotyping are listed in Supplementary Table 1.

Phyllotactic pattern measurement

The phyllotactic pattern was measured as described before (Peaucelle *et al.*, 2007) on 2-month-old plants using a 3D clockwise protractor. The first 3 cm of the stem was not considered because elongation is incomplete in this region. The divergence angle was measured by considering the insertion point of the two successive floral pedicels, without considering the outgrowth direction of the flower. The clockwise or anticlockwise orientation of the phyllotaxis was determined by following the direction that gives the smallest average divergence angle.

Protein-protein interaction assays

Modeling was carried out with ColabFold V1.5.5 using AlphaFold2 and AlphaFold2-mutimer (Mirdita *et al.*, 2022). Yeast 2 Hybrid matrix screening was performed as described in Herrera-Ubaldo et al., 2023 (Herrera-Ubaldo *et al.*, 2023).

Yeast-2-Hybrid (Y2H) was performed on the AH109 strain, and yeast transformation was performed as described by (de Folter and Immink, 2011)The coding sequences of the genes of interest were cloned in the GAL4 system Gateway vectors (pGADT7 and pGBKT7; Clontech Laboratories, Inc.), primers employed for cloning are listed in Supplementary Table 1. The protein-protein interaction assays were performed on selective yeast synthetic dropout medium lacking Leu, Trp, and His, and supplemented with different concentrations of 3-aminotriazole. Plates were grown for 5 days at 28°C.

Yeast-3-Hybrid (Y3H) was performed on the AH109 and Y187 strains. The coding sequence of REM35 was cloned in the pTFT vector and transformed into the Y187 strain, which was then mated with AH109 colonies transformed with the pGADT7 and pGBKT7 vectors of interest. The protein-protein interaction assays were performed on selective yeast synthetic dropout medium lacking Leu, Trp, Ade and His, and supplemented with different concentrations of 3-aminotriazole. Plates were grown for 5 days at 28°C.

For the Bimolecular fluorescence complementation (BiFC) assay, the coding sequences of interest were cloned into the pYFPN43 and pYFPC43 vectors. Agrobacterium, co-transformed with the viral suppressor p19 construct, was used to infiltrate tobacco leaves. 3 days after inoculation, the abaxial surfaces of infiltrated leaves were imaged.

For both experiments, the already published REM35-REM35 and REM34-REM34 interactions were employed as positive and negative controls, respectively.

Gene expression analysis

RNA was extracted using the LiCl method (Verwoerd, Dekker and Hoekema, 1989). For each sample, 500 ng of RNA were retro-transcribed using iScript kit (BioRad) following the manufacturer's instructions. qRT-PCR assay was performed using iTaq Universal SYBR Green supermix (BioRad) in a Bio-Rad iCycler iQ Optical System (software version 3.0a). Three biological replicates, with three technical replicates for each sample, were analyzed. Relative transcript enrichment of the targets of interest was calculated by normalizing the amount of mRNA against the *UBIQUITIN* transcript. Expression of genes was calculated using the $2^{-\Delta\Delta Ct}$ method, using the Wild Type as normalizer. The primers used for this analysis are listed in Supplementary Table 1.

Lateral roots number determination

Seeds were surface-sterilized and sowed on MS/2 (1.05g Murashige & Skoog med. incl. Mod. Vitamins (Duchefa), 0.5g MES, 0.7% plant agar/L). After two days of stratification in constant dark, plates were transferred at 22°C under long-day conditions. 7 days after germination, seedlings were treated with clearing solution (160 g chloral hydrate, 50 g glycerol, and H2O to a final volume of 250 ml) and lateral roots and primordia were counted with the aid of a Zeiss Axiophot® microscope. Root length was determined with Fiji. 10 seedlings for each genotype were analyzed and statistical significance was calculated with ANOVA followed by Dunnett's multiple comparison test.

Confocal microscopy analysis

For confocal imaging, the Laser Scanning Confocal Microscope Nikon A1 was used. With the help of a Leica® MZ 6 microscope floral buds were removed, leaving exposed only flower primordia and the inflorescence meristem. The steam of the inflorescence was included in a 2% solution of low melting agar. When necessary, samples were stained for two minutes in a 1 mg/ml propidium iodide solution, to allow the visualization of cell walls. GFP was excited at 488 nm and the signal was acquired considering an emission range between 500 and 550 nm, Chlorophyll was excited at 488 nm and collected at 660-740 nm, while PI and RFP were excited at 561 nm and collected at 590 - 730 nm and 570-630 nm respectively. 3D and longitudinal reconstructions were obtained with Fiji (Schindelin et al., 2012)(Schindelin et al., 2012). L1 layer was extracted from z-stacks with the aid of SurfCut (Version v1.1.0). Zenodo. http://doi.org/10.5281/zenodo.2635737(Erguvan et al., 2019).

In situ hybridization

IM were fixed in FAA (50% ethanol, 5% acetic acid, 3.7% formaldehyde) under vacuum for 15 min, dehydrated in ethanol and bioclear (Bioptica) and embedded in Paraplast Plus (Sigma-Aldrich). *In situ* hybridization was performed as previously described (Coen et al., 1990) with slight modifications. Digoxigenin-labelled antisense probes were synthesized with T7 RNA polymerase (Promega). The *H4* probe was designed according to (Petrella et al., 2020) the *PUCHI* probe was designed according to (Karim et al., 2009). *LBD18* probe was newly designed, and the specificity of the signal was assessed by hybridizing the same tissues employed in the experiment with the sense probe (Supplementary Fig. 6). Slides were imaged with the aid of a Zeiss Axiophot® microscope equipped with differential interference contrast (DIC) optics. Primers employed for probe synthesis are listed in Supplementary Table 1.

Chromatin ImmunoPrecipitation (ChIP)

ChIP assays were performed as described in (Gregis et al., 2009) Dynabead Protein G for Immunoprecipitation (Invitrogen) conjugated with Anti-GFP antibody (Roche), GFP-Trap®Magnetic Agarose and RFP-Trap®Magnetic Agarose (Promotek) were employed for the immunoprecipitation. The enrichment of the fragments of interest was determined via real-time PCR, which was performed on three technical replicates as described above. *ACTIN7* was used to normalize the fold change and calculations were performed as described by

(Matias-Hernandez et al., 2010). Three biological replicates were performed for each experiment. Primers employed in this experiment are listed in Supplementary Table 1.

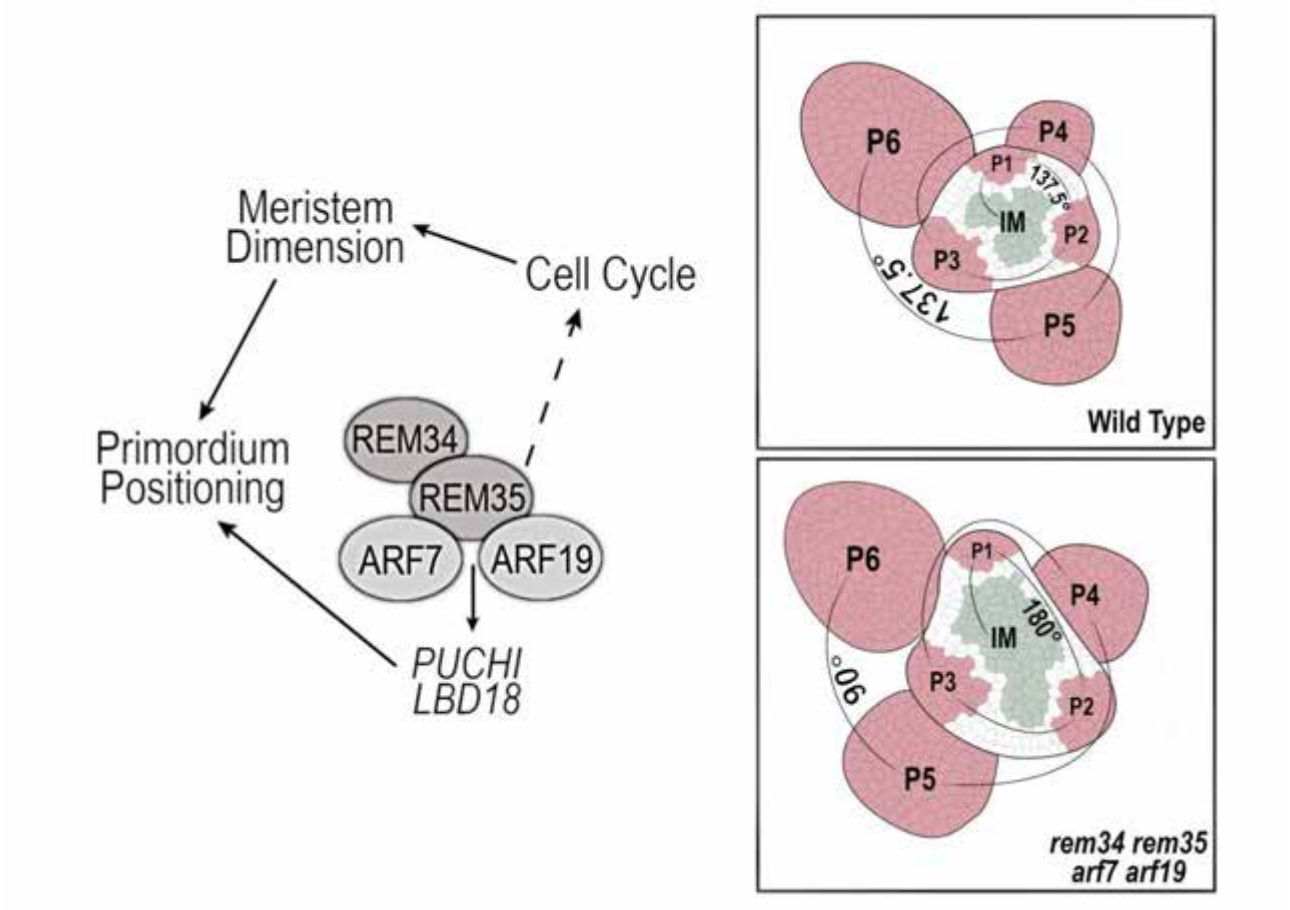

Author contributions

V.G, M.M.K and F.C. designed the experimental plan. F.C., V.M.B., C.F., S.G.A.T. conducted most of the experiments. R.D. designed and conducted the interaction prediction model. H.H.U. and S.d.F. designed and conducted the Y2H matrix screening. F.C. and V.G. wrote the manuscript.

Acknowledgments

We thank Mara Cucinotta, Alex Cavalleri, Francois Parcy for helpful suggestions and valuable discussions. We thank Valerio Parravicini and Mario Beretta for the technical assistance at the University of Milan Botanical Garden. *puchi-1* seeds were kindly provided by Tom Beeckman. The *pARF7:Venus* and *pARF19:Venus* lines were kindly provided by Teva Vernoux. Part of this work was carried out at NOLIMITS, an advanced imaging facility established by the Università degli Studi di Milano. FC was supported by PROCROP-H20MC_RISE15LCOLO_M. The PhD fellowship and post-doctoral fellowship for FC are funded by the University of Milan. V.M.B. PhD fellowship was founded from the Doctorate School in Molecular and Cellular Biology, Università degli Studi di Milano to V.M.B. and by a post-doctoral fellowship MUR–PRIN2020/2020RX4NWM.

Short legends for Supporting Information

Supplementary Figure 1. Models for interactions between REM35-REM35 and REM34-REM35.

Supplementary Figure 2. Description of *rem34* and *rem35* mutants and complementation test.

Supplementary Figure 3. Y2H matrix.

Supplementary Figure 4. Mutants employed

Supplementary Figure 5. *REM34* overexpression analysis in roots.

Supplementary Figure 6. *in situ* hybridization controls.

Supplementary Table 1. Primers employed in this work.

References

Azpeitia, E. *et al.* (2021) 'Cauliflower fractal forms arise from perturbations of floral gene networks', *Science*, 373(6551), pp. 192–197. Available at: https://doi.org/10.1126/SCIENCE.ABG5999.

Bartrina, I. *et al.* (2011) 'Cytokinin Regulates the Activity of Reproductive Meristems, Flower Organ Size, Ovule Formation, and Thus Seed Yield in Arabidopsis thaliana', *The Plant Cell*, 23(1), pp. 69–80. Available at: https://doi.org/10.1105/TPC.110.079079.

Benková, E. *et al.* (2003) 'Local, Efflux-Dependent Auxin Gradients as a Common Module for Plant Organ Formation', *Cell*, 115(5), pp. 591–602. Available at: https://doi.org/10.1016/S0092-8674(03)00924-3.

Berckmans, B. *et al.* (2011) 'Auxin-Dependent cell cycle reactivation through transcriptional regulation of arabidopsis E2Fa by lateral organ boundary proteins', *Plant Cell*, 23(10), pp. 3671–3683. Available at: https://doi.org/10.1105/tpc.111.088377.

Besnard, F. *et al.* (2014) 'Cytokinin signalling inhibitory fields provide robustness to phyllotaxis.', *Nature*, 505(7483), pp. 417–21. Available at: https://doi.org/10.1038/nature12791.

Boer, D.R. *et al.* (2014) 'Structural basis for DNA binding specificity by the auxin-dependent ARF transcription factors', *Cell*, 156(3), pp. 577–589. Available at: https://doi.org/10.1016/j.cell.2013.12.027.

Caselli, F. *et al.* (2019) 'REM34 and REM35 Control Female and Male Gametophyte Development in Arabidopsis thaliana', *Frontiers in plant science*, 10. Available at: https://doi.org/10.3389/FPLS.2019.01351.

Caselli, F. *et al.* (2020) 'Crop reproductive meristems in the genomic era: a brief overview'. Available at: https://doi.org/10.1042/BST20190441.

Cherenkov, P. *et al.* (2018) 'Diversity of cis-regulatory elements associated with auxin response in Arabidopsis thaliana', *Journal of Experimental Botany*, 69(2), pp. 329–339. Available at: https://doi.org/10.1093/jxb/erx254.

Coen, E.S. *et al.* (1990) 'floricaula: A homeotic gene required for flower development in antirrhinum majus', *Cell*, 63(6), pp. 1311–1322. Available at: https://doi.org/10.1016/0092-8674(90)90426-F.

Corson, F. *et al.* (2017) 'Self-organized Notch dynamics generate stereotyped sensory organ patterns in Drosophila', *Science*, 356(6337). Available at: https://doi.org/10.1126/science.aai7407.

Erguvan, Ö. *et al.* (2019) 'ImageJ SurfCut: A user-friendly pipeline for high-throughput extraction of cell contours from 3D image stacks', *BMC Biology*, 17(1), pp. 1–12. Available at: https://doi.org/10.1186/S12915-019-0657-1/FIGURES/6.

Farcot, E., Lavedrine, C. and Vernoux, T. (2015) 'A modular analysis of the auxin signalling network', *PLoS ONE*, 10(3). Available at: https://doi.org/10.1371/journal.pone.0122231.

Fauser, F., Schiml, S. and Puchta, H. (2014) 'Both CRISPR/Cas-based nucleases and nickases can be used efficiently for genome engineering in Arabidopsis thaliana', *Plant Journal*, 79(2), pp. 348–359. Available at: https://doi.org/10.1111/tpj.12554.

de Folter, S. and Immink, R.G.H. (2011) 'Yeast Protein–Protein Interaction Assays and Screens', in *Methods in molecular biology (Clifton, N.J.)*, pp. 145–165. Available at: https://doi.org/10.1007/978-1-61779-154-3_8.

Franco-Zorrilla, J.M. *et al.* (2014) 'DNA-binding specificities of plant transcription factors and their potential to define target genes.', *Proceedings of the National Academy of Sciences of the United States of America*, 111(6), pp. 2367–72. Available at: https://doi.org/10.1073/pnas.1316278111.

Galvan-Ampudia, C.S. *et al.* (2016) 'Phyllotaxis: from patterns of organogenesis at the meristem to shoot architecture', *Wiley Interdisciplinary Reviews: Developmental Biology*, 5(4), pp. 460–473. Available at: https://doi.org/10.1002/wdev.231.

Galvan-Ampudia, C.S. *et al.* (2020) 'Temporal integration of auxin information for the regulation of patterning', *eLife*, 9, pp. 1–65. Available at: https://doi.org/10.7554/eLife.55832.

Gray, W.M. *et al.* (2001) 'Auxin regulates SCFTIR1-dependent degradation of AUX/IAA proteins', *Nature*, 414(6861), pp. 271–276. Available at: https://doi.org/10.1038/35104500.

Gregis, V. *et al.* (2009) 'The Arabidopsis floral meristem identity genes AP1, AGL24 and SVP directly repress class B and C floral homeotic genes', *The Plant journal : for cell and molecular biology*, 60(4), pp. 626–637. Available at: https://doi.org/10.1111/J.1365-313X.2009.03985.X.

Guédon, Y. *et al.* (2013) 'Pattern identification and characterization reveal permutations of organs as a key genetically controlled property of post-meristematic phyllotaxis', *Journal of Theoretical Biology*, 338, pp. 94–110. Available at: https://doi.org/10.1016/j.jtbi.2013.07.026.

Hardtke, C.S. *et al.* (2004) 'Overlapping and non-redundant functions of the Arabidopsis auxin response factors MONOPTEROS and NONPHOTOTROPIC HYPOCOTYL 4', *Development*. Development, pp. 1089–1100. Available at: https://doi.org/10.1242/dev.00925.

Heo, J.B., Sung, S. and Assmann, S.M. (2012) 'Ca2+-dependent GTPase, extra-large G protein 2 (XLG2), promotes activation of DNA-binding protein related to vernalization 1 (RTV1), leading to activation of floral integrator genes and early flowering in Arabidopsis', *The Journal of biological chemistry*, 287(11), pp. 8242–8253. Available at: https://doi.org/10.1074/JBC.M111.317412.

Herrera-Ubaldo, H. *et al.* (2023) 'The protein–protein interaction landscape of transcription factors during gynoecium development in Arabidopsis', *Molecular Plant*, 16(1), pp. 260–278. Available at: https://doi.org/10.1016/J.MOLP.2022.09.004.

Himanen, K. *et al.* (2002) 'Auxin-Mediated Cell Cycle Activation during Early Lateral Root Initiation', *The Plant Cell*, 14, pp. 2339–2351. Available at: https://doi.org/10.1105/tpc.004960.

Jing, H. *et al.* (2022) 'Regulation of AUXIN RESPONSE FACTOR condensation and nucleo-cytoplasmic partitioning', *Nature Communications 2022 13:1*, 13(1), pp. 1–11. Available at: https://doi.org/10.1038/s41467-022-31628-2.

Kang, N.Y., Lee, H.W. and Kim, J. (2013) 'The AP2/EREBP gene PUCHI co-acts with LBD16/ASL18 and LBD18/ASL20 downstream of ARF7 and ARF19 to regulate lateral root development in arabidopsis', *Plant and Cell Physiology*, 54(8), pp. 1326–1334. Available at: https://doi.org/10.1093/pcp/pct081.

Karim, M.R. *et al.* (2009) 'A Role for Arabidopsis PUCHI in Floral Meristem Identity and Bract Suppression', *The Plant Cell*, 21(5), pp. 1360–1372. Available at: https://doi.org/10.1105/TPC.109.067025.

Kierzkowski, D. *et al.* (2013) 'Interaction between Meristem tissue layers controls phyllotaxis', *Developmental Cell*, 26(6), pp. 616–628. Available at: https://doi.org/10.1016/j.devcel.2013.08.017.

727 Landrein, B. *et al.* (2015) 'Meristem size contributes to the robustness of phyllotaxis in Arabidopsis', *Journal*
728 *of Experimental Botany*, 66(5), pp. 1317–1324. Available at: https://doi.org/10.1093/jxb/eru482.

729 Lavenus, J. *et al.* (2015) 'Inference of the Arabidopsis Lateral Root Gene Regulatory Network Suggests a
730 Bifurcation Mechanism That Defines Primordia Flanking and Central Zones', *The Plant Cell*, 27(5), p. 1368.
731 Available at: https://doi.org/10.1105/TPC.114.132993.

732 Lee, H.W. *et al.* (2009) 'LBD18/ASL20 regulates lateral root formation in combination with LBD16/ASL18
733 downstream of ARF7 and ARF19 in Arabidopsis', *Plant Physiology*, 151(3), pp. 1377–1389. Available at:
734 https://doi.org/10.1104/pp.109.143685.

735 Lee, H.W., Cho, C. and Kim, J. (2015) 'Lateral organ boundaries domain16 and 18 act downstream of the
736 AUXIN1 and LIKE-AUXIN3 auxin influx carriers to control lateral root development in arabidopsis', *Plant*
737 *Physiology*, 168(4), pp. 1792–1806. Available at: https://doi.org/10.1104/pp.15.00578.

738 Levy, Y.Y. *et al.* (2002) 'Multiple Roles of Arabidopsis VRN1 in Vernalization and Flowering Time Control',
739 *Science*, 297(5579), pp. 243–246. Available at: https://doi.org/10.1126/science.1072147.

740 Mandel, T. *et al.* (2016) 'Differential regulation of meristem size, morphology and organization by the
741 ERECTA, CLAVATA and class III HD-ZIP pathways', *Development (Cambridge)*, 143(9), pp. 1612–1622.
742 Available at: https://doi.org/10.1242/DEV.129973/256854/AM/DIFFERENTIAL-REGULATION-OF-MERISTEM-
743 SIZE.

744 Manrique, S. *et al.* (2023) 'Assessing the role of REM13, REM34 and REM46 during the transition to the
745 reproductive phase in Arabidopsis thaliana', *Plant Molecular Biology*, 1, pp. 1–15. Available at:
746 https://doi.org/10.1007/S11103-023-01357-1/FIGURES/7.

747 Mantegazza, O. *et al.* (2014) 'Analysis of the arabidopsis REM gene family predicts functions during flower
748 development', *Annals of Botany*, 114(7), pp. 1507–1515. Available at: https://doi.org/10.1093/aob/mcu124.

749 Marcon, L. and Sharpe, J. (2012) 'Turing patterns in development: What about the horse part?', *Current*
750 *Opinion in Genetics and Development*, 22(6), pp. 578–584. Available at:
751 https://doi.org/10.1016/j.gde.2012.11.013.

752 Matias-Hernandez, L. *et al.* (2010) 'VERDANDI is a direct target of the MADS domain ovule identity complex
753 and affects embryo sac differentiation in Arabidopsis.', *The Plant cell*, 22(6), pp. 1702–15. Available at:
754 https://doi.org/10.1105/tpc.109.068627.

755 Mendes, M.A. *et al.* (2016) 'Live and let die: a REM complex promotes fertilization through synergid cell
756 death in Arabidopsis', *Development*, 143(15), pp. 2780–2790.

757 Mirdita, M. *et al.* (2022) 'ColabFold: making protein folding accessible to all', *Nature Methods*, 19(6), pp.
758 679–682. Available at: https://doi.org/10.1038/s41592-022-01488-1.

759 Muto, H. *et al.* (2006) 'Fluorescence Cross-Correlation Analyses of the Molecular Interaction between an
760 Aux/IAA Protein, MSG2/IAA19, and Protein-Protein Interaction Domains of Auxin Response Factors of
761 Arabidopsis Expressed in HeLa Cells', *Plant and Cell Physiology*, 47(8), pp. 1095–1101. Available at:
762 https://doi.org/10.1093/pcp/pcj080.

763 Nguyen, U.T., Pandey, S.K. and Kim, J. (2023) 'LBD18 and IAA14 antagonistically interact with ARF7 via the
764 invariant Lys and acidic residues of the OPCA motif in the PB1 domain', *Planta*, 258(2), p. 26. Available at:
765 https://doi.org/10.1007/s00425-023-04183-3.

Okushima, Y., Overvoorde, Paul J, *et al.* (2005) 'Functional Genomic Analysis of the AUXIN RESPONSE FACTOR Gene Family Members in Arabidopsis thaliana : Unique and Overlapping Functions of ARF7 and ARF19', 17(February), pp. 444–463. Available at: https://doi.org/10.1105/tpc.104.028316.2.

Okushima, Y., Overvoorde, Paul J., *et al.* (2005) 'Functional Genomic Analysis of the AUXIN RESPONSE FACTOR Gene Family Members in Arabidopsis thaliana: Unique and Overlapping Functions of ARF7 and ARF19', *Plant Cell*, 17(12), pp. 3282–3300. Available at: https://doi.org/10.1105/tpc.105.036723.

Pandey, S.K. *et al.* (2018) 'LBD18 uses a dual mode of a positive feedback loop to regulate ARF expression and transcriptional activity in Arabidopsis', *The Plant Journal*, 95(2), pp. 233–251. Available at: https://doi.org/10.1111/tpj.13945.

Peaucelle, A. *et al.* (2007) 'Plants expressing a miR164-resistant CUC2 gene reveal the importance of post-meristematic maintenance of phyllotaxy in Arabidopsis', *Development*, 134(6), pp. 1045–1050. Available at: https://doi.org/10.1242/dev.02774.

Petrella, R. *et al.* (2020) 'BPC transcription factors and a Polycomb Group protein confine the expression of the ovule identity gene SEEDSTICK in Arabidopsis', *The Plant Journal*, 102(3), pp. 582–599. Available at: https://doi.org/10.1111/TPJ.14673.

Powers, S.K. *et al.* (2019) 'Nucleo-cytoplasmic Partitioning of ARF Proteins Controls Auxin Responses in Arabidopsis thaliana', *Molecular Cell*, 76(1), pp. 177-190.e5. Available at: https://doi.org/10.1016/j.molcel.2019.06.044.

Prusinkiewicz, P. *et al.* (2007) 'Evolution and development of inflorescence architectures', *Science (New York, N.Y.)*, 316(5830), pp. 1452–1456. Available at: https://doi.org/10.1126/SCIENCE.1140429.

Refahi, Y. *et al.* (2016) 'A stochastic multicellular model identifies biological watermarks from disorders in self-organized patterns of phyllotaxis', *eLife*, 5(2016JULY), pp. 1–51. Available at: https://doi.org/10.7554/eLife.14093.

Richter, R. *et al.* (2019) 'Floral regulators FLC and SOC1 directly regulate expression of the B3-type transcription factor TARGET OF FLC AND SVP 1 at the Arabidopsis shoot apex via antagonistic chromatin modifications', *PLoS genetics*, 15(4), p. e1008065. Available at: https://doi.org/10.1371/journal.pgen.1008065.

Rieu, P. *et al.* (2024) 'The ALOG domain defines a family of plant-specific transcription factors acting during Arabidopsis flower development', *Proceedings of the National Academy of Sciences*, 121(10), p. e2310464121. Available at: https://doi.org/10.1073/PNAS.2310464121.

Schindelin, J. *et al.* (2012) 'Fiji: An open-source platform for biological-image analysis', *Nature Methods*, 9(7), pp. 676–682. Available at: https://doi.org/10.1038/NMETH.2019.

Shi, B. *et al.* (2018) 'Feedback from Lateral Organs Controls Shoot Apical Meristem Growth by Modulating Auxin Transport', *Developmental Cell*, 44(2), pp. 204-216.e6. Available at: https://doi.org/10.1016/J.DEVCEL.2017.12.021.

Shin, R. *et al.* (2007) 'The Arabidopsis transcription factor MYB77 modulates auxin signal transduction', *Plant Cell*, 19(8), pp. 2440–2453. Available at: https://doi.org/10.1105/tpc.107.050963.

Shyer, A.E. *et al.* (2013) 'Villification: How the gut gets its villi', *Science*, 342(6155), pp. 212–218. Available at: https://doi.org/10.1126/science.1238842.

Somssich, M. *et al.* (2016) 'CLAVATA-WUSCHEL signaling in the shoot meristem', *Development (Cambridge, England)*, 143(18), pp. 3238–3248. Available at: https://doi.org/10.1242/DEV.133645.

Steven E. Clark, Mark P. Running and Elliot M. Meyerowitz (1993) 'CLAVATA1, a regulator of meristem and flower development in Arabidopsis', *Development*, (119), pp. 397–418. Available at: https://doi.org/10.1242/dev.119.2.397.

Strauss, S. *et al.* (2020) 'Phyllotaxis: is the golden angle optimal for light capture?', *New Phytologist*, 225(1), pp. 499–510. Available at: https://doi.org/10.1111/nph.16040.

Swaminathan, K., Peterson, K. and Jack, T. (2008) 'The plant B3 superfamily', *Trends in Plant Science*, 13(12), pp. 647–655. Available at: https://doi.org/10.1016/j.tplants.2008.09.006.

Szemenyei, H., Hannon, M. and Long, J.A. (2008) 'TOPLESS mediates auxin-dependent transcriptional repression during Arabidopsis embryogenesis', *Science*, 319(5868), pp. 1384–1386. Available at: https://doi.org/10.1126/science.1151461.

Truskina, J. *et al.* (2021) 'A network of transcriptional repressors modulates auxin responses Chromatin status of class A ARF loci', | *Nature* |, 589. Available at: https://doi.org/10.1038/s41586-020-2940-2.

Vernoux, T. *et al.* (2011) 'The auxin signalling network translates dynamic input into robust patterning at the shoot apex', *Molecular Systems Biology*, 7. Available at: https://doi.org/10.1038/msb.2011.39.

Verwoerd, T.C., Dekker, B.M.M. and Hoekema, A. (1989) 'A small-scale procedure for the rapid isolation of plant RNAs', *Nucleic Acids Research*, 17(6), pp. 2362–2362. Available at: https://doi.org/10.1093/NAR/17.6.2362.

Wang, J. *et al.* (2023) 'Dual regulations of cell cycle regulator DPa by auxin in Arabidopsis root distal stem cell maintenance', *Proceedings of the National Academy of Sciences of the United States of America*, 120(19). Available at: https://doi.org/10.1073/PNAS.2218503120/-/DCSUPPLEMENTAL.

Wang, L., Kim, J. and Somers, D.E. (2013) 'Transcriptional corepressor TOPLESS complexes with pseudoresponse regulator proteins and histone deacetylases to regulate circadian transcription', *Proceedings of the National Academy of Sciences of the United States of America*, 110(2), pp. 761–766. Available at: https://doi.org/10.1073/pnas.1215010110.

Yu, Y. *et al.* (2020) 'Arabidopsis REM16 acts as a B3 domain transcription factor to promote flowering time via directly binding to the promoters of SOC1 and FT', *Plant Journal* [Preprint]. Available at: https://doi.org/10.1111/tpj.14807.

Žádníková, P. and Simon, R. (2014) 'How boundaries control plant development', *Current Opinion in Plant Biology*, pp. 116–125. Available at: https://doi.org/10.1016/j.pbi.2013.11.013.

Zhang, K. *et al.* (2022) 'Cell- and noncell-autonomous AUXIN RESPONSE FACTOR3 controls meristem proliferation and phyllotactic patterns', *Plant Physiology*, 190(4), pp. 2335–2349. Available at: https://doi.org/10.1093/PLPHYS/KIAC370.

Behind phyllotaxis, within the meristem: a REM-ARF complex shapes inflorescence in *Arabidopsis thaliana*

Francesca Caselli[1], Carlotta Ferrario[1], Veronica Beretta[1], Sri Amarnadh Gupta Tondepu[1,4], Renaud Dumas[2], Humberto Herrera-Ubaldo[3,5], Stefan de Folter[3,] Martin M. Kater[1], Veronica Gregis[1,*]

[1] Dipartimento di Bioscienze, Università degli Studi di Milano, Milano 20133, Italy
[2] Laboratoire Physiologie Cellulaire et Végétale, Université Grenoble Alpes, Centre national de la recherche scientifique, Commissariat à l'énergie atomique et aux énergies alternatives, Institut national de recherche pour l'agriculture, l'alimentation et l'environnement, Département de Biologie Structurale et Cellulaire intégrée, Grenoble F-38054, France
[3] Unidad de Genómica Avanzada (UGA-Langebio), Centro de Investigación y de Estudios Avanzados del Instituto Politécnico Nacional, Irapuato, Mexico.
[4] Present address: Department of Biology and Biotechnology "L. Spallanzani", University of Pavia, Via Adolfo Ferrata 9, 27100 Pavia, Italy.
[5] Present address: Department of Plant Sciences, University of Cambridge, Cambridge CB2 3EA, UK

* Corresponding author: veronica.gregis@unimi.it

Supplementary Figures and Tables

Supplementary Figure 1. Models for interactions between REM35-REM35 and REM34-REM35.

Supplementary Figure 2. Description of *rem34* and *rem35* mutants and complementation test.

Supplementary Figure 3. Y2H matrix.

Supplementary Figure 4. *REM34* overexpression analysis in roots.

Supplementary Figure 5. *in situ* hybridization controls.

Supplementary Table 1. Primers employed in this work.

Supplementary Figures and Tables

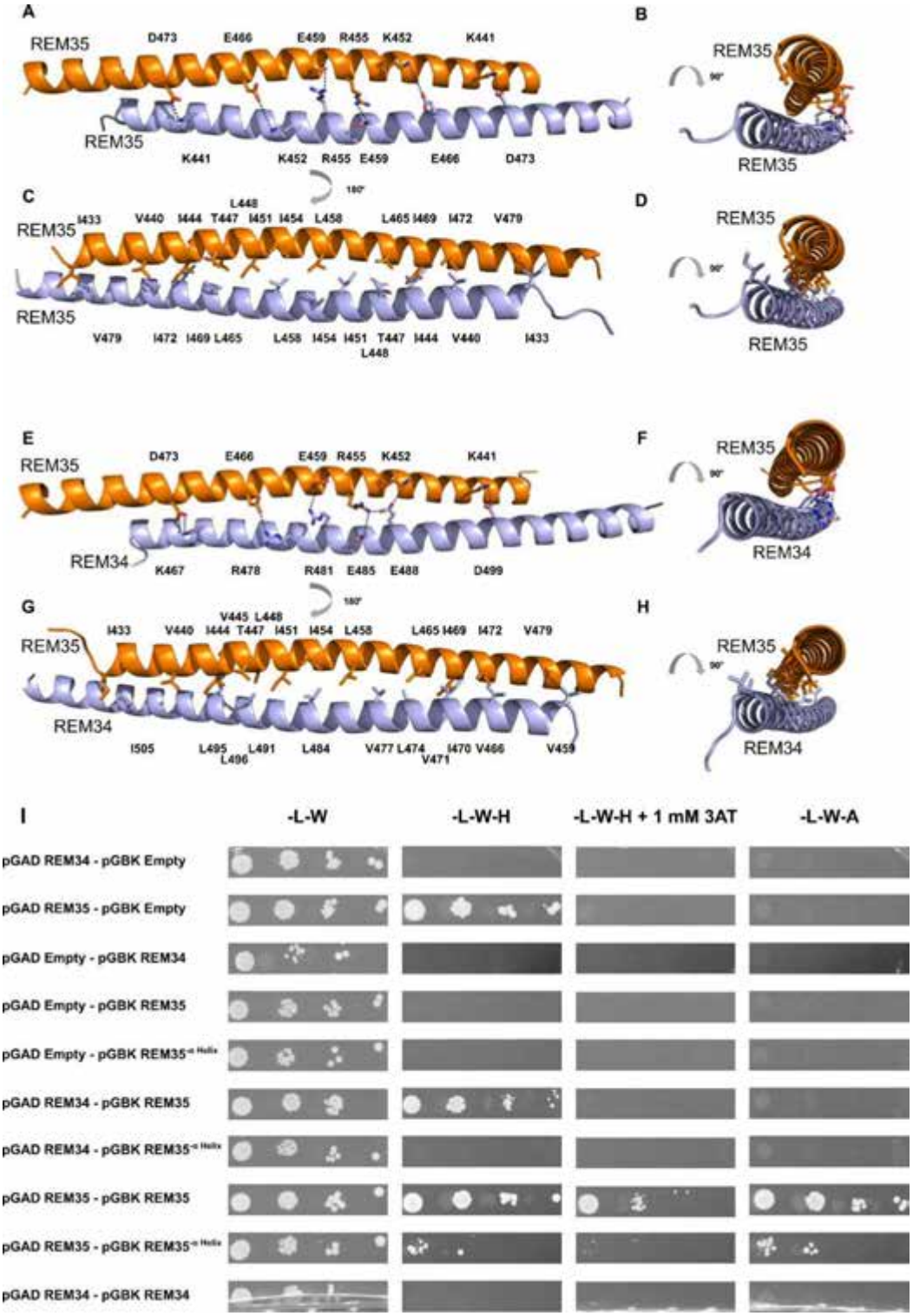

Supplementary Figure 1. Models for interactions between REM35-REM35 and REM34-REM35. AlphaFold models indicate that interaction between REM35 and REM35 or REM34 involved the C-terminal amphipathic helix with ionic interactions on one side of the helices and hydrophobic contacts on the other side (A-D). Interaction between REM35 and REM35. (A-B). Ionic interactions. (C-D) Hydrophobic contacts. (E-H) Interaction between REM34 and REM35. (E-F) Ionic interactions. (G-H) Hydrophobic contacts. (I) Yeast-2-Hybrid demonstrating the crucial role of the C-terminal helix of REM35 in mediating its interaction with REM34 and REM35. The interactions between REM34, REM35 and REM35 full length and a truncated version of the same protein, lacking the C-terminal domain (REM35$^{-\alpha\ Helix}$), were tested on different selective media. Serial dilutions of yeast colonies, starting from an OD600 of 0.5, harboring the vectors of interest were plated on different selective media. All the employed constructs were tested for autoactivation activity by cotransformation with the empty vectors. REM34-REM35, REM35-REM35 interactions were used as positive controls, while REM34-REM34 was employed as a negative control. The deletion of REM35 C-terminal abolishes its interaction with REM34 and clearly weakens the homodimerization of the protein.

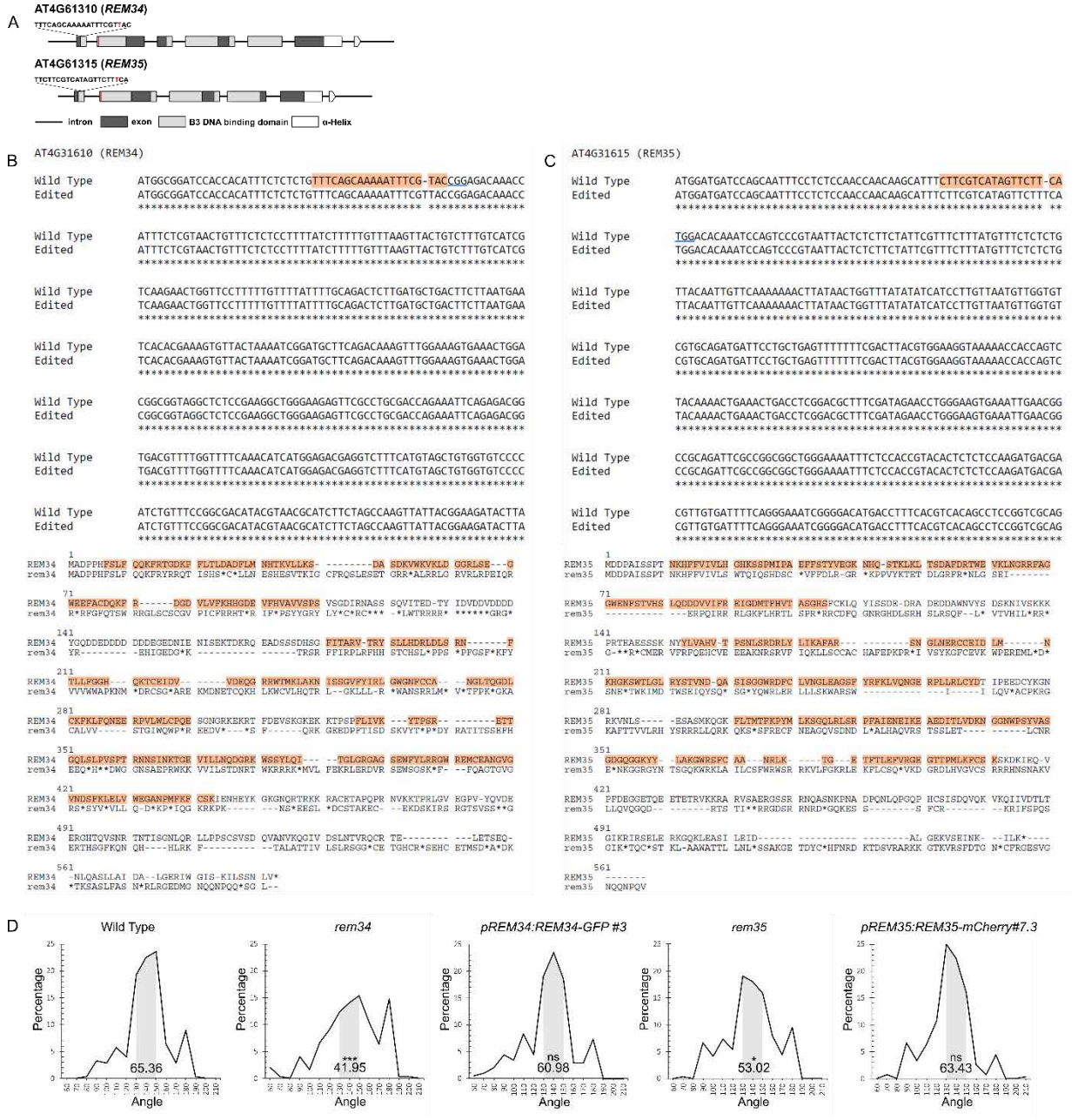

Supplementary Figure 2. Complementation of *rem34* and *rem35*. (A) Schematic representation of the structure of *REM34* and *REM35.* Boxes: exons, lines: introns. The two genes are characterized by three repetitions of the B3 DNA binding domain, indicated by the light gray boxes, the premature stop codon location is indicated in red at the beginning of the second exon. Above each gene, the protospacer sequence with the nucleotide insertion is indicated in red. (B) Comparison between *REM34* wild type and edited sequences. The top panel shows the alignment of the first 420 bp of the genomic region of *REM34* wild type and edited sequence, the edited sequence is characterized by the insertion of a T at position 45; the protospacer and PAM sequences are respectively highlighted and underlined in the wild type sequence. The panel below shows the protein alignment between REM34 and rem34, the T insertion causes a frameshift starting from aa15 which leads to the formation of a stop codon in position 25, at the beginning of the first B3 DNA binding domain; the three B3 DNA binding domains are highlighted in the wild type sequence. (C) Comparison between *REM35* wild type and edited sequences. The top panel shows the alignment of the first 420 bp of the genomic region of *REM35* wild type and edited sequence, the edited sequence is characterized by the insertion of a T at position 58; the protospacer and PAM sequences are respectively highlighted and underlined in the wild type sequence. The panel below shows the protein alignment between REM35 and rem35, the T insertion causes a frameshift starting from aa20 which leads to the formation of a stop codon in position 31, at the beginning of the first B3 DNA binding domain; the three B3 DNA binding domains are highlighted in the wild type sequence. (D)The phyllotactic pattern of wild type (10 plants, 280 angles), *rem34* (10 plants, 298 angles), *pREM34:REM34-GFP* in *rem34* (10 plants, 315 angles) *rem35* (10 plants, 315 angles), *pREM35:REM35-mCherry* in *rem35* (10 plants, 268 angles) was assessed. Compared to the wild type, the two mutants showed a significant decrease in the percentage of angles falling in the canonical 130°-150° range. The mutants transformed with the *pREM34:REM34-GFP* and *pREM35:REM35-mCherry* constructs exhibited a wild type-like phyllotactic pattern. Significance was calculated with a t-test (ns non-significative, *<0.05, ***<0.001).

SCR1 AT3G54220	CUC1 AT3G15170	CUC2 AT5G53950	HEC1 AT5G67060	WUS AT2G17950	YAB1 AT2G45190	CRC AT1G69180	BP AT4G08150	KNAT6 AT1G23380	STM AT1G62360	KNAT2 AT1G70510	
REM13 AT3G46770	PHV AT1G30490	ALC AT5G67110	AS2 AT1G65620	BEE1 AT1G18400	ARR4 AT1G10470	ARR16 AT2G40670	TCP15 AT1G69690	REV AT5G60690	LSH1 AT5G28490	IAA27 AT4G29080	ARR15 AT1G74890
NGA1 AT2G46870	BEL1 AT5G41410	RPL AT5G02030	STY1 AT3G51060	STY2 AT4G36260	ARF19 AT1G19220	LSH3 AT2G31160	ARF8 AT5G37020	IAA27 AT4G29080	PHB AT2G34710	BHLH14 AT4G00870	
NIN AT4G24020	JAG AT1G68480	REM11 AT2G24681	ARR10 AT4G31920	SEU AT1G43850	WIP3 AT3G13360	KAN2 AT1G32240	LUG AT4G32551	PNF AT4G29080	ARR12 AT2G25180	GIK AT2G35270	TPL AT1G15750
AS1 AT2G37630	AG AT4G18960	ARF18 AT3G61830	LSH4 AT3G23290	ARF4 AT5G60450	MSI1 AT5G58230	ETT AT2G33860	FIE AT3G20740	NGA2 AT3G61970	KAN1 AT5G16560	HEC2 AT3G50330	ARF17 AT1G77850
ARR14 AT2G01760	YAB3 AT4G00180		LEP AT5G13910	ARR7 AT1G19050	HEC3 AT5G09750	NGA3 AT1G01030	WIP6 AT1G13290	DRN AT1G12980	JAIBA/HAT1 AT4G17460.1	JAIBA/HAT1 AT4G17460.2	JAIBA/HAT1 AT4G17460.3
ARF1 AT1G59750	VDD AT5G18000	ANT AT4G37750	DKM AT2G21230	SHP2 AT2G42830	STK AT4G09960	AG AT4G18960	SHP1 AT3G58780	AGL14 AT4G11880	FUL AT5G60910	SEP3 AT1G24260	AGL63 AT1G31140
BPC1 AT2G01930	BPC2 AT1G14685	BPC3 AT1G68120	BPC6 AT5G42520	EMF2 AT5G51230	VRN2 AT4G16845	SWG AT4G02020	LHP1 AT5G17690	REM34 AT4G31610	REM35 AT4G31615	REM36 AT4G31620	BPC4 AT2G21240

Supplementary Figure 3. Y2H matrix. Schematic representation of the yeast-2-hybrid library employed to identify novel interactors of REM34 and REM35. For the screening REM34 and REM35 were cloned in the pDEST32 bait vector, containing the GAL4 DNA Binding Domain, and tested against the matrix of factors, previously cloned into the pDEST22 bait vectors, in frame with the GAL4 Activation Domain. Positive interactions were screened on media lacking Leu, Trp, Ade and His. A LacZ assay was also performed to confirm the detected interactions.

Supplementary Figure 4. Mutants employed. Photo of the inflorescence and rosette of all the mutants employed in this study.

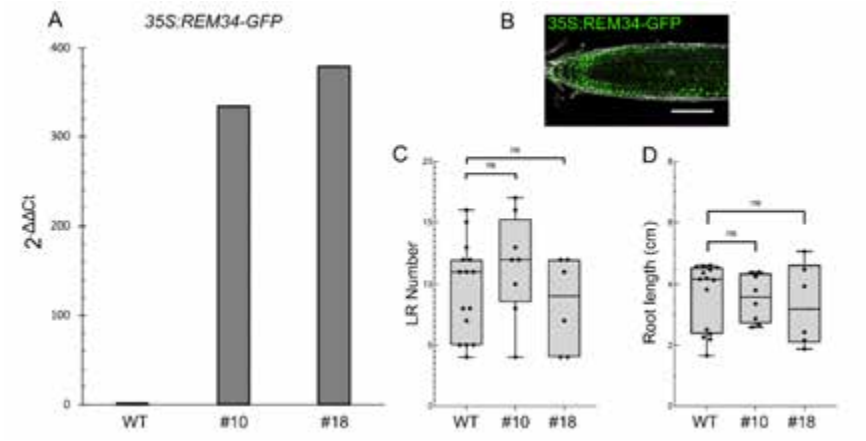

Supplementary Figure 5. *REM34* overexpression analysis in roots (A) Levels of overexpression of REM34 in the seedling of two independent 35S:REM34-GFP lines, compared to the wild type. (B) Confocal images showing the ectopic expression of REM34 (green), under the control of the 35S CaMV promoter (top) Cell walls were stained with PI (gray). Scale bars= 100 µm. (C-D) LR number and primary root length in wild type (n=15) and two *35S:REM34-GFP* lines (#10 n=8, #18 n=6). Statistical significance was determined with ANOVA followed by Dunnett's multiple comparison test (ns non-significative).

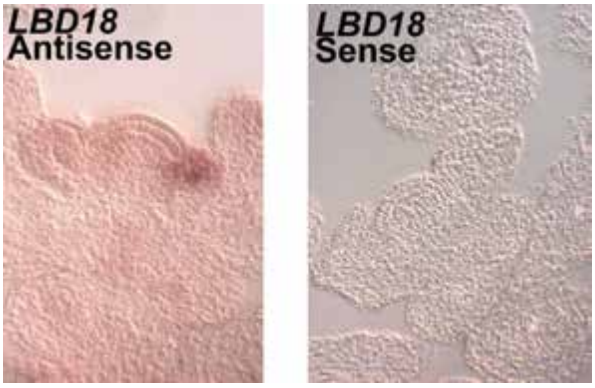

Supplementary Figure 6. *in situ* hybridization controls *in situ* hybridization showing longitudinal section of inflorescence meristems. To assess the specificity of the newly designed *LBD18* probe, both antisense and sense probes were used on the same tissues. While the antisense probe showed a strong signal in wild type inflorescences, localizing in the developing primordia, no signal was visible when the sense probe was used.

Supplementary Table 1. Primers employed in this work

Description	Primer Sequence
arf7-1 genotyping	fw TGCACTCCTCTTTGAACCATC
	rv TGGTTCACGTAGTGGGCCATCG
ARF7 genotyping	fw TGCACTCCTCTTTGAACCATC
	rv AAGAGGAAGGTGCATCTCCTC
arf19-1 genotyping	fw ACACTTGCTTACCACAGGTTGG
	rv TGGTTCACGTAGTGGGCCATCG
ARF19 genotyping	fw ACACTTGCTTACCACAGGTTGG
	rv CTGCAACAAACCACCAAGGTTAG
lbd18-1 genotyping	fw ACACTTGCTTACCACAGGTTGG
	rv TGGTTCACGTAGTGGGCCATCG
LBD18 genotyping	fw GGAAACGTATGTATGACTCGGG
	rv TTTTAAAATAACACGTACTAACTAGC
puchi-1 genotyping	fw GGTTACTTGGATTGCATTGT
	rv CTAAAAGACTGAGTAGAAGC
REM34 expression	fw AGCTTGTGAGACTGCTCCAC
	rv CCTGATCGGAGACTGAGCAC
REM35 expression	fw CATTTGATGAAGGAGGGGAGAC
	rv CTTTCTAGCTCTGACCGAATCC
H4 ISH probe	fw ATGGCAGGAAGAGGAAAAG
	rv+T7 TAATACGACTCACTATAGGGTCAACCACCAAATCCATATAG
PUCHI ISH probe	fw CTCCACAGTTTGTCATCGATC
	rv+T7 TAATACGACTCACTATAGGGGACTGAGTAGAAGCCTGTAG
LBD18 ISH probe	fw AGCTACCTCAACCGCAAACG
	rv+T7 TAATACGACTCACTATAGGGTAGTTCGAGACGGCGAGTGG
pPUCHI I ChIP	fw gactatgagcaattttcttg
	rv agtcaacaacaatcttagtc
pPUCHI II ChIP	fw ttatttcagctggttaagcc
	rv agaatggaagtgaagtgttg
pLBD18 I ChIP	fw attcaaggcaacatttctac
	rv tattcatagcaactacaacc

pLBD18 II ChIP	fw tcatttatccatcttgttcg
	rv tctcacatttagttgtttgc
ACTIN7 ChIP	fw CGTTTCGCTTTCCTTAGTGTTAGCT
	rv AGCGAACGGATCTAGAGACTCACCTTG
ARF19 CDS	fw+GW ggggacaagtttgtacaaaaaagcaggcttcACCATGAAAGCTCCTTCA
	rv+GW GGGGACCACTTTGTACAAGAAAGCTGGGTG CTATCTGTTGAAAGAAGC
ARF19^{B3} CDS	fw+GW ggggacaagtttgtacaaaaaagcaggcttcACCATGAAAGCTCCTTCA
	rv+GW GGGGACCACTTTGTACAAGAAAGCTGGGTTTaTCCCATCCAAGGCATTGC
ARF19^{B3MR} CDS	fw+GW ggggacaagtttgtacaaaaaagcaggcttcACCATGAAAGCTCCTTCA
	rv+GW GGGGACCACTTTGTACAAGAAAGCTGGGTTCaTTGAGTCTGATTGGG
ARF19^{MRPB1} CDS	fw+GW GGGGACAAGTTTGTACAAAAAAGCAGGCTccATGCCTTGGATGGGAGAAGAC
	rv+GW GGGGACCACTTTGTACAAGAAAGCTGGGTG CTATCTGTTGAAAGAAGC
ARF19^{PB1} CDS	fw+GW GGGGACAAGTTTGTACAAAAAAGCAGGCTccATGCGAACATATACAAAGGTTC
	rv+GW GGGGACCACTTTGTACAAGAAAGCTGGGTG CTATCTGTTGAAAGAAGC
REM35$^{-\alpha\ Helix}$ CDS	fw+GW GGGGACAAGTTTGTACAAAAAAGCAGGCTTCATGGATGATCCAGCAATTTC
	rv+GW GGGGACCACTTTGTACAAGAAAGCTGGGTCTTAATGTGGTTGCCCAGGCTGCAAG
ARF7 CDS	fw+GW ggggacaagtttgtacaaaaaagcaggcttcACCATGAAAGCTCCTTCA
	rv+GW GGGGACCACTTTGTACAAGAAAGCTGGGTG TCACCGGTTAAACGAAGTGG

LATERAL BRANCHING OXIDOREDUCTASE specificity for strigolactone branching inhibition in barley

Maiko Inoue[1], Apriadi Situmorang[2], Jack H. Kelly[2], Weiwei Chen[2], Hui Zhou[2], Carlotta C. Ferrario[3,4], Veronica Gregis[3], Alessandro Vajani[4], Salar Shaaf[4,5], Abhisek Biswas[4], Dabing Zhang[2], Stephanie J. Watts-Williams[2], Agnieszka Janiak[6], Marek Marzec[6], Beata Chmielewska[6], Laura Rossini[4], Kaori Yoneyama[1], Philip B. Brewer[2,3,4]

[1] Department of Biochemistry and Molecular Biology, Saitama University, 255 Shimo-Okubo, Sakuraku, Saitama 338-8570, Japan

[2] Waite Research Institute, School of Agriculture Food & Wine, The University of Adelaide, Adelaide, SA 5064, Australia

[3] University of Milan, Department of Biosciences, Via Celoria 26, 20133 Milan, Italy

[4] University of Milan, Department of Agricultural and Environmental Sciences (DiSAA), Via Celoria 2,20133 Milan, Italy

[5] Leibniz Institute of Plant Genetics and Crop Plant Research (IPK) Gatersleben, 06466 Seeland,Germany

[6] University of Silesia in Katowice, Institute of Biology, Biotechnology and Environmental Protection,Jagiellonska 28, 40032 Katowice, Poland

[7] Australian Research Council Centre of Excellence for Plant Success in Nature and Agriculture, The University of Queensland, Brisbane, QLD 4072, Australia

[8] Institute for Future Farming Systems, Central Queensland University, Rockhampton, QLD 4701, Australia

Resubmitted on February 2025, Journal Of Experimental Botany

In this paper the impact of LBO, a gene encoding a 2-oxoglutarate and Fe dependent oxygenase part of the strigolactones biosynthetic pathway, is described in barley. Mutants analysis revealed that *LBO* is involved in the tillering process and in the plant response to nutrient, but not in root fungal symbiosis.

I contributed to this paper by performing the *HvLBO* and *Hvlbo.f* complementation tests. Specifically, I cloned the *35S:HvLBO* and *35S:Hvlbo.f* constructs, developed the *Atlbo-1 35S:HvLBO* and *Atlbo-1 35S:Hvlbo.f* lines and performed the expression analysis and phenotypic analysis of those lines.

LATERAL BRANCHING OXIDOREDUCTASE specificity for strigolactone branching inhibition in barley

Maiko Inoue[1], Apriadi Situmorang[2], Jack H. Kelly[2], Weiwei Chen[2], Hui Zhou[2], Carlotta C. Ferrario[3,4], Veronica Gregis[3], Alessandro Vajani[4], Salar Shaaf[4,5], Abhisek Biswas[4], Rana Alqusumi[6], Mart T. Waters[6], Matthew R. Tucker[2,7], Dabing Zhang[2,7], Stephanie J. Watts-Williams[2], Agnieszka Janiak[8], Marek Marzec[8], Beata Chmielewska[8], Laura Rossini[4], Kaori Yoneyama[1], Philip B. Brewer[2,9,10]

[1] Department of Biochemistry and Molecular Biology, Saitama University, 255 Shimo-Okubo, Sakura-ku, Saitama 338-8570, Japan

[2] Waite Research Institute, School of Agriculture Food & Wine, The University of Adelaide, Adelaide, SA 5064, Australia

[3] University of Milan, Department of Biosciences, Via Celoria 26, 20133 Milan, Italy

[4] University of Milan, Department of Agricultural and Environmental Sciences (DiSAA), Via Celoria 2, 20133 Milan, Italy

[5] Leibniz Institute of Plant Genetics and Crop Plant Research (IPK) Gatersleben, 06466 Seeland, Germany

[6] School of Molecular Sciences, The University of Western Australia, Perth WA 6009, Australia

[7] ARC Training Centre for Future Crops Development, The University of Adelaide, Adelaide, SA 5064, Australia

[8] University of Silesia in Katowice, Institute of Biology, Biotechnology and Environmental Protection, Jagiellonska 28, 40032 Katowice, Poland

[9] Australian Research Council Centre of Excellence for Plant Success in Nature and Agriculture, The University of Queensland, Brisbane, QLD 4072, Australia

[10] Institute for Future Farming Systems, Central Queensland University, Rockhampton, QLD 4701, Australia

*Corresponding author: Philip B. Brewer, email: philip.brewer@adelaide.edu.au

Maiko Inoue: inoue.m.322@ms.saitama-u.ac.jp
Apriadi Situmorang: apriadi.situmorang@adelaide.edu.au
Jack H. Kelly: jack.h.kelly@adelaide.edu.au
Weiwei Chen: weiwei.chen@adelaide.edu.au
Hui Zhou: hui.zhou@adelaide.edu.au
Carlotta C. Ferrario: carlotta.ferrario@unimi.it
Veronica Gregis: veronica.gregis@unimi.it
Alessandro Vajani: alessandrovajani1@gmail.com
Salar Shaaf: shaafs@ipk-gatersleben.de
Abhisek Biswas: abhisek.biswas@unimi.it
Rana Alqusumi: 22804678@student.uwa.edu.au
Mark T. Waters: mark.waters@uwa.edu.au
Matthew R. Tucker: matthew.tucker@adelaide.edu.au
Dabing Zhang: (deceased)
Stephanie J. Watts-Williams: stephanie.watts-fawkes@adelaide.edu.au
Agnieszka Janiak: agnieszka.janiak@us.edu.pl
Marek Marzec: marek.marzec@us.edu.pl
Beata Chmielewska: beata.chmielewska@us.edu.pl
Laura Rossini: laura.rossini@unimi.it
Kaori Yoneyama: yoneyamak@mail.saitama-u.ac.jp
Philip B. Brewer: philip.brewer@adelaide.edu.au

Number of figures: 5

Word count (Introduction to Acknowledgments, excluding Materials and Methods): 5,505

Highlight

Barley *lateral branching oxidoreductase* mutants reveal functional divergence between strigolactones involved in tillering and those involved in root exudates.

Abstract

Strigolactone (SL) mutants display a range phenotypes, such as increased branching, reduced stature and a loss of SLs exuded from roots into soil. SL biosynthesis is complex and divergent between plant species. Recently, mutants defective in specific SL biosynthesis genes have shown a loss of exuded SLs, but no obvious change in branching (tillering). This means that functional specification may exist between certain SL sub-types. It has been suggested that the LATERAL BRANCHING OXIDOREDUCTASE (LBO) enzyme acts in a sub-pathway of SLs that is specific for branching. Here we report that barley plants mutants in *hvlbo* have increased tillering, but normal production of SLs detected in roots and root exudates. This finding supports the idea that SLs have functional or tissue-specific differences and that the LBO pathway has specificity for bud outgrowth rather than exudates.

Key words

Strigolactone, biosynthesis, branching, tillering, root exudate, barley, crop, yield

Abbreviations

SL, strigolactone; D14, DWARF14; CLAMT, CLA METHYLTRANSFERASE; LBO, LATERAL BRANCHING OXIDOREDUCTASE; TILLING, Targeting Induced Local Lesions in Genomes; WT, wild type; *Hor*TILLUS,

Hordeum vulgare TILLING University of Silesia; CDS, coding sequence; CaMV, Cauliflower Mosaic Virus; SD, short-day; LD, long-day; AM, arbuscular mycorrhizal; 2-OGD, 2-oxoglutarate and Fe(II)-dependent dioxygenase; DSBH, double-stranded β-helix conserved catalytic domain; GP, Golden promise; Seb, Sebastian, CL, carlactone; CLA, carlactonoic acid; MeCLA, methyl carlactonoate; 1'-HO-MeCLA, hydroxymethyl carlactonoate.

Introduction

Strigolactone (SL) biosynthesis consists of a core conserved pathway from β-carotene to carlactone (CL), which then diverges through a range of enzymatic pathways to produce various SL types depending on each plant species (Dun *et al.*, 2023; Marzec *et al.*, 2020b; Nomura *et al.*, 2024; Yoneyama and Brewer, 2021). SLs are plant hormones perceived by the DWARF14 (D14) receptor, which is encoded by a single gene copy in most species (Waters *et al.*, 2012). Mutants that fail to produce the core biosynthesis pathway, such as rice *dwarf17* (*d17*) or maize *zmccd8*, display the full range of SL-related phenotypes, such as excessive branching/tillering, dwarfism and the absence of SLs exuded from roots (Brewer *et al.*, 2013; Chen *et al.*, 2023; Ito *et al.*, 2022; Li *et al.*, 2023). Failure to exude SLs can result in reduced fungal symbiosis or parasitic weed infestation (Gomez-Roldan *et al.*, 2008; Umehara *et al.*, 2008). SLs, including those that are exuded, can inhibit branching when artificially added onto buds (Arite *et al.*, 2009). Hence, it has been assumed that any SL exuded from roots, also contributes to branching inhibition as an internal hormone. However, recently, SL mutants have been reported to be defective in exudates (and some plant phenotypes), but normal in branching/tillering (Chen *et al.*, 2023; Ito *et al.*, 2022; Li *et al.*, 2023; Li *et al.*, 2024; Wakabayashi *et al.*, 2019; Wang *et al.*, 2024; Zhou *et al.*, 2025).

The phenotypic separation of exudate content and shoot branching suggests there are SL biosynthesis pathways for distinctive compounds with different physiological functions. For instance, Os900 is a CYP711A2 enzyme in rice involved in the production of deoxyorobanchol (4DO), which is

further converted to orobanchol (oro) by Os1400 (CYP711A3). However, although rice *os1400* and/or *os900* mutants showed loss of SL exudate, they did not show the increased tillering phenotype of the core biosynthesis mutant, *d17* (Chen *et al.*, 2023; Ito *et al.*, 2022). Moreover, *os1400* single mutants were specifically shorter due to a build-up of 4DO (Chen et al., 2023). In maize, ZmCYP706C37 and ZmMAX1b (a CYP711A enzyme) are required for the production of prominent exuded SLs, including zealactone. However, plants defective in those enzymes did not show the branching increase that was observed in the core biosynthesis mutant, *zmccd8* (Li *et al.*, 2023). Also, OsCYP706C2 and two methyl transferases are involved in converting CL to 4-oxo-methyl carlactonoate (4-oxo-MeCLA). However, although *oscyp706c2* mutants were defective in 4-oxo-MeCLA exudate, root mycorrhizal colonization and root architecture, they did not show increased tillering (Li *et al.*, 2024). CYP722C is involved in the production of oro. In tomato, loss of *slcyp722c* caused deficiencies of oro and solanacol in exudates, but did not affect branching or height (Wakabayashi *et al.*, 2019). Moreover, recent findings showed that CYP722A converts carlactonoic acid (CLA) into 16-hydroxy-CLA. However, Arabidopsis *atcyp722a* mutants showed no increase in branching (Zhou *et al.*, 2025).

The production and identity of hormone-specific SLs remains unclear, together with how they may function specifically in branching. The most-likely pathway involves the enzymes CLA METHYLTRANSFERASE (CLAMT) and LATERAL BRANCHING OXIDOREDUCTASE (LBO) (Brewer *et al.*, 2016; Haider *et al.*, 2023; Li *et al.*, 2023; Mashiguchi *et al.*, 2022; Wakabayashi *et al.*, 2021; Yoneyama *et al.*, 2020a; Zhou *et al.*, 2025). CLAMT is a methyl-transferase that catalyzes CLA to MeCLA. Arabidopsis *atclamt* mutants still produced CLA, but were deficient in MeCLA, and yet showed increased branching (Mashiguchi *et al.*, 2022; Wakabayashi *et al.*, 2021).

MeCLA can be further converted to 1'-OH-MeCLA by LBO, which is a 2-oxoglutarate and Fe(II)-dependent dioxygenase (2-OGD) (Brewer *et al.*, 2016; Yoneyama *et al.*, 2020a; Zhou *et al.*, 2025).

However, the role of 1'-OH-MeCLA is uncertain (Brewer et al., 2016). Arabidopsis *atlbo* mutants still produced upstream compounds CL and MeCLA, and yet branching was not fully repressed (Brewer et al., 2016). This means that LBO produces from MeCLA one or more SLs that inhibit branching, which contrasts with the pathway steps described above that relate to SL exudates, but not branching. Moreover, *clamt* and *lbo* double mutant plants were additive in branching, attaining the same level as the core biosynthesis mutant, *atccd7* (Zhou et al., 2025). This confirms that the CLAMT-LBO pathway is a key regulator of branching, and MeCLA bioactivity is enhanced by LBO for full branching inhibition.

Hydroxylated versions of CLA can also be processed into hydroxylated derivatives by CLAMT and LBO (Yoneyama et al. 2020a; Zhou et al., 2025). Accordingly, a group of related compounds could be produced internally in plants as branching inhibitors (Zhou et al., 2025). Moreover, it was recently reported that branching could be repressed in Arabidopsis *clamt* mutants by engineering plants to produce 5-deoxystrigol (5DS) using *GaCYP722C* from cotton (Mizutori *et al.*, 2024). However, mutants engineered to produce 18-oxo-CLA (using *SlCYP722C* from tomato) or 4DO (using *Os900* from rice) did not show branching repression (Mizutori *et al.*, 2024). This suggests that 5DS can be an endogenous branching inhibitor, in addition to the CLAMT-LBO pathway.

Further research into the CLAMT-LBO pathway may help identify branching-specific SLs and discover how they relate to exuded SLs and other plant traits. Arabidopsis lacks the complexity in SL production and exudates required to fully understand LBO function (Mizutori *et al.*, 2024). Therefore, we generated a range of barley *hvlbo* mutants by TILLING and gene editing. Intriguingly, the resultant mutants displayed hallmark phenotypes that suggest lack of SL production specific for branching. However, the mutants still produced exuded root SLs and showed no obvious defect in fungal symbiosis. These data support a model whereby (1) the LBO pathway produces branching SLs,

(2) exuded SLs are produced via a split in the SL pathway upstream of LBO, and (3) exuded SLs do not normally inhibit branching.

We attempted to discover a branching SL in *hvlbo* mutants shoot tissue. However, we could not yet identify a missing SL. We previously showed in Arabidopsis that the product of LBO was poorly mobile over a graft (Brewer *et al.*, 2016). Hence, the branching influence of LBO likely breaks down quickly in tissue extracts. Further research is required to discover this branching SL and to determine why the root-exuded SLs in *hvlbo* are not involved in internal branching inhibition.

Materials and Methods

Plant materials

For work at the University of Milan, seeds of the *Arabidopsis thaliana lbo-1* mutant line (Ws-4 ecotype; T-DNA insertional mutant; code 119G09 (DYK9)) and the corresponding wild type background (Ws-4, code 530AV) were acquired from the French National Institute for Agricultural Research (INRA). Barley *lbo.f* homozygous mutants in Sebastian background and Sebastian wild-type (WT) seeds originated from University of Silesia in Katowice stocks (see below). For the production of gene edited *hvlbo* alleles at The University of Adelaide, Golden Promise was acquired from University seed stocks.

Screening for mutants in the *hvlbo* gene using the *Hor*TILLUS TILLING population

To isolate mutants carrying point mutations in the *HvLBO* gene a TILLING (Targeting Induced Local Lesions IN Genomes) strategy was used. The procedure was carried out on the population developed at the University of Silesia in Katowice, Poland called *Hor*TILLUS (*Hor*deum *vulgare* TILLING University of Silesia), which was created by double treatment of spring barley variety Sebastian with two chemical mutagens: sodium azide (NaN_3) and N-Methyl-N-nitrosourea (MNU) (Szurman-Zubrzycka

178 *et al.*, 2018). DNA extracted from nearly 7000 M_2 individuals from the *Hor*TILLUS population was
179 combined into eight-fold DNA pools and screened for the presence of mutations in a gene fragment
180 encompassing the LBO catalytic domain, using the following primer pair, forward 5'-
181 ACGAGATGGAGAGGTTGTCG-3', labelled with IRD800 dye and reverse 5'-
182 CGATCAACTTCAGTGTGTTTTG-3', labelled with IRD700 dye. The primers were anchored in the second
183 exon of the *HvLBO* gene. The protocol for TILLING analysis followed previous recommendations
184 (Szurman-Zubrzycka *et al.*, 2017). Briefly, the target amplicons was generated using eight-fold pools
185 of DNAs from M_2 individuals, using a 20 µl PCR mixture contacting 5 pmol of each primer, 0.2 mM of
186 each of dNTP, 1 U of Color Taq DNA polymerase (EurX, Gdansk, Poland), 150 ng of template DNA and
187 1 x PCR buffer containing 1.5 mM $MgCl_2$. The PCR reaction profile was as follows: 3 min at 95°C, 8
188 cycles of touch-down with denaturation at 95°C for 30 s, annealing at 64°C for 50 s (decreasing 0.5°C
189 per cycle) and amplification at 72°C for 1 min 30 s, followed by 30 cycles with denaturation at 95°C
190 for 30 s, annealing at 60°C for 50 s and amplification at 72°C for 1 min 30 s. The reaction was
191 completed by final amplification step of 5 min at 72°C. Next, the heteroduplex formation step was
192 performed at 95°C for 3 min for initial denaturation, followed by slow renaturation in a touchdown
193 type of reaction (70 cycles of 20 sec starting from 70°C with 0.1°C decrease per cycle). Then, the
194 samples were treated for 15 min at 45°C with 20 µl of 0.1× Celery Juice Extract (CJE) containing Cel I
195 enzyme that specifically cuts DNA mismatches. The products of cleavage were analyzed using
196 polyacrylamide gel electrophoresis on LI-COR 4300 DNA Analyzer. Gel images were manually
197 screened to detect the signals indicating putative mutations in the eight-fold DNA pools. The
198 identification of single plants carrying the mutations was done by mixing equal amounts of DNA
199 from each of M_2 plants that composed the specific pool with DNA from parent variety Sebastian.
200 Such mixtures were then analyzed using the same protocol as described for the eight-fold DNA
201 pools. All putative mutations were confirmed by Sanger sequencing.
202

Isolation of *hvlbo* gene edited mutant alleles

Construction of pY-LCRISPR-HvLBO was conducted following a prior protocol (Ma *et al.*, 2015), including the thermocycler setups and Golden Gate assembly reactions (GGA), unless otherwise stated. The construct targeted two positions, one in exon1, HvLBO-Target-1: GAAGCTCAGGAGAGCCTGCG***AGG*** (PAM sequences bold and italic), and one in exon2, HvLBO-Target-2: CGGGTAGAAGTTCATCCGCA***CGG*** and was driven by OsU6a promoter and OsU6b promoter, respectively. Phusion® High-Fidelity DNA Polymerase (NEB) was used for all PCR reaction during plasmid construction. Overlapping PCR was used to introduce the target sequence into sgRNA cassette. All PCR fragments were confirmed by Sanger sequencing prior to use. Following sequence verification to confirm successful introduction of target sequence 1 and 2, both verified fragments were combined with binary vector pYLCRISPR/Cas9Pubi-H in a GGA reaction. For 10 µl reaction, ~40 ng of pYLCRISPR/Cas9Pubi-H plasmid was combined with ~10 ng of each sgRNA cassette fragment (7:1 vector:insert ratio), 1 unit of BsaI-HFv2 (NEB) in 1X T4 ligase buffer (NEB). The reaction was incubated at 37^{o}C for 3 min and 16^{o}C for 4 min (30 cycles) followed by 5 min at 60^{o}C for enzyme inactivation. 2 µl of the reaction was transformed into 20 µl of *E. coli* TOP10 competent cells. Transformants were selected on LB media plates containing 50 µg.ml^{-1}. Prior to transformation into *Agrobacterium* AGL1, the resulting plasmid, pYLCRISPR-HvLBO, was verified using restriction enzymes and Sanger sequencing using the M13F primer 5'-TGTAAAACGACGGCCAGT-3'. The construct was transformed into immature embryos (Harwood, 2014). Following transgenic plant regeneration, transformants were screened for successful edits using PCR and Sanger sequencing of PCR products overlapping the regions using primers for Target 1: LBO-T1-F 5'-CTGACCTCGGCGGAGTACCT-3' and LBO-T1-R 5'-TTGTGAAGATCGGGCGGGTG-3' and Target 2: LBO-T2-F 5'-TTGTACCTGCCGTTGGTGAG-3' and LBO-T2-R 5'-CCACGCCTTCGTCTTCTCCG-3'. Only HvLBO-Target-1 was successful to generate *hvlbo* mutants.

HvLBO and *hvlbo.f* complementation test in the Arabidopsis *atlbo-1* mutant

To obtain the *HvLBO* CDS, gene expression in different tissues and developmental stages was analyzed mining publicly available transcriptomic data through the IPK website (https://apex.ipk-gatersleben.de/apex/f?p=284:10). The seedling stage was chosen for RNA extraction because of the early *HvLBO* expression. To clone *HvLBO* and *hvlbo.f* CDSs, RNA was extracted by Trizol protocol (Invitrogen®) from root samples of 8 day old WT Sebastian and *hvlbo.f* homozygous mutant seedlings. After DNAse I treatment and LiCl purification, reverse transcription was performed by the SUPERSCRIPT III Reverse-Transcriptase (Invitrogen®) according to the manufacturer's protocol. The CDS was amplified with high-fidelity Platinum SuperFi II DNA Polymerase (Invitrogen®) by specific tailed primers, AK365108 FW 5'-GGGGACAAGTTTGTACAAAAAAGCAGGCTATGGCTTCTGCGGCCGTCTG-3' and AK365108 RV 5'-GGGGACCACTTTGTACAAGAAAGCTGGGTCTAGTTGATCTTGGCGAAGTCCAG-3', and cloned by Gateway reaction in the p221 pDONR and pH2GW7 pDEST containing the 35S Cauliflower Mosaic Virus (CaMV) promoter and terminator.

Agrobacterium tumefaciens GV3101 was used to transform *atlbo-1* homozygous mutants by floral dip (Clough and Bent, 1998). T1 seeds were screened on hygromycin selective media and resistant seedlings were checked for transgene presence by PCR employing primers HvLBO/hvlbo.f FW 5'-CGAGATGGAGAGGTTGTCGA-3' and HvLBO/hvlbo.f RV 5'-GTCTTCTTGCCCTCGAGCTT-3'. Transgene expression was assessed by qRT-PCR. To test the expression in transgenic Arabidopsis plants, RNA was extracted from rosette leaves using the LiCl method (Verwoerd *et al.*, 1989). After DNAse treatment, for each sample, RNA was retro-transcribed using iScript kit (BioRad). qRT-PCR assay was performed using iTaq Universal SYBR Green supermix (BioRad) in a Bio-Rad iCycler iQ Optical System (software version 3.0a). Three technical replicates for each sample were analyzed. Relative transcript enrichment of the targets of interest was calculated by normalizing the amount of mRNA against the ubiquitin-like *RCE1* transcript (At4g36800). Expression of the genes was calculated using the $2^{-\Delta\Delta Ct}$

method, employing WT as the normalizer. The primers used for qPCR were HvLBO-SEED1 5'-TCTTCTCCGAAGACCAGAAGC-3', HvLBO-SEED2 5'-CTCGGCGGAGTACCTTTCC-3' used to evaluate the expression level of both *HvLBO* and *hvlbo.f* transcript, and RCE1-147 5'-CTGTTCACGGAACCCAATTC-3' and RCE1-148 5'-GGAAAAAGGTCTGACCGACA-3'. T2 and T3 seeds were selected on selective hygromycin media in order to track the plants bearing the transgene in homozygosity. Those T3 seeds were used for phenotypic analysis. In order to check for expression and transgene silencing, a representative T3 plant from each line was analyzed for the expression as described above.

Plant treatments and phenotypic analyses

Arabidopsis seeds were sown in multipot plateaus (2.5 cm diameter each pot) and stratified in soil for 2 days. Plants were grown in SD condition (8h day/16h night, 20-22 °C) for 14 days and then moved to LD (16h day/8h night, 20-22 °C). The SD condition was used to delay flowering and increase rosette leaf production and branching. As near as possible to the first senescent silique, the number of rosette branches bigger than 5 mm was counted (Brewer *et al.*, 2016). 25-27 plants per genotype were used and grown in a partially block-randomized setting.

A greenhouse experiment (2019-2020) was set up to phenotype barley *Hor*TILLUS lines carrying point mutations in *hvlbo* (Table 1) and WT cultivar Sebastian, following a random block design, with 19 incomplete blocks. In the final design we included 27 Sebastian plants and 19 *hvlbo.f* plants. Seeds were sterilized for 1 min in 1% sodium hypochlorite, rinsed in water once, then 2 min in 70% ethanol, and rinse three times in water. Seeds were then sown on a rooting medium containing 2.15 g L^{-1} Murashige and Skoog salts with vitamins (Duchefa Biochemie), 30 g L^{-1} sucrose, 8 g L^{-1} plant agar (Duchefa Biochemie), and 5 mL L^{-1} indole-3-butyric acid (IBA; 0.1 mg mL^{-1} stock) (Sparkes *et al.*, 2006) and incubated in a growth room in the dark at 24C°. When they reached one-leaf stage, seedlings were transplanted in soil in 14x14x16 cm pots (one plant per pot) and grown in a greenhouse at Orto Botanico Città Studi, located in Via Camillo Golgi 18 in Milan, under long day

280 photoperiod (16 hours light at 20°C and 8 h dark at 17°C), 60-65% humidity, 200 µE m^{-2} s^{-1} light. The
281 number of tillers at different days after sowing (DAS) was recorded for each plant, along with plant
282 height (distance between the point of emergence from the soil and the base of the spike) and tiller
283 number at harvest stage.
284
285 Gene edited alleles were developed and assessed in a glasshouse under long days (16/8 h) at
286 21/16°C with daylight supplemented with 400W Metal Halide lamps (Plusrite) at the South Australia
287 Research & Development Institute (SARDI) Plant Research Centre, University of Adelaide Waite
288 Campus. Plants were grown in SARDI's proprietary Cocopeat soil mix, containing 56% coir fibre, 44%
289 quarried drainage sand and controlled release fertilizer (N added separately) at 2 cm sowing depth in
290 17.5 cm diameter, 11.6 cm height, 2.8 L pots with calcium nitrate watered in at the start at the
291 specified rates. Hormone treatments contained either 2 µM GR24 (*rac*-GR24, PhytoTech Labs,
292 G3324) or mock without hormone addition. Treatment solutions contained one drop of Triton X
293 surfactant and 10 µL acetone (GR24 was dissolved in acetone) per 50 mL MilliQ water. Hormone
294 solutions were applied to tiller buds under the leaf sheaths using a pipette starting from mid-tillering
295 phase (Zadok stage 24). Treatments were applied 3 times per week (Mon, Wed, Fri) over a 6-week
296 period. 200 µL of solution was applied for early development, increasing to 400 µL, 800 µL and 1200
297 µL as plant size progressively increased. Tiller number was manually scored at the end of
298 development.
299
300 For hydroponic experiments in Japan, barley plants were assessed in half-strength Tadano and
301 Tanaka (TT) (Tadano and Tanaka, 1980) liquid culture using our reported plastic cup hydroponic
302 method (Yoneyama *et al.*, 2020b) and including the specified nutrient restrictions.
303

SL collection from root tissues and exudates and LC-MS/MS

SLs were collected and analyzed following our reported methods for root tissues and exudates (Inoue *et al.*, 2024; Yoneyama *et al.*, 2022). Barley SLs were analyzed using ultra performance liquid chromatography coupled to tandem mass spectrometry (UPLC-MS/MS). For this, the Acquity UPLC System (Waters) coupled to a Xevo TQD triple-quadrupole mass spectrometer (Waters MS Technologies) with electrospray (ESI) interface was used. Chromatographic separation was achieved using an ODS column (ACQUITY UPLC, BEH C18, 2.1 × 100 mm, 1.7 µm; Waters) with a water-MeOH gradient containing 4% 50 mM ammonium acetate to promote ionization. Separation started at 35% MeOH, followed by a 2 min gradient to 55% MeOH, followed by a 13 min gradient to 95%, kept 96% MeOH for 2 min to wash column and then back to 35% MeOH for 3 min. The column was equilibrated at this solvent composition for 5 min before the next run. Total run time was 25 min. The column oven temperature was maintained at 40°C with a flow-rate of 0.2 mL min^{-1} (sample injection volume of 1 µL). MRM transitions for 6-*epi*-heliolactone eluting at 5.5 min were monitored for m/z 361/97 at a collision energy (CE) of 18 V and m/z 361/233 at CE of 18 V with a cone voltage of 25 V. The MRM transitions of m/z 377/97 at CE of 20 V and m/z 377/231 at CE of 15 V with a cone voltage of 25 V were used for the detection of barleylactone 2 (a novel epoxy variant of 6-*epi*-heliolactone) eluting at 4.4 min. SLs are inherently low-abundance molecules that are difficult to precisely measure, hence we could only determine relative levels (“peak areas”) between samples rather than absolute concentrations.

Arbuscular mycorrhizal fungi colonization assay

Arbuscular mycorrhizal (AM) fungi colonization assays were carried out at the Adelaide SARDI facilities using a clay loam that was dried and then sieved to <2 mm. A fine sand and the sieved soil were then sterilized by autoclaving at 121^{o}C for 20 min, two times with >24 hours between autoclave runs. Free-draining, 0.8L plastic pots were used, and each pot held 1.1 kg of the soil mix

(loam soil:dry sand, 1:1). Soil and sand were homogenously mixed prior to potting. The AM treatment was inoculated with four isolates of the AM fungus *Rhizophagus irregularis* as a commercial product (Start Up Ultra, Microbe Smart Pty Ltd, Australia) at a rate of 1 g kg^{-1} soil (corresponding to approximately 800 spores pot^{-1}) and then mixed thoroughly with the soil. The non-AM control pots had no inoculum mixed with the soil. For AM fungus un-inoculated (-AMF) treatment, there were 6 pots prepared for each genotype (GP WT, *lbo-2* and *lbo-3*). For AM fungus inoculated (+AMF), there were 10 pots prepared for each genotype, where 6 pots were for the main experiment and 4 extra pots were prepared for mid-experiment destructive sampling. 3-4 seeds were directly sown onto the soils. Plants were watered approximately every two days with 50 mL water. Pots with more than 3-4 seedlings emerged were thinned to 2 seedlings, 14 days after sowing. At 48 days after planting, plants were gently removed from the soil and any roots with attached soil were washed clean. A representative sub-sample of fresh roots (approx. 200 mg) was taken and placed in a tissue cassette, submerged in 50% ethanol for at least 24 hours to fix. The fresh root subsamples were subsequently rinsed and placed into 10% potassium hydroxide (KOH) (w/v) solution for clearing at room temperature for seven days. Then, the samples were rinsed well and stained in a 5% ink in vinegar solution (Vierheilig *et al.*, 1998) and then de-stained in acidified RO water for at least 24 hours, before being stored in a 50% glycerol solution. The roots were then quantified for percentage root length colonized by AM fungi under a stereomicroscope using the gridline intersect method (Giovannetti and Mosse, 1980).

Parasitic weed seed germination bioassay

2.5 mL of each exudate collected sample was concentrated and applied to seeds of branched broomrape (*Phelipanche ramosa*) and Egyptian broomrape (*Phelipanche aegyptiaca*), and assessed for percentage germination, according to our published method (Inoue *et al.*, 2024).

Data analysis

Data obtained from the above experiments were obtained via manual collection and were arranged in Microsoft Excel. All data was transferred to GraphPad Prism for statistical analysis and visualization. Comparisons between 2 groups used parametric *t*-tests to determine statistical relationships. For multiple comparison tests between more than 2 groups, one-way and two-way ANOVA with Tukey *post hoc* tests were used to determine statistical relationships.

Results

Barley *HvLBO* shows functional conservation in *Arabidopsis thaliana*

Sequence searches identified a single barley gene (HORVU.MOREX.r3.3HG0314210) in the Morex V3 reference genome (Mascher *et al.*, 2021), encoding a protein of 375 amino acids with high similarity to proteins from related species, rice, *Brachypodium distachyon* and sorghum, and to Arabidopsis *AtLBO* (59% identity, 77% similarity) (Supplementary Fig. S1). The sequence contains within exon 2 a conserved double-stranded β-helix conserved catalytic domain (DSBH), which is a hallmark of 2-OGDs (Fig. 1A). We previously showed that the enzymatic activity of this protein was the same whether it came from tomato, maize, sorghum or Arabidopsis (Yoneyama *et al.*, 2020a). To validate functional orthology of this candidate *HvLBO* from barley, an interspecific complementation of the Arabidopsis *atlbo-1* mutant was employed. Whereas *atlbo-1* showed increased branching (Brewer *et al.*, 2016), 35S-driven constitutive expression of *HvLBO* CDS in the Arabidopsis mutant fully restored branching to WT (Ws-4) levels in four independent lines (Fig.1B). This confirms functional conservation of *LBO* across monocotyledonous and dicotyledonous plants. Expression of *HvLBO* in Arabidopsis did not inhibit branching below WT levels (Fig. 1C). However, high SL production would be expected to repress the endogenous SL pathway in Arabidopsis as a form of feedback (Hellens *et al.*, 2023).

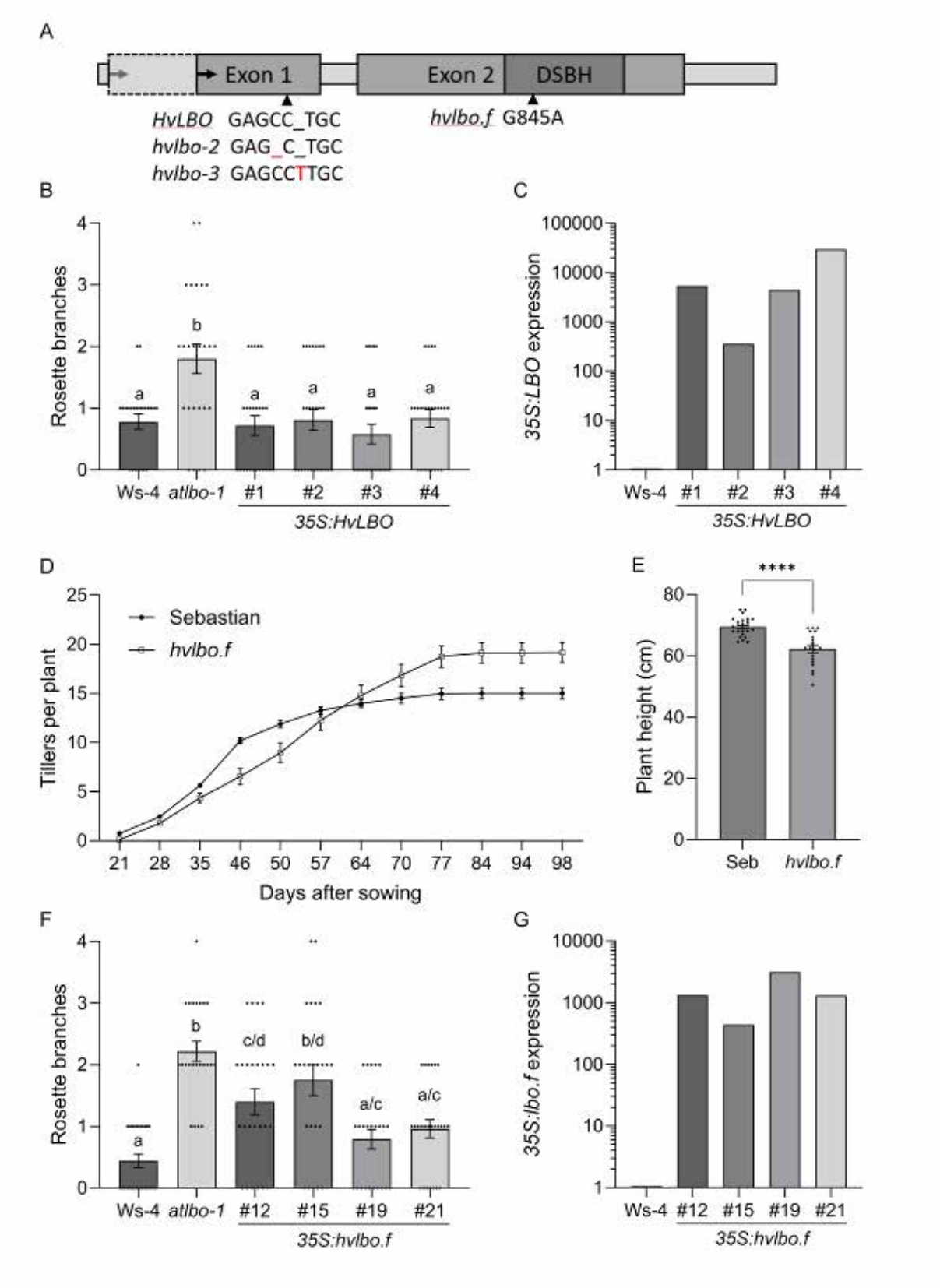

Fig. 1. Analysis of the *hvlbo.f* mutant. (A) *HvLBO* encodes a 2-oxoglutarate and Fe(II)-dependent dioxygenase (2-OGD) across two exons, including a conserved double-stranded β-helix conserved

catalytic domain (DSBH). A start codon was predicted (pale arrow). However, a second site is likely the real start codon (arrow), because this matches the protein sequence of BAJ96311 derived from a full length cDNA library, which we confirmed by PCR of a cDNA sample. The locations of three independent mutant alleles are shown (arrowheads) (an in-frame mutation, *hvlbo-1*, was not included in this study). (B) A *35S:HvLBO* construct was transformed into the *atlbo-1* mutant allele of Arabidopsis. The rosette branch number was reduced to WT (Ws-4) levels in four independent transgenic T3 lines. Data are mean ± SEM, *n* = 23-26. (C) Primers specific for *HvLBO* were used to detect relative expression of the transgene in a plant sample from each T3 line. (D) Mutant *hvlbo.f* plants isolated from the *Hor*TILLUS TILLING population showed increased tiller number compared to the WT Sebastian cultivar (Seb) during the later phase of growth, but not earlier. Data are mean ± SEM, *n* = 19-27. (E) Plant height was reduced in *hvlbo.f*. Data are mean ± SEM, *n* = 19-27. (F) A 35S construct expressing the barley mutant *hvlbo.f* CDS was also transformed into the *atlbo-1* mutant of Arabidopsis. The rosette branch number was only partially reduced to WT (Ws-4) levels in two out of four independent transgenic T3 lines. Data are mean ± SEM, *n* = 23-27. (G) Primers specific for *HvLBO*/*hvlbo.f* were used to detect relative expression of the transgene in a T3 plant sample from each line. Different letters indicate statistically significant differences by one-way ANOVA Tukey's test, $P < 0.05$. Asterisks show significant differences by student's *t*-test, **** $P \leq 0.0001$.

Barley *hvlbo* mutants display a sub-set of SL phenotypes

We employed TILLING using the *Hor*TILLUS mutagenized population of two-row spring barley (*Hordeum vulgare* L. cv. 'Sebastian') (Szurman-Zubrzycka *et al.*, 2018) to find potential *hvlbo* mutant alleles. Screening of 6912 M_2 plants resulted in the identification of 12 lines harboring distinctive point mutations in the target gene. Out of these, four lines carrying independent missense mutations (Table 1) showed viable seed germination and were further examined under glasshouse conditions. All mutations in these *hvlbo* alleles fell within the putative LBO catalytic domain near the C-terminus. One allele in particular, *hvlbo.f*, contained a point mutation in the coding sequence at

G845A, which would result in residue change D251N (Supplementary Fig. S1; Fig. 1A). Residue 251 is a conserved aspartic acid (D) residue that is predicted to play a critical role in iron binding within the LBO catalytic domain (Brewer *et al.*, 2016). Thus, this mutation is predicted to significantly interrupt *lbo* enzymatic function, and we analyzed this line further. Consequently, the *hvlbo.f* line exhibited increased tiller number at harvest compared to WT Sebastian (Fig. 1D) and reduced plant height (Fig. 1E), similar to SL-defective phenotypes reported in rice and other species (Gomez-Roldan *et al.*, 2008; Umehara *et al.*, 2008). Tiller number reached a plateau 64-70 days after sowing in the WT, but continued to increase for a further two weeks in the *hvlbo.f* line (Fig. 1D).

Table 1. *HvLBO* alleles isolated from screening of *Hor*TILLUS mutagenized population.

Allele	Nucleotide change (from ATG)	Effect	Mutation type
lbo.d	G815A	D241N	missense
lbo.e	G834A	S247N	missense
lbo.f	G845A	D251N	missense
lbo.ia	C915T	A274V	missense

To validate these results, a construct expressing the *hvlbo.f* CDS under the control of the 35S CaMV constitutive promoter was introduced in the Arabidopsis *atlbo-1* mutant and branch number (Fig. 1F) and the relative expression of the transgene was evaluated in T3 lines (Fig. 1G). According to the phenotype of four T3 independent lines, *hvlbo.f* was not able to fully complement the *atlbo-1* branching phenotype in any of the analyzed lines. Indeed, we detected a partial complementation only in two out of the four analyzed lines (Fig. 1F), which roughly aligned with expression level (Fig. 1G). These results suggest only a partial functionality of the *lbo.f* allele.

Further barley mutant alleles were generated by targeting exon 1 and exon 2 of *HvLBO* with a CRISPR-Cas9 site-directed nuclease construct transformed into barley (*Hordeum vulgare* L. cv. 'Golden Promise'), which generated several mutant alleles. Two alleles, *hvlbo-2* and *hvlbo-3*, were found to have single base changes that resulted in frame-shifts early in the coding sequence, which

would result in severe protein truncation and loss of the catalytic domain (Fig. 1A). We grew *hvlbo-2* and *hvlbo-3* mutants individually in hydroponic cups and compared plants to *hvd14.d*, a previously isolated mutant in the SL receptor gene (Marzec *et al.*, 2020a; Marzec *et al.*, 2016). The *hvlbo* mutants showed increased tillers (Fig. 2A-C). Mutant plants of *hvd14* showed on average 2.2 (± 0.4) extra tillers at 18 days old compared to the WT variety (*Hordeum vulgare* L. cv. 'Sebastian'), while *hvlbo-2* and *hvlbo-3* showed 1.3 (± 0.3) and 1.6 (± 0.5) extra tillers respectively, compared to Golden Promise (Fig. 2B). Plants in hydroponic cups have a limited lifespan and can experience some stress, which may affect tillering. Hence, we examined other plants grown individually in pots with normal soil and nutrients. Analysis of tiller number over time revealed that *hvlbo-2* mutant tiller numbers were not different during early growth compared to WT (Golden Promise), but *hvlbo-2* ended up with more tillers (Fig. 2C), consistent with results obtained with *hvlbo.f* (Fig. 1D). This confirms that SLs are more important for tiller repression in older plants. Other individual plants were grown in hydroponic cups and transferred at 18 days into phosphorus (P) starvation conditions to boost SL production. At 28 days, the root tissues were extracted and assessed for any SLs. 6-*epi*-heliolactone and barleylactone 2 (a novel epoxy variant of 6-*epi*-heliolactone) have recently been detected as predominant SLs in barley (Inoue *et al.*, 2024). We also detected these SLs in root tissues in all genotypes (Fig. 2D, E). Surprisingly, the peak areas of the mass spectrum were all very similar, including from *hvlbo-2* and *hvlbo-3*, indicating similar levels of SL production, regardless of the genetics (Supplementary Fig. 2; Fig. 2D, E). Root biomass was not greatly different, suggesting that root growth is not a compounding factor that may affect SL production (Fig. 2F). Similar SL levels in WT and *lbo* mutants suggests that LBO is not required for 6-*epi*-heliolactone and barleylactone 2 production within roots. Lack of SL signaling in *d14* might be expected to increase SL production due to feedback (Arite *et al.*, 2009). However, we did not see increased SL in *hvd14.d*, which may indicate a lack of *D14*-dependent feedback in barley (at least for 6-*epi*-heliolactone and barleylactone 2 content within roots).

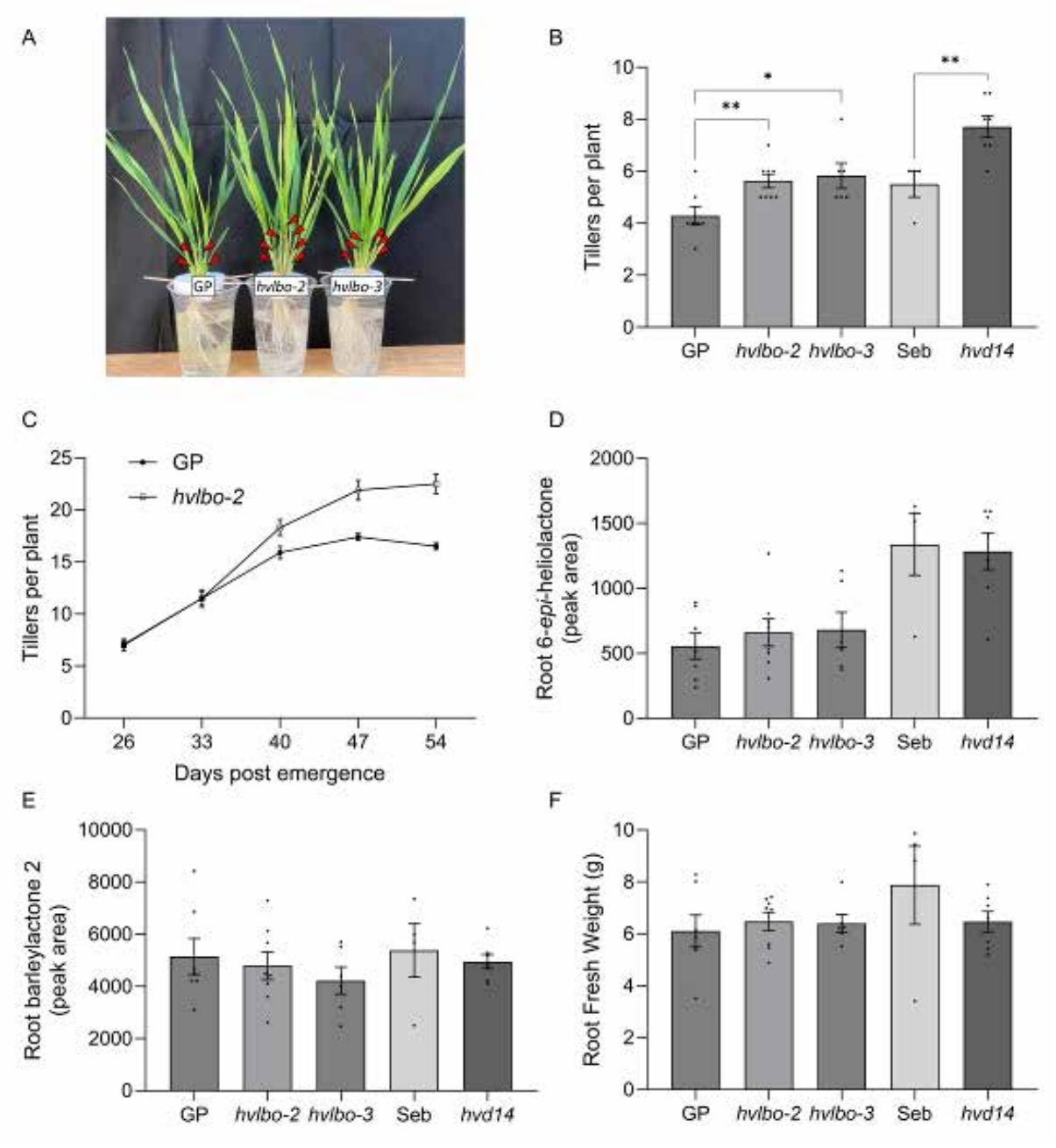

Fig. 2. Analysis of *hvlbo* gene edited mutants. (A) Mutant *hvlbo-2* and *hvlbo-3* plants grown in hydroponic cups. Red arrowheads indicate tillers. (B) Mutant *hvlbo-2 and hvlbo-3* plants showed increased tillering at 18 days old compared to the WT variety (Golden promise (GP)), but not as much as *hvd14.d* (compared to WT Sebastian (Seb)). (C) In pots with soil and normal nutrients, *hvlbo-2* tiller number was not different in at 33 days post emergence, but became greater in older plants. Root tissue was collected from the plants in hydroponic cups at 28 days old, after 10 days of P starvation. Extracts from the root tissues were analyzed for SLs by LC-MS/MS. (D) 6-*Epi*-

heliolactone was detected in the WTs and mutants, at similar relative levels. (E) Barleylactone 2 was detected in the WTs and mutants, at similar levels. Other SLs were not detected. (F) Root biomass was not significantly different. Data are mean ± SEM, *n* = 4-8. Asterisks show significant differences by student's *t*-test, * $P \leq 0.05$, ** $P \leq 0.01$.

Barley *hvlbo* mutant tiller number is greater and less reactive to nutrient conditions

As noted above, nutrients can repress SL production, and P or nitrogen (N) starvation is a common way to boost SL production for research (Brewer *et al.*, 2013). Nutrients promote the number of grain-bearing shoots (branches/tillers), which enables plants to increase progeny in proportion to greater resource availability (Brewer *et al.*, 2013). Hence, fertilizer can increase yield in crops by boosting the number of tillers. Conversely, this relationship can have adverse effects on tiller number and yield if growers seek to reduce fertilizer use (Francis *et al.*, 2023; Kelly *et al.*, 2023). SL biosynthesis gene expression, including *LBO*, can also be highly suppressed by N (Lailheugue *et al.*, 2023). We supposed that LBO, as a key SL enzyme, would also be part of nutrient responses in barley. Hence, we examined *hvlbo-2* in more detail. Plants were grown in pots in soil with low, intermediate and normal N levels and phenotypic changes were examined. Mutant *hvlbo-2* plants consistently displayed greater tiller numbers than the WT control variety (Golden Promise) (Fig. 3A). Tiller number aligned well with grain number (Fig. 3B) and yield per plant (Fig. 3C), and inversely with average individual grain (kernel) mass (Fig 3D). In each case, WT response to N was greater than *hvlbo-2* and tended to converge with the mutant at higher N. This aligns with the known role of SLs in adapting plants to nutrient levels (Brewer *et al.*, 2013). Mutant and WT phenotypes tend to converge in high N, because the SL pathway becomes suppressed by N in the WT (Sun *et al.*, 2023; Wu *et al.*, 2020). Hence, under optimal conditions, SL levels in the WT and mutant plants are similarly low and the plants appear more similar in phenotype.

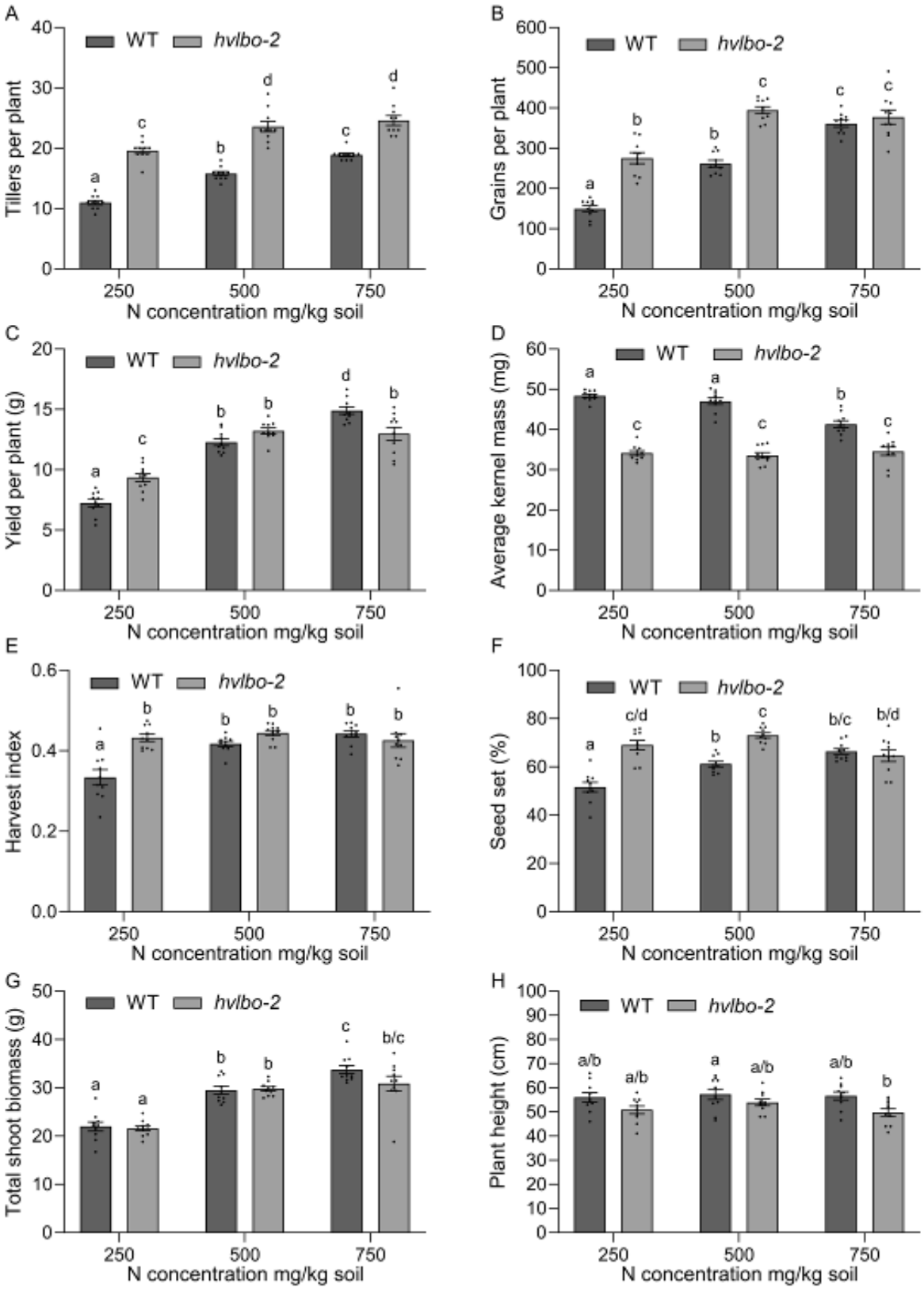
A
Tillers per plant
WT
hvlbo-2
N concentration mg/kg soil
B
Grains per plant
C
Yield per plant (g)
D
Average kernel mass (mg)
E
Harvest index
F
Seed set (%)
G
Total shoot biomass (g)
H
Plant height (cm)
250
500
750

Fig. 3: *hvlbo* mutant phenotype on low (250 mg/kg soil), intermediate (500 mg/kg) and normal (750 mg/kg) nitrate (N) added at sowing, compared to WT (Golden Promise). (A) *hvlbo-2* mutant tiller number, (B) grains per plant, (C) yield per plant, (D) average grain (kernel) mass per plant, (E) harvest index (yield as a proportion of total shoot biomass), (F) Percentage of seed set (a grain present) at each seed position, (G) total shoot biomass including grains, and (H) plant height. Data are mean ± SEM, $n = 10$. Different letters indicate statistically significant differences by two-way ANOVA Tukey's test, $P < 0.05$.

Barley *hvlbo* mutants retain yield and fertility at low N, but produced grains of reduced mass

Interestingly, *hvlbo-2* showed 29% greater yield than WT at 250 mg/kg N (Fig. 3C). Harvest index (Fig. 3E) and seed set (Fig. 3F) were also higher at 250 mg/kg N. This means that, in WT, SLs produced by LBO contribute to a repressive effect on yield, harvest index and fertility in low N, because these inhibitions were not as strong in the mutant. Hence, mutant variants of *lbo* may be useful in breeding to preventing yield loss from poorly fertile soil or low fertilizer use. On the other hand, yield was 13% lower in *hvlbo-2* at 750 mg/kg N. This was mostly due to lower individual grain mass that offset increased tiller and grain number. Smaller grain size has been observed in SL mutants in rice and maize (Guan *et al.*, 2023; Yamada *et al.*, 2019). This implies that SLs produced by LBO in the WT help plants to maintain the high mass of individual grains, even if grain number increases. Hence, LBO-related SLs may have positive or negative effects on yield and grain mass, depending on the conditions. Shoot biomass (Fig. 3G) and plant height (Fig. 3H) were only slightly different, indicating that the mutants did not show a strong growth or stature defect, which might otherwise repress grain mass. Likewise, root biomass was not greatly different in various experiments (Fig. 2F and see below).

Barley *hvlbo* responded to SL treatment, but showed normal root fungal symbiosis

To further test *hvlbo* mutants, we added a synthetic SL (*rac*-GR24) to *hvlbo-2* mutants and observed that tiller number was repressed to near the level of WT (Fig. 4A). This suggests that barley tiller buds are responsive to SLs and that *hvlbo* mutants are deficient in the production of a branching inhibiting SL. SL branching repression below control WT was not observed. SL feedback homeostasis, whereby SLs repress SL biosynthesis, is proposed to explain resistance to exogenous SLs in WT (Dun *et al.*, 2023). The lack of increased SL production in *hvd14.d* roots (Fig. 2D, E) may contradict that, but autoregulation of the signaling complex may also provide SL resistance (Dun *et al.*, 2023).

We also examined the capacity for arbuscular mycorrhizal (AM) fungal colonization in *hvlbo-2* and *hvlbo-3* mutant roots at 48 days post inoculation (dpi). Hyphae, vesicles and arbuscules were observed in roots, indicating that colonization had occurred. However, no significant differences were observed between mutants and WT in terms of overall colonization and fungal morphology (Fig. 4B). In addition, we confirmed no change in AM fungal colonization in *hvlbo-2* and *hvlbo-3* in an independent laboratory using alternative inoculation and scoring methods (Supplementary Fig. 3 and Supplementary Protocol). AM fungal colonization coincided with slightly repressed root and shoot biomass at 34 dpi (Fig. 4C, D). This result may indicate a carbon drain, negatively affecting plant growth, as has been reported in barley previously (Grace *et al.*, 2009; Kaur *et al.*, 2022). Importantly, similar biomass reduction trends were seen across WT, *hvlbo-2* and *hvlbo-3* (Fig. 4C, D), suggesting that the fungal interaction is functioning in a similar way in the mutant and WT. Root biomass was slightly reduced compared to the WT in *hvlbo-2* and *hvlbo-3*, and the shoot biomass trended slightly higher, which suggests that the *LBO* pathway may play a minor role in balancing root and shoot growth, in a manner unrelated to AM fungal colonization. A thorough examination of *hvlbo* root architecture responses to nutrients would be useful for future studies.

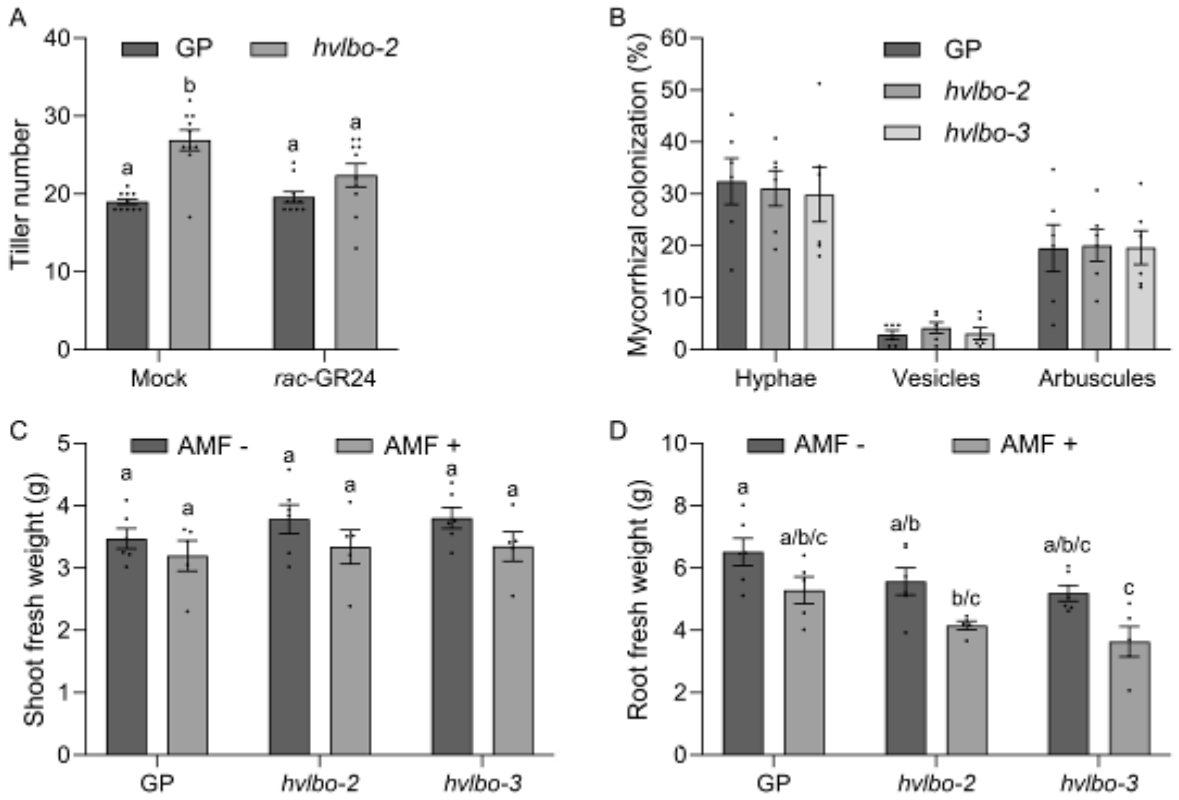

Fig. 4. The effects of SL treatment and AM fungal inoculation (*Rhizophagus irregularis*) on barley *hvlbo* mutants. (A) Doses of 2µM *rac*-GR24 repressed tiller number in *hvlbo-2* but not WT Golden Promise (GP). Data are mean ± SEM, *n* = 10. (B) The percentage presence of each of AM hyphae, vesicles and arbuscules were not obviously different between WT Golden Promise (GP), *hvlbo-2* and *hvlbo-3* at 48 dpi. Data are mean ± SEM, *n* = 6. (C) Shoot fresh weight at 34 dpi trended upwards in the mutants compared to WT (GP), and downwards with AM fungal inoculation. (D) Root fresh weight trended downwards in both the mutants and with AM fungal inoculation. Data are mean ± SEM, *n* = 5-6. Different letters indicate statistically significant differences by two-way ANOVA Tukey's test, $P < 0.05$.

Barley *hvlbo* mutants have normal SL root exudates

Having established that *lbo* mutant plants show phenotypes that align with SL deficiency, and yet show normal SL production in root tissues, and no obvious signs of deficient AM fungal symbiosis activity, we next sought to test whether exuded SL was defective in mutants. We grew *hvlbo-2* mutant plants in P- and N-deficient conditions to boost SL production, and the SLs exuded from roots were collected and analyzed by liquid chromatography with tandem mass spectrometry (LC-MS/MS). We detected and identified the same two SLs (Fig. 2D, E): 6-*epi*-heliolactone and barleylactone 2 (Supplementary Fig. 4; Fig. 5A, B). As expected, SL secretion greatly increased in the WT: 6-*epi*-heliolactone (Fig. 5A) and barleylactone 2 (Fig. 5B). This was especially so for N deficiency. Remarkably, *hvlbo-2* mutants showed very similar increases. Parasitic weed seed germination is a reliable bioassay used to verify that bioactive SLs are present in a sample , particularly when SL levels are near the limit of detection (Ablazov *et al.*, 2024). The WT and mutant collected exudate stimulated parasitic weed seed germination with trends matching the SL detection data (Fig. 5C, D). confirming similarity of SL levels. This implies that the product of LBO is not an important contributor to SL exudate production.

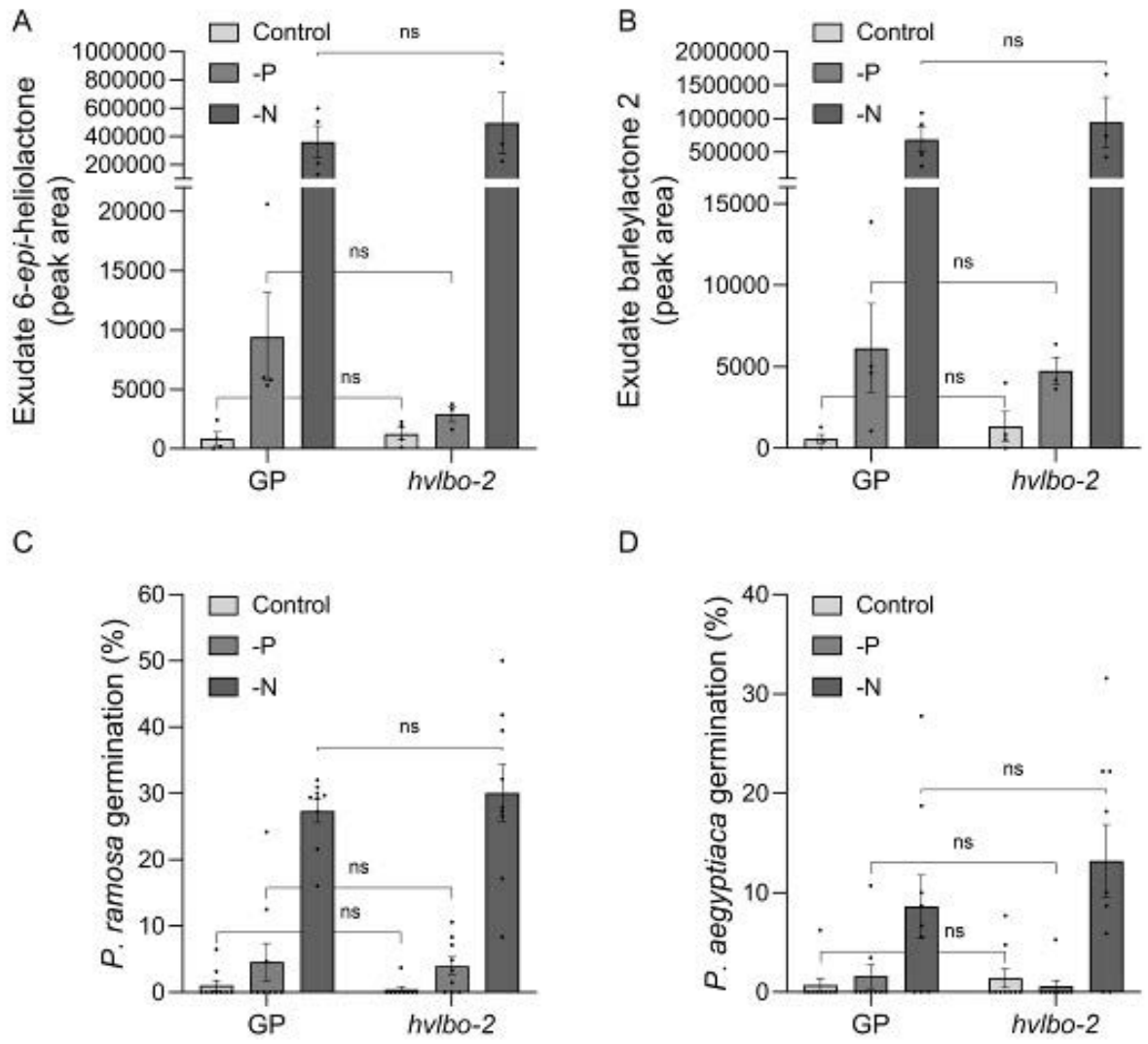

569

570 Fig. 5. *lbo* mutant plants grown in hydroponics with phosphorus (-P) or nitrogen (-N) starvation
571 conditions. SL exudates analyzed by LC-MS/MS. WT (Golden promise; GP) and mutant show similar
572 large increases in (A) 6-*epi*-heliolactone and (B) barleylactone 2. Data are mean ± SEM, *n* = 2-5. SL
573 exudate collected samples were also applied to parasitic weed seeds, (C) Branched broomrape
574 (*Phelipanche ramosa*) and (D) Egyptian broomrape (*Phelipanche aegyptiaca*), and assessed for
575 percentage germination. Data are mean ± SEM, *n* = 9. Not significant (ns) is as per two-way ANOVA
576 Tukey's test, $P > 0.05$.

577

578

Discussion

Until recently, all reported SL mutants were highly branched. Also, SLs can inhibit buds when applied exogenously, and there usually exists only one copy of the SL receptor in a species. Hence, it had been assumed that all SLs produced within plants will inhibit buds. However, research into the sub-pathway of SL biosynthesis that involves CLAMT and LBO, along with new SL biosynthesis mutants that are not highly branched, suggest that there may be (at least) exudate- and branching-specific SL pathways (Chen *et al.*, 2023; Ito *et al.*, 2022; Li *et al.*, 2023; Wakabayashi *et al.*, 2019; Wang *et al.*, 2024). This may mean that, despite years of research into branching and SLs, the branching-specific SL is yet unknown (Dun *et al.*, 2023; Nomura *et al.*, 2024; Yoneyama and Brewer, 2021). Therefore, it is useful to discover whether *lbo* mutants are defective in exuded SLs. In this study, we show that *lbo* mutants in barley fail to produce the SL-related branching inhibitor, but are still able to make exuded SLs.

Exudate SLs may include various structures, including four-ringed types (canonical) and non-four-ringed types (non-canonical). The production of known canonical SLs mostly involves consecutive reactions from P450 enzymes deriving from carlactonoic acid (CLA), a non-bioactive, two-ringed SL intermediate (Dun *et al.*, 2023). Plant species and varieties can exude their own distinctive mix of SLs. This is presumably to avoid parasitic weed infection but still retain AM fungal interactions (Yoneyama and Brewer, 2021). It is not yet well known how the diversity in exuded SLs relates to internal hormone function and evolution. Branching-specific SLs are likely to be CLA-derived and non-canonical. Methyl carlactonoate (MeCLA) is produced from CLA by the CLAMT enzyme (Haider *et al.*, 2023; Li *et al.*, 2023; Mashiguchi *et al.*, 2022; Wakabayashi *et al.*, 2021) and MeCLA is a precursor for non-canonical SLs (so far). MeCLA was shown to be the precursor to lotuslactone, zealactone or avenaol, all found in root exudates (Dun *et al.*, 2023; Yoneyama and Brewer, 2021). LBO is a 2-OGD enzyme that acts to convert MeCLA into hydroxymethyl carlactonoate (1'-HO-MeCLA), a function that appears to be conserved in monocotyledonous and dicotyledonous plants

(Brewer *et al.*, 2016; Yoneyama *et al.*, 2020a). Mutants of *clamt* or *lbo* in Arabidopsis show increased branching, suggesting that this pathway produces a branching inhibiting SL (Brewer *et al.*, 2016; Zhou *et al.*, 2025). This also means that LBO is currently the enzyme in the most distal position in the pathway that produces the branching SL. However, the identity of that SL, or what further conversions or transport may occur, are unknown. The LBO enzyme, when heterologously expressed in *Escherichia coli*, produces 1'-HO-MeCLA, but it also produces CLA, and at greater levels (Yoneyama *et al.*, 2020a). Mutants of *lbo* have high levels of MeCLA and undetectable levels of 1'-HO-MeCLA (Yoneyama *et al.*, 2020a). 1'-HO-MeCLA is predicted to be unstable and CLA may be a non-enzymatic reversion from 1'-HO-MeCLA that occurs perhaps in the absence of further enzymatic processing or perception (such as would occur in *E. coli*). However, the instability of 1'-HO-MeCLA may mean it cannot be chemically synthesized for further testing. Likewise, further research into the *in planta* function of LBO remains challenging.

Meanwhile, *lbo* mutants have been so far only revealed in Arabidopsis (Brewer *et al.*, 2016; Zhou *et al.*, 2025). However, Arabidopsis seems to have a simplified SL biosynthesis pathway, perhaps because hormone function has been retained but AM fungal symbiosis has been lost during evolution. Hence, sub-pathways of SL biosynthesis relating to AM fungi appear to be also lost. Therefore, it may be useful to study *lbo* mutants in species that have the capacity to associate with AM fungi. Hence, we isolated *hvlbo* mutants in barley by TILLING and gene editing. The mutants showed the expected increased tillering phenotype of SL mutants (Fig. 1D, 2A-C, 3A, 4A), although not as strong as *hvd14* (Fig. 2B). Previously, Arabidopsis mutants of *lbo* showed intermediate branching, perhaps due to a buildup of MeCLA, which presumably is only weakly bioactive (Brewer *et al.*, 2016). It is also important to consider that SLs are not the only signal that regulates branching. Cytokinins, sugar signaling and bud auxin transport also promoter tillering and still function in SL mutants (although they may be altered by complex feedback mechanisms) (Beveridge *et al.*, 1997; Salam *et al.*, 2021; Zhang *et al.*, 2020).

Mutants of *hvlbo* also showed a decrease in average individual grain mass (Fig. 3D). This is similar to rice and maize SL mutants (Guan *et al.*, 2023; Yamada *et al.*, 2019). Increased grain number in *hvlbo* was largely offset by reduced grain mass, which tended to make yield per plant similar to WT (Fig. 3C). Further research is needed to determine whether the lower grain mass in *hvlbo-2* is due to resource limitation from too many tillers or any defect directly in grain development. The latter is currently favored based on tiller removal in rice SL mutants that did not restore the smaller grain size (Yamada *et al.*, 2019). The *hvlbo* mutants had levels of two SLs in root tissues that were similar to WT and the *hvd14.d* mutant (Fig. 2D, E), yet tiller number was repressed by adding SL (Fig. 4A). This may indicate that LBO is defective in making some type of SL, but not these two. It is unclear if other SLs are made by barley. There are five *MAX1* homolog genes in barley that are partly conserved and partly divergent from the MAX1 homologs in rice (Marzec *et al.*, 2020b), so other SLs may exist. 5-deoxystrigol was previously reported for barley (Wang *et al.*, 2018), however, we could not yet detect it or any other SLs. We are currently isolating a range of SL biosynthesis mutants, which will help to elucidate the entire SL pathway in barley, and clarify the role of LBO.

The *hvlbo* mutants showed a general lack of response to nitrate, which would be expected for an SL mutant. The lack of response ultimately meant that yield was higher at low nitrate, but lower at higher nitrate (Fig. 3C). This opens up the potential to develop *lbo*-related genetic variants to employ in poorly fertile soils or when less fertilizer is used (Kelly *et al.*, 2023). Field trials will be useful to further explore this concept. In the case of barley, consistent grain size, germination and protein content is important for malting. So, grain quality analysis, such as germination and protein levels will be useful in future. A trade-off of low grain mass may not be desirable for malting barley, but may be acceptable for livestock feed. Also, because barley *hvd14* mutants were shown to be defective in drought response (Marzec *et al.*, 2020a), *hvlbo* mutants should also be assessed for this trait in future. We do not yet know exactly what traits may be regulated by the *LBO* pathway, in

addition to branching and grain size. For instance, AM fungi symbiosis was not obviously affected in the mutants (Fig. 4B), but stress response is yet unknown. Plants were shorter in *hvlbo.f* (Fig. 1E) compared to *lbo-2* (Fig. 3H). Further research is needed to test whether the growth conditions, cultivar background or a second-site mutation may have specifically enhanced dwarfing in *hvlbo.f*. To date, we would not yet rule out shade avoidance as a trait regulated by *LBO*.

We observed normal SL exudation and effects in *hvlbo* mutants. AM fungi symbiosis (Fig. 4B), the production of two SLs in root tissue (Fig. 2E, F) and exudates (Fig. 5A, B), and exudate germination stimulation of parasitic weed seeds (that are extremely sensitive to SLs) (Fig. 5C, D) suggest that SL production in roots is normal in *hvlbo* mutants. SLs affect root architecture (Brewer *et al.*, 2013). The root biomass of *hvlbo* mutants was not greatly different, but it will be important to discover whether there are subtle differences. Remaining important questions are: does LBO have any role in roots, and can root SL exudate production can be separated from root architecture?

We uncovered two SLs at similar levels in WT and *hvlbo* roots and exudates. Importantly, this means that LBO is not required to produce those SLs and that those SLs are not involved in branching. 6-*epi*-heliolactone has been identified as a biosynthetic intermediate between MeCLA and avenaol in black oat (Moriyama *et al.*, 2022). Treatment with prohexadione, a 2-OGD inhibitor, repressed the conversion of 6-*epi*-heliolactone to avenaol in black oat (Moriyama *et al.*, 2022). However, our results suggest that LBO is not involved in 6-*epi*-heliolactone production, at least in barley. Another 2-OGD may produce avenaol, such as LOTUSLACTONE-DEFECTIVE (LLD), a 2-OGD involved in lotuslactone production in the legume *Lotus japonicus* (Mori *et al.*, 2020), or a yet unknown 2-OGD.

The detection of normal levels of SLs in roots and exudates in *lbo* mutant suggests that the LBO enzyme is not significantly involved in the biosynthesis or exudation, or even the feedback, of those SLs. This supports the hypothesis that LBO has specificity for branching, but not exudation. *hvlbo*

mutant plants can make SLs, and those SLs are not able to significantly inhibit branching as an internal hormone. It is possible that they simply cannot travel to tissues where branching inhibition occurs. It has been suggested that the hormonal function of LBO is to convert MeCLA into branching SLs close to buds (Brewer *et al.*, 2016; Dun *et al.*, 2023; Yoneyama and Brewer, 2021). Differences in chemistry may mean that CLA is a soluble transported form that is converted to MeCLA in target tissues for further processing by LBO (Dun *et al.*, 2023). Thus, specialized transport and delivery near buds may be a key specification for the branching SL and may explain why other SLs cannot functions in that way. Novel SLs are regularly being discovered, even in well-studied species. Work will continue to discover the gamut of SLs in barley, especially those particularly involved in bud outgrowth.

Acknowledgments

This article is dedicated to our esteemed colleague and mentor, the late Prof. Dabing Zhang. Thanks to Ghazwan Karem, Toby Gerard, Saffron Gerard, Mitchell Booker, Amber Walker, Ethan Habets, Breanna Forster, and Antonella Monte for technical assistance, and Elizabeth Dun for discussions

Author contributions

LR, KY, and PBB: conceptualization; AS, JHK, WC, AJ, LR, KY, and PBB: methodology; MI, AS, JHK, WC, HZ, CCF, SS, SJWW, AJ, BC, LR, KY, and PBB: formal analysis; MI, AS, JHK, WC, HZ, CCF, VG, AV, SS, SJWW, AJ, RA, BC, LR, KY, and PBB: investigation; DZ, AJ, MM, LR, KY, and PBB: resources; LR and PBB: writing – original draft; AS, JHK, CCF, VG, MTW, MRT, SJWW, AJ, LR and PBB; writing – review and editing; KY and PBB: visualization; VG, MRT, DZ, LR, KY, and PBB: supervision; JHK, VG, DZ, AJ, MM, LR, KY, and PBB: funding acquisition.

Conflict of interest

No conflict of interest declared.

Funding statement

This research was supported by the Australian Research Council (ARC) Fellowship (FT180100081) and South Australian Grain Industry Trust grant (UAD 02023) to PBB, an ARC Discovery Project (DP24 0102441) to MTW and PBB; an Australian Government Research Training Program (RTP) Scholarship and a Thyne Reid Foundation/Playford Trust Scholarship to JHK, the ERA-NET Cofund FACCE SURPLUS (BarPLUS grant id. 93) funded by MIUR in Italy to LR and by NCBR in Poland to AJ. AR was supported by a scholarship from the Saudi Arabia Ministry of Higher Education-King Saud University. Work at University of Milan was in part supported by the CLIMBER project funded under the University's 2019 SEED call (grant number 1253 to LR and VG). LR also acknowledges financial support under the National Recovery and Resilience Plan (NRRP), Mission 4, Component 2, Investment 1.1, Call for tender No. 104 published on 2.2.2022 by the Italian Ministry of University and Research (MUR), funded by the European Union – NextGenerationEU– Project Title "RADICALS - Root and shoot developmental insights for crop agricultural traits affecting resilience, competitiveness and sustainability" – CUP G53D23004030006 - Grant Assignment Decree No. n. 1048 adopted on 14/07/2023 by the Italian Ministry of Ministry of University and Research (MUR). KY was supported by Japan Science and Technology Agency (FOREST, JPMJFR220F) and the Japan Society for the Promotion of Science (KAKENHI 21H02125, 22H02270).

Data availability statement

All data are presented in the article and supplementary figures.

References

Ablazov A, Jamil M, Haider I, Wang JY, Melino V, Maghrebi M, Vigani G, Liew KX, Lin PY, Chen GE, Kuijer HNJ, Berqdar L, Mazzarella T, Fiorilli V, Lanfranco L, Zheng X, Dai NC, Lai MH, Caroline Hsing YI, Tester M, Blilou I, Al-Babili S. 2024. *Zaxinone Synthase* overexpression modulates rice physiology and metabolism, enhancing nutrient uptake, growth and productivity. Plant, Cell & Environment **47**, 3647–3661.

Arite T, Umehara M, Ishikawa S, Hanada A, Maekawa M, Yamaguchi S, Kyozuka J. 2009. *d14*, a Strigolactone-Insensitive Mutant of Rice, Shows an Accelerated Outgrowth of Tillers. Plant and Cell Physiology **50**, 1416-1424.

Beveridge CA, Symons GM, Murfet IC, Ross JJ, Rameau C. 1997. The *rms1* Mutant of Pea Has Elevated Indole-3-Acetic Acid Levels and Reduced Root-Sap Zeatin Riboside Content but Increased Branching Controlled by Graft-Transmissible Signal(s). Plant Physiology **115**, 1251-1258.

Brewer PB, Koltai H, Beveridge CA. 2013. Diverse roles of strigolactones in plant development. Molecular Plant **6**, 18-28.

Brewer PB, Yoneyama K, Filardo F, Meyers E, Scaffidi A, Frickey T, Akiyama K, Seto Y, Dun EA, Cremer JE, Kerr SC, Waters MT, Flematti GR, Mason MG, Weiller G, Yamaguchi S, Nomura T, Smith SM, Yoneyama K, Beveridge CA. 2016. *LATERAL BRANCHING OXIDOREDUCTASE* acts in the final stages of strigolactone biosynthesis in Arabidopsis. Proc Natl Acad Sci U S A **113**, 6301-6306.

Chen GE, Wang JY, Votta C, Braguy J, Jamil M, Kirschner GK, Fiorilli V, Berqdar L, Balakrishna A, Blilou I, Lanfranco L, Al-Babili S. 2023. Disruption of the rice *4-DEOXYOROBANCHOL HYDROXYLASE* unravels specific functions of canonical strigolactones. Proc Natl Acad Sci U S A **120**, e2306263120.

Clough SJ, Bent AF. 1998. Floral dip: a simplified method for Agrobacterium-mediated transformation of Arabidopsis thaliana. Plant Journal **16**, 735-743.

Dun EA, Brewer PB, Gillam EMJ, Beveridge CA. 2023. Strigolactones and Shoot Branching: What Is the Real Hormone and How Does It Work? Plant and Cell Physiology **64**, 967-983.

Francis B, Aravindakumar CT, Brewer PB, Simon S. 2023. Plant nutrient stress adaptation: A prospect for fertilizer limited agriculture. Environmental and Experimental Botany **213**, 105431.

Giovannetti M, Mosse B. 1980. An Evaluation of Techniques for Measuring Vesicular Arbuscular Mycorrhizal Infection in Roots. New Phytologist **84**, 489–500.

Gomez-Roldan V, Fermas S, Brewer PB, Puech-Pages V, Dun EA, Pillot JP, Letisse F, Matusova R, Danoun S, Portais JC, Bouwmeester H, Becard G, Beveridge CA, Rameau C, Rochange SF. 2008. Strigolactone inhibition of shoot branching. Nature **455**, 189-194.

Grace EJ, Cotsaftis O, Tester M, Smith FA, Smith SE. 2009. Arbuscular mycorrhizal inhibition of growth in barley cannot be attributed to extent of colonization, fungal phosphorus uptake or effects on expression of plant phosphate transporter genes. New Phytol **181**, 938-949.

Guan JC, Li C, Flint-Garcia S, Suzuki M, Wu S, Saunders JW, Dong L, Bouwmeester HJ, McCarty DR, Koch KE. 2023. Maize domestication phenotypes reveal strigolactone networks coordinating grain size evolution with kernel-bearing cupule architecture. Plant Cell **35**, 1013-1037.

Haider I, Yunmeng Z, White F, Li C, Incitti R, Alam I, Gojobori T, Ruyter-Spira C, Al-Babili S, Bouwmeester HJ. 2023. Transcriptome analysis of the phosphate starvation response sheds light on strigolactone biosynthesis in rice. Plant Journal **114**, 355-370.

Harwood WA. 2014. A Protocol for High-Throughput *Agrobacterium*-Mediated Barley Transformation. Methods in Molecular Biology **1099**, 251-260.

Hellens AM, Chabikwa TG, Fichtner F, Brewer PB, Beveridge CA. 2023. Identification of new potential downstream transcriptional targets of the strigolactone pathway including glucosinolate biosynthesis. Plant Direct **7**, e486.

Inoue M, Xie X, Yoneyama K. 2024. Barley is a potential trap crop for root parasitic broomrape weeds. J Pestic Sci **49**, 255-261.

Ito S, Braguy J, Wang JY, Yoda A, Fiorilli V, Takahashi I, Jamil M, Felemban A, Miyazaki S, Mazzarella T, Chen GE, Shinozawa A, Balakrishna A, Berqdar L, Rajan C, Ali S, Haider I, Sasaki Y, Yajima S, Akiyama K, Lanfranco L, Zurbriggen MD, Nomura T, Asami T, Al-Babili S. 2022. Canonical

783 strigolactones are not the major determinant of tillering but important rhizospheric signals in rice.
784 Science Advances **8**, eadd1278.
785 **Kaur S, Campbell BJ, Suseela V**. 2022. Root metabolome of plant-arbuscular mycorrhizal symbiosis
786 mirrors the mutualistic or parasitic mycorrhizal phenotype. New Phytologist **234**, 672-687.
787 **Kelly JH, Tucker MR, Brewer PB**. 2023. The Strigolactone Pathway Is a Target for Modifying Crop
788 Shoot Architecture and Yield. Biology (Basel) **12**, 95.
789 **Lailheugue V, Merlin I, Boutet S, Perreau F, Pouvreau JB, Delgrange S, Ducrot PH, Cottyn-Boitte B,**
790 **Mouille G, Lauvergeat V**. 2023. Vitislactone, a non-canonical strigolactone exudated by grapevine
791 rootstocks in response to nitrogen starvation. Phytochemistry **215**, 113837.
792 **Li C, Dong L, Durairaj J, Guan JC, Yoshimura M, Quinodoz P, Horber R, Gaus K, Li J, Setotaw YB, Qi J,**
793 **De Groote H, Wang Y, Thiombiano B, Flokova K, Walmsley A, Charnikhova TV, Chojnacka A, Correia**
794 **de Lemos S, Ding Y, Skibbe D, Hermann K, Screpanti C, De Mesmaeker A, Schmelz EA, Menkir A,**
795 **Medema M, Van Dijk ADJ, Wu J, Koch KE, Bouwmeester HJ**. 2023. Maize resistance to witchweed
796 through changes in strigolactone biosynthesis. Science **379**, 94-99.
797 **Li C, Haider I, Wang JY, Quinodoz P, Suarez Duran HG, Mendez LR, Horber R, Fiorilli V, Votta C,**
798 **Lanfranco L, Correia de Lemos SM, Jouffroy L, Moegle B, Miesch L, De Mesmaeker A, Medema MH,**
799 **Al-Babili S, Dong L, Bouwmeester HJ**. 2024. OsCYP706C2 diverts rice strigolactone biosynthesis to a
800 noncanonical pathway branch. Science Advances **10**, eadq3942.
801 **Ma X, Zhang Q, Zhu Q, Liu W, Chen Y, Qiu R, Wang B, Yang Z, Li H, Lin Y, Xie Y, Shen R, Chen S,**
802 **Wang Z, Chen Y, Guo J, Chen L, Zhao X, Dong Z, Liu YG**. 2015. A Robust CRISPR/Cas9 System for
803 Convenient, High-Efficiency Multiplex Genome Editing in Monocot and Dicot Plants. Molecular Plant
804 **8**, 1274-1284.
805 **Marzec M, Daszkowska-Golec A, Collin A, Melzer M, Eggert K, Szarejko I**. 2020a. Barley
806 strigolactone signalling mutant hvd14.d reveals the role of strigolactones in abscisic acid-dependent
807 response to drought. Plant, Cell & Environment **43**, 2239-2253.

Marzec M, Gruszka D, Tylec P, Szarejko I. 2016. Identification and functional analysis of the *HvD14* gene involved in strigolactone signaling in *Hordeum vulgare*. Physiologia Plantarum **158**, 341-355.

Marzec M, Situmorang A, Brewer PB, Braszewska A. 2020b. Diverse Roles of MAX1 Homologues in Rice. Genes (Basel) **11**, 1348.

Mascher M, Wicker T, Jenkins J, Plott C, Lux T, Koh CS, Ens J, Gundlach H, Boston LB, Tulpova Z, Holden S, Hernandez-Pinzon I, Scholz U, Mayer KFX, Spannagl M, Pozniak CJ, Sharpe AG, Simkova H, Moscou MJ, Grimwood J, Schmutz J, Stein N. 2021. Long-read sequence assembly: a technical evaluation in barley. Plant Cell **33**, 1888-1906.

Mashiguchi K, Seto Y, Onozuka Y, Suzuki S, Takemoto K, Wang Y, Dong L, Asami K, Noda R, Kisugi T, Kitaoka N, Akiyama K, Bouwmeester H, Yamaguchi S. 2022. A carlactonoic acid methyltransferase that contributes to the inhibition of shoot branching in *Arabidopsis*. Proc Natl Acad Sci U S A **119**, e2111565119.

Mizutori Y, Nishiyama K, Seto Y. 2024. Inhibition of shoot branching in Arabidopsis by the artificially produced canonical-strigolactone. Biosci Biotechnol Biochem.

Mori N, Nomura T, Akiyama K. 2020. Identification of two oxygenase genes involved in the respective biosynthetic pathways of canonical and non-canonical strigolactones in *Lotus japonicus*. Planta **251**, 40.

Moriyama D, Wakabayashi T, Shiotani N, Yamamoto S, Furusato Y, Yabe K, Mizutani M, Takikawa H, Sugimoto Y. 2022. Identification of 6-*epi*-heliolactone as a biosynthetic precursor of avenaol in *Avena strigosa*. Bioscience, Biotechnology, and Biochemistry **86**, 998-1003.

Nomura T, Seto Y, Kyozuka J. 2024. Unveiling the complexity of strigolactones: exploring structural diversity, biosynthesis pathways, and signaling mechanisms. Journal of Experimental Botany **75**, 1134-1147.

Salam BB, Barbier F, Danieli R, Teper-Bamnolker P, Ziv C, Spichal L, Aruchamy K, Shnaider Y, Leibman D, Shaya F, Carmeli-Weissberg M, Gal-On A, Jiang J, Ori N, Beveridge C, Eshel D. 2021. Sucrose promotes stem branching through cytokinin. Plant Physiology **185**, 1708-1721.

Sparkes IA, Runions J, Kearns A, Hawes C. 2006. Rapid, transient expression of fluorescent fusion proteins in tobacco plants and generation of stably transformed plants. Nature Protocols **1**, 2019-2025.

Sun H, Guo X, Zhu X, Gu P, Zhang W, Tao W, Wang D, Wu Y, Zhao Q, Xu G, Fu X, Zhang Y. 2023. Strigolactone and gibberellin signaling coordinately regulate metabolic adaptations to changes in nitrogen availability in rice. Molecular Plant **16**, 588-598.

Szurman-Zubrzycka M, Chmielewska B, Gajewska P, Szarejko I. 2017. Mutation Detection by Analysis of DNA Heteroduplexes in TILLING Populations of Diploid Species. In: Jankowicz-Cieslak J, Tai TH, Kumlehn J, Till BJ, eds. *Biotechnologies for Plant Mutation Breeding*. Cham.: Springer, 281–303.

Szurman-Zubrzycka ME, Zbieszczyk J, Marzec M, Jelonek J, Chmielewska B, Kurowska MM, Krok M, Daszkowska-Golec A, Guzy-Wrobelska J, Gruszka D, Gajecka M, Gajewska P, Stolarek M, Tylec P, Sega P, Lip S, Kudelko M, Lorek M, Gorniak-Walas M, Malolepszy A, Podsiadlo N, Szyrajew KP, Keisa A, Mbambo Z, Todorowska E, Gaj M, Nita Z, Orlowska-Job W, Maluszynski M, Szarejko I. 2018. *Hor*TILLUS-A Rich and Renewable Source of Induced Mutations for Forward/Reverse Genetics and Pre-breeding Programs in Barley (*Hordeum vulgare* L.). Frontiers in Plant Science **9**, 216.

Tadano T, Tanaka A. 1980. The effect of low phosphate concentrations in culture medium on early growth of several crop plant (in Japanese, translated by the authors). Jpn. J. Soil Sci. Plant Nutr. **51**, 399–404.

Umehara M, Hanada A, Yoshida S, Akiyama K, Arite T, Takeda-Kamiya N, Magome H, Kamiya Y, Shirasu K, Yoneyama K, Kyozuka J, Yamaguchi S. 2008. Inhibition of shoot branching by new terpenoid plant hormones. Nature **455**, 195-200.

Verwoerd TC, Dekker BM, Hoekema A. 1989. A small-scale procedure for the rapid isolation of plant RNAs. Nucleic Acids Research **17**, 2362.

Vierheilig H, Coughlan AP, Wyss U, Piche Y. 1998. Ink and vinegar, a simple staining technique for arbuscular-mycorrhizal fungi. Applied and Environmental Microbiology **64**, 5004-5007.

Wakabayashi T, Hamana M, Mori A, Akiyama R, Ueno K, Osakabe K, Osakabe Y, Suzuki H, Takikawa H, Mizutani M, Sugimoto Y. 2019. Direct conversion of carlactonoic acid to orobanchol by cytochrome P450 CYP722C in strigolactone biosynthesis. Science Advances **5**, eaax9067.

Wakabayashi T, Yasuhara R, Miura K, Takikawa H, Mizutani M, Sugimoto Y. 2021. Specific methylation of (11R)-carlactonoic acid by an Arabidopsis SABATH methyltransferase. Planta **254**, 88.

Wang H, Chen W, Eggert K, Charnikhova T, Bouwmeester H, Schweizer P, Hajirezaei MR, Seiler C, Sreenivasulu N, von Wiren N, Kuhlmann M. 2018. Abscisic acid influences tillering by modulation of strigolactones in barley. Journal of Experimental Botany **69**, 3883-3898.

Wang JY, Chen GE, Braguy J, Al-Babili S. 2024. Distinguishing the functions of canonical strigolactones as rhizospheric signals. Trends in Plant Science **29**, 925-936.

Waters MT, Nelson DC, Scaffidi A, Flematti GR, Sun YK, Dixon KW, Smith SM. 2012. Specialisation within the DWARF14 protein family confers distinct responses to karrikins and strigolactones in *Arabidopsis*. Development **139**, 1285-1295.

Wu K, Wang S, Song W, Zhang J, Wang Y, Liu Q, Yu J, Ye Y, Li S, Chen J, Zhao Y, Wang J, Wu X, Wang M, Zhang Y, Liu B, Wu Y, Harberd NP, Fu X. 2020. Enhanced sustainable green revolution yield via nitrogen-responsive chromatin modulation in rice. Science **367**, eaaz2046.

Yamada Y, Otake M, Furukawa T, Shindo M, Shimomura K, Yamaguchi S, Umehara M. 2019. Effects of Strigolactones on Grain Yield and Seed Development in Rice. Journal of Plant Growth Regulation **38**, 753–764.

Yoneyama K, Akiyama K, Brewer PB, Mori N, Kawano-Kawada M, Haruta S, Nishiwaki H, Yamauchi S, Xie X, Umehara M, Beveridge CA, Yoneyama K, Nomura T. 2020a. Hydroxyl carlactone derivatives are predominant strigolactones in *Arabidopsis*. Plant Direct **4**, e00219.

Yoneyama K, Brewer PB. 2021. Strigolactones, how are they synthesized to regulate plant growth and development? Current Opinion in Plant Biology **63**, 102072.

Yoneyama K, Xie X, Nomura T, Yoneyama K. 2020b. Do Phosphate and Cytokinin Interact to Regulate Strigolactone Biosynthesis or Act Independently? Frontiers in Plant Science **11**, 438.

Yoneyama K, Xie X, Nomura T, Yoneyama K, Bennett T. 2022. Supra-organismal regulation of strigolactone exudation and plant development in response to rhizospheric cues in rice. Current Biology **32**, 3601-3608 e3603.

Zhang J, Mazur E, Balla J, Gallei M, Kalousek P, Medveďová Z, Li Y, Wang Y, Prat T, Vasileva M, Reinöhl V, Procházka S, Halouzka R, Tarkowski P, Luschnig C, Brewer PB, Friml J. 2020. Strigolactones inhibit auxin feedback on PIN-dependent auxin transport canalization. Nature Communications **11**, 3508.

Zhou A, Kane A, Wu S, Wang K, Santiago M, Ishiguro Y, Yoneyama K, Palayam M, Shabek N, Xie X, Nelson DC, Li Y. 2025. Evolution of interorganismal strigolactone biosynthesis in seed plants. Science **387**, eadp0779.

Supplementary data

```
tr|Q9LIF4|Q9LIF4_ARATH          --------------------MAPLPISSIRVGKIDDVQELIKS--KPNKVPERFIREEYE      38
tr|I1HUZ6|I1HUZ6_BRADI          MASAV-CSSKQQQ---------KEEESEIEIGQVDDVQELQRA--CLDTVPERYIRDGDD      48
Os01t0935400-00                 MDS------------GAAAVCAEKASEIIKIGQVDDVQELQRRLCSATTVPERYIRDGDD      48
HvLBO                           MASAAVCSPKQQQQQRRRDEEGETDGGVVKIGRVDDVQELQKA--CAGDVPERYLRDGDD      58
tr|C5XH53|C5XH53_SORBI          MRSRFCCIGGAY--------AMAAAENEIKIGQVDDVQELHRT--GLTTVPDRYIRDGDD      50
                                                      :.:*::****** :       **:*::*:  :

tr|Q9LIF4|Q9LIF4_ARATH          RGVVVSSLKTHHLHHQIPVIDLSKLSKPDNDDFFFEILKLSQACEDWGFFQVINHGIEVE      98
tr|I1HUZ6|I1HUZ6_BRADI          RPDGV-NL----CGKQIPVIDAGELRRGA--P--EELAKLRLACQDWGFFQVVNHGVEPE      99
Os01t0935400-00                 RPDHA-VVDDERAQERIPVIDVGELQRGS--E--DELDNLRLACEQWGFFQVVNHGVEEE      103
HvLBO                           RPGGA-NV---CAHAEIPVIDAGELRRGGGGG--DELEKLRRACEEWGFFQVVNHGIDGE      112
tr|C5XH53|C5XH53_SORBI          RPDGD-NV---CALAHIPVIDVGDLPRG---D--DELDKLRLACEEWGFFQVVNHGIAHE      101
                                *      :       .***** ..* :        *: :*  **::******:***:  *
```

```
tr|Q9LIF4|Q9LIF4_ARATH          VVEDIEEVASEFFDMPLEEKKKYPMEPGTVQGYGQAFIFSEDQKLDWCNMFALGVHPPQI   158
tr|I1HUZ6|I1HUZ6_BRADI          LMEDMAKLAREFFMLPLEEKSRYPMAPGGIQGYGHAFVFSADQKLDWCNMLALGVAPQSI   159
Os01t0935400-00                  TMEEMEKAAREFFMLPLEEKEKYPMEPGGIQGYGHAFVFSDDQKLDWCNMLALGVEPAFI   163
HvLBO                            LLDEMERLSREFFMLPLEEKERYPMAPGGIQGYGHAFVFSEDQKLDWCNMLALGVSPAFI   172
tr|C5XH53|C5XH53_SORBI           LLDEMEKLTREFFMLPLEEKEKYPMAPGGIQGYGHAFVFSEDQKLDWCNMLALGVEPASI   161
                                  :::: . : *** :*****.:*** ** :****:**:** *********:**** *  *

tr|Q9LIF4|Q9LIF4_ARATH          RNPKLWPSKPARFSESLEGYSKEIRELCKRLLKYIAISLGLKEERFEEMFGE--AVQAVR   216
tr|I1HUZ6|I1HUZ6_BRADI          RQPALWPTNPASFTTTLENYSAEIRDLCLDLLSHIAETLGLERSTFSGMFGGEKAVQAVR   219
Os01t0935400-00                  RRPNLWPTTPANFSKTLEKYSVEIRELCVRLLEHIAAALGLAPARLNGMFGE--AVQAVR   221
HvLBO                            RQPKLWPTTPAAFTDTLERYSAEVRALCHRLLERIAETLGLAPGTFAGMFGD--AVQAVR   230
tr|C5XH53|C5XH53_SORBI           RQPKLWPTAPARFRETLEAYSAEVRKLCRTLLAHIAETLGLAPATFGDMFGE--AVQAVR   219
                                  *.* ***: ** *  :** ** *:* **  **  ** :***    :  ***   ******

tr|Q9LIF4|Q9LIF4_ARATH          MNYYPPCSSPDLVLGLSPHSDGSALTVLQQSKNSCVGLQIL-KDNTWVPVK--PLPNALV   273
tr|I1HUZ6|I1HUZ6_BRADI          MNFYPPCPRPELVLGLSPHSDGSALTVLQQDG-AGGGLQVR-HGGDWVPVGHGGVPGALV   277
Os01t0935400-00                  MNFYPPCPRPELVLGLSPHSDGSAVTVLQQDA-AFAGLQVLRGGGGWVAVH--PVPGALV   278
HvLBO                            MNFYPPCPRPDLVLGLSAHSDGSAVTVLQQDA-GRAGLQVL-RDGAWVPVH--PVPHALV   286
tr|C5XH53|C5XH53_SORBI           MNFYPPCPRPELVMGLSAHSDGSAVTVLQQDM-SCAGLQVRSKAGAWVPVH--PVQHALV   276
                                  **:****  *:**:*** ******:*****.  .  ***:    . ** *    :  ***

tr|Q9LIF4|Q9LIF4_ARATH          INIGDTIEVLSNGKYKSVEHRAVTNRE-KERLTIVTFYAPNYEVEIEPMSELVDDETNPC   332
tr|I1HUZ6|I1HUZ6_BRADI          VNVGDSLEVLTNGRYKSVEHRAVVDGAGRDRLSVVTFYAPAYDVELGPMPELLGDG-EPC   336
Os01t0935400-00                  VNVGDTLEVLTNGRYKSVEHRAVASGE-HDRMSVVTFYAPAYDVELGPLPELVADG-EPR   336
HvLBO                            VNLGDSLEVLTNGRYKSVEHRAVTNGE-QDRLSIVTFYAPAYDVELGPLPELVADG-EPC   344
tr|C5XH53|C5XH53_SORBI           VNLGDTLEVLTNGRYKSVEHRAVVNGE-QDRLSVVTFYAPAYDVELGPLPEFVTDE-APC   334
                                  :*:**::***:**:*********..   ::*:::****** *:**: *: *:: *   *

tr|Q9LIF4|Q9LIF4_ARATH          KYRSYNHGDYSYHYVSNKLQGKKSLDFAKILN----   364
tr|I1HUZ6|I1HUZ6_BRADI          RYRRFNHGEYSRHYVTSKLEGKKTLDFAKIN-----   367
Os01t0935400-00                  RYRTYNHGEYSRHYVTSRLQGKKTLEFAKI------   366
HvLBO                            RYRRFKHGEYSRHYVTSKLEGKKTLDFAKIN-----   375
tr|C5XH53|C5XH53_SORBI           RYRRFNHGEYSRHYVTSRLEGKKTLEFAMVNPPVGR   370
                                  :** ::**:** ***:.:*:***:*:** :
```

Supplementary Fig. S1. Amino acid sequence alignment of barley HvLBO (BAJ96311.1) with *Arabidopsis thaliana* AtLBO (Q9LIF4) and homologs from rice (Os01t0935400-00), sorghum (C5XH53) and *Brachypodium distachyon* (I1HUZ6). The highly-conserved amino acid residue highlighted in blue Asp 251 (D) is substituted to Asn (N) in the barley *lbo.f* mutant.

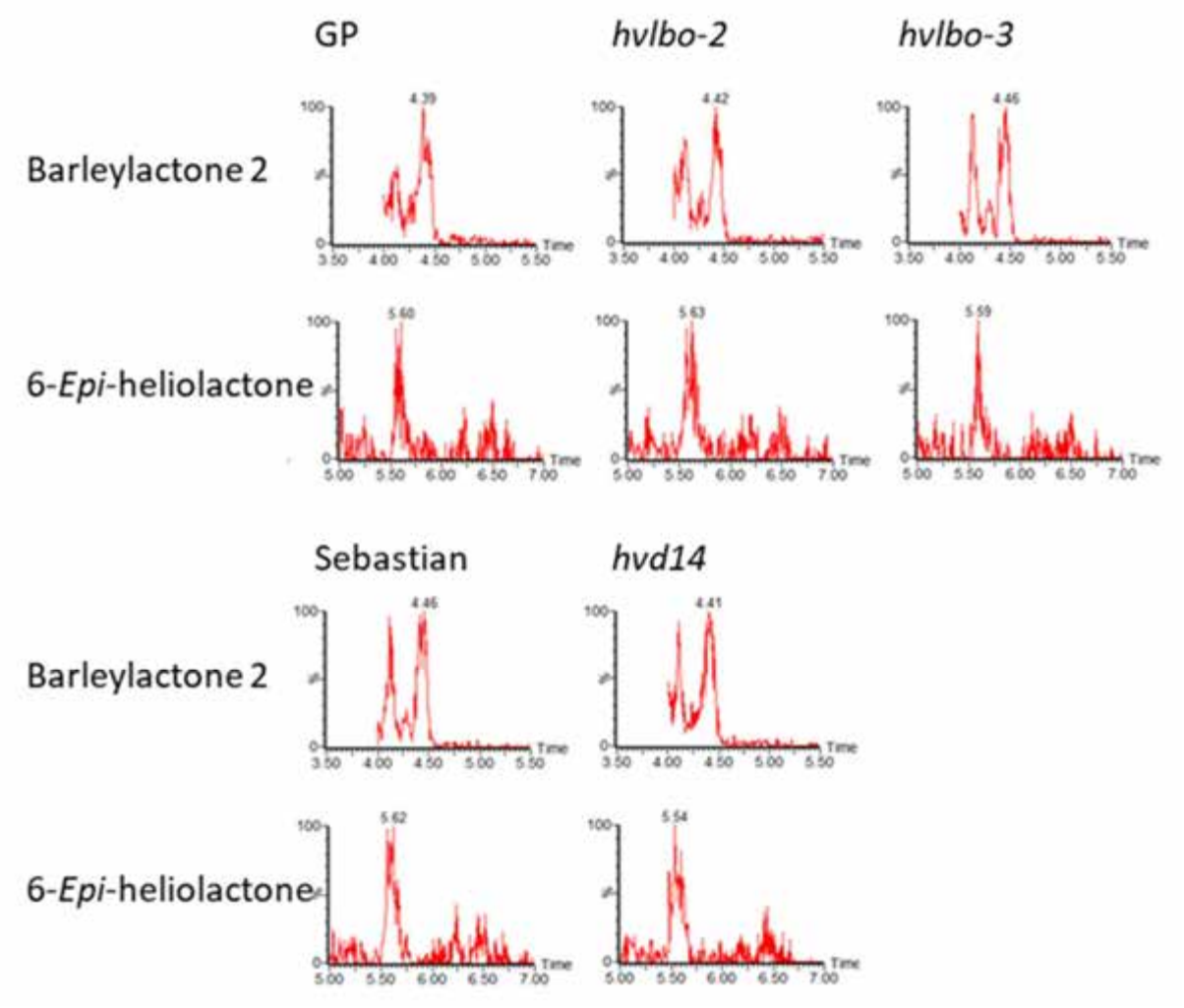

Supplementary Fig. S2. Mass-spectrum data for Fig. 2. Endogenous barleylactone 2 (a novel epoxy variant of 6-*epi*-heliolactone) and 6-*epi*-heliolactone in root tissues of Golden Promise (GP), *hvlbo-2*, *hvlbo-3*, Sebastian and *hvd14* plants. MRM chromatograms of barleylactone 2 (377.0/97.0; m/z in positive mode) and 6-*epi*-heliolactone (361.0/97.0; m/z in positive mode) are shown.

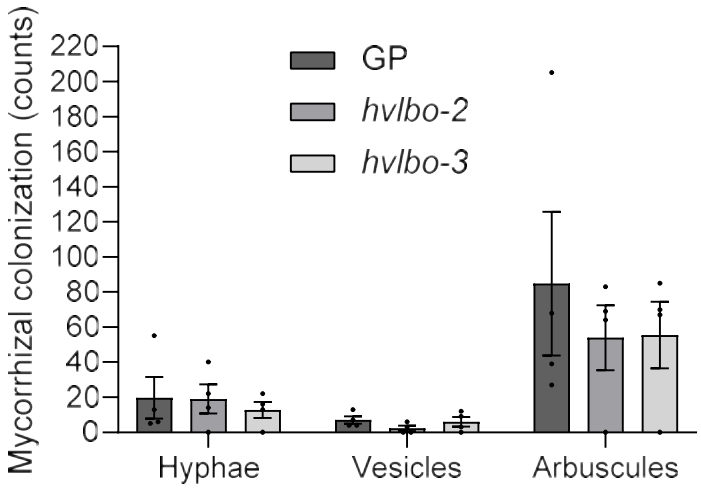

915

916 Supplementary Fig. S3. Arbuscular mycorrhizal fungal colonization in 6-week-old GP (wild type
917 Golden Promise cultivar), *hvlbo-2*, and *hvlbo-3* roots. Hyphae, vesicles and arbuscules were counted
918 from 10 fields of view across each of three full-length roots per replicate. Data are mean ± SEM, *n* =
919 4.

920

921 Supplementary Protocol S1. AM fungi colonization in barley *hvlbo* mutants for Supplementary Fig.
922 S3.

923

924 Barley seeds were surface sterilized with 70% EtOH for 30 seconds, followed by 10% bleach for 3
925 min, and then rinsed with sterile water 3-5 times. Seeds were placed on 90-mm square plates
926 containing two layers of filter paper wetted with approx. 7 mL of sterilized water and then stratified
927 in darkness at 4 °C for 3-4 days. After stratification, plates were moved to a growth chamber under
928 constant white light (38-42 µmol $m^{-2}s^{-1}$) at 20-22 °C for 5 days. 100x100 mm pot was filled with
929 approx. 600 g of sterilized sand then the sand was watered with 100 mL of tap water. Five-day-old
930 seedlings were transferred into pots with one seedling per pot and a total of 4-6 seedlings per
931 genotype.

Spores of *Rhizophagus irregularis* (Agronutrition DAOM 197198, Grade C) were collected with a 10 µm cell strainer, rinsed five times with sterile water, and finally resuspended in water at 1000 spores/mL. Each seedling was inoculated with 2000 spores on the day of transfer to pots. Plants were grown under 16 h light and 8 h darkness and under approx. 22 °C and 60% relative humidity and 440-475 µmol m^{-2} s^{-1} light supplied by broad-spectrum white LEDs. Plants were watered with 50 mL tap water every 2-3 days. After the first week, plants were supplied with 50 mL of 0.5x Hoagland's solution (25 µM phosphate) once a week. After six weeks (44-45 days post inoculation), roots were harvested and washed thoroughly with water to remove sand, and then stored in 50% ethanol at 4 °C until staining.

Before staining, stored roots were rinsed with water. For each plant, three full-length roots were treated with 10% KOH (w/v) for 30 mins at 95 °C, rinsed with water, and then rinsed with 10% acetic acid (v/v) to equilibrate the root for staining. The roots were stained with 5% ink (Pelikan Ink 4001 Brilliant Black, v/v) and 5% acetic acid (v/v) at 95 °C for 10 mins. Roots were rinsed with water then destained with 5% acetic acid and incubated at room temperature overnight. Roots were rinsed with water to remove the 5% acetic acid and then each full-length root was mounted on 50 % glycerol (v/v) on a slide.

Colonization was scored for three roots on separate slides for every plant. For each root, ten random fields of view were used to count the number of arbuscules, hyphae, and vesicles using a 10x objective lens (overall 100x magnification). To avoid counting the same field twice, each field was assigned different coordinates on the microscope stage. After scoring for fungal morphology, the totals were divided by three to derive a mean count across the three roots.

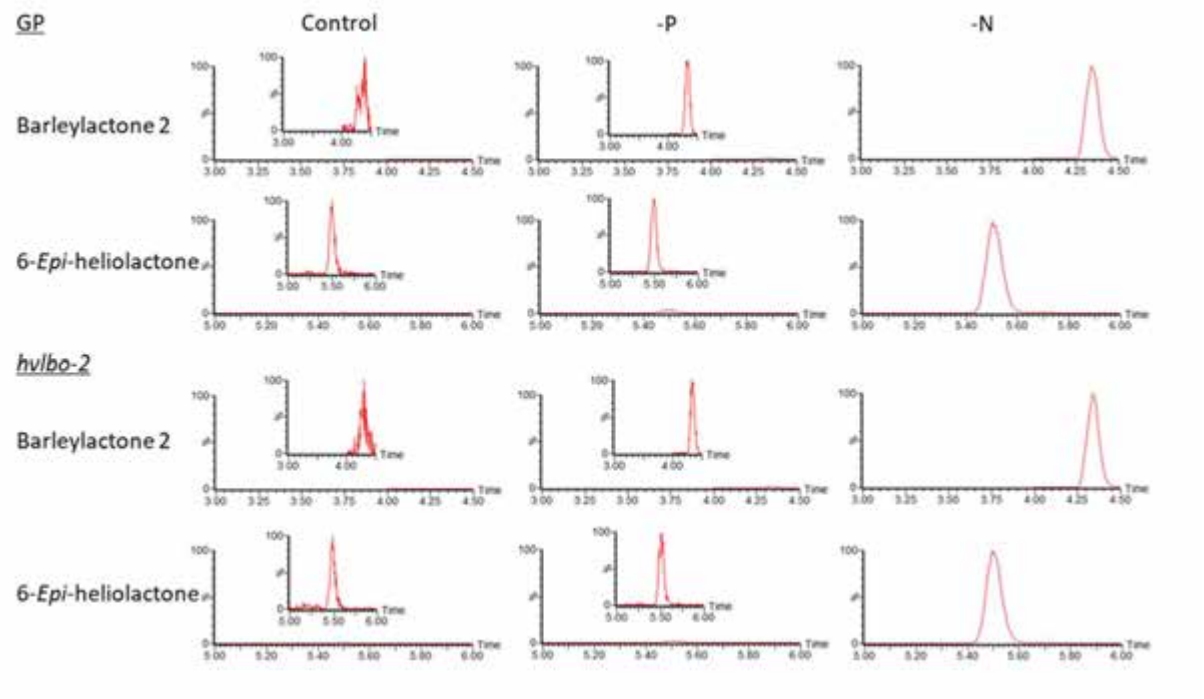

Supplementary Fig. S4. Mass-spectrum data for Fig. 5. Detection of barleylactone 2 (a novel epoxy variant of 6-*epi*-heliolactone) and 6-*epi*-heliolactone in root exudates of Golden Promise (GP) and *hvlbo-2* plants grown under control, -P and -N. MRM chromatograms of barleylactone 2 (377.0/97.0; m/z in positive mode) and 6-*epi*-heliolactone (361.0/97.0; m/z in positive mode) are shown.